Alma Mater Studiorum – Università di Bologna

DOTTORATO DI RICERCA IN

Ingegneria Civile, Chimica, Ambientale e dei Materiali

Ciclo XXXIII

Settore Concorsuale: 03/B2

Settore Scientifico Disciplinare: CHIM/07

NEW BIO-BASED POLYMERS: FROM SYNTHESIS TO CHARACTERIZATION

Presentata da: Silvia Quattrosoldi

Coordinatore Dottorato	**Supervisore**
Prof. Luca Vittuari	Prof.essa Nadia Lotti
	Co-supervisore
	Dott.essa Michelina Soccio

Esame finale anno 2021

Abstract

The environmental problems caused by human activity are one of the main themes of debate of the last Century. As regard plastics, the use of non-renewable sources together with the accumulation of waste in natural habitats are causing serious pollution problems. For this reason, a continuously growing interest is recorded around sustainable materials, potential candidate for the replacement of traditional recalcitrant plastics. Promising results have been obtained with biopolymers, in particular with the class of biopolyesters. Their potential biodegradability and bio-based nature is particularly interesting mainly for food packaging, where the multilayer systems normally used and the contamination by organic matter create severe recycling limits. In this framework, the present research has been conducted with the aim of synthetizing, modifying and characterizing biopolymers for food packaging application. New bioplastics based on monomers derived from renewable resources were successfully synthetized by two-step melt polycondensation and chain extension reaction following the "Green chemistry" principles. Moreover, well-known biopolyesters have been modified by blending or copolymerization, both resulting effective techniques to *ad hoc* tune the polymer final characteristics. The materials obtained have been processed and characterized from the chemical, structural, thermal and mechanical point of view; more specific characterizations as compostability tests, surface hydrophilicity film evaluation and barrier property measurements were conducted.

Tables of contents

List of Abbreviations

AFM	Atomic Force Microscopy
b	Degree of Randomness
BD	1,4-Butanediol
BDA	1,4-Butandiammine
BEPD	2-Butyl-2-ethyl propanediol
CC	Catechol Carbonate
^{13}C-NMR	Carbon Nuclear Magnetic Resonance
DEG	Diethylene Glycol
DMI	Dimethyl Isophthalate
DMS	Dimethyl Succinate
DP	Degree of Polymerization
DSC	Differential Scanning Calorimetry
E	Elastic Modulus
FDCA	Furandicarboxylic Acid
FESEM	Scanning Electron Microscope of Fractured Surfaces
FSC	Fast Scanning Chip Calorimetry
FVEs	Free Volume Elements
GPC	Gel Permeation Chromatography
GTR	Gas Transmission Rate
^{1}H-NMR	Proton Nuclear Magnetic Resonance
HDA	1,6-Hexandiammine
Hex	1,6-Hexandiol
IR	Infrared Spectroscopy (IR)
IV	Intrinsic Viscosity
PBCE	Poly(butylene-1,4-cyclohexanedicarboxylate)
PBF	Poly(butylene furanoate)
PBI	Poly(butylene isophthalate)
PBS	Poly(butylene succinate)

PBT	Poly(butylene terephthalate)
PD	1,3-Propanediol
PDA	1,5-Pentandiammine
PDEF	Poly(diethylene 2,5-furaoate)
PEF	Poly(ethylene furanoate)
PEI	Poly(ethylene isophthalate)
Pent	1,5-Pentandiol
PET	Poly(ethylene terephthalate)
PHAs	Polyhydroxyalkanoates
PHB-OH	Poly(3-hydroxybutyrate)-OH
PHexCE	Poly(hexylene-1,4-cyclohexanedicarboxylate)
PHF	Poly(hexamethylene furanoate)
POM	Polarized optical microscopy
PPCE	Poly(propylene 1,4-cyclohexanedicarboxylate)
PPeF	Poly(pentamethylene furanoate)
PPentCe	Poly(pentylene-1,4-cyclohexanedicarboxylate)
PPF	Poly(propylene furanoate)
PPI	Poly(propylene isophthalate)
PPT	Poly(propylene terephthalate)
T_c	Melt Crystallization
T_{cc}	Cold Crystallization
T_g	Glass Transition Temperature
T_m	Melting Temperature
TGA	Thermogravimetric Analysis
***Trans*-CEDA**	Trans 1,4-cyclohexanedicarboxylic acid
SEM	Scanning Electron Microscopy
WAXS	Wide-Angle X-Ray Diffraction
ε_b	Elongation at Break
σ_b	Stress at Break
σ_y	Stress at Yielding
ΔC_p	Heat Capacity
ΔH_m	Enthalpy of Crystallization
χ_c	Crystallinity Degree

Chapter I
INTRODUTION

1   PLASTIC MATERIALS

"Plastics" have been defined by the "International Union of Pure and Applied Chemistry" (IUPAC) as "polymeric materials that may contain other substances to improve performance or reduce costs". Normally these materials are constituted of synthetic or natural macromolecules that can be easily melted and molded in a solid final product. Due to their excellent properties - as low cost of production, easy manufacturing, low density, high mechanical performance and versatility- plastics prevailed over traditional materials, succeeding in disparate industrial fields.

The historians commonly used the characteristic materials of certain period to classify the early ages of man, as the Stone Age, the Iron Age and the Bronze Age. This fact underlines the importance of materials in the development of society. Until the end of 1800, tools, objects and furniture had been made with traditional materials; then, a new class was introduced, and a kind of new Age started. Indeed, plastics have not only prevailed over traditional materials but also made possible new products that brought a revolution in different fields. The massive production of plastic started in the 1930, but some traces of use of natural plastic could be found also in the antiquity. For example, the use of bitumen was mentioned in the Genesis (Chapter 11) from the builder during the planning of Babylonia. In the Ancient Egypt, the mummies were wrapped in cloth wet of solution of bitumen and lavender. Once expose to light, the solution reacted and cross-link bonds determined an insoluble and hard final product. Early traces were also found in the Middle Ages, when sealing wax based on shellac has used. Then, in the 17th century, John Tradescant introduced gutta-percha, a natural polymer of isoprene forming a rubber-like elastomer. This material, employed as a cable insulator and for general molding products, reached high popularity during the 19th century. Different studies were performed on this new material, and in the 1930 Goodyear became able to vulcanize the natural rubber. While Goodyear was studying the base of the chemistry of rubber, other scientists worked on this topic around Europe. Schönbien found the condition to produce nitrated cellulose, i.e. celluloid, that marked the beginning of researches and discoveries of novel materials: Parkesine (1856), Xylonite (1862), Galalith (1897). Then in the 1907, Leo Hendrik Baekeland

found how to modify and control the reaction between phenol and aldehyde, obtaining 119 patents. After the General Bakelite Company was founded, the new material conquered different industrial fields and in the 1944 the production reached 175 000 tons/year. If celluloid was the first example of chemical modification of natural polymer, Bakelite was the first synthetic and commercially available product. Starting from the success of Bakelite, new resins were developed as urea-formaldehyde resins and thiourea-formaldehyde resins. In those years, also a new thermoplastic derivate of cellulose was synthetized: cellulose acetate.

Between 1930 and 1940, the industrial production of polystyrene (PS), polyvinyl chloride (PVC), polyolefins and polymethyl meta acrylate (PMMA) begun. The second war world boosted the research of new materials. The main goal of the researches was to find synthetic substitutes of natural materials, in short supply but with a strategic importance. Nylon was synthetized by Carothers and his team, for Du Pont. After the war, these new plastic materials conquered the market, being produced in large scale and used in different fields, ousting the natural polymers and their chemically modified derivatives.

In more recent years, the industrial synthetic processes and quality of the existing polymers improved significantly. In particular, a new grade of Polypropylene was synthetized by Phillips, using the new catalyst discovered by Zigler-Natta, both awarded with the Noble Prize[1].

1.1   Market and production of plastics

As already mentioned, after the second War World, plastics became the alternative to traditional materials in different fields, for their lower price but also for their great potential.
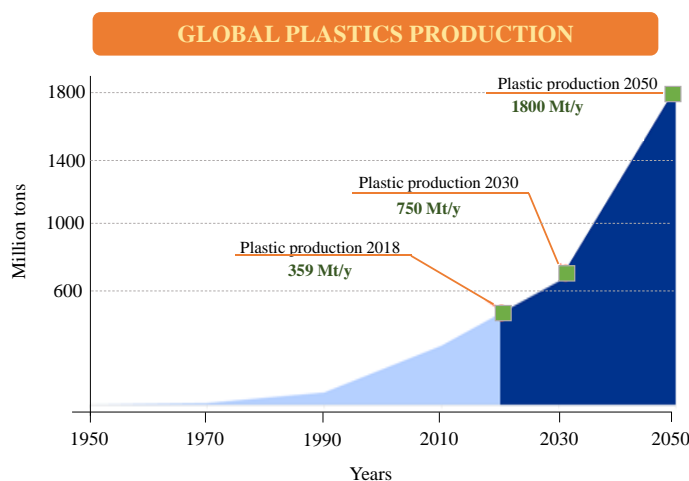
Figure 1.1: *Global plastics and fiber production measured in tones per years.*

In this view, large-scale investments for the development of new technologies were fundamental to favor the consistent increasing of production; considering the data collected by the Modern Plastic Source, while in 1939 the word production of plastic materials was around 300 000 tons, in 1998 the tons of materials produced reached 135 000 000 tons[1].

Production has been still growing today and the market, as shown in the annual report published by Plastics Europe, has still expanding (**Figure 1.1**). In 2018, around 359 million tons of plastics have been produced worldwide, and 61.8 million tons only in Europe[2], as reported in **Figure 1.2**.
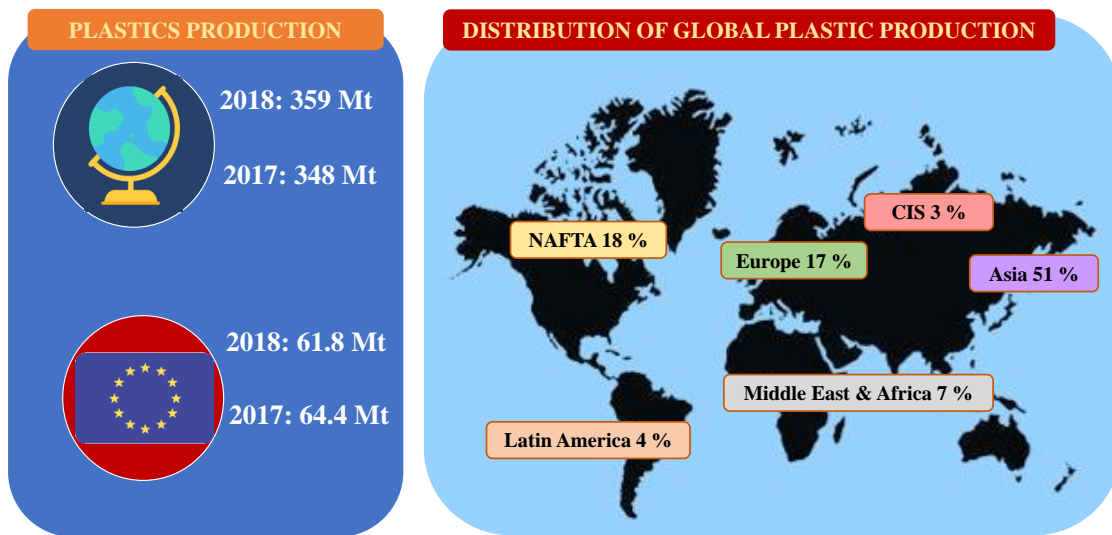
***Figure 1.2**: World and European plastics production and the global distribution.*

The value reported is relative only to thermoplastics, thermosets, polyurethanes, adhesives, coatings and sealants; other materials as fibers of PET, polyamides PA, PP and polyacrylic are not included[2]. The main amount of plastics produced has employed in packaging field, but a high percentages find application in construction, automotive and electronics, as well[2].

1.1.1 Environmental impact

Plastic materials boast different and unique properties as lightweight, high strength-to-weight ratio, inexpensive and easy production, thermal and electrical insulating, water and shock resistance. Durability and low density are real benefits during the using of the objects but determine environmental threat. Indeed, plastic products when become wastes persisting in the environment, and in same case, 50 years or even more are needed for their degradation. Moreover, around 60% of the plastic produced is less dense than seawater, determining an easy dispersion around the globe[3]. For this reason, wind and water

can transport the wastes far from the source area[4], reaching the most remote region of the world: plastic debris are spreading around in all major ocean basins[5] (**Figure 1.3**). In 2010, it is estimated that 4 to 12 million metric tons (Mt) of plastic waste enter the marine system[6], becoming ubiquitous in the environment. In particular, floating islands of wastes are accumulating in different zone: the biggest one, "Great Pacific garbage patch" located between California and Hawaii, has an extension of 1.6 million square kilometers and contains about 80,000 metric tons of plastic[7]. In these conditions, the massive plastic waste is partially degraded into smaller pieces[5] by the action of sun, temperature variations, waves and marine life[6], or lose buoyancy and sink[8] realizing micro/nano fragments: increasingly numbers of reports are documenting their contamination of freshwater and terrestrial habitats[9–11]. As a direct consequence, the exposition of living organisms to chemicals can damage their biological function, compromising their surviving.
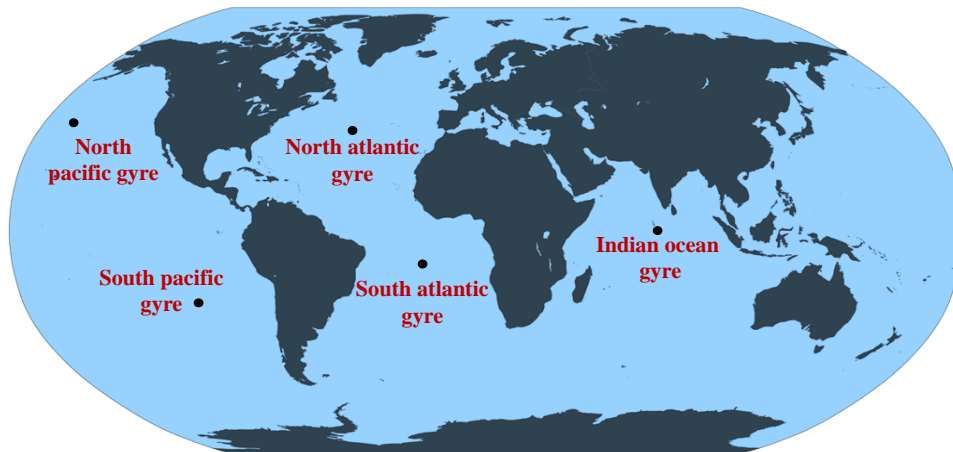
Figure 1.3: World map of garbage gyres.

Considering the growth rate of production and the characteristics of these materials, the management of the end-life products is becoming a real problem. The Plastics Europe reports that 29.1 million tons of plastic waste have been collected in Europe in 2018[2]. The main source of waste, 16.7 million tons (around 62%), is the packaging sector[2]: plastic bottles are appreciated because of their lightness and unbreakability - in contrast with glass ones-, small containers are produced in pharmaceutical field to pack tablets or solution, film are also widely used to wrap bags and object. As it is possible to understand, the main application of plastic materials in this field are for single-use or for products with a short-term life. In particular, the global trend to shift from reusable to single use, accelerated the accumulation[6].

Despite the significant contribution of plastics to improve of standard of living, the current opinion of the public citizen on these materials is not completely positive. In the new Century, the concern for environment brings an increasing awareness for pollution and natural resources. Recycling and destructive thermal treatment, as combustion or pyrolysis, are developed as alternative to the landfill: from 2006 to 2018, recycling increased by 110% and the thermal treatment increased by 77%, while landfill decreased by 44%[2], as reported in **Figure 1.4 B**.
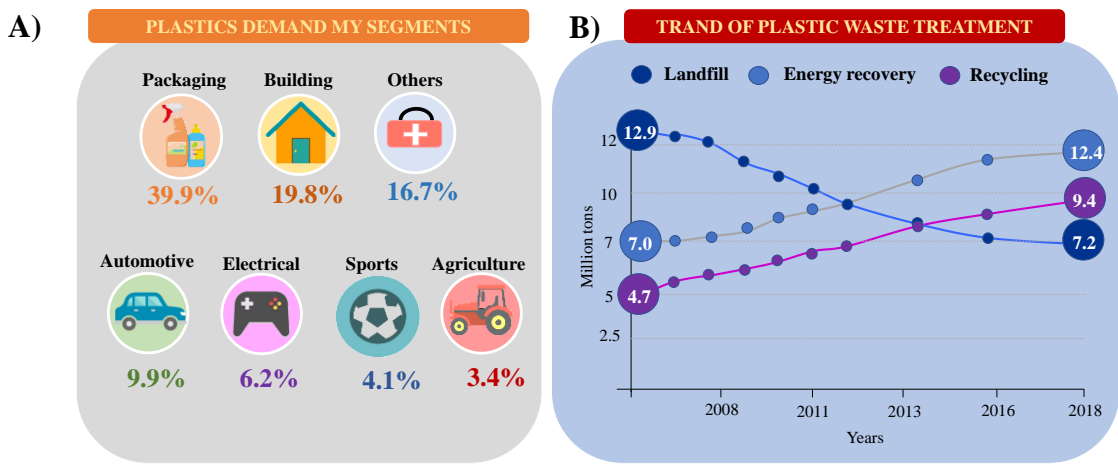
Figure 1.4: A) Distribution of plastics converters demand by segment in 2018 for Europe; B) the trend of plastic waste treatment.

New long-term waste management policy and legislations are developed, both at national and European level [12]. The 2008/98/EC Directive introduces a multistep hierarchy, which classifies the different waste treatment strategies (prevention, re-use, recycling, other forms of recovery and landfill) according to their ability to preserve the limited fossil resources[13]. Even if these data are very promising, it is also true that in many southern and eastern European countries landfill is still the first solution.

1.2 Bioplatics

As previously explained, reducing the usage of finite fossil resources and mitigating the environmental impact of plastics are becoming very urgent needs[14]. For this reason, the development of plastics based on renewable sources and able to degrade after the use, the so-called bioplastics, with performances comparable to traditional plastics in terms of cost and properties, is one of the main challenges of the scientific community.

According to the European Bioplastics Association, the word "Bioplastics" includes a family of materials, which can be divided in three broad categories, **Figure 1.5**:

- obtained by chemical polymerization of bio-based building blocks and not biodegradable, as bio-PET, bio-PE[15];
- obtained by chemical polymerization of oil-based building blocks and biodegradable, as poly(butylene/adipate terephthalate) PBAT and polycaprolactone PCL;
- obtained by chemical polymerization of biobased building blocks or by micro-organisms, and biodegradable, as polyhydroxyalkanohates PHA, polylactic acid PLA, poly(butylene adipate) PBA, poly(butylene succinate) PBS.
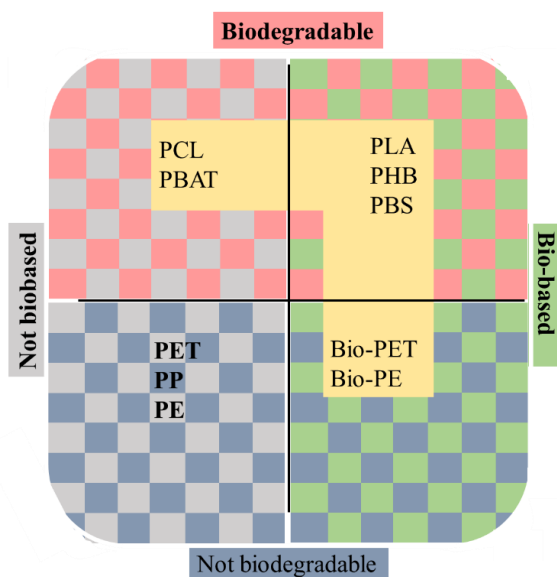
Figure 1.5: Bioplastic subdivision.

The application of renewable and degradable materials in daily life represents a valid solution in the case of products characterized by short life, such those employed for food packaging, to cite an example among several others. Bioplastics possess performances comparable to petrochemical-based polymers, can be manufactured and processed with the same technologies, and their whole production chain is greener. Biodegradable bioplastics can be incorporated into the organic waste stream, where are converted into CO_2, CH_4, water and organic matter for soil, by action of micro-organisms or by hydrolysis[16,17]. For this reason, the derived wastes do not need to be separated from organic waste, unlike traditional plastic, saving time and expensive processes, since a system of waste disposal will be not required. The lowering of waste management costs is also promoted by the decreasing of the total volume of wastes placed in landfills, in this way their longevity and stability is favored. Alternatively, via microbial and/or enzymatic treatment at the end life, bioplastics could be converted to useful monomers

and oligomers. Of course, for those applications requiring products with long life term, recycling is the optimal strategy to manage waste in accordance with the principles of the circular economy. In this view, bioplastics from renewable resources represent the best choice.

The fields of use of bioplastics follow the main applications of petrochemical-based plastics: packaging, (as film wrapping, bags, laminated paper, food containers), hygiene products (cotton swabs, soup disposal), consumer goods (toys, tableware, general containers), and agricultural tools (mulch films, pots)[17,18].

The market of biopolymers is rapidly growing, favored by the European Union and the public opinion. Even if nowadays the global production capacity is only 2.05 million tons per year (about 1% of total plastic production), it is expected a huge increment, increasing from 2.05 million tons in 2017 to 2.44 million tons in 2022[19]. Among biodegradable polymers, PBS, PLA and PHA are the most required by the market. Bio-based PE, bio-based PET, and bio-based PA, bio-based and not biodegradable materials, cover the 57% (1.2 million tons) of the global bioplastics production[19].

1.2.1 Renewable green platforms

The bio-based nature, defined as the possibility to derive chemicals from renewable sources, is a relevant aspect proper of most bioplastics. In this way the dependence on fossil resources, which are limited and with a price subjected to continuous and uncontrolled fluctuations, could be decreased. Bioplastics are a suitable option, but some criticisms need to be considered. A number of monomers used for synthesis of biopolymers, derive from natural substances which can also be consumed as food: wheat, corn, sugar cane and rice. In addition, the processes to refine biomasses could require important quantities of energy, higher than those used for oil. In this situation, the benefits can easily become issues. To critically assess the balance between advantages and disadvantages and then estimate whether the whole process is truly sustainable, Life Cycle Assessments (LCAs) studies must be conducted, taking into account also the ethical and moral factors[20]. To date, several non-edible renewable resources have been reported as usable to synthetize polymers; moreover, some products constituted by natural polymers (such as chitin and chitosan, silk, cotton, cellulose and its derivatives) are already commercialized[21].

There are some examples which seem encouraging to synthetize renewable polymers. Several processes based on fermentation of biomass have been proposed for the production of important diacids – for example succinic acid[22] and isophthalic acid[23–25] - and glycols[26–28]. In order to take advantage from the

wide range of functional groups and structural variations of natural products, different strategies of synthesis have been developed. For example, vegetable oils and fatty acids, mostly triglycerides, are functionalized employing their different reactive sites to facilitate the conversion in useful monomers/polymers[29–35]. Terpenes and terpenoids are also promising organic feedstock for the production of green plastics and composites[36–38]. In literature, different strategies report dye-sensitized photooxygenation of these compounds to obtain bio-based polyhydroxylated monomers and their use for the production of functionalized polyesters[39–49]. Terpenes are demonstrated being useful starting materials for the synthesis of biobased terephthalic acid and 1,4-cyclohexane dicarboxylic acid[50]. Another important bio-based platform obtained starting from hexoses, mainly fructose, is 5-hydroxymethyl furfural (HMF). HMF together with one of its most promising derivate, 2,5-furandicarboxylic acid (FDCA), have been included in the "Top 10+4" bio-based chemical evaluated by U.S Department of Energy (DOE)[51,52]. HMF demonstrated to be pretty versatile molecule, being converted into several sustainable chemicals such as:

- direct furan derivates: 5-hydroxymethylfuroic acid, alkoxymethylfurfurals, 2,5-furandicarboxylic acid;
- non direct furan derivates: caprolactam and caprolactone, adipic acid, levulinic acid and 1,6-hexanediol[53].

FDCA has been proven being a good alternative of terephthalic acid[54] and polymerized with ethylene glycol led to 100% bio-based polyester, which will be in the near future commercialized[54,55].

Another important class of molecules, organic carbonates (OCs), can be originated from biomass[56], but also from microbial metabolites of fungi and bacteria[57]. OCs have found a wide range of applications both as chemical intermediates, due to their non-toxicity and biodegradability[58,59], and for the synthesis of polymers[58,60]. In this latter field, production of phosgene-free polycarbonates is reported with the advantages of avoiding the use of hazardous chemicals as phosgene[61–64]

2 POLYESTERS

Polyesters are a class of polymers characterized by the presence of ester functional groups along the chain (**Figure 2.1**). They are generally synthetized via polycondensation between diacids (or diesters) and diols, as well as hydroxy acids, producing water (or alcohol in case of diesters) as side product. It is a class of extremely versatile materials characterized by interesting properties.

R_x= Aliphatic
  Aromatic

R_y= Aliphatic
  Aromatic
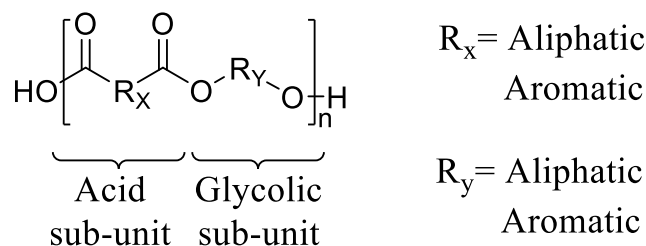
Figure 2.1: *General structure for polyesters.*

Nowadays, polyesters are the most promising candidates as bioplastics. The raw materials for their production are easy to access, indeed, a large variety of diacids/diesters and diols can be used. In addition, the monomers can be treated in a simple synthetic route and the final polymeric products are stable and can be processed even in complex shapes. Moreover, chemical and/or physical modifications of both bulk and surface are possible, as well as immobilization of biomolecules inside the materials. Despite some issues, as the release of low molecular weight substances - monomers, catalysts, additives- in the environment and easy absorption of water and biomolecules from the surroundings (even in applications where it is not required), the final balance on polyesters is positive, even because, as already mentioned, it is possible to *ad hoc* tune their final properties depending on the application envisioned. For these reasons, polyesters are widely used in large-scale productions (packaging, as insulating films and tapes), as well as for more specific applications (as electronic components, biomedical devices, technical clothing).

2.1 Aliphatic polyesters

Aliphatic polyesters are polymers, which contain the ester functional group along a non-aromatic main chain (**Figure 2.1**). In February 1928, a research group in organic chemistry was set up by Du Pont. Wallace H. Carothers joined the group with the purpose to study the nature of polymers, by using simple synthetic method: building up a long chain adding molecules by defined reactions in such a way that

there could be no doubt about the structure. Therefore, he followed and studied the proceeding of the polymerization process[65]. The first studies were performed reacting aliphatic alcohols and aliphatic carboxylic acids, a really well-known process, with very few side-reactions. Carothers and his research group synthesized many polyesters, nearly all of them aliphatic. These investigations led to determine the "Carothers equation", where the degree of polymerization, X_n, was correlated to the monomer conversion. In 1931, the first basic patent of Carothers was accepted[66,67]. The scientific community has been deeply influenced by this work, because it proves that polymers are macromolecules, not assemblies of small molecules in a special state of association. Then, the focus of the research group turned to set up the synthesis of polyamides, previously briefly explored by Carothers and Hill, without any success. These researches have opened the production of nylon fibers, nylon 9, nylon 5,10 and then, early in 1935 with Berchet, of nylon 6,6[65]. Further systematic studies to understand the formation and the properties of aliphatic polycondensated polyesters have been carried out. An important contribute was given by Paul Flory with his studies on the kinetics of polyesterification and polyester molar mass distribution.

The versatility and suitability of monomers make aliphatic polyesters one of the most important classes of synthetic polymers: packaging, automotive, pharmaceutics, are just some of the fields in which these materials are intensively used. There can be no doubt that polyesters will continue to be one of the most important classes of polymers, also considering their possible nature of biodegradable and biocompatible materials. Moreover, it is possible to replace the oil-based reagents with bio-based monomers, i.e. obtained by fermentation of vegetable oils or sugars, including dicarboxylic acids, like adipic, succinic, sebacic, azelaic acid, and fatty acids, or diols like 1,3-propanediol, 1,4-butanediol, 1,3-butanediol, 1,10-decanediol[68–73] or polyesters themselves. Moreover, polyesters are found in nature inside bacteria and also in high plants[74,75]. In the light of these features, they are applied in high adding value sectors, as medical and biomedical engineering, including drug delivery systems and functional materials in tissue engineering, but also as a single use material for degradable packaging.

The class of biodegradable aliphatic polyesters is including both natural materials and polymers obtained by chemical synthesis[76].

2.1.1 Polyhydroxyalkanoates (PHAs)

Polyhydroxyalkanoates (PHAs) (**Figure 2.2**) are polyesters synthetized by bacteria. The most common types are poly(3-hydroxybutyrate) (PHB), 3-hydroxyvalerate (PHV) and their copolymers[74].
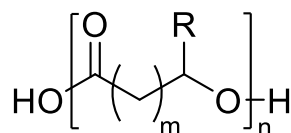
Figure 2.2*: General structure of PHAs.*

PHB has firstly isolated in 1925, by Lemoigne[77,78], who discovered that bacteria synthetize the polymer as an energy storage. The extracted material boasts properties comparable with polyethylene (PE) and polypropylene (PP) ones. Several natural bacteria - as Gram-positive and Gram-negative, aerobic and photosynthetic - result to be able to produce PHB, with a feedstock of carbohydrate origin but also with other organic chemicals such as methanol[79]. The main problems of PHB are its brittleness and stiffness and very narrow workability window. A good way to increase its flexibility, is through copolymerization with 3-hydroxyvalerate. Despite several companies as Meredian, Tianan Biologic Materials, PolyForm Canada are producing PHAs, the real applications are limited mainly due to the large amount of biomass waste produced (5 kg of raw material to obtain only 1 kg polymer). This aspect, together with the high cost of the process, the difficult extraction and purification procedures, and the small production volumes, are retarding the success of polyhydroxyalkanoates in the market[80].

2.1.2 Poly(butylene succinate) (PBS)

Poly(butylene succinate) (PBS) (**Figure 2.3**) represents one of the most important biobased, biodegradable and biocompatible synthetic polyester known nowadays.
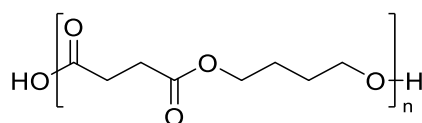
Figure 2.3*: Chemical structure of PBS.*

In the late of 1800s, Agostinho Vicente Lourenço[81] synthetized for the first time PBS. Then Carothers, during his studies regarding polyester, synthesized the polymer with the highest molecular weight among those prepared up to then. Despite that, the final product did not show features good enough to enter the market[82]. The real Golden Age for this material started in 1990s with the introduction of new catalysts permitting to obtain high molecular weight PBS, together with the growing interest in bio-based polymers. The polymer is semicrystalline, with quite high melting temperature and a glass transition below room temperature.

In 1993, Showa Denko[83] entered the market with the first bio-based PBS (Bionolle), with a molecular weight of 40'000-100'000g/mol. Then, PBS found commercial applications in different sectors as food packaging, agriculture, fishery, forestry, construction and other industrial fields[84]. Moreover, thanks to its biocompatibility, PBS has been applied in high added value market as medical and biomedical field in form of implants, scaffolds and devices for tissue engineering and drug delivery systems.

The reagents, BD and SA, can be obtained from conventional oil-based chemistry or produced from biomasses. Regarding SA, the conventional process is starting utilizing the C4-fraction of naphtha, as n-butane or butadiene, oxidized to maleic anhydride. Then, the product is hydrogenated to produce succinic anhydride. An additional hydrogenation led to the final product, SA[22,73,85]. The bio-based monomer is, instead, obtained via fermentation of glucose sources. Suitable yeasts and bacteria metabolize many C5 and C6 sugars as well as their derivatives, like lignocellulose. Despite fermentation processes require large volumes, have low yields and long reaction times, the process has been optimized including the purification step, becoming more economically sustainable. Indeed, SA has been included by US department of energy in the first 12 added-value bio-based chemicals[51]; in 2018, its market reached USD 131.7 million and is predicted to increase up to USD 183 million by 2023[86]. The giants of the chemical market have already started its production in large scale: BioAmber has opened two plants (France 2010 and North America 2013) where the process is feed by sugar beet and wheat, and new plants are going to be opened in Thailand, North America and Brazil[87]. Different substrate are used, for example Myriant[88] starts from lignocellulose, Revedia employs starch, through a fermentation process (Biosuccinium). Moreover, a joint venture between Corbion and BASF set up a process by using micro-organism Basfia succiniproducens, with glycerol as substrate (Succinity).

Also 1,4-butanediol can be easily obtained starting from oil-based reagents or from renewable sources. A direct catalytic hydrogenation of SA leads to bio-based BD. BioAmber has a working plant where bio-BD and bio-THF are produced; Novamont, in a joint venture with Genomatica, has also set up a fermentation process to obtain the glycol[89–91].

PBS has conquered the market thanks to its properties. Beside its thermoplastic and semi-crystalline nature (crystallinity degree around 35-45%), PBS displays one of the highest melting temperature among the family of the poly(alkylene dicarboxylate)s, with a value between 110-130°C[92]. The glass transition is below room temperature, usually between -34 and -15°C[93], while in the range 70 and 95°C melt crystallization is recorded. Due to its crystallinity, high molecular weight PBS exhibits brittle behavior

with Young's modulus (E) of about 300-500 MPa[94,95], and limited elongation at break[96]. This behavior can be mitigated through different strategies, such as copolymerization, polymer blending, ect[97]. Good results are obtained by incorporation of urethane bonds through the use of isocyanates[14], or blending PBS with polylactic acid (PLA) or starch,[98,99] obtaining mechanical responses comparable to those of polyolefins[100]. Moreover, PBS can be considered completely compostable, according to the standard tests EN13432, US, BPI and OK-Compost, because susceptible to microbiological attacks and even abiotic degradation.

2.1.3 Poly(alkylene 1,4-cyclohexanedicarboxylate)s

Poly(alkylene 1,4-cyclohexanedicarboxylate)s, (**Figure 2.4 A**), belonging to the class of aliphatic polyesters, are characterized by the presence of a cyclohexane ring along the repeating unit. This architecture affects the final properties, increasing the rigidity of the chains, together with the thermal stability that overtakes the values of aromatic counterparts[101–103]. Nonetheless, the compostability is preserved[104] and considering the good resistance to heat, light, and humidity, poly(alkylene 1,4-cyclohexanedicarboxylate)s result suitable for packaging applications. In 1980s, the Eastman Chemical Company started the investigation of this class of polymers, due to their high tensile strength and high impact properties.

The diacid required for the synthesis, 1,4-cyclohexane dicarboxylic acid, is currently produced as oil-based derivate but the bio-based process, employing bio-based terephthalic acid obtained from limonene and other terpenes[50], is in progress.

For 1,4-cyclohexane dicarboxylic acid, two isomers are possible: *trans* and *cis* (**Figure 2.4 B**). The different configuration has a considerable impact on the final properties of the material: in the *trans* isomer chain packing is favored, more effective and the capacity of the polymer to crystallize is higher[101,102]. Consequently, by decreasing the amount of *trans* isomer these properties are reduced. Only polymers constituted by at least 70% of *trans* 1,4-cyclohexane dicarboxylic units are able to crystallize. Differently, polymers containing amounts of cis-isomer around 50-80% are completely amorphous, becoming unable to organize themselves in an ordered state[91]. Recent studies conducted on poly(alkylene 1,4-cyclohexanedicarboxylate)-based systems have highlighted the good barrier properties to different gases at different temperature and percentage of humidity, suggesting a possible application in

packaging[105–107]. Despite that, nowadays there are no commercial grades available of these class of polyesters.

A)

B)

Cis　　　　　　**Trans**
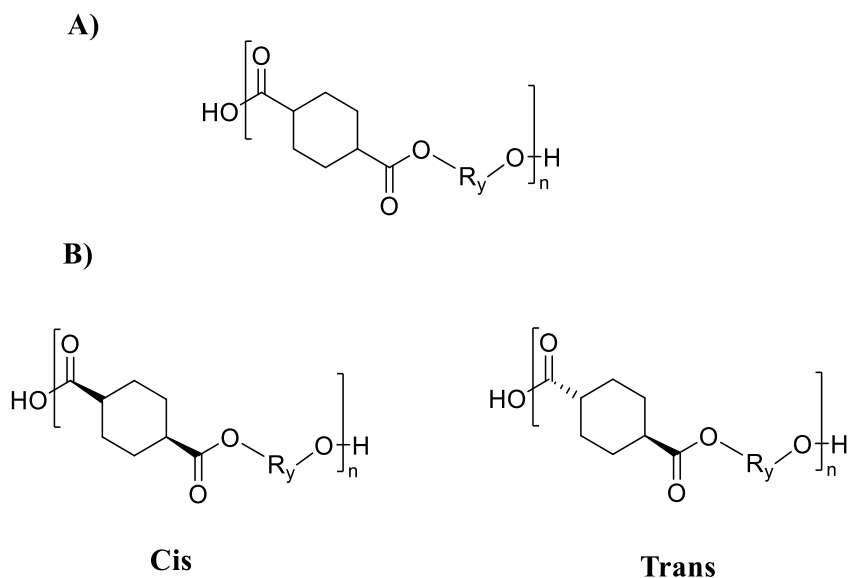
*Figure 2.4:A) General structure of poly(alkylene 1,4-cyclohexanedicarboxylate)s; **B)** cis and trans poly(alkylene 1,4-cyclohexanedicarboxylate) isomers.*

2.2 Aromatic polyesters

Aromatic polyesters are characterized by the presence of aromatic moieties along the chain of the macromolecules, as reported in **Figure 2.1**. In the 1940s, in UK a group of researchers of Calico Printers Association has commissioned the synthesis of a polyester starting from ethylene glycol and terephthalic acid, poly(ethylene terephthalate) (PET)**.** One year later, the first patent was filed[108]. The discovery attracted the attention of the British Ministry of Supply, who arranged for further experimental work the government's Chemical Research Laboratory at Teddington, where the production of PET was scaled up in autoclave. As it is reported, almost at the same time Schlack and Whinfield together with Dickson, set up the process to produce polyester fibers. Then, Schlack focused his attention on the synthesis of PBT, made by terephthalic acid and 1,4-butanediol[109]. In 1942 the patent has been filed[109,110]. The discovery of this class of polymers was only at the beginning: thank to their chemical structure directly affecting the mechanical behavior, improving hardness and rigidity, and favoring the heat stability, several other polyesters have been explored. Nowadays, aromatic polyesters are widely used, mainly in form of films and fibers or bottles, and the production of PET alone covers 8% of the global market of plastic[2]. The

main producers of these polymers are SABIC, Du Pont, Invista, BASF and Celanese, all of them selling several grades, which differ for the additives and the kind of reinforcement.

Terephthalic acid (TPA)   Isophthalic acid (IA)   2,5-Furandicarboxylic acid (FDCA)
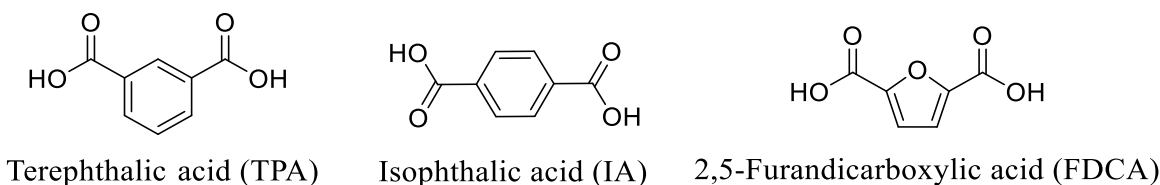
Figure 2.5: *Chemical structure of terephthalic acid, isophthalic acid and 2,5-furandicarboxylic acid.*

2.2.1 Terephthalic polyesters

As previously reported, terephthalic polyesters are one of the main class of polymers produced in 2018[111]. The family is characterized by the presence of terephthalic acid (TPA), represented in **Figure 2.5**, which in presence of glycolic subunit of adequate length, is capable to crystallize. The ease tendency of terephthalic polyesters to form packed systems is connect to their intrinsically symmetrical structure and the possibility to have interchain interactions help the segmental disposition. The crystalline structure formed confers good mechanical properties and resistance to solvents to the final polymer.

Regarding the production, besides the oil-based pathway, several recent papers and patents report the possibility to obtain TPA from bio-based source. For example monoterpenes as limonene[50,112] can lead directly to TPA, while p-cymene[113–117] as well as a-pinene[118–122], eucalyptolo[122,123] can convert in p-cymene, then oxidized to TPA[50,112,124–126]. Also muconic acid[127] and isobutylene (obtained from isobutanol[128]) are employed for the synthesis of TPA. Moreover , also fermentation processes are set up and the literature is rich of patents[129–131]. Despite that, nowadays no commercial processes are available for the production of bio-based TPA. Several companies are developing methods at laboratory scale, and with pilot facilities already available for the processes, as Anellotech, Gevo and Virent[132].

Poly(ethylene terephthalate) (PET)   Poly(propylene terephthalate) (PPT)   Poly(butylene terephthalate) (PBT)
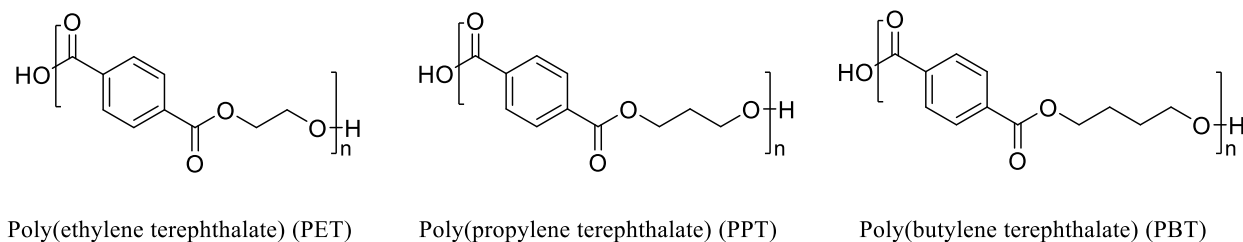
Figure 2.6: *Chemical structure of PET, PPT and PBT.*

15

2.2.1.1 Poly(ethylene terephthalate) (PET)

The most important example of terephthalic polyester is poly(ethylene terephthalate) (PET) (**Figure 2.6**): the process of synthesis requires a two-step melt polycondensation between terephthalic acid (TPA) and ethylene glycol (EG), catalyzed by Pb and Zn acetates or titanium alkoxides[133]. PET is a semicrystalline material, colorless and light. The just mentioned characteristics together with the stability in contact with food and water, make PET one of the best options in packaging sector[134]. Bottles are probably the most well-known application, but PET is widely used also to produce fibers for clothing, containers, elements for electronics, and in crystalline form is also applied as thermoplastic material for automotive, in the electric and electronic fields. In order to modify its properties, it can be combined with other materials as carbon nanotubes and glass, to cite a few of the several choices.

2.2.1.2 Poly(propylene terephthalate) (PPT)

Poly(propylene terephthalate) (PPT) (**Figure 2.6**), as well as PET, is synthetized via two-step melt polycondensation between TPA and propylene glycol (PG), together with titanium alkoxides as catalysts. PPT is mainly applied as fiber, thanks its better mechanical behavior with respect to the other polymer of the family. Besides textile application, PPT is used in the production of ropes for musical instruments, umbrellas, food packaging and artificial leather.

2.2.1.3 Poly(butylene terephthalate) (PBT)

Poly(butylene terephthalate) (PBT) (**Figure 2.6**) is obtained by polycondensation of TPA and 1,4-butanediol (BD) catalyzed by titanium alkoxides. PBT boasts good hardness and shine surface together with high resistance to chemical agents and heat. For these features, this polymer has found space of application in high added-value market as electrical, electronic and automotive parts.

2.2.2 Isophthalic polyesters

Isophthalic acid (IA), reported in **Figure 2.5**, is the isomer of phthalic acid containing the two carboxylic groups in meta position. Isophthalic acid can be produced from fossil resources, but several examples of processes based on fermentation and renewable resources are also reported[23,25,70]. These latter methods comprise a cycloaddition reaction of bio-isoprene and bio-acrylic acid to produce bio-3-methyl-3-cyclohexene-1-carboxylic. An aromatization reaction produces bio-meta-toluic acid, then an oxidation leads to the final bio-isophthalic acid. The isophthalic-based polyesters are characterized by lower rate of crystallization and melting temperature with respect to their terephthalic counterparts, ascribed to the lower symmetry of the molecule containing the meta isomer (IA) compared to para one (TPA). However,

16

the isophthalic derivates can be crystallized by annealing. In this condition, the colorless soft resins gradually become hard and opaque, suggesting the proceeding of crystallization[135].

Poly(ethylene isophthalate) (PEI)   Poly(propylene isophthalate) (PPI)   Poly(butylene isophthalate) (PBI)
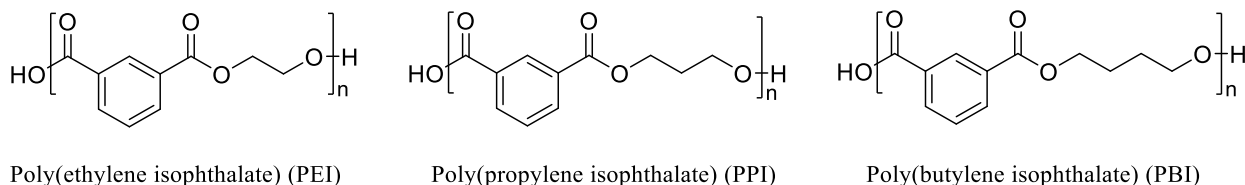
Figure 2.7: *Chemical structure of PEI, PPI and PBI.*

2.2.2.1   Poly(ethylene isophthalate) (PEI)

PEI (**Figure 2.7**) is synthetized by two step polycondensation between isophthalic acid (IA) and ethylene glycol (EG). The final material has some difficult to crystallize with respect to PET, due to its asymmetrical molecular structure. Therefore, the final material has Young´s modulus and stress at break sensibly lower than PET. Regarding barrier properties, PEI boasts lower permeability to CO_2 compared to PET. This behavior is due to the hindering of phenyl ring flipping in the meta isomer compared to the para one, that limits the diffusion of gasses through the polymer film[136,137].

2.2.2.2   Poly(propylene isophthalate) (PPI)

The synthesis proceeds via two step polycondensation of IA and 1,3-propanediol catalyzed by Ti(OBu)$_4$, obtaining a polymer with the chemical structure reported in **Figure 2.7**. The crystallization is still hampered by the presence of isophthalate ring, but the longer glycol subunit confers higher crystallinity degree to PPI. The thermal stabilities of PPI and PPT are pretty similar[138].

2.2.2.3   Poly(butylene isophtalate) (PBI)

Two step polycondensation catalyzed by Ti(OBu)$_4$ of IA and 1,4-butanediol permits to obtain poly(butylene isophthalate) (PBI). The chemical structure is reported in **Figure 2.7**. The as synthetized material is amorphous, but similarly to other family members, can slowly crystallize under specific conditions. Its counterpart, PBT, crystallizes faster and to higher extent. The mechanical behavior of the two polymers reflects the microstructure: stress-strain test shows lower Young´s modulus and higher elongation at break for PBI with respect to PBT[135,139].

2.2.3   2,5-furandicarboxylate-based polyesters

In the last few years, several researches have been focused on the substitution of the benzene ring with another aromatic moiety: 2,5-furan ring (**Figure 2.5**). Of particular interest, the diacid sub-unit containing

such moiety, i.e the 2,5-furandicarboxylic acid (FDCA). FDCA has been combined through polycondensation, with good results[140], with many different glycols[141] like ethylene glycol[142–144], 1,3-propanediol[142] and 1,4-butanediol[69,71,145–147]. The great interest on FDCA is mainly due to its bio-based nature. The diacid can be obtained from renewable sources, as cellulose or hemicellulose. The process requires a series of steps, including bioconversion, dehydration and oxidation, where hexose and 5-hydroxymetifurfural are important intermediates[148]. Specifically, 5-hydroxymethylfurfural can be easily obtained dehydrating glucose or fructose[149].

| Poly(ethylene furanoate) (PEF) | Poly(propylene furanoate) (PPF) | Poly(butylene furanoate) (PBF) |

| Poly(pentamethylene furanoate) (PPeF) | Poly(hexamethylene furanoate furanoate) (PHF) |
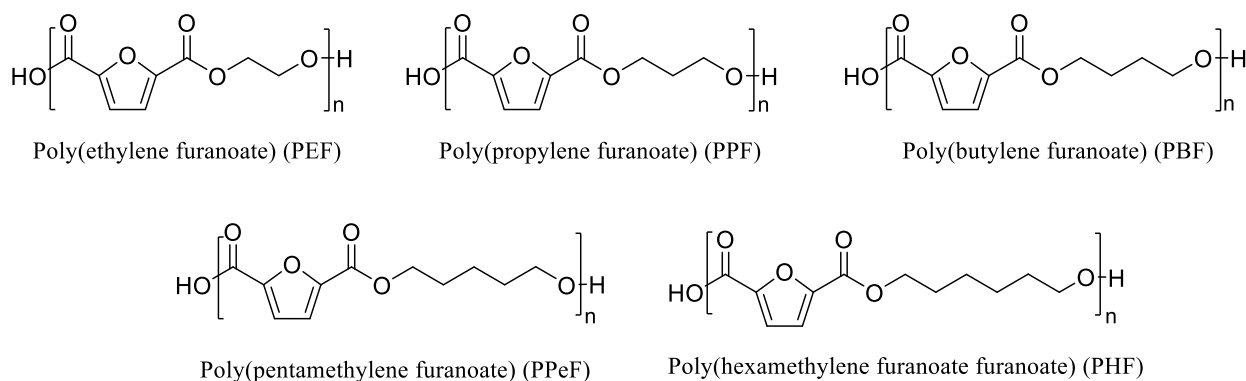
Figure 2.8: Chemical structure of PEF, PPF, PBF, PPeF, PHF.

2.2.3.1   Poly(ethylene furanoate) (PEF)

Poly(ethylene furanoate) (PEF), (**Figure 2.8**), is the most important FDCA-based polymer. It is obtained by two-step melt polycondensation of FDCA (or its dimethyl ester) and ethylene glycol (EG), catalyzed by Ti(OBu)$_4$ and Ti(OiPr)$_4$[142–144,150]. Authors report the use of dimethyl ester derivate of FDCA, permits to avoid darkening of the final material and increase the molecular weight[151]. Besides that, solid state synthesis has also been explored to further increase the molecular weight, leading to final polymer of 80 KDa[151]. High molecular weight PEF boasts surprising properties, similar and even better than PET[152]. In PEF samples the presence of furan ring helps the stacking of the chains[55]. The final structure is similar to PET, indeed the thermal transition and the mechanical performance are similar too. Regarding the barrier properties, PEF is hampering the diffusion of gasses, thanks to the intrinsic stacking of the chains, better organized than PET. For this reason, Avantium, cooperating with Coca-Cola and other companies, is scaling up a new process, according to the patented "YXY" technology, to synthesize PEF by reacting a silanic dicarboxylic acid, obtained from biomasses such as sugar cane, agricultural residues or cereals, and bio-ethylene glycol. In this way, the replacement of PET bottles sounds possible: indeed, the first

100% bio-PEF bottle (PlantBottle™), completely synthetized with natural carbohydrates, has been already presented by The Coca-Cola Company during Milan EXPO 2015.

2.2.3.2 Poly(propylene furanoate) (PPF)

PPF (**Figure 2.8**) can be synthetized by two step polycondensation process starting from FDCA (or its dimethyl ester) and 1,3-propanediol (PD) in presence of $Ti(OBu)_4$ and $Ti(OiPr)_4$, similarly to PEF. As reported for PEF, solid state reaction permits to reach higher molecular weight. PPF is characterized by higher stiffness than the terephthalic derivate, PPT[141]. Moreover, also for PPF outstanding permeability properties, even higher than PEF ones, are reported[153]. A deep investigation has been conducted by Professor Lotti[154–156] and coworkers, where this experimental work took place.

2.2.3.3 Poly(butylene furanoate) (PBF)

Poly(butylene furanoate) PBF, reported in **Figure 2.8**, also can be obtained from FDCA or dimethyl ester of FDCA and BD, through two step polycondensation catalyzed by $Ti(OBu)_4$ and titanium(IV) isopropoxide. The reaction has been optimized in terms of conditions and catalysts to maximize the final molecular weight, obtaining value around 46000 Da[71,146,148,150,157,158]. High molecular weight PBF presents similar thermal and mechanical properties with respect to PBT. Despite that, permeability values overtakes not only PBT but even Nylon 6 and PET, making PBF suitable material for packaging application[154].

2.2.3.4 Poly(pentamethylene furanoate) (PPeF)

Poly(pentamenthylene furanoate) (PPeF), **Figure 2.8**, has been successfully synthetized employing the dimethyl ester derivate of FDCA and 1,5-pentandiol, through one pot polycondensation, catalyzed by TBT and TTIP. Firstly, Bikiaris et al. prepare PPeF and investigate its thermal properties[159]; then our group optimize the process of synthesis and deeply characterized the material from the chemical, thermal and mechanical point of view. Permeability tests conducted show outstanding barrier properties, explained by the presence of partially ordered layers of furanic rings (intermolecular C−H···O bonds)[160].

2.2.3.5 Poly(hexamethylene furanoate) (PHF)

Poly(hexametylene furanoate) (PHF) synthesis has been carried out in bulk, via two step polycondensation between dimethyl furan-2,5-dicarboxylate (DMF) and 1,6-hexandiol catalyzed by TTIP and TBT. The structure is reported in **Figure 2.8**. Detailed investigation of this furan derivate has been conducted by our group, that reported a good thermal stability and mechanical response in line with

the characteristics require for flexible packaging application. Moreover, the permeability tests show decent barrier properties together with high perm-selectively between CO_2 and O_2, opening the scenario for smart packaging application[154].

2.3 Synthesis

Polyesters are generally synthetized by polycondensation involving difunctional monomers as hydroxy acids, for the so-called self-condensation, or two different monomers bearing diacid/diester/diacid chloride groups and hydroxylic ones, respectively. Besides that, lactones and lactide can undergo ring-opening polymerization (ROP)[161]. Polycondensation and ROP are widely used for the industrial production of polyesters. Despite that, both pathways present advantages and drawbacks that have to be considered during the scaling up of the process. Polycondensation process is flexible and can be used for various diols and diacids, but normally needs to be conducted at high temperature for long time and generates by-reaction products, which need to be removed in order to favor the increasing of the molecular weight of the final product. Moreover, the resulting polymer polydispersity index (PDI) cannot be completely controlled. Differently, in case of ring-opening polymerization, a narrow range of monomers can be involved, but, by setting the proper conditions, it is possible to reach high molecular weight under milder condition compared to polycondensation and the polymers are characterized by a lower polydispersity[162].

In the last few years, an increasing interest is growing around enzymatic-catalyzed polymerization. The main advantage is the possibility to obtain regio- and stereospecific products with controlled molecular weight, under very mild conditions[76,163–165]. For example, *Candida antarctica* lipase B is successfully employed as a biocatalyst to obtain high molecular weight derivate of poly(butylene succinate) via two step polycondensation process[166], despite the possibility to lead depolymerization processes. Lastly, worthy of note are the research conducted by Katia Loos and co-worker that successfully employed enzymes to obtain polymers of different nature -as polyester, polyurethanes, polyamide- and more complex systems as copolymers from renewable sources[15,167–171].

2.3.1 Polycondensation

Polycondensation is used to synthetize polymers through the condensation of organic small molecules, as by-product. The synthesis usually starts from monomers as diacids/diesters and glycols, which react with each other, producing water/alcohol. A bishydoxyl terminated dimers is obtained. Then a second

step is conducted, where the condensation of bishydoxyl terminated dimers is observed. The increasing of temperatures and decreasing of pressure favor the distillation of the sub-product as glycols. Several commercial aliphatic polyesters, as PBS, PBA and PLA, and aromatic polyesters, as PET are synthetized by melt polycondensation[162].

The main drawback of this synthetic process is low molecular weight. All the reactions are reversible and reach an equilibrium state. To obtain high molecular weight values, the equilibrium constant (K_c) needs to be high, guaranteeing good average value of degree of polymerization, DP_n[172].

$$DPn = Kc_{0.5} + 1 \qquad\qquad Eqn.\ 1$$

In most cases, K_c is below 10, implying a value of DP_n of about 4. The degree of conversion (p)[172] of reactive groups at the equilibrium condition is 0.76, as predicted by *Eqn 2*.

$$DPn = \frac{1}{1-p} \qquad\qquad Eqn.\ 2$$

In order to obtain high molecular weight values, i.e. $DP_n \geq 100$, the final conversion needs to be around 0.99 and the corresponding $K_c \geq 104$. This result can be obtained by removing the low molar mass by-products of esterification. The removal of side product results easier starting from acid chlorides (Schotten-Baumann reaction), acid anhydrides or activated carboxylic acids.

Eqn.3 which is derived from *Eqn.1* by assuming $K_c \gg 1$, provides a dependence of the degree of polymerization on the extent of removal of the by-products (q):

$$DPn = \frac{Kc}{q} * 0.5 \qquad\qquad Eqn.\ 3$$

where $q = \frac{N_e}{N_0}$, i.e., the ratio of the concentration of the by-products at a given equilibrium to its hypothetical concentration resulting from reactive groups conversion degree related to the required DP_n.

A good value of DP_n, for instance 102, can be reached with K_c of 104, i.e. q should be lower than 10^{-3}, that means only 0.1% of by-products can remain in the system. With the increasing of the degree of conversion, system viscosity increases making the removal of by-products more difficult.

Another important factor influencing the final polymer molecular weight, is the stoichiometry ratio between the starting reagents. The dependence of the average degree of polymerization of the polyester

formed in heteropolycondensation from the stoichiometric imbalance parameter, r, is given by the following equation:

$$DPn = \frac{1+r}{1+r-2p}$$
Eqn. 4

where $r = \frac{NOH}{NCOOH}$ for NOH < NCOOH *or* $r = \frac{NCOOH}{NOH}$ for NOH > NCOOH

NOH and NCOOH are the concentrations of hydroxyl and carboxylic groups, respectively.

Considering a value of p = 0.99, DP_n reaches a value of 100. This situation corresponds to a value of r = 1. If r = 0.99, DP_n decreases to the value of 67.

If reagents are feed in 1:1 ratio, unbalancing of chemicals is highly probable, due to the higher volatility or more responsive towards side reactions of one of them.

The theoretical kinetic equations rarely represent what is really happening during polycondensation. Even if the fundamental assumptions of equal reactivity of functional groups are respected, different viscosity or dielectric constant can have a huge impact on the course of the reactions. Indeed, at high viscosities the "diffusion in" is slowed down, compensated by equally slowing down of the "diffusion out"[173].

In 1936, Flory developed a theoretical equation to describe the molar mass distribution (or polymerization degree) of linear polyesters obtained by polycondensation. The number (n_i) and weight fractions (w_i) of macromolecules having a degree of polymerization equal to i at a given degree of conversion, p, is:

$$n_i = p^{i-1} * (1 - p)$$
Eqn. 5

$$n_i = i * p^{i-1} * (1 - p)^2$$
Eqn. 6

The number average polymerization degree, DP_n, and weight average polymerization degree, DP_w, are defined respectively by the *Eqn.7* and *Eqn.8*

$$DPn = \frac{1}{1-p}$$
Eqn. 7

$$DPw = \frac{1+p}{1-p}$$
Eqn. 8

such as, the polydispersity index:

$$\frac{DPw}{DPn} = 1 + p = 2 - DPn^{-1} \qquad\qquad\qquad Eqn.\ 9$$

$\frac{DPw}{DPn}$ is assuming a different value in case of polyesters prepared by polycondensation or by ROP. In this latter case, as the kinetic control of the entire polymerization process is higher, the molar mass distribution is usually narrower and the ratio between DP_w and DP_n around 1. In case of polycondensation, the value of $\frac{DPw}{DPn}$ is normally around 2. This is due to the formation of a fraction of macrocyclic products. However, the phenomenon of cyclization can be considered as a side reaction of secondary importance because critical concentrations of macrocycles (in terms of repeating units) are well below 1 g/l[174].

Tetrabutyl titanate(IV) (TBT)   Titanium(IV) isopropoxide (TTIP)
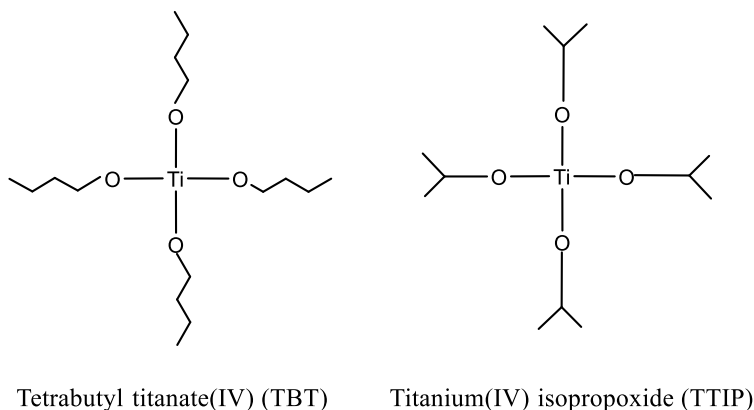
Figure 2.9: Chemical structure of TBT and TTIP.

Another important element to consider, is the role of the catalysts. These compounds must be active enough to interact with the monomers and have to avoid decomposition or degradation of the macromolecules formed. One of the main class of catalyst used in the synthesis of polyesters are organometallic compounds. Tetrabutyl titanate(IV) (TBT) and titanium(IV) isopropoxide (TTIP) (**Figure 2.9**) are clear example of this class of catalyst, characterized by the presence of an atom of metal coordinated to organic moieties. The general mechanism of action, reported here below in **Scheme 1**, is based on the coordination of the lone pair of the carboxylic oxygen with the unoccupied orbitals of the metal, then a sequence of insertion and exchanges favor the growing of the chain.

As regard catalytic systems, different studies have been carried out to find catalyst active at low temperature. Polycondensation process conducted with mild condition could virtually eliminate thermal

degradation, avoiding side reactions. Also, milder polymerization conditions make possible the synthesis of polymers containing thermally unstable moieties. Good results have been obtained with silicon-phosphorus active for polycondensation in the range 0°-150°C. Other experiments employed aliphatic dicarboxylic acids (ADAs) polymerized with 1,4-butanediol or 1,6-hexanediol at 80 - 100 °C, in presence of triflates of sodium, magnesium, aluminum, zinc, tin(II), scandium, and hafnium bismuth triflate. The best results have been obtained conducting the reaction with Bi(OTf)$_3$, as catalyst[175].
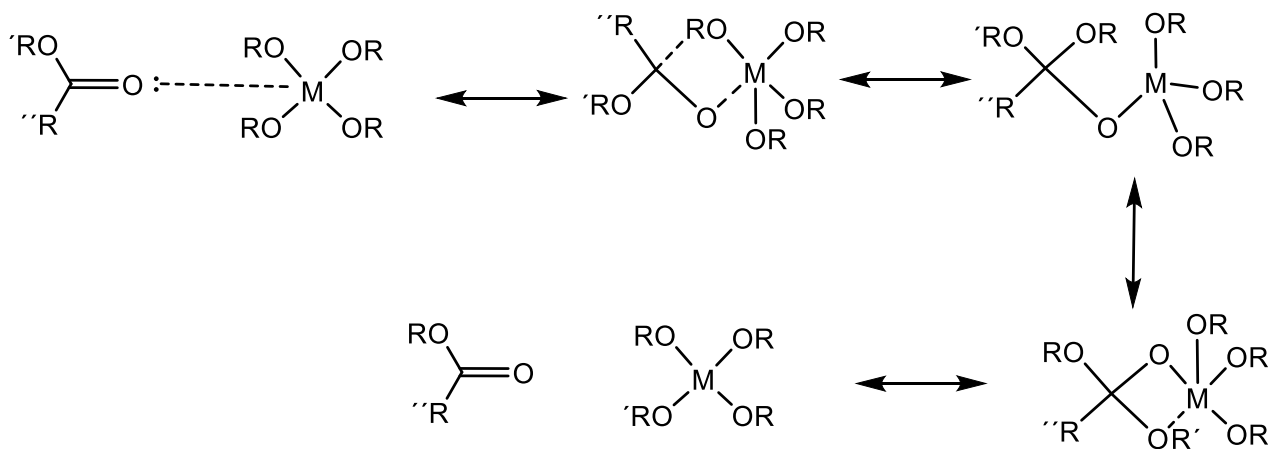
Scheme 1: Schematic representation of catalytic mechanism.

Further investigations have been focused on the impact of the catalyst on the color of the resulting polyesters. The using of combined systems as titanyl oxalate catalyst with catalyst enhancer, metallic oxalate, and a metallic cocatalyst such as antimony oxide or antimony triacetate lead to fast reactions with good final color for the resulting polyester and a substantially reduction of the amount of catalysts needed.

In terms of molecular weight, the effect of catalysts has also deeply studied: for example, regarding the synthesis of PEF, Terzopoulou et al. find that TTIP, lead to polymers with 5500 Da at the end of melt polycondensation. PEF molecular weight is even lower if TBT and DBTO, dibutyltin oxide, are used[176]. The effect of TiBO, THE, tin(II) 2-ethylhexanoate, SnOBu, GeO$_2$, and Sb(Ac)$_3$ has been also investigated[177]. SnOBu is found to be the most active in term of final molecular weight. In case of PBS, Jacquel et al. report low M_n and low yield employing TEH, ascribed to the generation of cyclic products[178]. Other studies compared the two active catalysts as titanium(IV) isopropoxide and butyltin(IV) tris(octoate) and found that with certain amount of titanium the M_n do not increase while PDI increased[179].

Besides the catalysis with organometallic compounds, alternative synthesis for the preparation of high molecular weight aliphatic polyesters are performed in presence of inorganic acid. Good examples are the results reported by Sokolsky-Papkov et al. that catalyze the reaction of adipic acid or sebacic acid with aliphatic diols with H_3PO_4 or H_2SO_4, as catalyst, combined with mild temperatures and low vacuum[180].

2.3.2 Ring-opening polymerization (ROP)

Polyesters have historically first synthesized via step-growth polycondensation, the ring-opening polymerization (ROP) is an alternative synthetic pathway that leads to high molecular weight aliphatic polyesters with low polydispersity under mild condition[181]. The reaction is conducted in the presence of cyclic monomers, lactones and lactides, with different ring-size and functional groups. The conversion of the monomers to linear macromolecules must be allowed kinetically and thermodynamically. As such, the equilibrium needs to shift to the formation of polymer in operable reaction time.

ROP can be written as follow.
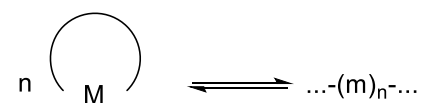
Where M represents the monomer, and m is the polymer repeating unit derived from M. Reached the equilibrium, in most cyclic reagents, high concentration of unreacted monomer can be present. This is due to the reversibility of propagation step (high depolymerization constant, K_d, low polymerization constant, K_p). The equilibrium monomer concentration $[M]_{eq}$ is used to define the monomer thermodynamic tendency to polymerize. First Dyton and Ivin in 1948, then Tobolsky and Eisenberg developed the corresponding thermodynamic laws[182,183].

At the beginning, is fundamental that the monomer M is reacting with initiator agents in order to give an active species, m*, able to react faster with M without being involved in side reaction, as monomer transfer (K_t) or termination (K_{tr})[184].
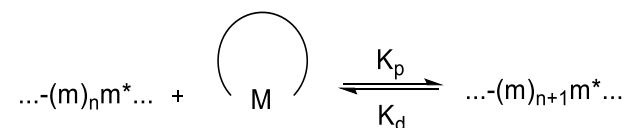
In order to obtain "living process", the transfer constant, K_t, and termination constant, K_{tr}, need to be equal to 0. In this conditions, it is possible to control, and predict by the monomer-to-initiator molar ratio, the molecular weight with a final tight distribution[184,185].

$$I \quad + \quad M \xrightarrow{K_i} \quad I\text{-}m^*$$

$$\ldots\text{-}(m)_n m^* \quad + \quad M \underset{K_d}{\overset{K_p}{\rightleftharpoons}} \quad \ldots\text{-}(m)_{n+1} m^*$$

$$\ldots\text{-}(m)_n m^* \quad + \quad X \xrightarrow{K_t} \quad \ldots\text{-}(m)_n m\text{-}X$$

$$\ldots\text{-}(m)_n m^* \quad + \quad M \xrightarrow{K_{tr}} \quad \ldots\text{-}(m)_n m \quad + \quad m^*$$
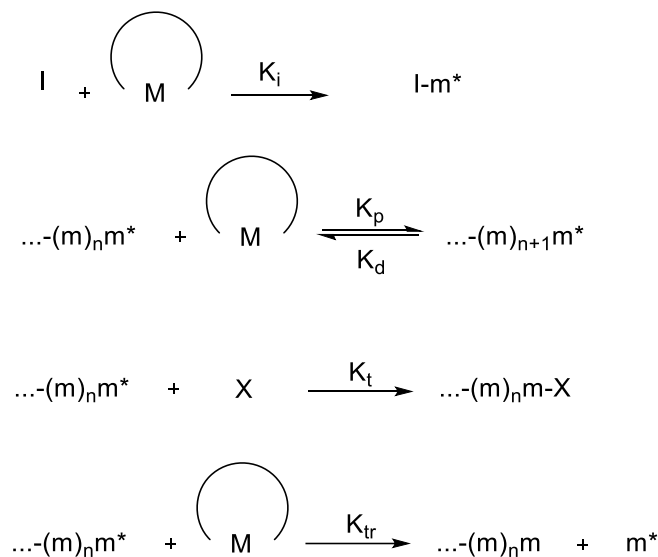
The interest around lactones has increased in the last 30 years, when heterocycle systems have been identified as key structural constituent of natural products[186]. Despite that, the studies around this molecules starts in 1883[187]. Nowadays, the synthetic routes involve the cyclization of β-halocarboxylate salts and the diazotation of β-amino acids[188,189] or the direct conversion of ketones and aldehydes to β–lactones[188,190].

Lactone polymerization is usually performed in bulk or in solvents as THF, dioxane, toluene- emulsion, or dispersion. The temperature of polymerization has been investigated in order to minimize the side reactions. In bulk, the best results have been obtained in a range between 100 °C and 170 °C, while for polymerization in solution lower temperatures are required, around 0 - 25 °C[185].

Another factor affecting the reaction is the nature of the initiator. Depending on it, ROP can proceed through different mechanisms: cationic, anionic (nucleophilic), or with coordination mechanism[184]. Organometallic compounds derivatives of Al, Ca, Sn, Nd, Fe, Y, Yb, Sm, La, Ti, Zn, Zr and Mg, in form of oxides, carboxylates, and alkoxides are the most common initiators because able to effectively control the polymerization[181]. Differently, the use of ionic compounds shows unwanted inter- and intra-molecular transesterification reactions that are causing low molecular weight and broad distribution. Depending on the nature of the organometallic catalysts, ROP reactions can occur with two different

polymerization mechanisms. The first one involves complexation with the carbonyl group, followed by polymerization, which can start with nucleophile molecules, as water or alcohol. In the second case, the initiator is the organometal itself; the polymerization is proceeding through an 'insertion– coordination' mechanism, see **Scheme 2**. The most common metal alkoxides operating with this mechanism, are Sn(Oct)$_2$ and Al(Oi-Pr)$_3$, which have been widely investigated for their good activity and polymerization control[185,191–193]. The polymerization proceeds via a three-steps coordination/insertion mechanism, reported in **Scheme 2**.
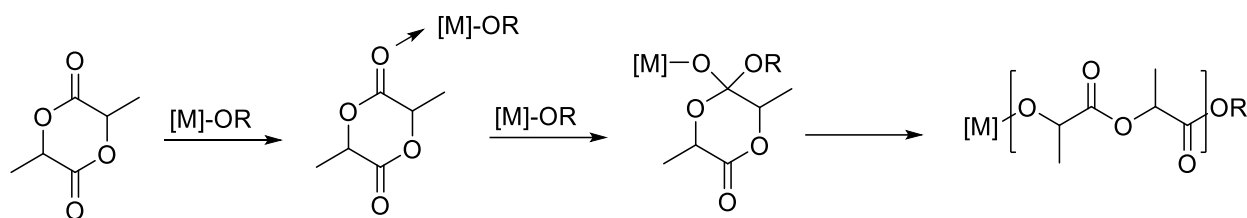
Scheme 2: *coordination/insertion mechanism.*

The good results obtained with this mechanism of polymerization push the researches to design new homoleptic complexes featuring alkoxy and carboxy ligands[194]. For example, trivalent yttrium and lanthanum alkoxides Ln(OR)$_3$ (Ln = La, Y and R = i-Pr, n-Bu) have proved being able to promote the ROP of lactide at room temperature with more efficiency with respect to aluminum alkoxides[195,196].

2.3.3 Chain extension

High molecular weight polymers can be also obtained by chain extension. The method consists in coupling two prepolymers, which can be homopolymers or copolymers, through a small molecule, acting as linker in between the two chains. This reactant, defined as chain extender, is a bifunctional low molecular weight chemical that is reacting readily with the terminal groups of the prepolymer. The most used molecules are diphenyl carbonates, aliphatic and aromatic bisoxazolines, bisepoxides, diisocyanates, phosphites, caprolactam phosphite, bisketenimines, dianhydrides, oxazolinones and dicyanates. Among these, diisocyanates[197–199] have been deeply investigate for their reactivity and good results have been reported in literature regarding the chain extensions of PLA[198,200–205].

3 COPOLYESTERS

Copolymers can be defined as polymeric materials with at least two different repeating units[206]. The process of synthesis, copolymerization, has the aim of incorporating all the different monomers in a single polymeric chain. Copolymerization permits to have a wide *plethora* of possible final properties, allowing their fine tuning according to the application envisioned. Beside composition, also the structure and architecture of the copolymers can be modified. In particular, linear copolymers are formed by a single macromolecule and depending on how the different monomers are lined along the polymer chain, it is possible to discern four categories[207], graphically schematized in **Figure 3.1**:

-   random copolyesters: the sequence of comonomeric units follows bernoullian statistics;

-   alternating copolyesters: constituted of regularly alternating A and B units;

-   block copolyesters: constitute of two or more homopolymers linked by covalent bonds.
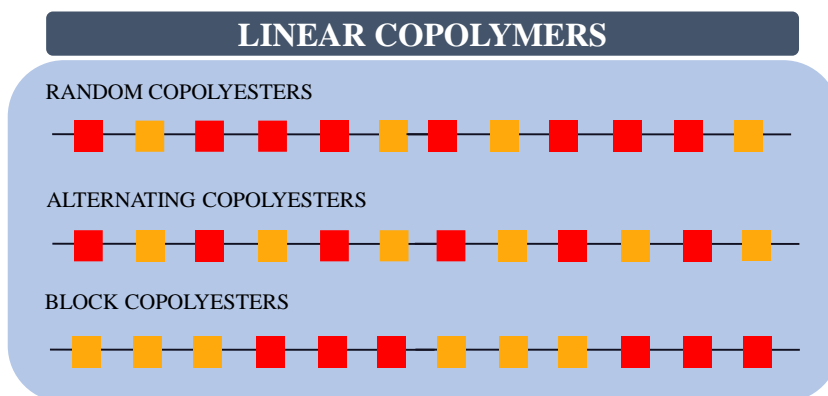
***Figure 3.1**:Architectural structure of copolyesters.*

Beside linear copolymers, there are several chemical architectures for non-linear macromolecules, defined as branched copolymers, **Figure 3.2**:

-   graft copolymers: branched copolymers in which the side chains are structurally distinct from the main chain;

-   star copolymers: characterized by the presence of several polymer chains connected to a central core.
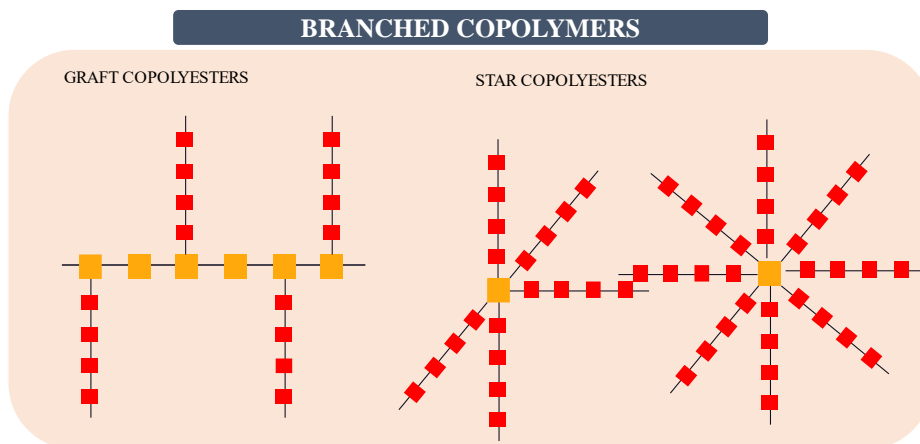
Figure 3.2*: Architecture of branched copolymers.*

The final properties of the material are defined by the physic-chemical properties of the subunits but also by the structure and architecture of the copolymer. An important role is also played by the molecular weight and its distribution and presence of ramifications, cyclic structure or crosslinks.

3.1 Aliphatic copolyesters

3.1.1 PBS-based copolymers

PBS-based copolymers have been widely studied for biomedical and food packaging applications. In both cases, copolymerization results an adequate tool to decrease the crystallinity degree of the homopolymer, increasing the flexibility together with biodegradability, maintaining good the thermal stability and biocompatibility. Through the main pathways of synthesis –polycondensation, chain extension and reactive blending - several examples of random and multiblock copolymers have been reported[14]. In more detail, PBS has been copolymerized with comonomers characterized by ether and thioether bonds, and with natural sub-units as glucose derivates (mannitol or sorbitol). Moreover, the direct mixing of PBS with organic materials, as chitosan or collagen, or inorganic materials, as hydroxyapatite of fluorapatite, revealed to be an alternative effective strategy to tailor and improved final material properties for biomedical applications[14,95,208–210].

3.1.2 PHA-based copolymers

PHB is the most studied polymer of the family of PHA. Thanks to its structural regularity, it is crystalline with high Young´s modulus and low elongation at break[211], resulting brittle and stiff. Moreover, PHB is insoluble in the most common solvents and relatively resistant to hydrolytic degradation. Synthetizing high molecular weight copolymers of PHB can be a good strategy to improve its physical properties[212].

Copolymers can be obtained directly from microorganisms, choosing the right substrate and microbials strain. For example, poly(3-hydroxybutyrate-co-4-hydroxybutyrate)[P(3HB-co-4HB) can be obtained from *R. Eutropha*[213] in presence of fructose and Y-butyrolactone. Besides that, copolymers containing PHB copolymerized with PLA, can be synthetized from glucose by introducing the *Cupriavidus necator β-ketothiolase* and *acetoacetyl-CoA reductase* genes[214].

3.1.3 Alkylene dicarboxylate-based copolymers

Early studies regarding copolyesters containing cycloaliphatic rings have been carried out in 80´ by Eastman Chemical Company. The great interest has increased in the last few years, driven by the possibility to obtain homopolyesters completely from renewable sources[50] that, added to its well-known biodegradability[215], good stability, high crystallization rate, and thermal properties strictly connected to the length of the aliphatic chain, makes this class of polymers suitable for various applications; despite that, mechanical performances are not comparable with the commercial aromatic polyesters. Copolymerization has been employed to modify the unsatisfying properties of poly(alkylene dicarboxylate)s. For example, some polyesters have been modified into poly(ester amide)s where an improvement of the mechanical properties has been observed[216,217]; other studies insert new diacid sub-units along the polymeric chains. Good results have been reported, adding PBT repeating unit into PBCE, that led to higher thermal transitions and improved mechanical properties[218].

Multiblock thermoplastic elastomers have been obtained reacting 1,4-cyclohexanedicarboxylic acid with terephthalic acid, butanediol and ethylene glycol[219]. A series of PBCE derived random copolymers are prepared in the presence of triethylene glycol, obtaining lower crystallinity degree and lower melting temperature with respect to homopolymer, while the thermal stability is maintained[220]. Besides that, random copolymers of PBCE and diglycolic acid reveal a notable and controllable effect on thermal, mechanical, and barrier properties. More complex systems have been also explored: poly(ester urethane) are prepared from poly(butylene 1,4-cyclohexanedicarboxylate) coupled in different ratios with poly(butylene succinate)-based random copolymers containing ether linkages[221]. Multiblock copolyesters characterized by thioether linkages along the PBCE chains are synthetized, displaying good thermal stability, lower crystallinity degree and melting point respect to the homopolymer. These factors have in turn a remarkable effect on the mechanical and barrier properties of the investigated copolymers[222].

3.2 Aromatic copolyesters

As known, the use of aromatic polyesters is preferred for those applications which require materials with excellent physico-mechanical stability.

3.2.1 Terephthalate based copolyesters

Terephthalic acid is one of the most used monomer in copolymeric systems. Some examples are copolyesters based on PET with lactic acid[223], isophtalate[224–232] or furan acid[233]. Another important member of the class of terephthalate-based polyester is PPT, which has been copolymerized with adipic or sebacic acid as comonomers[234–239]. Some papers report the use of PBT repeating unit, that in presence of 1,4-cyclohexanedicarboxylic acid determine higher thermal transitions and improved mechanical properties[218,219] with respect to the homopolymer[240–245].

3.2.2 Isophthalate based copolyesters

Thanks to the characteristics previously mentioned, derivates of isophthalic acid have been copolymerized in order to tune the final properties of the material. A wide number of papers report copolymerization of PEI; in particular, the system poly(ethylene isophthalate-co-ethylene terephthalate) (PEI/PET) has been deeply investigated: various compositions and molecular weights are synthesized by melt polycondensation and different characterizations in terms of chemical structure, thermal behavior and rheological properties[224–232,246,247] are performed. Regarding PPI, the polyester has been randomly copolymerized in bulk, for example with poly(propylene adipate) (PPA), then the system has been deeply characterized in terms of chemical structure, molecular weight and thermal properties[248]. Random systems of PPI and poly(propylene succinate) (PPS) are also reported[249]. Further copolymerizations have been conducted starting from PBI as parent homopolymer. The Authors observed the decreasing of the crystallization capability and of melting temperature, while glass transition temperature results not significantly affected[250]. Sulfonated poly(butylene isophthalate) random copolymers have been also synthesized and characterized from the molecular and thermal point of view, with particular attention devoted to crystallization kinetics studies[251]. The segmental dynamics of poly(butylene isophthalate/butylene adipate) copolyester are investigated[252]. More complex systems, as branched poly(butylene isophthalate)-co-poly(tetramethylene glycol)-co-poly(ethylene glycol) are synthetized and processed in form of fibers, showing an excellent elastic recovery[253]. Poly(tetramethylene isophthalate) (PTMI) and poly(tetramethylene oxide) (PTMO) are polymerized, evidencing, as expected, a direct correlation between composition and transition temperatures[254].

3.2.3 Furanic based copolyesters

2,5-furandicarboxylate polyesters display excellent thermal, mechanical and barrier properties, but there is no mention to possible (bio)degradability, since, as already observed with the terephthalic-based counterparts, they are potentially strongly resistant to hydrolysis but also to bacterial attack[255]. With the aim to increase the degradability[256], decrease the rigidity of the derivates and tune the final properties, the literature reports several examples of copolymers based on 2,5-furandicarboxylate[257,258], as PEF copolymerized with lactic acid[143], ethylene glycol[259], terephthalic acid[260], 1,4-cyclohexanedimethylene[261]. Different works are also centered on PPF, where new copolymers are synthetized in presence of fatty acid[262] and terephthalic acid[233]. Also PBF is widely copolymerized: the fully bio-based system poly(butylene 2,5-furanoate/diglycolate) showed really good barrier properties. Different studies reported copolymers of PBF also with succinic acid[148], diglycolic acid[147], 1,4 butandiol[263], adipic acid[145] and with PEF.

3.2.4 Aliphatic/aromatic copolyesters

Aromatic polyesters boast excellent physico-mechanical stability together with low biodegradability. This latter feature is, instead, characteristic of aliphatic polyesters that, in turn, show poor mechanical properties[264]. In order to obtain materials with the mechanical properties of aromatic derivates, and characterized by the high biodegradability of aliphatic ones, several copolyesters containing both the moieties have been synthetized. In this way, the peculiar problems of the two classes of polymers can be overcome, and these materials can be considered a real alternative for replacing the common plastics. As a confirmation of their potentiality, several studies have been also conducted from the industrial point of view[265].

Commonly, the biodegradability is strictly bonded to the chemical structure, in particular to the number of hydrolysable and /or susceptible to microbial attack bonds in the polymeric chain. Secondary factors - degree of crystallinity, molecular weight, morphology and stereoregularity- also affect the biodegradation process. With the aim of proving the biodegradability of aliphatic/aromatic copolyesters, many studies have been carried out[265,266], showing that thermophilic bacteria, as *Thermomonospora Fusca*, in conditions of high temperatures, and microorganisms present in the soil, like R. bacteria, *Depolimerans* and *Leptothrix*, are able to attack and degrade these copolyesters in a few weeks. During the process, the bacteria start to degrade the aliphatic part, which is acting as trigger for the degradation of the whole chain. The literature is rich of example of aliphatic/aromatic copolymers, as poly(butylene

succinate) (PBS) and poly(ethylene adipate) (PEA) modified with phenyl side chains[267] or based on poly(butylene terephthalate) (PBT) with aliphatic polyesters[234,235,268–271], 2,5-furandicarboxylic acid or 2,5-thiophenedicarboxylic acid copolymerized with adipic acid[147,266]. Regarding commercial products, adipic acid, terephthalic acid and 1,4-butanediol are employed to produce poly(butylene adipate-co-terephthalate) (PBAT), named Ecoflex® by BASF, Easter Bio® from Eastman Chemical and Origo-B from Novamont. PBAT boasts the European (DIN EN 13432) and American (ASTM D 6400) certifications of biodegradability and compostability[235,272,273] together with properties similar to LDPE. Ecoflex® is a good solution when high resistance to humidity and fat is needed, like for compost bags for organic waste, agricultural and household films, coating materials for starch-based products (e.g., plates, cups). Moreover, BASF declares also good compatibility of Ecoflex® with PLA and starch products. Other example is Ecovio®, a blend of Ecoflex® and PLA, this latter derived from fermentation process of sugars. The main applications of the material are bags for organic waste, films for agriculture, coffee capsules and as protecting aroma outer package.

3.3   Synthesis of copolyesters

3.3.1   Polycondensation

Polycondensation is one of the most common technique to synthetize polymers. In case of homopolymers, the reaction is occurring between only one kind of diacid and diol, in case of copolymers higher numbers of monomers can be involved in the reaction. More details have been reported in section 2.3.1.

3.3.2   Chain extension

Chain extension is a good strategy to obtain high molecular weight polymers. As previously reported in section 2.3.3, this strategy con be adopted also to synthetize high molecular weight block copolymers.

3.3.3   Reactive blending

Reactive blending is versatile strategy of synthesis for copolymers. The selected homopolymers are reacting in melt, in the presence of catalyst for a certain time. It has several advantages compared to performing the reaction in solid state or solution. First, the absence of any solvents limits environmental issues, bond to the removal and recovery of the fluids, and the cost connected. Moreover, the probability of contamination of the products is lower with respects to reaction in solid state and solution. Besides that, it is necessary to consider the high temperatures needed and for this reason, thermal stability is a

basic requirement to perform reactive blending in molten state. As a consequence, the list of chemicals employable is short: imidization, ring opening, amidation reactions, and interchange reactions between polycondensates, are the most common. Reacting blending involving polyesters are mainly occurring via interchange as intermolecular alcoholysis, intermolecular acidolysis and esterolysis. The latter mentioned has a relevant industrial role because is used for the production of plastics like PET. Another aspect of reactive blending is related to the versatility of the strategy. The final architecture of the copolymers can be modified changing the reaction time, from block structures to random ones (**Figure** *3.3*).
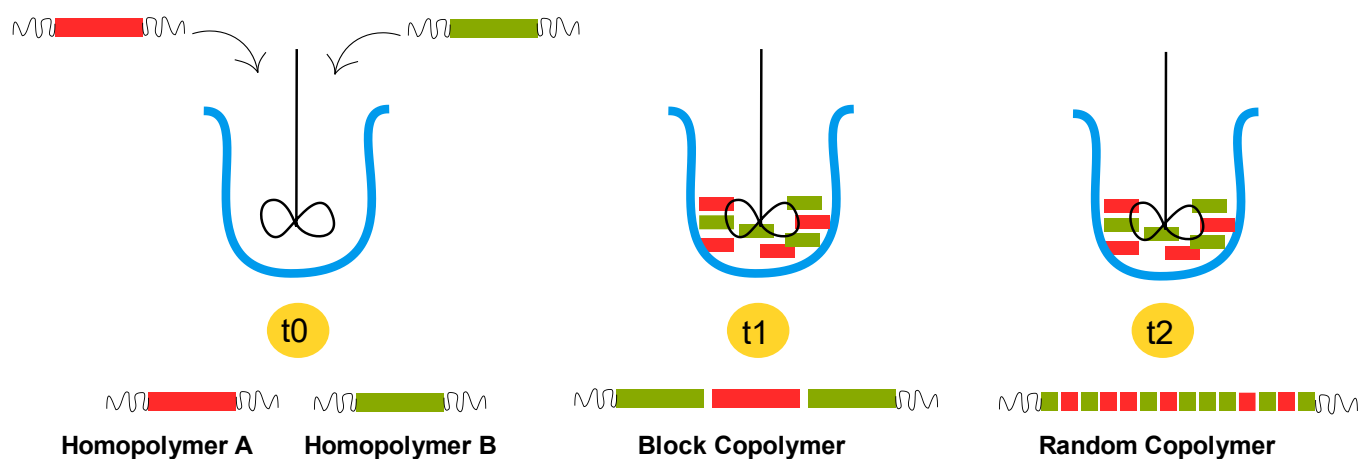
Figure 3.3: *Effect of reaction time on the final copolymeric architecture.*

4 PHYSICAL PROPERTIES

Solid-state properties of aliphatic and aromatic polyesters are strictly correlated to several factors as crystallinity degree, presence of polar groups, mobility of polymer chains, molecular mass, presence of branching, etc. For example, as reported in literature, short-chain branches hamper the crystallization, while long branches reduce the viscosity and confer plastic behavior[274]. Moreover, the final properties can be further modulated by copolymerization, both in terms of composition as well as of macromolecular architecture.

4.1 Structure of polymers

Polymeric materials can be classified as a function of the arrangement of the macromolecules as follow: amorphous, if completely disordered and semicrystalline, if partially ordered (see **Figure 4.1**). In some cases, the development of short-range order can also occur leading to the formation of the so-called mesophase.
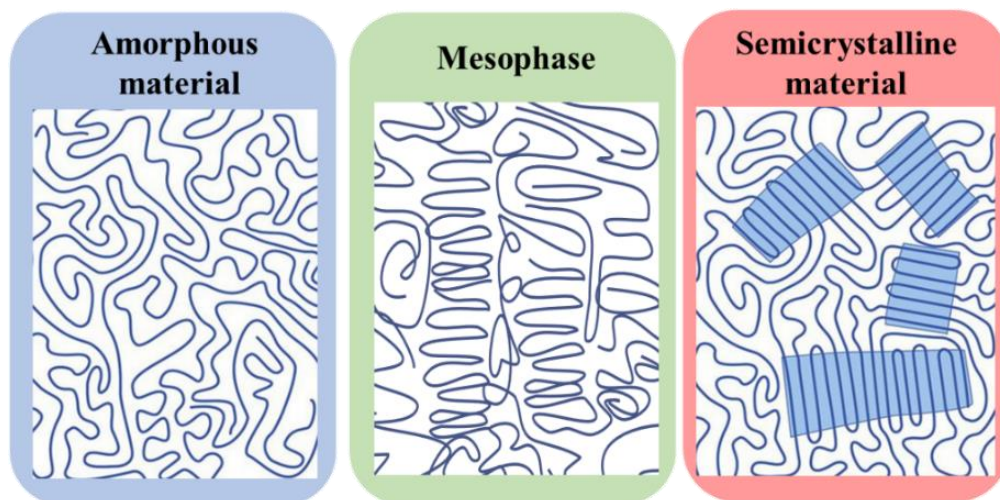
Figure 4.1*: Graphical representation of amorphous phase, mesophase and semicrystalline structures.*

4.1.1 Amorphous phase

Amorphous polymers are characterized by a second order transition, called glass transition. This phenomenon is defined as kinetic process because the temperature at which the transition is occurring depends on the cooling rate: for a given polymer, slowly cooling of the melt produces a glass at lower temperature than a fast cooling would do. The glass transition temperature, T_g, is associated with the

main change in the dynamic properties and for this reason is also defined as α relaxation. Below T_g the material is resulting rigid and fragile, a glass, made of dense and less dense regions, defined density fluctuations, defects or heterogeneities[275–277]. These less dense zones are mobile islands where the local motions of chains, or translational motions of entrapped gas/small molecules, are still possible[278]. However, the mobility is restricted to vibrational movements without directly involving the surrounding atoms or molecules[278]. These phenomena are called as "sub-T_g relaxations", considering their position relative to the glass transition. Different secondary sub-T_g relaxations can be observed in polymeric materials, mainly β relaxations have been studied showing dependence to the Arrhenius law, with a characteristic activation energy (E_a) reflecting the degree of cooperativity and non-cooperativity movements. When the material is heated above T_g, the large multitude of cooperative movements become possible as showed in **Figure 4.2**, determining changes in the physical properties of the material (increasing in heat capacity, entropy, and volume and decreasing in both rigidity and viscosity[279]).
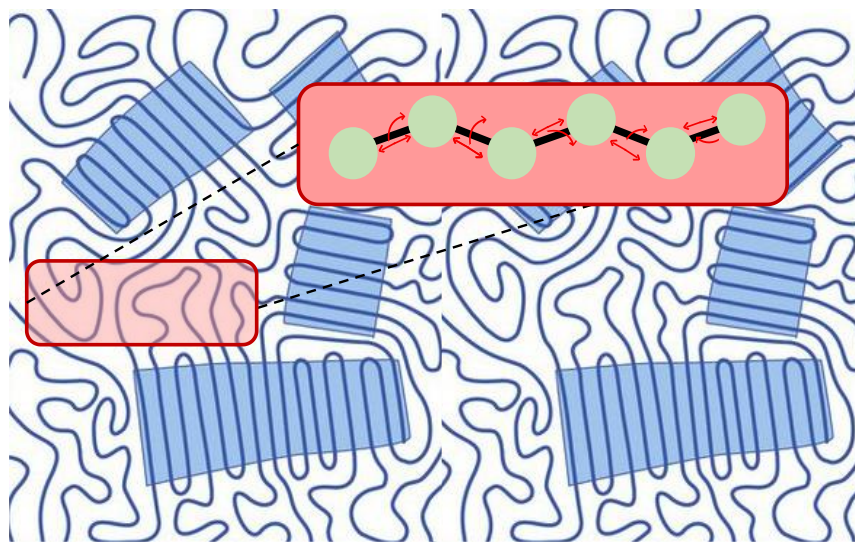
Figure 4.2*: Cooperative movements interesting the amorphous phase above T_g.*

Appling different cooling rates, amorphous polymers can be frozen in a non-equilibrium condition with the corresponding values of entropy/enthalpy and volume being above those corresponding to the most stable situation[280]. Of course, the material will tend to relax towards the equilibrium condition, over a defined amount of time - called "relaxation time"- and energy - identified as "enthalpy of relaxations". This process occurs slowly but the rate can be increased by changing the temperature. Indeed, raising the temperature near T_g, the relaxation time can be significantly reduced. From the microscopical point of view, chain rearrangements and densifications are observed. As a consequence, the molecular

organization is compacting and the strengthened interactions produce changes in mechanical behavior - the rigidity is increasing[281] - and in gas barrier properties, where the molecules diffusivity through the material is hampered[282].

4.1.2 Mesophase

In recent years, the transient states (mesophases) in the ordering of polymers into crystalline structure, have been deeply investigated. These mesomorphic states or mesophases are intermediate between complete disordered amorphous state and the three-dimensional structures of the crystalline phase. In these conditions, an ordered short range unit cell is forming; despite the absence of 3D structure, mesophases present a partially ordered structure (1D or 2D) since the classical technique used to investigate crystalline phases can be employed. For example, X-ray detect the mesophase as a relatively narrow diffraction peak rising over a diffuse halo[283]. Wunderlich established the first classification of mesophases into three categories[284,285] (**Figure 4.3**):

- liquid crystals: are defined as liquids with some orientational order;
- plastic crystals: are crystals with a large degree of orientational disorder;
- condis crystals: identified as crystals with complete or partial conformational disorder.

A list of the typical differences and properties of the mesophases are reported in **Table 4.1**.

Table 4.1: *Properties of liquid crystals, plastic crystals and condis crystals.*

Liquid crystals	Plastic crystals	Condis crystals
"Liquid"	"Plastic"	"Solid"
Birefringence	Not birefringence	Birefringence
Small ΔS (2-5 J/K*mol)	Fixed ΔS (7-14 J/K*mol)	ΔS=7-12 J/K*mol for each ratable bond
100% crystallinity	100% crystallinity	Limited crystallinity for macromolecules
Small and large molecules	Small molecules	Small and large molecules
No positional order, some orientational order	Positional order, no/limited orientational order	Positional ordered, and orientational ordered
Full conformational disorder, as in melt	Full conformational disorder, similar as melt	Partial of full conformational order
Mesogen shape: rod, disc and board	Mesogen shape: close to spherical	Rotational shape that keep the chains parallel

A less fine classification proposed a subdivision just in two categories, solid mesophases and liquid crystal mesophases[283,286]. In particular plastic crystals and condis crystals are composing the solid mesophases, while liquid crystals, being closer to liquids, are defining as liquid crystal mesophases.

As well represented by **Figure 4.3**, plastic crystals and condis crystals, solid mesophases, present long range order with high structural disorder; differently, liquid crystalline mesophases are resembling crystals with long-range orientational order but, as liquid, are characterized by absence of three-dimensional positional order[283,286].

Many researchers are investigating the formation of mesophase, proposing a possible assembling during formation and growth of lamellar crystals, proceeding as multistep process[287–290]. Firstly, a mobile mesomorphic layer is formed with a thickness up to a critical value; then, a solidification by core crystallization is occurring followed by further stabilization into lamellar crystallites by surface ordering[291]. The base of this concept is proposed by Ostwald[292], who observes that a general phase transformation is proceeding through metastable states[287–289]. Further studies have taken into account the peculiar chemical structure needed to develop mesophases. In details, there are essentially two components that need to be present: a semirigid anisometric group (mesogenic group) and a flexible alkyl spacer; these two elements favor the formation of mesophase independently if they are located in the main backbone or in the side chain of the polymers[293,294]. The consequence of the intermediate order exhibited by mesophases lead to new and unexpected properties. In particular, liquid crystalline polymers, LCPs, boast the anisotropic behavior proper of liquid crystals with the excellent characteristics of polymers, as good strength, reprocessability and low gas permeability[295]. As reported in **Figure 4.3** LCPs[295] can be divided into three different groups in function of degree of order:

- nematic, where the macromolecules are oriented along one direction;
- smectic, where the macromolecules are oriented in parallel and arranged in well-defined planes;
- other partially ordered systems as cholesteric, arranged in layers with the long molecular axes parallel to the plane and disposed to give a final helical stacking.
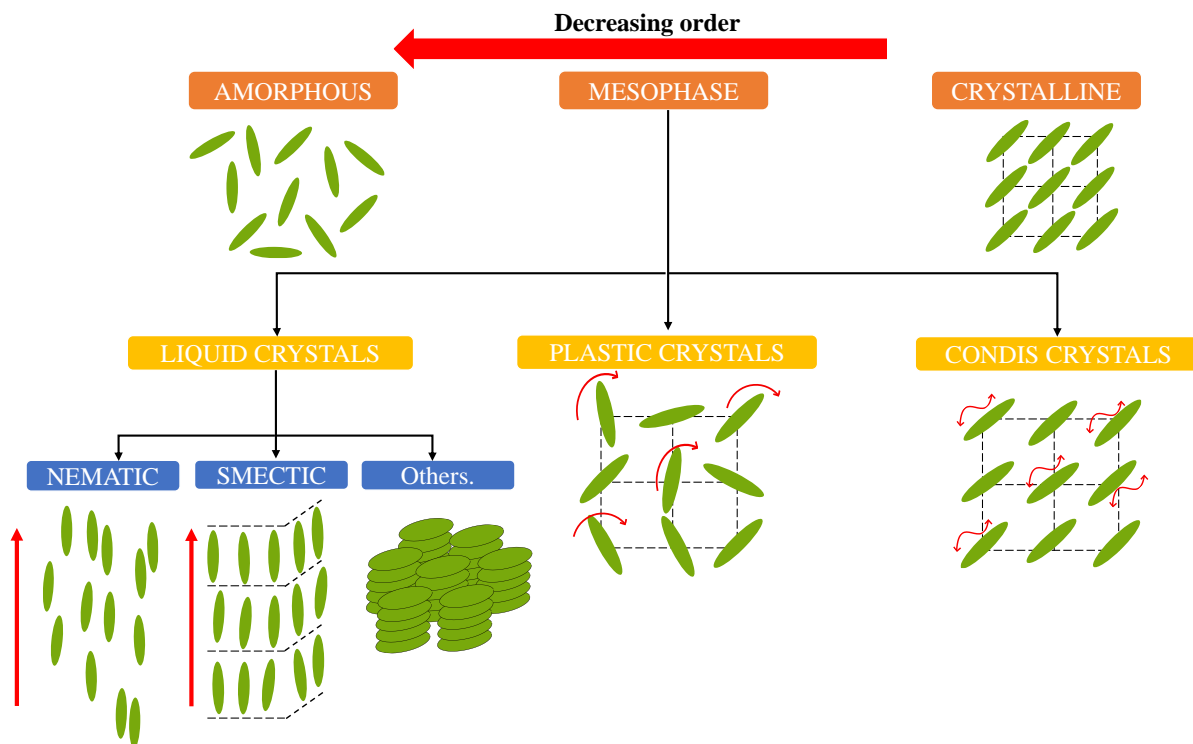
Figure 4.3*: Schematic representation of mesophases.*

The type of mesophase assumed by LCPs is deeply influenced by length and length/diameter ratio of the rigid unit together with the length of the flexible spacer unit. Moreover, also the characteristic transition temperature, from smectic to nematic to isotropic, is affected from the chemical structure of the polymer. In detail, nematic phase is more stable with the increasing of the length and length/diameter ratio of the rigid unit and with the shortening of flexible moiety. So far, the shortest rigid unit that permits nematic formation is of about 1.1 nm[295]. Moreover, odd-even effect on the crystal nematic has been reported with the increasing numbers of methylene units in the spacer group[296–298]. In general, LCPs constituted by even number of methylenes show higher transition temperatures and entropy changes than those having odd units.

4.1.3   Crystalline phase

Beside the condition of completely amorphous materials, the polymeric chains can organize in 3D structure. Due to the dimension of the chains, polymeric materials are unable to reach 100% of crystallinity. As a consequent, an amorphous portion is always present even if constrained between crystals, causing the shift of T_g to higher temperatures compared to the same polymer in a completely amorphous state. Not only the T_g is affected by the presence of crystalline phase, but relevant changes

are observed in density, transparency, mechanical response. The temperature at which the 3D structure is losing its order is called "melting temperature", T_m, and the corresponding process identified as an endothermic phenomenon (**Figure 4.4**).
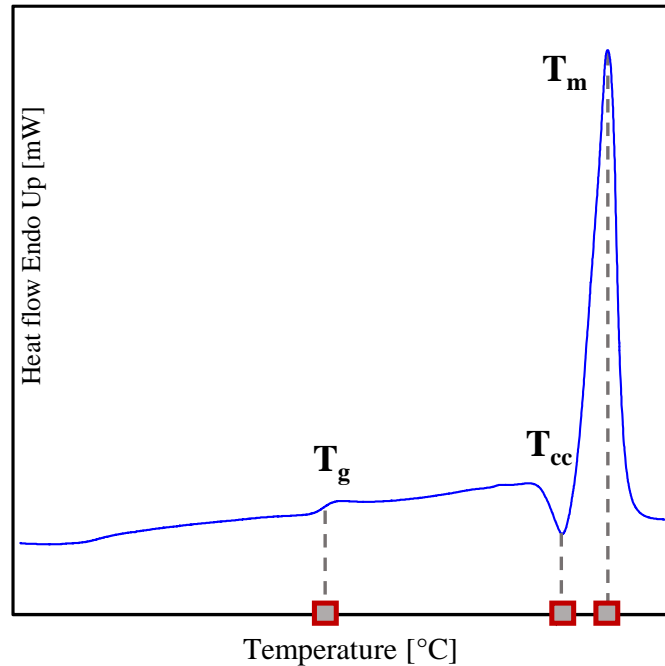
Figure 4.4: DSC analysis of polyester.

The process by which the macromolecules are organizing into crystalline structure is called "crystallization". The organization can start from the melt, defining the "melt crystallization" process and happening at T_c (**Figure 4.5**) but also heating up the material from the glass – the so-called "cold crystallization", indicated as T_{cc}.

TIME

Figure 4.5: Crystallization process conducted at defined temperature.

In order to be able to crystalize, the polymer has to boast sufficient structural regularity. If this is occurring, the phenomenon can happen in the range between T_g and the melting temperature with a rate, defined as crystallization rate, strictly connected to the temperature. If the intrinsic structure of the polymer is adequate, the first step is the formation of nuclei, defined as nucleation[299]. This phenomenon

can take place both in "homogeneous conditions" or "heterogeneous conditions". The spontaneous nucleation starts with the organization of the macromolecules by themselves, without external force and, consequentially, the rate of crystallization can be significantly slow. As reported[300–302], applying a high supercooling, the formation of homogenous nuclei can be encouraged. Due to their small size and low enthalpy, their detection can be complicated. In order to overcome this problems, Tammann's two-stage crystal nuclei development method could be applied. The experiment is based on difference between temperatures of maximum rate of homogenous crystal nucleation and the temperature of crystal growth[303,304]. This method consists in the formation of nuclei at high supercooling/glassy state with a subsequent growing at higher temperature favouring the nuclei detection (**Figure 4.6**).
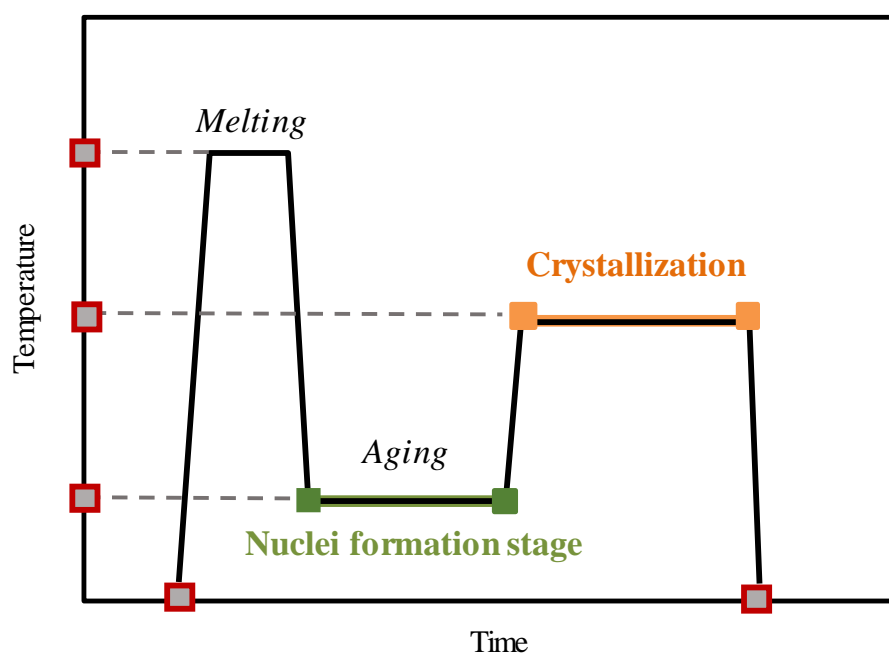
Figure 4.6*: Graphical scheme of Tammann´s nuclei formation method.*

Firstly, Tammann´s method has been applied to study the crystallization of glycerol[303,304], organic liquids[305] and silicate glasses[306,307]. Then, it was employed in polymeric chemistry to study the homogeneous nucleation of poly (ε-caprolactone) (PCL)[308–310], isotactic poly(butene-1) (iPB-1)[311], polyamide 6 (PA 6)[312] and PET[313].

Besides that, "heterogeneous nucleation" is the typical technique applied at industrial level. Different strategies have been reported. One example is the partial melting of the crystalline material, where the

crystalline fragments act as "self-nuclei" for the polymer melt, during the subsequent cooling[299].
Moreover, the addition of "nucleating agents" is quite effective.

Once the nuclei are formed, they can growth with different rates in different condition. Usually, the growth rate is represented as "bell shaped curve", **Figure 4.7**, as a function of temperature. Growth rate assumes a value equal to 0 at [314]:

- T_g, because the mobility of the polymeric chains is restricted not allowing chain folding;
- T_m, because the equilibrium between liquid and crystal is reached.
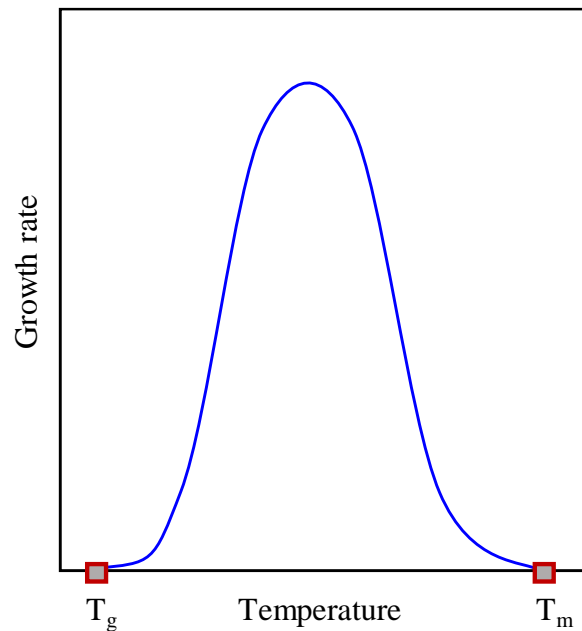
Figure 4.7: Growth rate curve in function of temperature.

The crystallization process can be theoretically evaluated as a function of temperature and time. When temperature is a constant factor, it is spoken of "isothermal crystallization". The crystal growth rate under this condition can be described by the Avrami equation[314]:

$$X(t) = 1 - log(-Kt^n) \qquad\qquad Eqn.\ 10$$

X(t) is the crystallinity fraction in the crystallizable material at time t. K is the rate constant that is temperature dependent; n represents a factor which takes into account the dependence of time of nucleation step and the dimensionality of the growth process typical of a given morphology and type of nucleation. If during the process the temperature is changing time by time, we speak of "non-isothermal

crystallization". In this case the theoretical treatments of the crystallization is more complex because one has to take into account the temperature as a function of time, $T(t)$[314].

4.1.4 Phase transitions

Both glass transition temperature and melting temperature, as well as crystallization temperature, are affected by composition, chain symmetry, flexibility and tacticity. For example, the presence of chemical groups as -O-, -COO-, OCOO- and -(CH_2)- favors the flexibility while polar groups, responsible of intermolecular bonds, increase the T_g and T_m values and decrease T_c (or T_{cc}).

4.1.4.1 Homopolyesters

Regarding polyesters, thermoplastic ones have lower T_g compared to thermoset derivates. Besides that, linear aliphatic polyesters with x and y (**Figure 4.8**) higher than 2, present excellent crystallization skills with consequent high crystallinity degree, with a T_m around 40°-90°C, and glass transition temperature between –70 and –30°C.
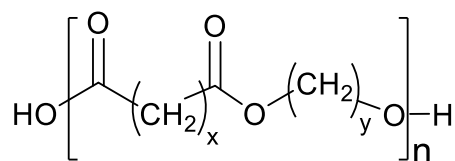
Figure 4.8: General chemical structure of polyesters.

Melting temperature can be deeply affected by the ratio between methylene and carboxylic groups in the polymer chain. As reported[14,315], the lower the ratio, the higher the T_m. As such, poly(butylene adipate) melts at 47°C, while of poly(butylene succinate) at 116°C.

Aromatic polyesters are characterized by higher crystallinity degree and melting temperature compared to aliphatic polyesters. Also in this case, the T_m is deeply connected to the length of alkyl chains, in particular is decreasing alternately passing from an even number of alkyl units to an odd one: T_m of PET is 290 °C, T_m of PPT is 237 °C and T_m of PBT is 236 °C[316–318].

4.1.4.2 Random Copolymers

As previously explained and graphically reported in **Figure 3.1**, random copolymers are constituted by two or more repeating units statistically bonded. The different composition is affecting the glass and the

melt transition. In particular, Fox equation is the simplest relation between copolymer composition and glass transition temperature (T_g):

$$\frac{1}{T_g} = \frac{\omega_A}{T_{g,A}} + \frac{\omega_B}{T_{g,B}}$$

Eqn. 11

where ω_A and ω_B are the weight fractions of the two comonomeric units A and B, while $T_{g,A}$ and $T_{g,B}$ represent the glass transition temperatures of the two homopolymers A and B.

Such equation interpolates well the experimental data when the two comonomeric units are characterized by similar chemical structure. If this condition is not satisfied, other more complex equations containing adjustable parameters have to be utilized.

More complex is the situation regarding the crystallization ability. If only A comonomeric units are able to crystallize, AB random copolymer can exhibit two behaviors:

- comonomer exclusion: the crystalline phase is composed by A and is in equilibrium with the amorphous phase, composed by A and B units. As such, crystallization involves only A units, with the complete exclusion of B units;

- comonomer inclusion: the crystalline phase is a solid solution of A and B, where B co-units are producing defects in the ordered phase, constituted by A.

As reported by Sanchez in 1973, commonly the structures of copolymers are intermediate among to the two situation described above[319].

The thermodynamics of the comonomer exclusion during crystallization has been studied by Flory during 1947[320]. He defines the upper limit of the copolymer melting temperature, (i.e. the T_m of crystals formed by "infinitely long" sequences of A units) as:

$$\frac{1}{T_m^\circ} - \frac{1}{T_{m_{XB}}^\circ} = \frac{R}{\Delta H_m^\circ} * ln(1 - X_B)$$

Eqn. 12

with T_m° and ΔH_m° being the equilibrium melting temperature and heat of fusion of 100% crystalline homopolymer; X_B represents the concentration of B units in the copolymer while R is the gas constant.

The model is based on an unrealistic assumption: the homopolymer sequences of infinite length build up unfolded crystals of the length of A sequences. To overcome this limit, it is necessary to consider that

only sequences of ξ length can be included into crystals with ξ lamellar thickness. Baur's equation is defining the behavior of T_m of infinitely long homopolymer sequences (*Eqn. 13*).

$$\frac{1}{T_m^\circ} - \frac{1}{T_{m\,XB}^\circ} = \frac{R}{\Delta H_m^\circ} * [\ln(1 - X_B) - < \tfrac{1}{\xi} >]$$

Eqn. 13

Where $\frac{1}{<\xi>}$ corresponds to $[2X_B(1-X_B)]$, the average length of homopolymer sequences in melt.

Usually, the experimental data are well fitted by Baur´s model even if it ignores the fixed nature of homopolymeric sequence due to the covalent bounds[319,321–324]. For that reason, the prediction of melting temperature depression for random comonomers needs to consider the comonomer inclusion. The last mentioned case, comonomers B included as defects into crystals constituted by A comonomer, was early investigated by Helfand and Lauritzen[325] then by Sanchez and Eby[319].

According to their model, T_m is then given by *Eqn 14*.

$$\frac{1}{T_{m\,XB}^\circ} - \frac{1}{T_m^\circ} = \frac{R}{\Delta H_m^\circ} * \left\{ \frac{\varepsilon X_{CB}}{R * T_m} + (1 - X_B) \cdot ln\left[\frac{1-X_{CB}}{1-X_B}\right] + X_{CB} \cdot ln\left[\frac{X_{CB}}{X_B}\right] \right\}$$

Eqn. 14

where X_{CB} is the concentration of B units in the co-crystal, and ε the free energy of defects.

Considering $X_{CB} = X_B$, uniform inclusion can be derivate from *Eqn.15*:

$$T_{m(XB)} = T_m^\circ \cdot \left[\frac{1-\varepsilon X_B}{\Delta H_m^\circ}\right]$$

Eqn. 15

When the equilibrium is reached, X_{CB} can be written as:

$$X_{CB}^{eq} = \frac{X_B * e^{\frac{-\varepsilon}{RT}}}{1 - X_B + X_B * e^{\frac{-\varepsilon}{RT}}}$$

Eqn. 16

and the equilibrium melting point is derived from *Eqn.14* as:

$$\frac{1}{T_{m\,XB}^\circ} - \frac{1}{T_m^\circ} = \frac{R}{\Delta H_m^\circ} \cdot ln[1 - X_B + X_B \cdot e^{\frac{-\varepsilon}{RT}}]$$

Eqn. 17

The difference respect to Flory's equation is the inclusion of term $X_B \cdot e^{\frac{-\varepsilon}{RT}}$, the equilibrium fraction of repeating crystallizable units B. Considering the case of high defects, *Eqn.17* is reduced to *Eqn.11* theorized by Flory. Moreover, the free energy of the defects is underestimated, while T_m for $\varepsilon \gg 0$ is

resulting overestimated. The value of T_m obtained from *Eqn.17* can be defined as an upper limit of the melting temperature.

In the case of $\varepsilon \gg 0$, the Sanchez-Eby model encountered the main limits; considering high value of ε the cocrystallization is suppressed, *Eqn.17* should converge to Bauer´s equation (*Eqn.13*) instead it is reduced to the Flory model *Eqn.12*.

Wendling and Suter[326] in 1998, present a new model where the conversion of *Eqn.17* in *Eqn.13* is possible. The melting temperature was expressed as follows:

$$\frac{1}{T^\circ_{m_{XB}}} - \frac{1}{T^\circ_m} = \frac{R}{\Delta H^\circ_m} \cdot \left\{ \frac{\varepsilon X_{CB}}{R*T_m} + (1 - X_{CB}) \cdot ln\left[\frac{1-X_{CB}}{1-X_B}\right] + X_{CB} \cdot ln\left[\frac{X_{CB}}{X_B}\right] + \frac{1}{<\xi>} \right\} \qquad Eqn.\ 18$$

In case of monomer inclusion, *Eqn. 18* can be simplified as:

$$\frac{1}{T^\circ_m} - \frac{1}{T^\circ_{m_{XB}}} = \frac{R}{\Delta H^\circ_m} \cdot ln[1 - X_B + X_B \cdot e^{\frac{-\varepsilon}{RT}}] - \frac{1}{<\xi>} \qquad Eqn.\ 19$$

With $\dfrac{1}{<\xi>} = \dfrac{2*(X_B - X_B * e^{\frac{-\varepsilon}{RT}})}{1 - X_B - X_B * e^{\frac{-\varepsilon}{RT}}}$

Both the models, for the inclusion and exclusion crystallization, describe a depression of melting temperature. In the inclusion model, this phenomenon can be explained as defective heat of fusion during crystallization; in case of exclusion, the reason is the need of copolymeric chains to allow the crystallization which leads to an increasing of entropy of fusion.

4.1.4.3 Block copolymers

Block copolymers are complex macromolecules, which can contain two or more different homopolymeric sequences, with consequent wide possibility of architectures:

- linear di-block A-B;

- linear tri-block A-B-A;

- multiblock or segmented $(AB)_n$;

- star di-blocks $(AB)_{nX}$.

When a third monomer is involved, linear A-B-C, A-C-B, and B-A-C triblock copolymers can be prepared[327].

Block copolymers are not available as natural products but have to be synthetized. An early example of commercial block copolymer is Pluronics, a surfactant constituted of propylene oxide and poly(ethylene oxide). In 1959 Du Pont launched the first product designed on the concept of soft and hard segments, Spandex, an elastomeric polyurethane.

The crystallization process is complex due to two different self-organizing mechanisms competing each other: microphase separation and crystallization. Considering a di-block copolymer where only one of the two blocks can crystallize, the thermal transitions are influenced by both blocks. The thermal behavior is more complicated when both two or more block can crystallize. If the two blocks present different melting temperature, one block can crystallize predominantly influenced by the crystallization of the other block, depending on several parameters (segregation strength, crystallization temperature and molecular weight of the blocks)[328].

4.1.5 Thermal properties

Considering the thermo-mechanical behavior of plastics, it is possible to divide them in two categories: thermoplastics and thermosets[329].

Thermoplastics are material that can be repeatedly softened by heating, molded and hardened by cooling, thanks to the presence of secondary bond which can soften reversibly, without undergoing chemical transformation. Some examples are: saturated polyesters, polycarbonates, polyamides.

Thermosets are, instead, materials that are hardening after heating, loosing completely the possibility to be processed again. These polymers are characterized by chemical groups or double bonds that undergo cross link reactions; some examples are unsaturated polyesters, resins or polyurethanes.

4.1.6 Thermal stability

Thermal degradation is one of the main problems occurring during synthesis and processing of polymeric materials, due to the high temperature involved. Heat is causing thermal degradation and consequent chemical modifications in the macromolecular structure. The bonds are breaking and volatile products are forming, modifying the final properties of the material. For this reason, the thermal stability

evaluation is fundamental to define the maximum temperature that can be reached, avoiding polymer degradation.
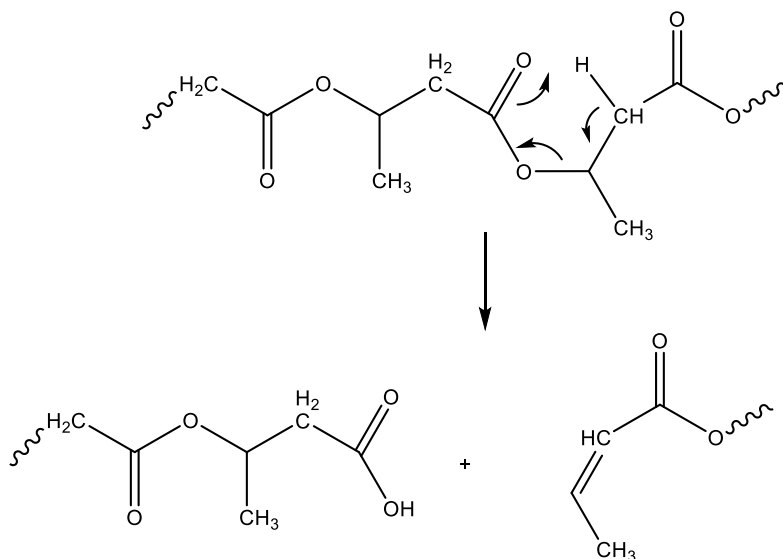
Figure 4.9: β-scission mechanism.

Thermal degradation mechanism has been deeply investigated and it involves two simultaneous distinct reactions. Random bonding scission is responsible of the decreasing of molecular weight while chain-end scission of C-C bonds, is generating volatile sub-products. This latter phenomenon, also known as depolymerization reaction, is occurring when bonds in the main chain are weaker than those of the side groups, taking place at the gas-liquid interface of the system[330]. Usually, it starts from the end of the chains, releasing progressively monomeric units. Differently, random body scission can start at any bond along the chain. Regarding polyesters, β-scission is one of the most common mechanism (**Figure 4.9**) of random degradation, taking place in presence of β-hydrogen atoms in the diol sub-unit[330,331]. The hydrogen bonded to a carbon atom in β position to carbonyl group is extracted, breaking the O-CH bond[332–334]. The degradation mechanisms are forming –COOH and $CH_2 = CH$- terminal groups.

The presence of methylene groups in aliphatic and aromatic polyesters increases the probability of chain scission[333]. As a prove of that, PBT or PPT are degrading faster than PET, this last containing a lower number of methylene groups; as well, poly(ethylene succinate) (PES) is more thermally stable than poly(butylene succinate) (PBS) at high temperature. Thermal degradation is producing sub-products of different natures as H_2O or CO_2 or formaldehyde, acetaldehyde, formic and acetic acids. In particular,

the presence of acetaldehyde in plastics for food packaging applications is a huge issue not only because of the colored by-products that can be formed, but mainly for its high toxicity.
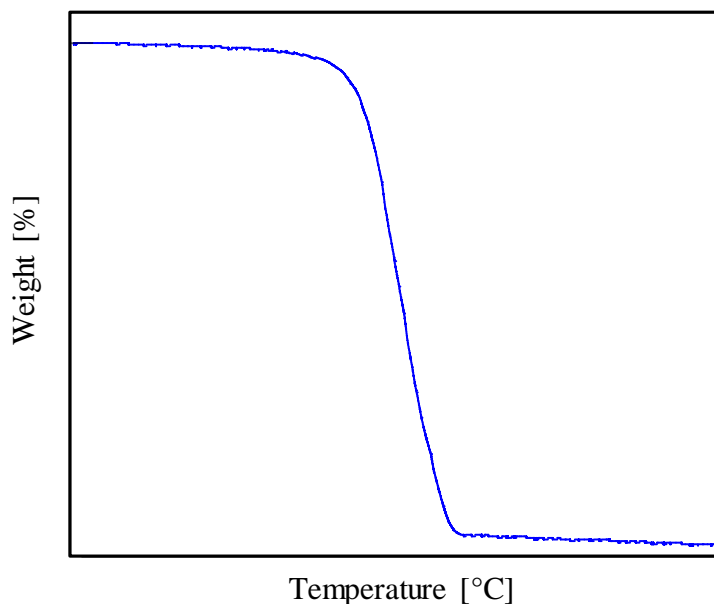
Figure 4.10: Typical thermal gravimetric analysis (TGA) of polyester.

One of the main techniques to investigate thermal degradation phenomenon is thermogravimetric analysis. During the test, the mass loss can be monitored as a function of temperature under a controlled and fix heating rate or under isothermal conditions, i.e. keeping a selected temperature constant. An example of thermogram recorded in no-isothermal conditions is reported above, (see **Figure 4.10**): in this case, the material is showing the main mass loss in one stage. Smaller mass losses at lower temperature are due to degradation of low molecular weight residues as unreacted monomers, catalyst, oligomers or water. In order to obtain information of thermal degradation mechanism, it is possible to equip the instrument with mass spectrometer or Fourier transform infrared spectrophotometer.

4.1.7 Mechanical properties

Polymers can show both elastic and plastic behavior, and for this reason are defined as viscoelastic materials. Depending on the load applied, these materials can be deformed and return to the original shape after removal of the stress (elastic behavior) or can be irreversibly deformed (plastic behavior). The mechanical tests can be conducted with different geometry and loads (static and dynamic)[335]. Widely used is the stress-strain test, where the strain – defined as change in sample length divided by the original length – is measured in response to the stress applied at constant rate – defined as the force applied to the

system divided by the cross-sectional area. An example of stress-strain curve of a thermoplastic material is reported below (**Figure 4.11**).
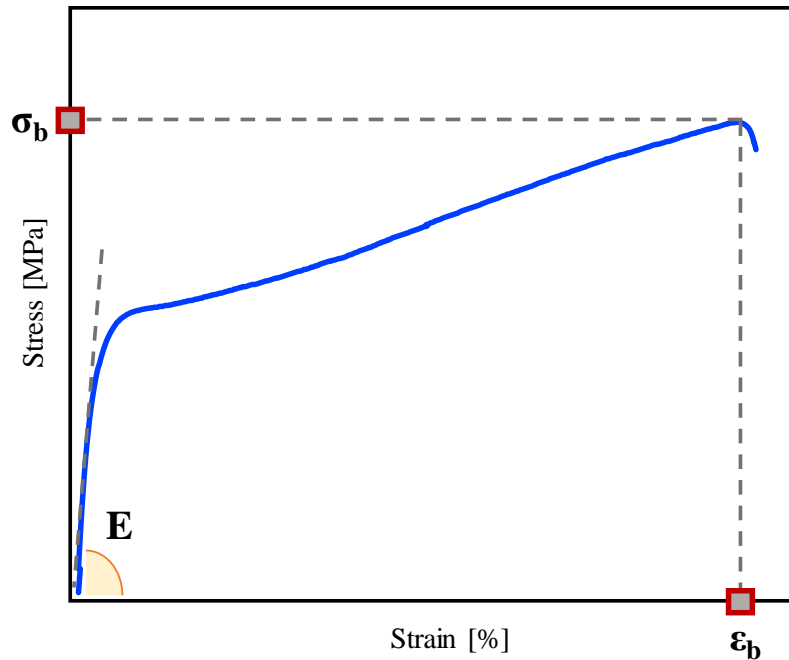
Figure 4.11: Stress strain curve of thermoplastic material.

From stress strain curves, several experimental data can be deducted:

- toughness: defined as the ability of a material to absorb energy and plastically deform without fracturing and identified as the area subtended the strass-strain curve;

- elastic modulus, E: is defined in the elastic region, determined through the slope of stress-strain curve in the initial linear part;

- stress (σ_y) and elongation (ε_y) at yielding: identified as the point of passage from the elastic region to the plastic one;

- stress (σ_b) and elongation (ε_b) at break: the point at which fracture is occurring.

Mechanical properties of polymers are strictly bonded to several factors related to the nature of the macromolecules. The most important elements are: molecular weight, molecular architecture, chain mobility and crystallinity degree. In particular, the molecular weight of the polymer needs to be sufficiently high in order to reach adequate final mechanical response. Moreover, the presence of crystals increases the rigidity and brittleness of the polymer, with a consequent lowering of the elongation at

break; differently, lack of crystals is favoring higher elongation at break and lower elastic modulus. Besides that, the temperature at which the measuring is performed is relevant. This is due to its influence on the chain mobility: polymers at glassy state are characterized by low elongation at break and high elastic modulus; differently, if the chains can move more easily (rubbery state) the elongation at break is increasing[336,337].

In absence of yielding, as observed in thermoplastic elastomers, cyclic measurements can be conducted (**Figure 4.12**). The tests imply the application and removal of defined deformation for an established amount of time. In this way, the elastic return, the ability of the material to resume its initial shape after the removal of the applied stress as well as the energy lost after each cycle (hysteresis), can be evaluated considering the difference in the area defined by the stress relaxation loop.
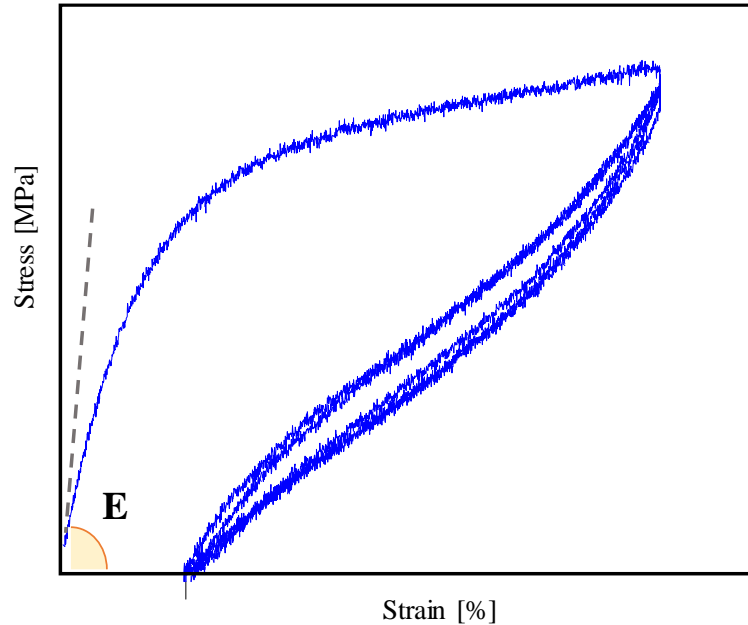
Figure 4.12: Cyclic curve of thermoplastic material.

4.1.8 Barrier properties

Plastics used for food packaging applications boast tunable barrier properties, because of the different nature of the packed products. For example oxygen can react with lipids, changing the color of the edibles, while the increasing of humidity can affect food freshness; differently, CO_2 inhibits the proliferation of a wide range of microorganisms and can extend the storage life of fresh food like meat, since it is incorporate in the envelop and it is necessary to be kept inside the pack[338]. At the same time,

the migration of lipids needs to be limited together with the releasing of additives (antioxidants, colors, and antimicrobial agents)[339].

Barrier properties are based on the capability of materials to hamper the passage of low molecular weight compounds, like gases or organic molecules[340]. The transport through the film depends on two different contributions: solubilization and diffusion (solution-diffusion mechanism, **Figure 4.13**)[341]. In particular, the phenomenon can be described in three phases:

- molecular adsorption: the low molecular weight compounds are dissolving in the surface exposed to the gas (upstream surface);

- molecular diffusion: the compounds are penetrating through the film with a defined gradient;

- molecular desorption: low molecular weight compounds diffuse to the opposite side of the film (downstream surface).
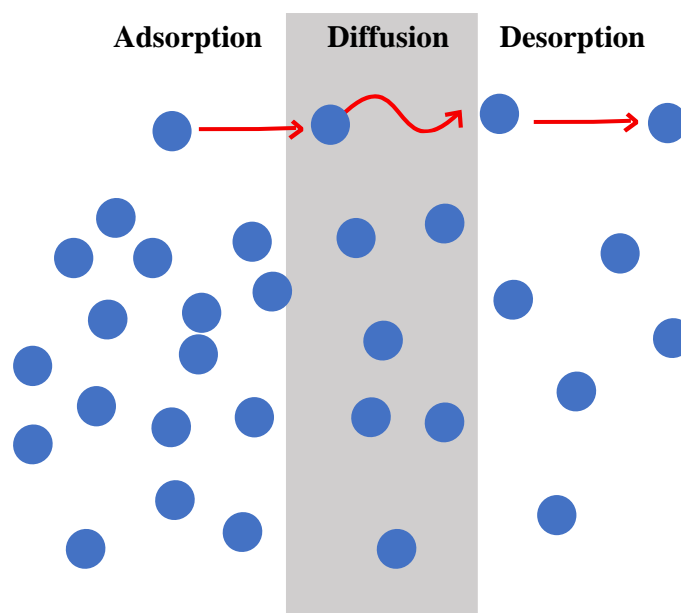
Figure 4.13: Solution-diffusion mechanism.

Thus, the steady state permeability of a certain penetrant P_1 is given by the following equation:

$$P_1 = \frac{J_{1,ss}}{p_1^u - p_1^d} \cdot \frac{l}{M_1} = <S_1> \cdot <D_1> \qquad\qquad Eqn.\ 20$$

Where $<S_1>$ is the average solubility and $<D_1>$ is the diffusivity coefficient. $J_{1,ss}$ represents the steady state diffusive mass flux of the low molecular weight compound penetrating while p_1^u and p_1^d are the

upstream and downstream penetrant partial pressures, respectively; M_1 is the molecular mass of the gas, l is the thickness of polymeric film.

Studying the transient permeation process through the diffusional time lag (τ_L) method, it is possible to define the average diffusion coefficient:

$$\tau_L = \frac{l^2}{6 \cdot <D_1>} \qquad\qquad Eqn.\ 21$$

Where D_1, diffusion coefficient, is the average ability of the molecule to pass through the macromolecules and is regulated by Fick's first law of diffusion. The diffusion coefficient is strictly related to the size of the penetrating molecules, stiffness of polymeric chains, presence of free volume and polymer crystallinity degree. S, solubility coefficient, is regulated by Henry's law and defined as:

$$S = \frac{C_{eq}}{P_i} \qquad\qquad Eqn.\ 22$$

Where C_{eq} is the equilibrium concentration of the dissolved molecules in the membrane and P_i represents the partial pressure in the gas phase. The solubility coefficient depends on several factors, condensability of penetrating molecule, cohesive energy density of the polymeric chains[342] and interactions between polymer and permeant molecule.

Low fractional free volume and high intermolecular cohesion ensure high barrier properties. Indeed, during the diffusion process, the molecules are passing through free volume elements (FVEs) inside the polymer matrix. FVEs are thermally generated nanometric voids, and for this reason are not stable but continuously form and disappear. The penetrating molecules can occupy the voids until another chain motion occurs nearby. Considering the amorphous portion, the voids present are named free volume[343]. Thermal treatments are an efficient tool to modify the free volumes in glassy state polymers, in particular slow cooling is decreasing the formation of voids. Besides that, also the chemical structure can affect the amount of free volume, for instance the presence of polar groups with low specific volumes can decrease the presence of FVEs and favor the chain packaging[344]. Moreover, the chemical structure is also responsible to the affinity with the potential penetrating molecule. If the solubility is low, also the permeability will be low even if the diffusion kinetics is favorable[340]. Crystallinity, another important factor, impacts on solubility and diffusion processes. In particular, these regions are more ordered and denser with respect amorphous parts, precluding the adsorption of molecules. Crystals are acting as

barrier, increasing the length of the path must diffuse through. Particular mechanical stretching, favoring the chain orientation, can modify the barrier properties. This effect is not only due to the oriented lamellar structures that are formed but also to the stress-induced crystallization and the consequent orientation of the amorphous portion[345,346].

Permeation processes have different impact depending on the temperature at which they occur. Indeed, if the temperature of tests is above the T_g of the material, increase in free volume is recorded, because the movements of the macromolecules are favored and the penetrating molecules can cross easily through the material.

In the last few years, liquid crystalline polymers have aroused a lot of interest, thanks to their high mechanical strength and outstanding barrier properties, due to their highly ordered morphology[347]. This behavior is probably due to the presence of short-range ordered structure that hampers the gas diffusion, as previously explained.

The simultaneous presence of the differently ordered phases, i.e. amorphous, mesophase and crystalline, generates great amounts of disclinations/interphases, these last responsible for higher transmission rate of gases through the polymer matrix.

4.1.9 Degradation processes

Biodegradation is defined as "*capability of a material to undergo decomposition into water, carbon dioxide, methane, inorganic compounds and biomass, whether by hydrolysis or by the enzymatic action of microorganisms*"[348], according to the standard regulation (ASTM D6400, ASTM D6866, ASTMD 7081, EN13432). The degradation time is the fundamental parameter to define a material as degradable or not. In particular, degradable materials are degenerating during their application or right after it; while, for non-degradable material the degradation time is longer than their application[349]. Corruption, oxidation/photo-oxidation, hydrolysis, thermal or mechanical stimuli lead to scission of main polymeric chain or side chains. In particular, biodegradable polymers are able to degrade in biological environments (seas, rivers, soil, human body) thanks to living cells or microorganisms as fungi, algae and bacteria. Several studies are carried out in literature regarding the degradation in soil and in compost, the only categories regulated by standard regulations and recognized by the market. In these conditions, microorganisms can catalyze the degradation both under aerobic and anaerobic conditions.

The final products are water, carbon dioxide and biomasses obtained by three steps [350]:

1. bio-deterioration: the chemical and physical properties of the material are modified;

2. bio-fragmentation: the macromolecular chains are broken via enzymatic process;

3. assimilation: the microorganisms are consuming the fragmented molecules;

4. mineralization: the oxidized metabolites are released by the microorganism in the environment.

The process can be described, in aerobic and anaerobic conditions, respectively, as follows:

$$C_{polymer} + O_2 \rightarrow CO_2 + H_2O + C_{residue} + C_{biomass} + salts \qquad Eqn.\ 23$$

$$C_{polymer} + CO_2 \rightarrow CH_4 + H_2O + C_{residue} + C_{biomass} + salts \qquad Eqn.\ 24$$
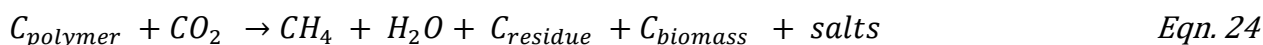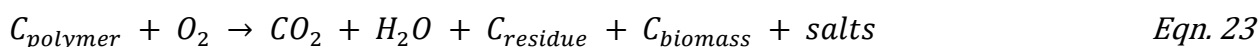
C is representing carbon atoms of polymer chain.

In presence of oxygen, carbon dioxide is produced while, in anaerobic condition, methane is obtained as final product[351].

In vivo degradation processes, taking place in human body, are proceeding via enzymatic or chemical hydrolysis. Specifically, polymers that degrade in this condition are more correctly defined as absorbable, resorbable or bioabsorbable[352]. The process proceeds via two steps:

1. chemical hydrolysis: it is an autocatalytic mechanism, where the broken chains form carboxylic end groups that increase the acidity and accelerate the further hydrolytic degradation;

2. metabolic reactions: nontoxic products are obtained from the conversion of the fragmented polymer. These are easily excreted by metabolism[353].

Degradation process is influenced by different factors, some related to the chemistry of polymeric material- as chemical and stereochemical structure, molecular weight, molecular weight distribution, chain orientation, thermal properties, sequence disposition, presence of unreacted monomers or oligomers- some other to the physic features of the sample - as shape, size and porosity - and also from the environment - as pH and temperature, humidity, presence of microorganisms or enzymes[354]-. In particular, crystallinity is one of the most impacting factors on the degradation rate, indeed enzymatic or

non-enzymatic degradation proceeds faster in amorphous regions due to the easier diffusion of water and enzymes. Subsequently, also crystals can be eventually degraded from the edges inward.

Figure 4.14: Degradation of PLA bottle. Source: yoursustainabledevelopment.com

Ester bonds typical of polyesters can be subjected to hydrolysis and enzymatic scission (for example by lipases), for this reason are considered biodegradable materials (**Figure 4.14**). Despite that, common polyesters as PET or PBT are quite insensitive to hydrolytic degradation, and enzymatic degradation is not effective. The aromatic groups are limiting the accessibility of lipase to ester bonds[355]. Anyway, low molecular weight esters constituted by aromatic ring show hydrolysis processes[356]. Moreover, it is reported that *Thermobifida fusca* is able to depolymerize low crystalline PET used to produce drink bottles with rate of 17 µm/week at a temperature of 55°C. A 100 µm film would totally dissolve in 3 weeks[355].

A possible solution that accelerates the degradation of the most common aromatic polyesters is the introduction of aliphatic subunits, which enhance both water uptake and speed up hydrolytic chain scission. One commercial example is represented by Ecoflex®, which, as mentioned before, is compostable. The process do not provide aromatic oligomers, and no ecotoxic effects are observed[357].

4.1.9.1   Hydrolytic degradation

Hydrolytic degradation is a bulk process, involving a reaction between water and some specific functional groups of polymeric chains, which causes scission of the macromolecules in oligomers and, later, in monomers. Firstly, water molecules, by imbibition in matrix or by accessing the surface of the material, react via nucleophilic attack with the electron rich macromolecule sites causing the breaking of the bonds[358,359]. The hydrolysis reaction can be catalyzed by enzymes but also by acid or base chemicals. In the light of this, the presence of hydrolysable functional groups such those present in ethers, esters,

orthoesters, anhydrides, carbamides, amides, or ester amides[360] is fundamental to allow the degradation process. In particular, the chemical nature of these functional groups is strictly connected to the hydrolytic rate. Those characteristics of orthoesters and anhydrides are reacting more readily than the other cited ones. Another important factor to consider is the hydrophilicity/hydrophobicity ratio of the material; hydrophilic polymers are able to retain large amounts of water, degrading consequentially faster than hydrophobic polymers[349]. Moreover, the degradation process can take place at the surface, as homogeneous phenomenon, or in heterogeneous condition, in bulk. The actual way by which the degradation proceeds, is influenced by several factors as the matrix dimensions, the degradation rate of the functional groups of the polymer and the diffusion of water inside the system[361]. When the diffusion of water is happening more readily than the scission of polymeric bonds, bulk erosion is the predominant mechanism. Differently, when the polymeric chains are degraded faster than the diffusion of water molecules, the degradation occurs at the surface[361].

Other relevant aspect is the presence of crystals/mesophase. Indeed, the ordered phase hampers the accessibility of water, limiting the degradation of the amorphous zone[362].

Considering the specific case of aliphatic polyesters, the hydrolytic process is mainly happening via bulk degradation. Firstly, a random cleavage of the chains is observed, causing a significant decreasing of molecular weight, but negligible gravimetric weight losses, with a consequent impact on the mechanical properties. Then, oligomers are obtained and if small enough can dissolve in the solution/medium[363]. In this case, gravimetric weight loss starts to be measurable and of course increases with incubation time.

4.1.9.2 Biodegradation in compost

Materials capable to degrade in compost (**Figure 4.15**) are defined as compostable. With the growing interest around this new class of compounds, several standard regulations as ISO and ASTM define a series of requirements necessary to assess the word "biodegradable". In particular, ASTM D 6400 and ASTM D 6002-96 standards consider the composting process as a biological action of decomposition and transformation of materials in substances called "compost". In order to reach this state, that is, to be considered compostable, a material should satisfy additional requirements as[364] :

-   a final conversion for 90% into carbon dioxide and less than 10% into residual material with a size of 2 mm;

-   under micro-bacterial action, a decomposition into water, carbon dioxide, and biomass;

- a rate of degradation comparable with the other known compostable materials as leaves, grass, paper;

- the total amount of time needed to degrade should be less than 180 days;

- there must be no negative effects on the composting process.

Figure 4.15: Production of compost. Source: www.ideagreen.it

According to Compost Council of Canada, to obtain high amount of biological activity, the compost has to satisfy some parameters as[365]:

- adequate amount of nutrients (carbonaceous materials and nitrogenous materials) and humidity (from nitrogenous materials, rainfall and water) must be supplied during the process;

- good air circulation, strictly connected to the porosity of the substrate and fundamental for oxidation and metabolization of organic compounds;

- proper temperature to development of micro-organisms;

- adequate pH for every phase of the process: 9 for the initial oxidation, 7-7.5 for the end of the maturation phase.

The degradation process has been deeply studied and three main phases have been identified[365,366].

Phase 1.) Mesophilic phase: lipids, monosaccharides and starch are degraded by fungi and mesophilic bacteria to soluble organic matter compounds. The organic acids produced decrease the pH to 5-5.5, while the temperature of the system is increasing because of the exothermic nature of process of degradation. Besides that, the degradation of proteins produces ammonia, that rises the pH to 8-9.

Phase 2.) Thermophilic phase: once the temperature reaches 40°C, the degradation rate is higher thanks to the presence of thermophilic bacteria and fungi. The temperature is continuing increasing until 55-60°C, where the biological activity decreases. This phase takes from some days to months.

Phase 3.) Cooling and maturation phase: after the degradation of the more accessible and easy carbon sources, compost becomes stable and cools down. Mesophilic bacteria together with actinomycetes, protists, fungi and macro-organisms populate the system. Then, maturation phase starts and the biological processes are slowing down; the compost, humidifying, is becoming mature.

The over mentioned steps have different durations, depending on the efficiency of the process, defined by the amount of oxygen consumption[364] and the composition of the organic matter.

Degradation of materials can be followed by measuring gravimetric weight loss of sample. The process indeed occurs as surface erosion process. Interesting is the Sturm Test, consists in the measurement of carbon dioxide evolved during degradation, to estimate the biodegradability of materials[350].

4.2 Applications

4.2.1 Food packaging

As reported from Plastics Europe annual report 2018, almost 40% of plastic is applied in packaging field, mainly related to food sector[367]. Thanks to the good barrier properties, adequate mechanical response and low cost, polyethylene (PE), polypropylene (PP) and PET are the main materials used[17]. It is clear that materials for food packaging should be versatile, with mechanical behavior, optical and barrier properties easy to tailor. General properties present in the most common materials used for food packaging application are flexibility and toughness, to ensure manipulation during transport and protection of food. On the light of this, flexible packaging is the main class of envelop used for edible products, covering the 39% of total packaging market. Moreover, in 2021 the volume is expected to increase by 11%. The use of films in this sector is really popular, indeed are occupying the 46% of the total amount of flexible packaging market; polyethylene (41%), polypropylene (28%), polyester (16%), Nylon (13%) and polystyrene (<1%) are the most common polymers used. Filmed materials can be easily folded, reducing the final waste volume, furthermore can decrease the weight/volume of the products lowering the energy needed for the transport[368,369].

Figure 4.16: Different types of foods packed. Source: www.meteoweb.eu

During the design of films for food packaging application, also all the chemical and enzymatic reactions, together with physical changing of the organic material (food), have to be taken into account. In this context, packaging is playing an important role, maintaining the nutritional, structural and chemical properties, hampering chemical and biological contamination. For example, products affected by degradation due to moisture need to be packed using materials with low permeation to the water vapor, while fresh fruits and vegetables (**Figure 4.16**) need a controlled environment to extend their shelf life, in particular a reduction of oxygen passage must be guaranteed, in order to limit oxidation and the production of ethylene[370]. To improve food quality and safety, new class of smart and active packaging are currently tested. For example, through modified atmosphere packaging (MAP)[371] (see **Figure 4.17**), is possible to control the atmosphere inside the package, maintaining the environment as natural as possible[372]. In this way, chlorophyll degradation is controlled by varying oxygen, nitrogen and carbon dioxide concentrations, together with the production of ethylene[373–375].
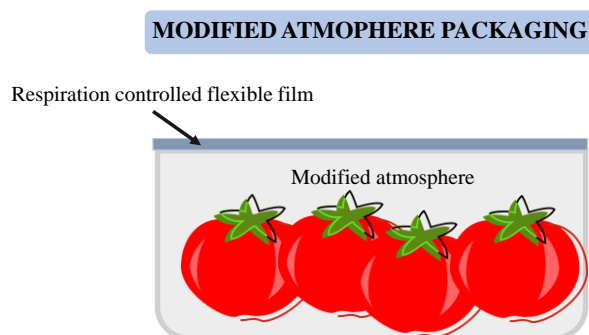
Figure 4.17: Typical structure of MAP.

Moreover, in order to extend the quality of edibles, plastic films are successfully laminated with different materials as aluminum foil or paper by co-extrusion or lamination production technology. This type of

packaging is usually named as "multilayer flexible packaging" (MFP), **Figure 4.18**, and is covering the 17% of all produced packaging films.

Figure 4.18: Some example of multilayer films. Source: weiyi-packaging.en.alibaba.com.

A two-layer package is projected with an inner layer side facing the product and an outer layer, resisting against abrasion and printable. The inner material is sealable and helps to maintain low-temperature inside the pack and is contributing to barrier performance. Ethylene-vinyl acetate (EVA), LDPE, linear-low-density polyethene (LLDPE) are standardly used to compose the inner items[376]. Due to lack of stiffness, structural integrity, and abrasion resistance the inner layer is combined with an outer one. In particular, the used of HDPE increases moisture resistance, while PA are employed for their exceptional mechanical properties; oriented PET films guarantee excellent surface for printing. Paper is also applied as outer layer, for its low-cost and is used in pouches and bags[376]. Adding a layer more, three-layer packaging, provides even more flexibility in packaging design.
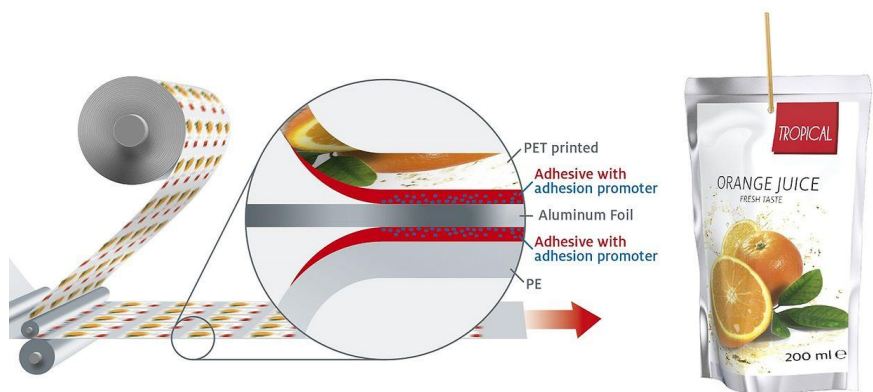
Figure 4.19; Example of five-layered films. Source: www.henkel.com.

The inner layer maintains the sealability as main function, while the outer layer is supposed to provide structural integrity, abrasion resistance and give a printable surface. The additional central layer can provide a variety of functions in accordance with the application: a very good oxygen barrier is given by

Ethylene-vinyl Alcohol (EVOH) or by a metallized layer; also a layer of recycled material can be incorporated into the center layer, being not allowed its direct contact with food, as specified in Regulation (EU) No 10/2011[376–378] . Moreover, in order to help the adhesion between two dissimilar materials an adhesive can be added in the central part. On the market we find up to five-layer films (**Figure 4.19**), the centered layer, often surrounded by two adhesive layers that help the adhesion of the most external and the most internal layers, as usually happens in case of barrier films containing PA-6 or EVOH, because of their poor adhesion to most common external layers and sealants. An overview of commonly used materials and their respective functions is shown in **Table 4.1**.

Table 4.1:*Overview of common functional layers* [376,378,379]

Mechanical Stability	Moisture Barrier	Oxygen Barrier	Light Barrier	Tie Layers	Sealant
HDPE PP, OPP OPET PS Paper	PE (LD, LLD, HD) PP, OPP, EVA, PVDC, Ionomers	EVOH PVDC polyamides(nylon) coatings (SiOx,Al2O3, PVOH, nanoparticles) Aluminum	Aluminum TiO$_2$ filled polymers	Polyurethanes Acid/anhydride Grafted polyolefins	LLDPE, LDPE, EVA, Ionomers, PP,OPP, PA, OPA, PET, OPET

Currently, the broad use of multilayer films suffers a contraction, due to their low environmental-friendly nature. Indeed, the complex multilayer structure hampers their recyclability, and consequently in most of the cases, film wastes are destined for landfill or incineration. This is absolutely not in line with the development of circular economy; in addition, for the production of most of them, large amounts of fossil finite resources are utilized. Considering the short life of packaging films, the market urgently needs to find alternative products. Synthetic biopolymers are a valid solution to overcome the problem of common multilayer films[380]. Biopolymeric films have to present particular characteristics, due to the complexity of the edible substances and to preserve or even prolong their shelf life (**Figure 4.16**). Therefore, not all the polymers can be applied in packaging sector.

The most important class of polymeric materials applied in this field are[97]:

- cellulose-based polyesters: due to the poor mechanical properties of the virgin material, the research is meanly focused on derivates. Good results have been obtained from cellulose acetate, whose film are used for fresh and cooked foods, but the poor barrier properties and the sensibility to hydrolysis are hampering their diffusion;

- starch-based polyesters: they are covering the higher volume in the market of biodegradable materials, thanks to their low permeability to oxygen. However, their hydrophilicity is still hampering the use in humid conditions;

- polyhydroxyalkanoates: the most widely used is PHB, that shows thermal properties and mechanical behavior similar to those of polypropylene (PP). However, fragility and rigidity of PHB together with high cost of production are undermining the success of this material in packaging field.

5 BIBLIOGRAPHY

1. Brydson, J. A. *Platics Materials*. (Butterworth-Heinemann, 1999).

2. Association of Plastics manifacturors. Plastics -The facts 2018. *Plast. Eur.* 1–57 (2018). doi:10.1016/j.marpolbul.2013.01.015

3. Andrady, A. L. Microplastics in the marine environment. *Mar. Pollut. Bull.* **62**, 1596–1605 (2011).

4. Peter G.R., Moore, C. J., van F. A. J. Monitoring the abundance of plastic debris in the marine environment. *Philos. Trans. R. Soc. B Biol. Sci.* **364**, 1999 (2009).

5. Barnes, D. K. A., Galgani, F., Thompson, R. C. Accumulation and fragmentation of plastic debris in global environments. *Philos. Trans. R. Soc.* **B 364**, 1985–1998 (2009).

6. Geyer, R., Jambeck, J. R., Law, K. L. Production, use, and fate of all plastics ever made. *Sci. Adv.* **3**, 25–29 (2017).

7. Lebreton, L., Slat, B., Ferrari, F., Sainte-Rose, B., Aitken, J., Marthouse, R., Noble, K. Evidence that the Great Pacific Garbage Patch is rapidly accumulating plastic. *Sci. Rep.* **8**, 1–15 (2018).

8. Richard C. Thompson R. C, Olsen, Y., Mitchell, R. P., Davi, A., Rowland, S. J., McGonigle, D. Lost at Sea: Where Is All the Plastic? *Science.* **304**, 838 (2004).

9. Wagner, M., Scherer, C., Alvarez-Muñoz, D., Brennholt, N., Bourrain, X., Buchinger, S., Fries, E., Grosbois, C., Klasmeier, J., Marti, T., Rodriguez-Mozaz, S. Urbatzka, R., Vethaak, A. D., Winther-Nielsen, M. Microplastics in freshwater ecosystems: What we know and what we need to know. *Environ. Sci. Eur.* **26**, 12 (2014).

10. Rillig, M. C. Microplastic in terrestrial ecosystems and the soil? *Environ. Sci. Technol.* **46**, 6453–6454 (2012).

11. Zubris, K. A. V. Synthetic fibers as an indicator of land application of sludge. *Environ. Pollut.* **138**, 201–211 (2005).

12. European Commission. Being wise with waste : the EU ' s approach to waste management. *Publ. Off. Eur. Union* 20 (2010). doi:10.2779/93543

13. Directive (2008/98/EC). Directive 2008/98/EC of the European Parliament.. *Off. J. Eur. Union* 3–30 (2008). doi:2008/98/EC.; 32008L0098

14. Gigli, M., Fabbri, M., Lotti, N., Gamberini, R., Rimini, B., Munari, A. (Poly(butylene succinate)-based polyesters for biomedical applications: A review in memory of our beloved colleague and friend Dr. Lara Finelli. *Eur. Polym. J.* **75**, 431–460 (2016).

15. Nakajima, H., Dijkstra, P., Loos, K. The recent developments in biobased polymers toward general and engineering applications: Polymers that are upgraded from biodegradable polymers,

analogous to petroleum-derived polymers, and newly developed. *Polymers (Basel).* **9**, 1–26 (2017).

16. Kale, G., Kijchavengkul, T., Auras, R., Rubino, M., Selke, S. E., Singh, S. P. Compostability of bioplastic packaging materials: An overview. *Macromol. Biosci.* **7**, 255–277 (2007).

17. Siracusa, V., Rocculi, P., Romani, S., Rosa, M. D. Biodegradable polymers for food packaging: a review. *Trends Food Sci. Technol.* **19**, 634–643 (2008).

18. Gross, R. A., Kalra, B. Biodegradable polymers for the environment. *Science,* **297**, 803–807 (2002).

19. European Bioplastics e.V. Available at: https://www.european-bioplastics.org/.

20. Yates, M. R., Barlow, C. Y. Life cycle assessments of biodegradable, commercial biopolymers - A critical review. *Resour. Conserv. Recycl.* **78**, 54–66 (2013).

21. Cok, B., Tsiropoulos I., Roses, A. L. Green building blocks for bio-based plastics. *Biofuels, Bioprod. Biorefining* **8**, 246–256 (2014).

22. Bechthold, I., Bretz, K., Kabasci, S., Kopitzky, R., Springer, A. Succinic acid: A new platform chemical for biobased polymers from renewable resources. *Chem. Eng. Technol.* **31**, 647–654 (2008).

23. Frost, J. W. US 9499465 B2 (2016).

24. Frost, J.W. Miermont, A.D. Schweitzer, V. Bui, E. Paschke, J.W. Frost, A. Miermont, D. Schweitzer, V. Bui, E. Paschke, D.A. Wicks, 2011/0288263 A1 (2011).

25. Bramucci, US 6 187 569 B1 (2001).

26. B. Cok, I. Tsiropoulos, A. L. R. Succinic acid production derived from carbohydrates: An energy and greenhouse gas assessment of a platform chemical toward a bio-based economy. *BIOFUEL BIOPROD BIOR* **8**, 16–29 (2014).

27. He, J., Huang, K., Barnett, K. J., Krishna, S. H., Alonso, D. M., Brentzel, Z. J., Hermans, I. New catalytic strategies for α,ω-diols production from lignocellulosic biomass. *Faraday Discuss.* **202**, 247–267 (2017).

28. Nakagawa, Y., Tomishige, K. Production of 1,5-pentanediol from biomass via furfural and tetrahydrofurfuryl alcohol. *Catal. Today* **195**, 136–143 (2012).

29. Montero De Espinosa, L., Meier, M. Plant oils: The perfect renewable resource for polymer science?! *Eur. Polym. J.* **47**, 837–852 (2011).

30. M. Van der Steen, C.V. Stevens. Undecylenic acid: a valuable and physiologically active renewable building block from castor oil. *ChemSusChem* **2**, 692–713 (2009).

31. Gandini, A., The irruption of polymers from renewable resources on the scene of macromolecular science and technology. *Green Chem* **13**, (2011).

32. Lligadas, G., Ronda, J. C., Galiá, M., Cádiz, V. Plant oils as platform chemicals for polyurethane synthesis: Current state-of-the-art. *Biomacromolecules* **11**, 2825–2835 (2010).

33. Y. Xia, R.C. Laroc. Vegetable oil-based polymeric materials: synthesis, properties, and applications. *Green Chem.* **12**, (2010).

34. Biermann, U. Oils and fats as renewable raw materials in chemistry. *Chem Int Ed* **50**, (2011).

35. Meier, M., Metzger, J.O., Schubert, U.S. Plant oil renewable resources as green alternatives in polymer science. *Chem Soc Rev* **36**, (2007).

36. Wilbon, P. A., Chu, F., Tang, C. Progress in renewable polymers from natural terpenes, terpenoids, and rosin. *Macromol. Rapid Commun.* **34**, 8–37 (2013).

37. Winnacker, M., Rieger, B. Recent Progress in Sustainable Polymers Obtained from Cyclic Terpenes: Synthesis, Properties, and Application Potential. *ChemSusChem* **8**, 2455–2471 (2015).

38. Thomsett, M. R., Storr, T. E., Monaghan, O. R., Stockman, R. A., Howdle, S. M. Progress in the synthesis of sustainable polymers from terpenes and terpenoids. *Green Mater.* **4**, 115–134 (2016).

39. Byrne, C. M., Allen, S. D., Lobkovsky, E. B., Coates, G. W. Alternating copolymerization of limonene oxide and carbon dioxide. *J. Am. Chem. Soc.* **126**, 11404–11405 (2004).

40. Chen, Y. Z., Wu, L. Z., Zhang, L. P., Tung, C. H. Confined space-controlled hydroperoxidation of trisubstituted alkenes adsorbed on pentasil zeolites. *J. Org. Chem.* **70**, 4676–4681 (2005).

41. Thomsett, M. R., Moore, J. C., Buchard, A., Stockman, R. A., Howdle, S. M. New renewably-sourced polyesters from limonene-derived monomers. *Green Chem.* **21**, 149–156 (2019).

42. Kobayashi, S., Lu, C., Hoye, T. R., Hillmyer, M. A. Controlled polymerization of a cyclic diene prepared from the ring-closing metathesis of a naturally occurring monoterpene. *J. Am. Chem. Soc.* **131**, 7960–7961 (2009).

43. Lowe, A. B. Thiol-ene 'click' reactions and recent applications in polymer and materials synthesis: A first update. *Polym. Chem.* **5**, 4820–4870 (2014).

44. Firdaus, M., Montero De Espinosa, L., Meier, M. Terpene-based renewable monomers and polymers via thiol-ene additions. *Macromolecules* **44**, 7253–7262 (2011).

45. Firdaus, M., Meier, M. Renewable polyamides and polyurethanes derived from limonene. *Green Chem.* **15**, 370–380 (2013).

46. Hauenstein, O., Reiter, M., Agarwal, S., Rieger, B., Greiner, A. Bio-based polycarbonate from limonene oxide and CO2 with high molecular weight, excellent thermal resistance, hardness and transparency. *Green Chem.* **18**, 760–770 (2016).

47. Roth, S., Funk, I., Hofer, M., Sieber, V. Chemoenzymatic Synthesis of a Novel Borneol-Based Polyester. *ChemSusChem* **10**, 3574–3580 (2017).

48. Parrino, F., Fidalgo, A., Palmisano, L., Ilharco, L. M., Pagliaro, M., Ciriminna, R. Polymers of Limonene Oxide and Carbon Dioxide: Polycarbonates of the Solar Economy. *ACS Omega* **3**,

4884–4890 (2018).

49. Stamm, A., Tengdelius, M., Schmidt, B., Engström, J., Syrén, P. O., Fogelström, L., Malmström, E. Chemo-enzymatic pathways toward pinene-based renewable materials. *Green Chem.* **21**, 2720–2731 (2019).

50. Berti, C., Binassi, E., Colonna, M., Fiorini, M., Kannan, G., Karanam, S. Synthesis and radiocarbon evidence of terephthalate polyesters completely prepared from renewable resources, Green Chem. **13**, 2543-2548 (2011).

51. Werpy, T., Petersen, G. Volume I - Results of Screening for Potential Candidates from Sugars and Synthesis Gas. *Top Value Added Chem. from Biomass* 76 (2004). doi:10.2172/15008859

52. *National Renewable Energy Laboratory: Golden*. (2004).

53. van Putten, R. J., Van Der Waal, J. C., De Jong, E. D., Rasrendra, C. B., Heeres, H. J., de Vries, J. GHydroxymethylfurfural, a versatile platform chemical made from renewable resources. *Chem. Rev.* **113**, 1499–1597 (2013).

54. Ray, P., Smith, C., Simon, G. P., Saito, K. Renewable green platform chemicals for polymers. *Molecules* **22**, 14–16 (2017).

55. De Jong, E., Dam, M. A., Sipos, L., Gruter, G. J. M. Furandicarboxylic acid (FDCA), A versatile building block for a very interesting class of polyesters. *ACS Symp. Ser.* **1105**, 1–13 (2012).

56. Choomwattana, C., Chaianong, A., Kiatkittipong, W. Chemical Engineering and Processing : Process Intensi fi cation Process integration of dimethyl carbonate and ethylene glycol production from biomass and heat exchanger network design $. *Chem. Eng. Process. Process Intensif.* **107**, 80–93 (2016).

57. Zhang, H., Liu, H., Yue, J. Organic Carbonates from Natural Sources. (2014). doi:10.1021/cr300430e

58. Tundo, P., Selva, M. The chemistry of dimethyl carbonate. *Acc. Chem. Res.* **35**, 706–716 (2002).

59. Schäffner, B., Schäffner, F., Verevkin, S. P., Börner, A. Organic carbonates as solvents in synthesis and catalysis. *Chem. Rev.* **110**, 4554–4581 (2010).

60. M. Selva, M. Noè, A. P. Carbonate, acetate and phenolate phosphonium salts as catalysts in transesterification reactions for the synthesis of non-symmetric dialkyl carbonates. *Org. Biomol. Chem.* **10**, 6569–6578 (2012).

61. Deshmukh, K. M., Qureshi, Z. S., Dhake, K. P., Bhanage, B. M. Transesterification of dimethyl carbonate with phenol using Brønsted and Lewis acidic ionic liquids. *CATCOM* **12**, 207–211 (2010).

62. S. Fukuoka, M. Kawamura, K. Komiya, M. Tojo, H. Hachiya, K. Hasegawa, M. Aminaka, H. Okamoto, I. F. novel non-phosgene polycarbonate production process using by-product CO2 as starting material. *Green Chem.* **497**–**507**, (2003).

63. Gross, S. M., Bunyard, W. C., Erford, K., Roberts, G. W., Kiserow, D. J., DeSimone, J. M. Determination of the Equilibrium Constant for the Reaction between Bisphenol A and Diphenyl Carbonate. 171–178 (2001). doi:10.1002/pola.10098

64. Shaikh, A. G. Organic Carbonates. (1996). doi:10.1021/cr950067i

65. Hermes, M. E. *Enough for One Lifetime: Wallace Carothers, Inventor of Nylon*. (1996).

66. Carothers, W. H., E. I. du Pont de Nemours and Company, Patent 2 071 250 (1931).

67. Carothers, W. H., E. I. du Pont de Nemours and Company, Patent 2 071 251 (1937).

68. Novamont, (2016).

69. Ma, J., Yu, X., Xu, J., Pang, Y. Synthesis and crystallinity of poly(butylene 2,5-furandicarboxylate). *Polymer (Guildf).* **53**, 4145–4151 (2012).

70. He, Y. C., Wu, Y. D., Pan, X. H., Ma, C. L. Biosynthesis of terephthalic acid, isophthalic acid and their derivatives from the corresponding dinitriles by tetrachloroterephthalonitrile-induced Rhodococcus sp. *Biotechnol. Lett.* **36**, 341–347 (2014).

71. Zhu, J., Cai, J., Xie, W., Chen, P. H., Gazzano, M., Scandola, M., Gross, R. A. Poly(butylene 2,5-furan dicarboxylate), a biobased alternative to PBT: Synthesis, physical properties, and crystal structure. *Macromolecules* **46**, 796–804 (2013).

72. Gómez, F., Quintana, R., De Ilarduya, A. M., Rudé, E., Muñoz-Guerra, S. Poly(butylene terephthalate-co-5-tert-butyl isophthalate) copolyesters: Synthesis, characterization, and properties. *J. Polym. Sci. Part A Polym. Chem.* **43**, 92–100 (2005).

73. Díaz, A., Katsarava, R., Puiggalí, J. Synthesis, properties and applications of biodegradable polymers derived from diols and dicarboxylic Acids: From Polyesters to poly(ester amide)s. *Int. J. Mol. Sci.* **15**, 7064–7123 (2014).

74. Kim, Y. B., Lenz, R. W., Babel, W. and Steinbuchel, A. Polyesters from Micro-organisms. in *In Advances in Biochemical Engineering/Biotechnology* (ed. Springer-Verlag) (Eds, 2001).

75. Barnes, C. E. Chemical Nature of Shellac. *Ind. Eng. Chem.* **30**, 449–451 (1938).

76. Okada, M. Chemical syntheses of biodegradable polymers. *Prog. Polym. Sci.* **27**, 87–133 (2002).

77. Lemoigne, M. Etudes sur L'autolyse Microbienne Acidification par Formation D'acide β-Oxybutyrique. *Ann. Inst. Pasteur* **39**, 144 (1925).

78. Lemoigne, M. Études sur l'autolyse microbienne origine de l'acide β-oxybutyrique formé par autolyse. *Ann. Inst. Pasteur* **41**, 148 (1927).

79. Scheirs, J. T. Modern polyesters: chemistry and technology of polyesters and copolyesters in *The Historical Development of Polyesters* (2003).

80. Kootstra, M., Elissen, H. *PHA's (Polyhydroxyalkanoates): General information on structure and raw materials for their production*. (2017).

81. Lourenço, A. V. Annales de Chimie et de Physique. *Ann. Chim. Phys.* **67**, (1863).

82. Carothers, W. H. Studies on polymerization and ring formation. I. An introduction to the general theory of condensation polymers. *J. Am. Chem. Soc.* **51**, 2548–2559 (1929).

83. Showa Denko. Available at: http://www.showa-denko.com.

84. Babu, R. P., O'Connor, K., Seeram, R. Current progress on bio-based polymers and their future trends. *Prog. Biomater.* **2**, 8 (2013).

85. Delhomme, C., Weuster-Botz, D., Kühn, F. E. Succinic acid from renewable resources as a C4 building-block chemical - A review of the catalytic possibilities in aqueous media. *Green Chem.* **11**, 13–26 (2009).

86. Ong, K. L., Fickers, P., Lin, C. Enhancing succinic acid productivity in the yeast Yarrowia lipolytica with improved glycerol uptake rate. *Sci. Total Environ.* **702**, 134911 (2020).

87. Dominguez de Maria, P. *Industrial Biorenewables: A Practical Viewpoint* (John Wiley & Sons, 2016).

88. Myriant Corporation.

89. Bikiaris, D. N., Achilias, D. S. Synthesis of poly(alkylene succinate) biodegradable polyesters, Part II: Mathematical modelling of the polycondensation reaction. *Polymer (Guildf).* **49**, 3677–3685 (2008).

90. Howe-Grant, M. Encyclopedia of chemical technology, vol 11, (Wiley, New York,1991).

91. Ihn, K. J., Yoo, E. S., Im, S. S., Ihn, K. J. Structure and Morphology of Poly(tetramethylene succinate) Crystals. *Macromolecules* **28**, 2460–2464 (1995).

92. Yoo, E. S., Im, S. S. Melting behavior of poly(butylene succinate) during heating scan by DSC. *J. Polym. Sci. Part B Polym. Phys.* **37**, 1357–1366 (1999).

93. Yue, W., Zhao, Y., Shao, S., Tian, H., Xie, Z., Geng, Y., Wang, F. Novel NIR-absorbing conjugated polymers for efficient polymer solar cells: effect of alkyl chain length on device performance. *J. Mater. Chem.* **19**, 2199 (2009).

94. Xu, J., Guo, B. H. Poly(butylene succinate) and its copolymers: Research, development and industrialization. *Biotechnol. J.* **5**, 1149–1163 (2010).

95. Gualandi, C., Soccio, M., Saino, E., Focarete, M. L., Lotti, N., Munari, A., Visai, L. Easily synthesized novel biodegradable copolyesters with adjustable properties for biomedical applications. *Soft Matter* **8**, 5466–5476 (2012).

96. Gigli, M., Negroni, A., Soccio, M., Zanaroli, G., Lotti, N., Fava, F., Munari, A. Influence of chemical and architectural modifications on the enzymatic hydrolysis of poly(butylene succinate). *Green Chem.* **14**, 2885–2893 (2012).

97. Liu, Z. Edible films and coatings from starches in *Innovations in food packaging* (pp. 318-337). (Academic Press, Elsevier, 2005).

98. Eslami, H., Kamal, M. R. Effect of a chain extender on the rheological and mechanical properties of biodegradable poly(lactic acid)/poly[(butylene succinate)-co-adipate] blends. *J. Appl. Polym. Sci.* **129**, 2418–2428 (2013).

99. Wang, Z., Li, W., Zhao, X., Zhu, D., You, J. Self-segregation behavior of n-ethyl-pentadecafluorooctanamide-terminated polybutylene isophthalate and its effects on film morphology and wettability. *J. Phys. Chem. B* **113**, 15204–15211 (2009).

100. Fujimaki, T. Processability and properties of aliphatic polyesters, 'BIONOLLE', synthesized by polycondensation reaction. *Polym. Degrad. Stab.* **59**, 209–214 (1998).

101. Berti, C., Celli, A., Marchese, P., Marianucci, E., Barbiroli, G., Di Credico, F. Influence of molecular structure and stereochemistry of the 1,4-cyclohexylene ring on thermal and mechanical behavior of poly(butylene 1,4-cyclohexanedicarboxylate). *Macromol. Chem. Phys.* **209**, 1333–1344 (2008).

102. Berti, C., Binassi, E., Celli, A., Colonna, M., Fiorini, M., Marchese, P., Marianucci, E., Gazzano, M., Di Credico, F. Poly(1,4-cyclohexylenedimethylene 1,4- cyclohexanedicarboxylate): Influence of Stereochemistry of 1,4-Cyclohexylene Units on the Thermal Properties. **46**, 619–630 (2008).

103. Genovese L., Lotti N., Gazzano M., Finelli L. New eco-friendly random copolyesters based on poly(propylene cyclohexanedicarboxylate): Structure-properties relationships. *Express Polym. Lett.* **9**, 972–983 (2015).

104. Gigli, M., Lotti, N., Vercellino, M., Visai, L., Munari, A. Novel ether-linkages containing aliphatic copolyesters of poly(butylene 1,4-cyclohexanedicarboxylate) as promising candidates for biomedical applications. *Mater. Sci. Eng. C* **34**, 86–97 (2014).

105. Guidotti, G., Soccio, M., Siracusa, V., Gazzano, M., Munari, A., Lotti, N. Novel random copolymers of poly(butylene 1,4-cyclohexane dicarboxylate) with outstanding barrier properties for green and sustainable packaging: Content and length of aliphatic side chains as efficient tools to tailor the material's final performance. *Polymers (Basel).* **10**, (2018).

106. Siracusa, V., Genovese, L., Ingrao, C., Munari, A., Lotti, N. Barrier properties of poly(propylene cyclohexanedicarboxylate) random eco-friendly copolyesters. *Polymers (Basel).* **10**, (2018).

107. Gigli, M., Lotti, N., Gazzano, M., Siracusa, V., Finelli, L., Munari, A., Dalla Rosa, M. Fully aliphatic copolyesters based on poly(butylene 1,4- cyclohexanedicarboxylate) with promising mechanical and barrier properties for food packaging applications. *Ind. Eng. Chem. Res.* **52**, 12876–12886 (2013).

108. Calico Printers Association, Whinfield, J. R. and Dickson, J. T. (1946).

109. Ludewig, H. *Polyester Fibres: Chemistry and Technology* (1971).

110. Bobingen, A.G. für Textil-Faser (Schlack, P.) (1955).

111. Plastics Europe, G. M. R. & Conversio Market & Strategy GmbH. Plastics - the Facts 2019. (2019).

112. Colonna, M., Berti, C., Fiorini, M., Binassi, E., Mazzacurati, M., Vannini, M., Karanam, S. Synthesis and radiocarbon evidence of terephthalate polyesters completely prepared from renewable resources. *Green Chem.* **13**, 2543–2548 (2011).

113. Linstead, R. P. *J. Chem. Soc.* **0**, 1139– 1147 (1940).

114. Weyrich, P. A., Hölderich, W. F. Dehydrogenation of α-limonene over Ce promoted, zeolite supported Pd catalysts. *Appl. Catal. A Gen.* **158**, 145–162 (1997).

115. Buhl, D., Roberge, D. M., Hölderich, W. F. Production of p-cymene from α-limonene over silica supported Pd catalysts. *Appl. Catal. A Gen.* **188**, 287–299 (1999).

116. Martin-Luengo, M. A., Yates, M., Rojo, E. S., Arribas, D. H., Aguilar, D., Hitzky, E. R. Sustainable p-cymene and hydrogen from limonene. *Appl. Catal. A Gen.* **387**, 141–146 (2010).

117. Pines, H., Schaap, L. Sodium and Potassium Alkoxides as Catalysts for Carbanion Reactions of Hydrocarbons. *J. Am. Chem. Soc.* **79**, 2956–2958 (1957).

118. Stanislaus, A., Yeddanapalli, L. M. Vapor Phase Catalytic Transformations of Terpene Hydrocarbons in the C 10 H 16 Series. II. Aromatization of α-Pinene over Chromia–Alumina . *Can. J. Chem.* **50**, 113–118 (1972).

119. Roberge, D. M., Buhl, D., Niederer, J. P. M., Hölderich, W. F. Catalytic aspects in the transformation of pinenes to p-cymene. *Appl. Catal. A Gen.* **215**, 111–124 (2001).

120. Bazhenov, Y. P., Kas' yanova, L. Z., Bokin, A. I., Kutepov, B. I., Khazipova, A. N., Travkin, E. A., Dzhemilev, U. M. Hydrogenation and Skeleton Rearrangements of α-Pinene on Heterogeneous Catalysts. *Russ. J. Appl. Chem.* **76**, 234–237 (2003).

121. Golets, M., Ajaikumar, S., Mohln, M., Wärnå, J., Rakesh, S., Mikkola, J. P. Continuous production of the renewable ρ-cymene from α-pinene. *J. Catal.* **307**, 305–315 (2013).

122. Leita, B. A., Warden, A. C., Burke, N., O'Shea, M. S., Trimm, D. Production of p-cymene and hydrogen from a bio-renewable feedstock-1,8-cineole (eucalyptus oil). *Green Chem.* **12**, 70–76 (2010).

123. Leita, B. A., Gray, P., O'Shea, M., Burke, N., Chiang, K., Trimm, D. The conversion of 1,8-cineole sourced from renewable Eucalyptus oil to p-cymene over a palladium doped γ-Al2O3 catalyst. *Catal. Today* **178**, 98–102 (2011).

124. S. Lundmark, WO 2014/133433 A1 (2014).

125. Neaţu, F., Culică, G., Florea, M., Parvulescu, V. I., Cavani, F. Synthesis of Terephthalic Acid by p-Cymene Oxidation using Oxygen: Toward a More Sustainable Production of Bio-Polyethylene Terephthalate. *ChemSusChem* **9**, 3102–3112 (2016).

126. Ospenson, J. N. *Acta Chem. Scand.,* **3**, 211–211 (1949).

127. Frost, J.W., Miermont, A., Schweitzer, D., Bui, V., Paschke, E., 2011/0288263 A1 (2011).

128. Peters, M.W. Taylor, J.D., Jenni, M., Manzer, L.E., Henton D. E. 2011/044243 A1 (2011).

129. Bramucci, M., Nagarajan, V., Thomas, S., 2003/0073206 A1 (2003).

130. Osterhout, R. E. 2011/0207185 A1 (2001).

131. Webley, S. D., Welsh, S. J., Jackman, A. L., Aherne, G. W. Pure bacterial isolates that convert p-xylene to terephthalic acid. *Appl. Microbiol. Biotechnol.* **58**, 255–259 (2002).

132. Smith P. B. Bio-Based Sources for Terephthalic Acid. *ACS Symp. Ser.* **1192**, 453–469 (2015).

133. Marsh, K., Bugusu, B. Food packaging - Roles, materials, and environmental issues: Scientific status summary. *J. Food Sci.* **72**, (2007).

134. Sonawane, T. A. Bio-based Materials: Past to Future. in *Bio-based Materials for Food Packaging Green and Sustainable Advanced Packaging Materials* (ed. Ahmed, 2018).

135. Conix, A., Van Kerpel, R. Crystallization behavior and melting properties of m-phenylene group containing polyesters. *J. Polym. Sci.* **40**, 521–532 (1959).

136. Kotek, R., Pang, K., Schmidt, B., Tonelli, A. Synthesis and gas barrier characterization of poly(ethylene isophthalate). *J. Polym. Sci. Part B Polym. Phys.* **42**, 4247–4254 (2004).

137. Karayannidis, G. P., Sideridou, I. D., Zamboulis, D. N., Bikiaris, D. N., Sakalis, A. J. Thermal behavior and tensile properties of poly(ethylene terephthalate-co-ethylene isophthalate). *J. Appl. Polym. Sci.* **78**, 200–207 (2000).

138. Roupakias, C. P., Bikiaris, D. N., Karayannidis, G. P. Synthesis, thermal characterization, and tensile properties of alipharomatic polyesters derived from 1,3-propanediol and terephthalic, isophthalic, and 2,6-naphthalenedicarboxylic acid. *J. Polym. Sci. Part A Polym. Chem.* **43**, 3998–4011 (2005).

139. Chiorboli, E., Pizzoli, M., Ciamician, C. G., Centro, U., Selmi, V. Effect of crystallinity on the dynamic mechanical relaxations of poly(butylene isophthalate). **84**, 77–84 (1989).

140. Sousa, A. F., Vilela, C., Fonseca, A. C., Matos, M., Freire, C. S., Gruter, G. J. M., Silvestre, A. J. Biobased polyesters and other polymers from 2,5-furandicarboxylic acid: A tribute to furan excellency. *Polym. Chem.* **6**, 5961–5983 (2015).

141. Papageorgiou, G. Z., Papageorgiou, D. G., Terzopoulou, Z., Bikiaris, D. N. Production of bio-based 2,5-furan dicarboxylate polyesters: Recent progress and critical aspects in their synthesis and thermal properties. *Eur. Polym. J.* **83**, 202–229 (2016).

142. R. B. Gomes M., Gandini A. Synthesis and characterization of poly(2,5-furan dicarboxylate)s based on a variety of diol,". *J. Polym. Sci. Part APolymer Chem.* **49**, 3759–3768 (2011).

143. Matos, M., Sousa, A. F., Fonseca, A. C., Freire, C. S., Coelho, J. F., Silvestre, A. J. A new generation of furanic copolyesters with enhanced degradability: Poly(ethylene 2,5-furandicarboxylate)-co-poly(lactic acid) copolyesters. *Macromol. Chem. Phys.* **215**, 2175–2184 (2014).

144. Codou, A., Guigo, N., Van Berkel, J., De Jong, E., Sbirrazzuoli, N. Non-isothermal Crystallization

Kinetics of Biobased Poly(ethylene 2,5-furandicarboxylate) Synthesized via the Direct Esterification Process. *Macromol. Chem. Phys.* **215**, 2065–2074 (2014).

145. Wu, B., Xu, Y., Bu, Z., Wu, L., Li, B. G., Dubois, P. Biobased poly(butylene 2,5-furandicarboxylate) and poly(butylene adipate-co-butylene 2,5-furandicarboxylate)s: From synthesis using highly purified 2,5-furandicarboxylic acid to thermo-mechanical properties. *Polymer (Guildf).* **55**, 3648–3655 (2014).

146. Gopalakrishnan, P., Narayan-Sarathy, S., Ghosh, T., Mahajan, K. Belgacem, M. N. Synthesis and characterization of bio-based furanic polyesters. *J. Polym. Res.* **21**, (2014).

147. Soccio, M., Costa, M., Lotti, N., Gazzano, M., Siracusa, V., Salatelli, E., Munari, A. Novel fully biobased poly(butylene 2,5-furanoate/diglycolate) copolymers containing ether linkages: Structure-property relationships. *Eur. Polym. J.* **81**, 397–412 (2016).

148. Wu, L., Mincheva, R., Xu, Y., Raquez, J. M., Dubois, P. High molecular weight poly(butylene succinate-co-butylene furandicarboxylate) copolyesters: From catalyzed polycondensation reaction to thermomechanical properties. *Biomacromolecules* **13**, 2973–2981 (2012).

149. De Melo, F. C., De Souza, R. F., Coutinhob, P. L. A., De Souza, M. O. Synthesis of 5-Hydroxymethylfurfural from dehydration of fructose and glucose using ionic liquids. *J. Braz. Chem. Soc.* **25**, 2378–2384 (2014).

150. Miyakoshi, R., Yokoyama, A., Yokozawa, T. Catalyst-transfer polycondensation. Mechanism of Ni-catalyzed chain-growth polymerization leading to well-defined poly(3-hexylthiophene). *J. Am. Chem. Soc.* **127**, 17542–17547 (2005).

151. Knoop, R. J. I., Vogelzang, W., Van Haveren, J., Van Es, D. S. High molecular weight poly(ethylene-2,5-furanoate); Critical aspects in synthesis and mechanical property determination. *J. Polym. Sci. Part A Polym. Chem.* **51**, 4191–4199 (2013).

152. Papageorgiou, G. Z., Tsanaktsis, V., Bikiaris, D. N. Synthesis of poly(ethylene furandicarboxylate) polyester using monomers derived from renewable resources: Thermal behavior comparison with PET and PEN. *Phys. Chem. Chem. Phys.* **16**, 7946–7958 (2014).

153. Vannini, M., Marchese, P., Celli, A., Lorenzetti, C. Fully biobased poly(propylene 2,5-furandicarboxylate) for packaging applications: excellent barrier properties as a function of crystallinity. *Green Chem.* **17**, 4162–4166 (2015).

154. Guidotti, G., Soccio, M., García-Gutiérrez, M. C., Ezquerra, T., Siracusa, V., Gutiérrez-Fernández, E., Lotti, N. Fully Biobased Superpolymers of 2,5-Furandicarboxylic Acid with Different Functional Properties: From Rigid to Flexible, High Performant Packaging Materials. *ACS Sustain. Chem. Eng.* **8**, 9558–9568 (2020).

155. Guidotti, G., Soccio, M., Lotti, N., Gazzano, M., Siracusa, V., Munari, A. Poly(propylene 2,5-thiophenedicarboxylate) vs. Poly(propylene 2,5-furandicarboxylate): Two examples of high gas barrier bio-based polyesters. *Polymers (Basel).* **10**, (2018).

156. Guidotti, G., Genovese, L., Soccio, M., Gigli, M., Munari, A., Siracusa, V., Lotti, N. Block copolyesters containing 2,5-furan and trans-1,4-cyclohexane subunits with outstanding gas barrier

properties. *Int. J. Mol. Sci.* **20**, 1–15 (2019).

157. Papageorgiou, G. Z., Tsanaktsis, V., Papageorgiou, D. G., Exarhopoulos, S., Papageorgiou, M., Bikiaris, D. N. Evaluation of polyesters from renewable resources as alternatives to the current fossil-based polymers. Phase transitions of poly(butylene 2,5-furan-dicarboxylate). *Polymer (Guildf).* **55**, 3846–3858 (2014).

158. Wilsens, C. H., Verhoeven, J. M., Noordover, B. A., Hansen, M. R., Auhl, D., Rastogi, S.. Thermotropic polyesters from 2,5-furandicarboxylic acid and vanillic acid: Synthesis, thermal properties, melt behavior, and mechanical performance. *Macromolecules* **47**, 3306–3316 (2014).

159. Tsanaktsis, V., Terzopoulou, Z., Nerantzaki, M., Papageorgiou, G. Z., Bikiaris, D. N. New poly(pentylene furanoate) and poly(heptylene furanoate) sustainable polyesters from diols with odd methylene groups. *Mater. Lett.* **178**, 64–67 (2016).

160. Guidotti, G., Soccio, M., García-Gutiérrez, M. C., Gutiérrez-Fernández, E., Ezquerra, T. A., Siracusa, V., Lotti, N. Evidence of a 2D-Ordered Structure in Biobased Poly(pentamethylene furanoate) Responsible for Its Outstanding Barrier and Mechanical Properties. *ACS Sustain. Chem. Eng.* **7**, 17863–17871 (2019).

161. Nair, L. S., Laurencin, C. T. Biodegradable polymers as biomaterials. *Prog. Polym. Sci.* **32**, 762–798 (2007).

162. Pang, K., Kotek, R., Tonelli, A. Review of conventional and novel polymerization processes for polyesters. *Prog. Polym. Sci.* **31**, 1009–1037 (2006).

163. Varma, I. K., Albertsson, A. C., Rajkhowa, R., Srivastava, R. K. Enzyme catalyzed synthesis of polyesters. *Prog. Polym. Sci.* **30**, 949–981 (2005).

164. Albertsson, A. C., Srivastava, R. K. Recent developments in enzyme-catalyzed ring-opening polymerization. *Adv. Drug Deliv. Rev.* **60**, 1077–1093 (2008).

165. Gross, R. A., Ganesh, M., Lu, W. Enzyme-catalysis breathes new life into polyester condensation polymerizations. *Trends Biotechnol.* **28**, 435–443 (2010).

166. Azim, H., Dekhterman, A., Jiang, Z., Gross, R. A. Candida antarctica Lipase B catalyzed synthesis of poly(butylene succinate): Shorter chain building blocks also work. *ACS Symp. Ser.* **999**, 285–293 (2008).

167. Maniar, D., Jiang, Y., Woortman, A. J. J., van Dijken, J., Loos, K. Furan-Based Copolyesters from Renewable Resources: Enzymatic Synthesis and Properties. *ChemSusChem* **12**, 990–999 (2019).

168. Skoczinski, P., Espinoza Cangahuala, M. K., Maniar, D., Loos, K. Enzymatic transesterification of urethane-bond containing ester. *Colloid Polym. Sci.* (2020). doi:10.1007/s00396-020-04689-2

169. Jiang, Y., Woortman, A. J. J., Alberda Van Ekenstein, G. O. R., Loos, K. A biocatalytic approach towards sustainable furanic-aliphatic polyesters. *Polym. Chem.* **6**, 5198–5211 (2015).

170. Jiang, Y., Loos, K. Enzymatic synthesis of biobased polyesters and polyamides. *Polymers (Basel).* **8**, (2016).

171. Maniar, D., Silvianti, F., Ospina, V. M., Woortman, A. J., van Dijken, J., Loos, K. On the way to greener furanic-aliphatic poly(ester amide)s: Enzymatic polymerization in ionic liquid. *Polymer (Guildf).* **205**, 122662 (2020).

172. Carothers, H. Polymers and polyfunctionality (1935).

173. Rabinovitch E. *Trans. Faraday Soc.* **33**, 1225 (1937).

174. Duda, A., Penczek, S. In Biopolymers, Vol. 3b (Steinbuechel, A.; Doi, Y., Eds., 2002).

175. Buzin, P., Lahcini, M., Schwarz, G., Kricheldorf, H. R. Aliphatic Polyesters by Bismuth Triflate-Catalyzed Polycondensations of Dicarboxylic Acids and Aliphatic Diols. 8491–8495 (2008).

176. Terzopoulou, Z., Karakatsianopoulou, E., Kasmi, N., Tsanaktsis, V., Nikolaidis, N., Kostoglou, M., Bikiaris, D. N. Effect of catalyst type on molecular weight increase and coloration of poly(ethylene furanoate) biobased polyester during melt polycondensation. *Polym. Chem.* **8**, 6895–6908 (2017).

177. Yu, Z., Zhou, J., Cao, F., Zhang, Q., Huang, K., Wei, P. Synthesis, Characterization and Thermal Properties of Bio-based Poly(ethylene 2,5-furan dicarboxylate). *J. Macromol. Sci., Part B* **55**, 1135–1145 (2016).

178. Jacquel, N., Freyermouth, F., Fenouillot, F., Rousseau, A., Pascault, J. P., Fuertes, P., Saint-Loup, R. Synthesis and properties of poly(butylene succinate): Efficiency of different transesterification catalysts. *J. Polym. Sci. Part A Polym. Chem.* **49**, 5301–5312 (2011).

179. M. Gruter, G. J., Sipos, L., Adrianus Dam, M. Accelerating Research into Bio-Based FDCA-Polyesters by Using Small Scale Parallel Film Reactors. *Comb. Chem. High Throughput Screen.* **15**, 180–188 (2011).

180. Palaniappan, S. Preparation of polyaniline-sulfate salt by emulsion and aqueous polymerization pathway without using protonic acid. *Polym. Adv. Technol.* **13**, 54–59 (2002).

181. Jérôme, C., Lecomte, P. Recent advances in the synthesis of aliphatic polyesters by ring-opening polymerization. *Adv. Drug Deliv. Rev.* **60**, 1056–1076 (2008).

182. Danton, F. S., Ivin, K. J. Reversibility of the propagation reaction in polymerization processes and its manifestation in the phenomenon of a 'ceiling temperature'. *Nature* **162**, 705–707 (1948).

183. Tobolsky, A. V., Eisenberg, A. Equilibrium Polymerization of Sulfur. *J. Am. Chem. Soc.* **81**, 780–782 (1959).

184. Philippe Dubois, Olivier Coulembier, A., Raquez, J.-M. *Handbook of Ring-Opening Polymerization*. (WILEY-VCH Verlag GmbH & Co. KGaA).

185. Von Schenck, H., Ryner, M., Albertsson, A. C., Svensson, M. Ring-opening polymerization of lactones and lactides with Sn(IV) and Al(III) initiators. *Macromolecules* **35**, 1556–1562 (2002).

186. Danheiser, R. L., Nowick, J. S. A Practical and Efficient Method for the Synthesis of β-Lactones. *J. Org. Chem.* **56**, 1176–1185 (1991).

187.	Einhorn, A. *Chem. Ber.* **16**, 2208 (1883).

188.	Searles, G. Comprehensive Heterocyclic Chemistry. (ed. Rees. Pergamon, 1984).

189.	Testa, E., Fontanella, L., Franco, G., Mariani, L. Uber p-lactone: eine neue allgemeine synthese. A*uf das Zentralnervensystem wirkende Substanzen, XIX*, **823**, (1960).

190.	Berichte, D. Condensationen ewieohen Maloneater und Aldehyden unter dem Einfluae von Ammoniak und or ganischen Aminen (1898).

191.	Kricheldorf, H. R., Kreiser-Saunders, I., Stricker, A. Polylactones 48. SnOct2-initiated polymerizations of lactide: a mechanistic study. *Macromolecules* **33**, 702–709 (2000).

192.	Degée, P., Dubois, P., Jérôme, R. Bulk polymerization of lactides initiated by aluminium isopropoxide, 2: Beneficial effect of Lewis bases and transfer agents. *Macromol. Chem. Phys.* **198**, 1973–1984 (1997).

193.	Eguiburu, J. L., Fernandez-Berridi, M. J., Cossío, F. P., San Román, J. Ring-opening polymerization of L-lactide initiated by (2-methacryloxy)ethyloxy-aluminum trialkoxides. 1. Kinetics. *Macromolecules* **32**, 8252–8258 (1999).

194.	Dechy-Cabaret, O., Martin-Vaca, B., Bourissou, D. Controlled ring-opening polymerization of lactide and glycolide. *Chem. Rev.* **104**, 6147–6176 (2004).

195.	Stevels, W. M., Ankone, M. J. K., Dijkstra, P. J., Feijen, J. Versatile and highly efficient catalyst system for the preparation of polyesters based on lanthanide tris(2,6-di-tert-butylphenolate)s and various alcohols. *Macromolecules* **29**, 3332–3333 (1996).

196.	Stevels, W. M., Ankoné, M. J. K., Dijkstra, P. J., Feijen, J. Kinetics and mechanism of L-lactide polymerization using two different yttrium alkoxides as initiators. *Macromolecules* **29**, 6132–6138 (1996).

197.	Shirahama, H., Kawaguchi, Y., Aludin, M. S., Yasuda, H. Synthesis and enzymatic degradation of high molecular weight aliphatic polyesters. *J. Appl. Polym. Sci.* **80**, 340–347 (2001).

198.	Cohn, D., Hotovely Salomon, A. Designing biodegradable multiblock PCL/PLA thermoplastic elastomers. *Biomaterials* **26**, 2297–2305 (2005).

199.	Chen, H. B., Wang, X. L., Zeng, J. B., Li, L. L., Dong, F. X., Wang, Y. Z. A novel multiblock poly(ester urethane) based on poly(butylene succinate) and poly(ethylene succinate- co -ethylene terephthalate). *Ind. Eng. Chem. Res.* **50**, 2065–2072 (2011).

200.	Ha, M., Hiltunen, K., Seppa, J. V. Lactic Acid Based Poly (ester – urethane) s : The Effects of Different Polymerization Conditions on the Polymer. 865–873 (1996).

201.	Kylmä, J., Tuominen, J., Helminen, A., Seppälä, J. Chain extending of lactic acid oligomers. Effect of 2,2′-bis(2-oxazoline) on 1,6-hexamethylene diisocyanate linking reaction. *Polymer (Guildf).* **42**, 3333–3343 (2001).

202.	Behniafar, H., Haghighat, S. Thermally stable and organosoluble one-pot preparation and

characterization. *Polym. Adv. Technol.* **19**, 1040–1047 (2008).

203. Zhong, W., Ge, J., Gu, Z., Li, W., Chen, X., Zang, Y., Yang, Y. Study on Biodegradable Polymer Materials Based on Poly-.pdf. 2546–2551 (1999).

204. Desbrières, J., Babak, V. G. Interfacial properties of amphiphilic natural. *Polym.* **55**, 1177–1183 (2006).

205. Genovese, L., Soccio, M., Lotti, N., Gazzano, M., Siracusa, V., Salatelli, E., Munari, A.. Design of biobased PLLA triblock copolymers for sustainable food packaging: Thermo-mechanical properties, gas barrier ability and compostability. *Eur. Polym. J.* **95**, 289–303 (2017).

206. Alison J Scott, A. P. *Reference Module in Chemistry, Molecular Sciences and Chemical Engineering*. (Elsevier, 2017).

207. Nicholas, P. *Condensed Encyclopedia of Polymer Engineering Terms*. (Elsevier, 2001).

208. Gigli, M., Lotti, N., Gazzano, M., Finelli, L., Munari, A. Novel eco-friendly random copolyesters of poly(butylene succinate) containing ether-linkages. *React. Funct. Polym.* **72**, 303–310 (2012).

209. Soccio, M., Lotti, N., Finelli, L., Gazzano, M., Munari, A. Influence of transesterification reactions on the miscibility and thermal properties of poly(butylene/diethylene succinate) copolymers. *Eur. Polym. J.* **44**, 1722–1732 (2008).

210. Gualandi, C., Soccio, M., Govoni, M., Valente, S., Lotti, N., Munari, A., Focarete, M. L Poly(butylene/diethylene glycol succinate) multiblock copolyester as a candidate biomaterial for soft tissue engineering: Solid-state properties, degradability, and biocompatibility. *J. Bioact. Compat. Polym.* **27**, 244–264 (2012).

211. Sudesh, K., Abe, H., Doi, Y. Synthesis, structure and properties of polyhydroxyalkanoates: Biological polyesters. *Prog. Polym. Sci.* **25**, 1503–1555 (2000).

212. Anjum, A., Zuber, M., Zia, K. M., Noreen, A., Anjum, M. N., Tabasum, S. Microbial production of polyhydroxyalkanoates (PHAs) and its copolymers: A review of recent advancements. *Int. J. Biol. Macromol.* **89**, 161–174 (2016).

213. Kim, J. S., Lee, B. H., Kim, B. S. Production of poly(3-hydroxybutyrate-co-4-hydroxybutyrate) by Ralstonia eutropha. *Biochem. Eng. J.* **23**, 169–174 (2005).

214. Yang, T. H., Kim, T. W., Kang, H. O., Lee, S. H., Lee, E. J., Lim, S. C., Lee, S. Y. Biosynthesis of polylactic acid and its copolymers using evolved propionate CoA transferase and PHA synthase. *Biotechnol. Bioeng.* **105**, 150–160 (2010).

215. Huang, S.J. *Encyclopedia of polymer science and engineering*. vol **2**, (eds Mark, Bikales, Overberger and Menges, 1985).

216. Montan, J., Armelin, E., Asn, L., Rodrguez-Galn, A., Puiggal, J. Comparative degradation data of polyesters and related poly(ester amide)s derived from 1,4-butanediol, sebacic acid, and amino acids. *J. Appl. Polym. Sci.* **85**, 1815–1824 (2002).

217. Tetsuka, H., Doi, Y., Abe, H. Synthesis and thermal properties of novel periodic poly(ester - Amide)s derived from adipate, butane-1,4-diamine, and linear aliphatic diols. *Macromolecules* **39**, 2875–2885 (2006).

218. Berti, C., Celli, A., Marchese, P., Barbiroli, G., Di Credico, F., Verney, V., Commereuc, S. Novel copolyesters based on poly(alkylene dicarboxylate)s: 1. Thermal behavior and biodegradation of aliphatic-aromatic random copolymers. *Eur. Polym. J.* **44**, 3650–3661 (2008).

219. Wang, L., Xie, Z., Bi, X., Wang, X., Zhang, A., Chen, Z., Feng, Z. Preparation and characterization of aliphatic/aromatic copolyesters based on 1,4-cyclohexanedicarboxylic acid. *Polym. Degrad. Stab.* **91**, 2220–2228 (2006).

220. Genovese, L., Soccio, M., Gigli, M., Lotti, N., Gazzano, M., Siracusa, V., Munari, A. Biodegradable aliphatic copolyesters containing PEG-like sequences for sustainable food packaging applications. *Polym. Degrad. Stab.* **105**, 96–106 (2014).

221. Genovese, L., Soccio, M., Gigli, M., Lotti, N., Gazzano, M., Siracusa, V., Munari, A. Gas permeability, mechanical behaviour and compostability of fully-aliphatic bio-based multiblock poly(ester urethane)s. *RSC Adv.* **6**, 55331–55342 (2016).

222. Gigli, M., Lotti, N., Siracusa, V., Gazzano, M., Munari, A., Dalla Rosa, M.. Effect of molecular architecture and chemical structure on solid-state and barrier properties of heteroatom-containing aliphatic polyesters. *Eur. Polym. J.* **78**, 314–325 (2016).

223. Soni, R. K., Soam, S., Dutt, K. Studies on biodegradability of copolymers of lactic acid, terephthalic acid and ethylene glycol. *Polym. Degrad. Stab.* **94**, 432–437 (2009).

224. Arencón, D., Velasco, J. I., Realinho, V., Antunes, M., Maspoch, M. L. Essential work of fracture analysis of glass microsphere-filled polypropylene and polypropylene/poly (ethylene terephthalate-co-isophthalate) blend-matrix composites. *Polym. Test.* **26**, 761–769 (2007).

225. Zhang, Y., Gu, L. Study of non-isothermal crystallization kinetics and sequence distribution in poly(ethylene terephthalate-co-isophthalate). *Eur. Polym. J.* **36**, 759–765 (2000).

226. Arencón, D., Velasco, J. I., Rodríguez-Pérez, M. A., De Saja, J. A. Poly(propylene)/poly(ethylene terephthalate-co-isophthalate) blends and glass bead filled composites: Microstructure and thermomechanical properties. *J. Appl. Polym. Sci.* **94**, 1841–1852 (2004).

227. Finelli, L., Fiorini, M., Siracusa, V., Lotti, N., Munari, A. Synthesis and Characterization of Poly (ethylene isophthalate- co -ethylene terephthalate) Copolyesters. (2003).

228. Shik Ha, W., Chun, Y. K., Soon Jang, S., Mook Rhee, D., Rae Park, C. Preparation of poly(ethylene terephthalate-co-isophthalate) by ester interchange reaction in the PET/PEI blend system. *J. Polym. Sci. Part B Polym. Phys.* **35**, 309–315 (1997).

229. Karayannidis, G. P., Bikiaris, D. N., Papageorgiou, G. Z., Pastras, S. V. Synthesis and characterization of poly(ethylene terephthalate-co-isophthalate)s with low content of isophthalate units. *J. Appl. Polym. Sci.* **86**, 1931–1941 (2002).

230. Lee, B., Shin, T. J., Lee, S. W., Yoon, J., Kim, J., Ree, M. Secondary crystallization behavior of

poly(ethylene isophthalate-co- terephthalate): Time-resolved small-angle X-ray scattering and calorimetry studies. *Macromolecules* **37**, 4174–4184 (2004).

231. Wu, T. M., Chang, C. C., Yu, T. L. Crystallization of poly(ethylene terephthalate-co-isophthalate). *J. Polym. Sci. Part B Polym. Phys.* **38**, 2515–2524 (2000).

232. Yu, J., Li, B., Lee, S., Ree, M. Relationship between physical properties and chemical structures of poly(ethylene terephthalate-co-ethylene isophthalate). *J. Appl. Polym. Sci.* **73**, 1191–1195 (1999).

233. Hua, H., Zhang, R., Wang, J., Bin Ying, W. Fully bio-based poly(propylene succinate-co-propylene furandicarboxylate) copolyesters with proper mechanical, degradation and barrier properties for green packaging applications. *Eur. Polym. J.* **102**, 101–110 (2018).

234. Witt U., Muller R. J., Augusta J., Widdecke H. *Macromol Chem Phys* **195**, 793 (1994).

235. Witt U., Muller R. J. *J Macromol Sci Pure Appl Chem* **A43**, 851 (1994).

236. Berti, C., Colonna, M., Finelli, L., Lorenzetti, C., Lotti, N., Vannini, M. Poly(propylene terephthalate) modified with 2,2-bis[4-(ethylenoxy)-1,4- phenylene]propane terephthalate) units: Thermal behaviour, crystallisation kinetics and morphology. *Macromol. Chem. Phys.* **205**, 2473–2485 (2004).

237. Lorenzetti, C., Finelli, L., Lotti, N., Vannini, M., Gazzano, M., Berti, C., Munari, A. Synthesis and characterization of poly(propylene terephthalate/2,6-naphthalenate) random copolyesters. *Polymer (Guildf).* **46**, 4041–4051 (2005).

238. Soccio, M., Lotti, N., Finelli, L., Gazzano, M., Munari, A. Neopentyl Glycol Containing Poly(propylene terephthalate)s: Structure–Properties Relationships. *J. Polym. Sci. B. Polym. Phys.* **46**, 170–181 (2008).

239. Lotti, N., Colonna, M., Fiorini, M., Finelli, L., Berti, C. Poly(propylene terephthalate) containing 4,4-sulfonylbisphenol units:effect of chemical composition on the physical-chemical properties. *Polym. Sci. Ser. B* **56**, 616–622 (2014).

240. Lotti, N., Finelli, L., Fiorini, M., Righetti, Colonna, M., Munari, A. Synthesis and characterization of poly (butylene terephthalate- co -diethylene terephthalate) copolyesters. **41**, 5297–5304 (2000).

241. Lotti, N., Finelli, L., Fiorini, M., Righetti, Colonna, M., Munari, A. Synthesis and Characterization of Poly (butylene terephthalate-co-triethylene terephthalate) Copolyesters. 981–990 (2001).

242. Lotti, N., Finelli, L., Siracusa, V., Munari, A. Synthesis and thermal characterization of poly(butylene terephthalate-co-thiodiethylene terephthalate. *Polymer (Guildf).* **43**, 4355–4363 (2002).

243. Finelli, L., Lotti, L., Munari, A., Berti, C., Colonna, M. Random terephthalate polyesters based on 1,4-butanediol and bis(hydroxyethyl ether) of bisphenol A: thermal properites and crystallisation kinetics. *Polymer (Guildf).* **44**, 1409–1420 (2003).

244. Lotti, N., Colonna, M., Fiorini, M., Finelli, L., Berti, C. Poly(butylene terephthalate) modified with ethoxylated bisphenol S with increased glass transition temperature and improved thermal stability. *Polymer (Guildf).* **52**, 904–911 (2011).

245. Lotti, N., Finelli, L., Milizia, T., Munari, A., Manaresi, P. Preparation and thermal behavior of random copolyesters of thiodipropionic acid. *Eur. Polym. J.* **36**, 929–936 (2000).

246. Li, B., Yu, J., Lee, S., Ree, M. Crystallizations of poly(ethylene terephthalate co ethylene isophthalate). *Polymer (Guildf).* **40**, 5371–5375 (1999).

247. Lee, S. W., Ree, M., Park, C. E., Jung, Y. K., Park, C. S., Jin, Y. S., Bae, D. C. Synthesis and non-isothermal crystallization behaviors of poly(ethylene isophthalate-co-terephthalate)s. *Polymer (Guildf).* **40**, 7137–7146 (1999).

248. Soccio, M., Finelli, L., Lotti, N., Gazzano, M., Munari, A. Novel random poly(propylene isophthalate/adipate) copolyesters: Synthesis and characterization. *Eur. Polym. J.* **42**, 2949–2958 (2006).

249. Soccio, M., Finelli, L., Lotti, N., Gazzano, M., Munari A. Poly(propylene isophthalate), Poly(propylene succinate), and Their Random Copolymers: Synthesis and Thermal Properties. *J. Polym. Sci.* **45**, 310–321 (2006).

250. Finelli, L., Lotti, N., Munari, A. Influence of branching on the thermal behavior of poly(butylene isophthalate). *J. Appl. Polym. Sci.* **84**, 2001–2010 (2002).

251. Lotti, N., Finelli, L., Munari, A., Siracusa, V. Melting behavior and crystallization kinetics of sulfonated poly(butylene isophthalate). *Polym. Eng. Sci.* **42**, 1590–1599 (2002).

252. Alvarez, C., Capitán, M. J., Lotti, N., Munari, A., Ezquerra, T. A. Anomalous enhanced mobility in a semicrystalline random poly(butylene isophthalate/butylene adipate) copolyester. *Colloid Polym. Sci.* **282**, 96–99 (2003).

253. Huang, X., Guo, R., Lan, J. Synthesis and characterizations of branched poly(butylene isophthalate)-co-poly(tetramethylene glycol)-co-poly(ethylene glycol) fibers with excellent low temperature elastic recovery. *Polym. Sci. - Ser. B* **57**, 313–321 (2015).

254. Phillips, R. A., McKenna, J. M., Cooper, S. L. Glass transition and melting behavior of poly(ether-ester) multiblock copolymers with poly(tetramethylene isophthalate) hard segments. *J. Polym. Sci. Part B Polym. Phys.* **32**, 791–802 (1994).

255. Chandra, R., Rustgi, R. *Prog. Polym. Sci.* **23**, 1273 (1998).

256. Guidotti G., Soccio M., Lotti N., Siracusa V., Gazzano M., Munari A. New multi-block copolyester of 2,5-furandicarboxylic acid containing PEG-like sequences to form flexible and degradable films for sustainable packaging. *Polym. Degrad. Stab.* **169**, (2019).

257. Terzopoulou, Z., Papadopoulos, L., Zamboulis, A., Papageorgiou, D. G., Papageorgiou, G. Z. Tuning the Properties of Furandicarboxylic Acid-Based Polyesters with Copolymerization: A Review. *Polymers (Basel).* **12**, (2020).

258. Xuan Fei A. *ACS Sustain. Chem. Eng.* **8**, 8471−8485 (2020).

259. Wang, G., Jiang, M., Zhang, Q., Wang, R. Biobased multiblock copolymers: Synthesis, properties and shape memory performance of poly(ethylene 2,5-furandicarboxylate)-b-poly(ethylene glycol). *Polym. Degrad. Stab.* **144**, 121–126 (2017).

260. Papageorgiou, Z., Konstantopoulou, M., Terzopoulou, Z., Nerantzaki, M., Tsagkalias, J., Achilias, D. A., Bikiaris, D.N, Exarhopoulosa, S. Poly(ethylene furanoate-co-ethylene terephthalate) biobased copolymers: Synthesis, thermal properties and cocrystallization behavior. *Eur. Polym. J.* **89**, 349–366 (2017).

261. Wang, J., Liu, X., Zhang, Y., Liu, F., Zhu, J. Modification of poly(ethylene 2,5-furandicarboxylate) with 1,4-cyclohexanedimethylene: Influence of composition on mechanical and barrier properties. *Polymer (Guildf).* **103**, 1–8 (2016).

262. Kwiatkowska, M., Kowalczyk, I., Kwiatkowski, K., Szymczyk, A., Rosłaniec, Z. Fully biobased multiblock copolymers of furan-aromatic polyester and dimerized fatty acid: Synthesis and characterization. *Polymer (Guildf).* **99**, 503–512 (2016).

263. Zhou, W., Zhang, Y., Xu, Y., Wang, P., Gao, L., Zhang, W., Ji, J. Synthesis and characterization of bio-based poly(butylene furandicarboxylate)-b-poly(tetramethylene glycol) copolymers. *Polym. Degrad. Stab.* **109**, 21-26 (2014).

264. Tserki, V., Matzinos, P., Pavlidou, E., Panayiotou, C. Biodegradable aliphatic polyesters. Part II. Synthesis and characterization of chain extended poly(butylene succinate-co-butylene adipate). *Polym. Degrad. Stab.* **91**, 377–384 (2006).

265. Shah, A. A., Kato, S., Shintani, N., Kamini, N. R., Nakajima-Kambe, T. Microbial degradation of aliphatic and aliphatic-aromatic co-polyesters. *Appl. Microbiol. Biotechnol.* **98**, 3437–3447 (2014).

266. Zhi, Wenbiao Hu, Y., Liang, M., Liu, Y., Li, J., Yin, J., Shi, Y. Solid-liquid equilibrium and thermodynamic of 2,5-thiophenedicarboxylic acid in different organic solvents. *Fluid Phase Equilib.* **375**, 110–114 (2014).

267. Jin, H. J., Lee, B. Y., Kim, M. N., Yoon, J. S. Thermal and mechanical properties of mandelic acid-copolymerized poly(butylene succinate) and poly(ethylene adipate). *J. Polym. Sci. Part B Polym. Phys.* **38**, 1504–1511 (2000).

268. Nagata, M., Goto, H., Sakai, W., Tsutsumi, N. Synthesis and enzymatic degradation of poly(tetramethylene succinate) copolymers with terephthalic acid. *Polymer (Guildf).* **41**, 4373–4376 (2000).

269. Ki, H. C., Ok Park, O. Synthesis, characterization and biodegradability of the biodegradable aliphatic-aromatic random copolyesters. *Polymer (Guildf).* **42**, 1849–1861 (2001).

270. Kim, Y. J., Park, O. O. Miscibilities and rheological properties of poly(butylene succinate)-poly(butylene terephthalate) blends. *J. Appl. Polym. Sci.* **72**, 945–951 (1999).

271. Kint, D. P. R., Alla, A., Deloret, E., Campos, J. L., Muñoz-Guerra, S. Synthesis, characterization,

and properties of poly(ethylene terephthalate)/poly(1,4-butylene succinate) block copolymers. *Polymer (Guildf).* **44**, 1321–1330 (2003).

272. Jacquel, N., Saint-Loup, R., Pascault, J. P., Rousseau, A., Fenouillot, F. Bio-based alternatives in the synthesis of aliphatic-aromatic polyesters dedicated to biodegradable film applications. *Polymer (Guildf).* **59**, 234–242 (2015).

273. Witt, U., Müller, R. J., Deckwer, W. D. Studies on sequence distribution of aliphatic/aromatic copolyesters by high-resolution 13C nuclear magnetic resonance spectroscopy for evaluation of biodegradability. *Macromol. Chem. Phys.* **197**, 1525–1535 (1996).

274. Albertsson, A. C, Varma, I. K. Aliphatic Polyesters: Synthesis, Properties and Applications. in *Advances in Polymer Science* (ed. Springer) 1–40 (2002).

275. Stillinger, F. H. Translation-rotationparadox for diffusion in fragile glass-forming liquids. *Phys. Rev.* **50**, 2064 –2068 (1994).

276. Perez, J. Quasi-punctual defects in vitreous solids and liquid-glass transition. *Solid State Ionics* **39**, 69–79 (1990).

277. Ediger, M. D., Inoue, T., Cicerone, M. T., Blackburn, F. R. Probe rotation near and belowT: relationship to viscoelasticitygand physical aging. *Macromol. Symp.* **101**, 139–146 (1996).

278. Chan, R. K., Pathmanthan, K., & Johari, G. P. Dielectricrelaxations in the liquid and glassy states of glucose and its watermixtures. *J. Phys. Chem.* **90**, 6358 –6362 (1986).

279. Roudaut, G., Simatos, D., Champion, D., Contreras-Lopez, E., Le Meste, M. Molecular mobility around the glass transition temperature: A mini review. *Innov. Food Sci. Emerg. Technol.* **5**, 127–134 (2004).

280. Parker, M. J. Test Methods, Nondestructive Evaluation, and Smart Materials. in *Comprehensive Composite Materials* (Zweben, A. K. and C.) (2000).

281. Struik, L. C. E. Effect of thermal history on secondaryrelaxation processes in amorphous polymers. *Polymer (Guildf).* **28**, 57–68 (1987).

282. Tiemblo, P., Guzman, J., Riande, E., Mijangos, C., Reinecke, H. Erratum: Effect of physical aging on the gas transport properties of PVC and PVC modified with pyridine groups. *Polymer (Guildf).* **42**, 8321 (2001).

283. Corradini, P., Auriemma, F., De Rosa, C. Crystals and crystallinity in polymeric materials. *Acc. Chem. Res.* **39**, 314–323 (2006).

284. Wunderlich, B. *Thermotropic mesophases and mesophase transitions of linear, flexible macromolecules.* (Heidelberg, 1994).

285. Wunderlich, B. Reversible crystallization and the rigid-amorphous phase in semicrystalline macromolecules. *Prog. Polym. Sci.* **28**, 383–450 (2003).

286. Auriemma, F., De Rosa, C., Corradini, P. Solid Mesophases in Semicrystalline Polymers:

Structural Analysis by Diffraction Techniques in *Interphases and Mesophases in Polymer Crystallization II*. 1–74 (Springer, Heidelberg, 2005).

287. Keller, A. Keller, A., Hikosaka, M., Rastogi, S., Toda, A., Barham, P. J., Goldbeck-Wood, G. An approach to the formation and growth of new phases with application to polymer crystallization: effect of finite size, metastability, and Ostwald's rule of stages. *J. Mater. Sci.* **29**, 2579–2604 (1994).

288. Strobl, G. Crystallization and melting of bulk polymers: New observations, conclusions and a thermodynamic scheme. *Prog. Polym. Sci.* **31**, 398–442 (2006).

289. Strobl, G. From the melt via mesomorphic and granular crystalline layers to lamellar crystallites: A major route followed in polymer crystallization? *Eur. Phys. J. E* **3**, 165–183 (2000).

290. Stribeck, N., Bayer, R., Bösecke, P., Camarillo, A. A. Visualisation of the structure transfer between an oriented polymer melt and the semi-crystalline state. *Polymer (Guildf).* **46**, 2579–2583 (2005).

291. Strobl, G. *The physics of polymers: Concepts for understanding their structures and behavior*. (Springer, 2007). doi:10.1007/978-3-540-68411-4

292. Ostwald, W. *Phys. Chem* **22**, (1986).

293. Imrie C.T. Comparison ofthe Mesogenic Properties of Monomeric, Dimeric, and Side-Chain Polymeric Liquid Crystals. *Macromolecules* **26**, (1993).

294. Craig, A. A., Imrie, C. T. Effect of Backbone Flexibility on the Thermal Properties of Side-Group Liquid-Crystal Polymers. 6215–6220 (1999). doi:10.1021/ma990525f

295. MacDonald, W. A. Thermotropic Main Chain Liquid Crystal Polymers. *Liq. Cryst. Polym. From Struct. to Appl.* 407–446 (1992). doi:10.1007/978-94-011-1870-5_8

296. Ober, C.K., Jin Lenz, R. W., Ober, CK., Jin, I.J., Lenz, R.W. *Adv. Polym. Sci.* **59**, 101 (1984).

297. Ciferri, A. *Polymer Liquid Crystals* (Academic Press, 1982).

298. Roviello, A., Sirigu, A. *Macromol. Chem* (1982).

299. Lotz, B. Phase Transitions and Structure Of Crystalline Polymers, Institut Charles Sadron, France.

300. Toda, A., Androsch, R., Schick, C. Insights into polymer crystallization and melting from fast scanning chip calorimetry. *Polymer (Guildf).* **91**, 239–263 (2016).

301. Schick, C., Androsch, R., Schmelzer, J. W. P Homogeneous crystal nucleation in polymers. *J. Phys. Cond. Matter* **29**, (2017).

302. Androsch, R., Schick, C. Crystal nucleation of polymers at high supercooling of the melt. *Adv. Polym. Sci.* **276**, 257–288 (2005).

303. Tammann, G., Jenckel, E. Abhängigkeit der Zahl der Kerne, welche sich in verschiedenen unterkühlten Flüssigkeiten bilden, von der Temperatur. *Z. Anorg. Allg. Chem* **25**, 441−479 (1898).

304. Tammann G., Die Kristallisationsgeschwindigkeit und die Kernzahl des Glycerins in Abhängigkeit von der Temperatur. *Z. Anorg. Allg. Chem.* **193**, 76–80 (1930).

305. Mikhnevich G. L., Stability of the Crystallization Centers of an Oraganic Liquid at Various Temperatures and Conclusions to Be Draw therefore Concerning Tammann´s Method. *Phys. Z. Sowjetunion* **13**, 113–122 (1938).

306. Nascimento, M. L. F., Fokin, V. M., Zanotto, E. D., Abyzov, A. S. Dynamic processes in a silicate liquid from above melting to below the glass transition. *J. Chem. Phys.* **135**, (2011).

307. Fokin, V. M., Zanotto, E. D., Yuritsyn, N. S., Schmelzer, J. W. P. Homogeneous crystal nucleation in silicate glasses: A 40 years perspective. *J. Non. Cryst. Solids* **352**, 2681–2714 (2006).

308. Zhuravlev, E., Schmelzer, J. W. P., Wunderlich, B., Schick, C. Kinetics of nucleation and crystallization in poly (3 -caprolactone) (PCL). *Polymer (Guildf).* **52**, 1983–1997 (2011).

309. Zhuravlev, E., Schmelzer, J. W. P., Androsch, R., Schick, C. Experimental test of tammann's nuclei development approach in crystallization of macromolecules. *Int. Polym. Process.* **31**, 628–637 (2016).

310. Wurm, A. Zhuravlev, E., Eckstein, K., Jehnichen, D., Pospiech, D., Androsch, R., Wunderlich, B., Schick, C. Crystallization and Homogeneous Nucleation Kinetics of Poly (ε - caprolactone) (PCL) with Di ff erent Molar Masses. (2012). doi:10.1021/ma300363b

311. Stolte, I., Androsch, R., Di Lorenzo, M. L., Schick, C. Effect of aging the glass of isotactic polybutene-1 on form II nucleation and cold crystallization. *J. Phys. Chem. B* **117**, 15196–15203 (2013).

312. Androsch, R., Schick, C., Schmelzer, J. W. P. Sequence of enthalpy relaxation, homogeneous crystal nucleation and crystal growth in glassy polyamide 6. *Eur. Polym. J.* **53**, 100–108 (2014).

313. Androsch, R., Schick, C., Rhoades, A. M. Application of Tammann's Two-Stage Crystal Nuclei Development Method for Analysis of the Thermal Stability of Homogeneous Crystal Nuclei of Poly(ethylene terephthalate). *Macromolecules* **48**, 8082–8089 (2015).

314. Lorenzo, M. L., Silvestre, C. *Non-isothermal crystallization of polymers*. **24**, (1999).

315. Soccio M., Lotti N., Gigli M., Finelli L., Gazzano M. Reactive blending of poly(butylene succinate) and poly(triethylene succinate): characterization of the copolymers obtained. *Polym. Int.* **63**, 1163 (2012).

316. Jang, J., Oh, J. H. In situ FT-IR spectroscopic investigation on the microstructure of hyperbranched aliphatic polyesters. *Polymer (Guildf).* **40**, 5985–5992 (1999).

317. Kricheldorf, H. R., Stöber, O., Lübbers, D. New Polymer Syntheses. 78. Star-Shaped and Hyperbranched Polyesters by Polycondensation of Trimethylsilyl 3,5-Diacetoxybenzoate. *Macromolecules* **28**, 2118–2123 (1995).

318. Žagar, E., Žigon, M. Molar mass distribution of a commercial aliphatic hyperbranched polyester based on 2,2-bis(methylol)propionic acid. *J. Chromatogr. A* **1034**, 77–83 (2004).

319. Sanchez, I. C., Eby, R. K. Crystallization of Random Copolymers. *J Res Nat Bur Stand Sect A Phys Chem* **77 A**, 353–358 (1973).

320. Flory, P. J. Thermodynamics of crystallization in high polymers II. Simplified derivation of melting-point relationships 1,2. *J. Chem. Phys.* **15**, 684 (1947).

321. Baur, V. H. Einfluß der sequenzlängenverteilung auf das schmelz-ende von copolymeren. *Die Makromol. Chemie* **98**, 297–301 (1966).

322. Windle, A. H., Viney, C., Golombok, R., Donald, A. M., Mitchell, G. R. Molecular correlation in thermotropic copolyesters. *Faraday Discuss. Chem. Soc.* **79**, 55–72 (1985).

323. Allegra, G., Marchessault, R. H., Bloembergen, S. Crystallization of markoffian copolymers. *J. Polym. Sci. Part B Polym. Phys.* **30**, 809–815 (1992).

324. Naoko, Y., Yoshio, I., Hee, Y. Y. Nuclear magnetic resonance study on isomorphous behaviour in random copolyesters: poly(ethylene terephthalate-co-1,4-cyclohexenedimethylene terephthalate). *Polymer (Guildf).* **35**, 1931–1935 (1994).

325. Helfand, E., Lauritzen, J. I. Theory of Copolymer Crystallization. *Macromolecules* **6**, 631–638 (1973).

326. Wendung, J., Gusev, A. A., Suter, U. W. Predicting the cocrystallization behavior of random copolymers via free energy calculations. *Macromolecules* **31**, 2509–2515 (1998).

327. Lodge, T. P. Block copolymers: Past successes and future challenges. *Macromol. Chem. Phys.* **204**, 265–273 (2003).

328. Alejandro J. Müller, María Luisa Arnal, V. B. Crystallization in Block Copolymers with More than One Crystallizable Block. in *Progress in Understanding of Polymer Crystallization* 229–259

329. Zheng, Y., Yanful, E. K., Bassi, A. S. A review of plastic waste biodegradation. *Crit. Rev. Biotechnol.* **25**, 243–250 (2005).

330. Singh, B., Sharma, N. Mechanistic implications of plastic degradation. *Polym. Degrad. Stab.* **93**, 561–584 (2008).

331. Sivasamy, P., Palaniandavar, M., Vijayakumar, C. T. The role of β-hydrogen in the degradation of polyesters. *Polym. Degrad. Stab.* **38**, 15–21 (1992).

332. Zimmermann H. *Faserforsch Textiltech.,* **24**, 445 (1973).

333. Chrissafis, K., Paraskevopoulos, K. M., Bikiaris, D. N. Thermal degradation mechanism of poly(ethylene succinate) and poly(butylene succinate): Comparative study. *Thermochim. Acta* **435**, 142–150 (2005).

334. Zimmermann H., Chu D.D. *Developments in Polymer Degradation* (1986).

335. Landel R.F., Nielsen L.E. *Mechanical Properties of Polymers and Composites* (Boca Raton, 1993).

336. Van Krevelen D.W., Te Nijenhuis K. *Properties of Polymers: Their Correlation with Chemical Structure; their Numerical Estimation and Prediction from Additive Group Contribution* (Elsevier, Amsterdam, 2009).

337. Ward I.M., Sweeney J. *Mechanical Properties of Solid Polymers* (Wiley, UK, 2013).

338. Jakobsen, M., Bertelsen, G. CO2 and Its Effect on Chemical, Quality Changes in the Meat : a Review. J*ournal of Muscle Foods*, **13**, 143–168 (2001).

339. Tharanathan, R. N. Biodegradable films and composite coatings: Past, present and future. *Trends Food Sci. Technol.* **14**, 71–78 (2003).

340. Lagaron, J. M., Catalá R., Gavara R. "Structural characteristics defining high barrier properties in polymeric materials." *Materials science and technology*, **20**, 1-7 (2004).

341. Sano, T., Hasegawa, M., Kawakami, Y., Yanagishita, H. Separation of methanolrmmethyl-tert-butyl ether mixture by pervaporation using silicalite membrane. *Journal of membrane science*, **107**, 193-196 (1995).

342. Minelli, M., Sarti, G. C. Gas transport in glassy polymers: Prediction of diffusional time lag. *Membranes (Basel).* **8**, 1–15 (2018).

343. Duda J.L., *Diffusion in Polymers* (ed. P. Neogi, Marcel Dekker, US, 1996).

344. Singh A., Koros W. J. in *Polymers* (San Francisco,1998).

345. Weinkauf, D. H., Paul D. R. *in Barrier Polymers and Structures*. (American Chemical Society, 1990).

346. Michaels A.S., Vieth W.R., *J. Appl. Phys.* **34**, (1963).

347. Chiou J. S., Paul D. R. *Polym. Sci.* **25**, (1987).

348. Bastioli, C. *Handbook of Biodegradable Polymers*. (2005).

349. Göpferich A. Polymer bulk erosion, *Biomaterials* **30**, 2598-2604 (1996).

350. Pathak, V. M., Navneet. Review on the current status of polymer degradation: a microbial approach. *Bioresour. Bioprocess.* **4**, (2017).

351. Leja, K., Lewandowicz, G. Polymer biodegradation and biodegradable polymers - A review. *Polish J. Environ. Stud.* **19**, 255–266 (2010).

352. Ikada, Y., Tsuji, H. Biodegradable polyesters for medical and ecological applications. *Macromol. Rapid Commun.* **21**, 117–132 (2000).

353. Boland, E. L., Shine, R., Kelly, N., Sweeney, C. A., McHugh, P. E. A Review of Material Degradation Modelling for the Analysis and Design of Bioabsorbable Stents. *Ann. Biomed. Eng.* **44**, 341–356 (2016).

354. Hakkarainen, M. Aliphatic polyesters: abiotic and biotic degradation and degradation products.

In *Degradable aliphatic polyesters* (Springer, Berlin, Heidelberg, 2002).

355. Muller R.J., Schrader H., Profe J., Dresler K., Deckwer W.D., *Macromol. Rapid Commun.* **26**, (2005).

356. Marten, E., Müller, R. J., Deckwer, W. D. Studies on the enzymatic hydrolysis of polyesters: Low molecular mass model esters and aliphatic polyesters. *Polym. Degrad. Stab.* **80**, 485–501 (2003).

357. Müller, R. J., Kleeberg, I., Deckwer, W. D. Biodegradation of polyesters containing aromatic constituents. *J. Biotechnol.* **86**, 87–95 (2001).

358. Azevedo H.S., Reis R.L. Natural Stimulus Responsive Scaffolds/Cells for Bone Tissue Engineering: Influence of Lysozyme upon Scaffold Degradation and Osteogenic Differentiation of Cultured Marrow Stromal Cells Induced by CaP Coatings. Biodegradable Systems, *in Tissue Engineering and Regenerative Medicine,* (CRC Press, US, 2004).

359. Rydz, J., Sikorska, W., Kyulavska, M. & Christova, D. Polyester-based (bio)degradable polymers as environmentally friendly materials for sustainable development. *Int. J. Mol. Sci.* **16**, 564–596 (2015).

360. Lucas, N., Bienaime, C., Belloy, C., Queneudec, M., Silvestre, F., Nava-Saucedo, J. E. Polymer biodegradation: Mechanisms and estimation techniques - A review. *Chemosphere* **73**, 429–442 (2008).

361. Von Burkersroda F., Schedl L. Why degradable polymers undergo surface erosion or bulk erosion. **23**, 4221–4231 (2002).

362. Zee, M. Van der. Structure-biodegradability relationship of polymeric material. *Dissertation,* University of Twente (1997).

363. Grima, S., Bellon-Maurel, V., Feuilloley, P., Silvestre, F. Aerobic biodegradation of polymers in solid-state conditions: A review of environmental and physicochemical parameter settings in laboratory simulations. *J. Polym. Environ.* **8**, 183–195 (2000).

364. Rudnik E. *Compostable Polymer Materials*. (Elsevir, Amsterdam, 2008).

365. Compost Council of Canada. Available at: www.compost.org.

366. Tuomela M. Degradation of lignin and other ^{14}C-labelled compounds in compost and soil with an emphasis on white-rot fungi. *PhD Dissertation*, University of Helsinki (2002).

367. Smart Packaging Market Size & Share, Industry Report. www.grandviewresearch.com/industry-analysis/smart-packaging-market.

368. Cooper T.A. SPE FlexPackCon (2017).

369. Flexible Packaging: state of the industry report. (2017).

370. Russo, G., Simon, G. P., Incarnato, L., Correlation between Rheological , Mechanical , and

Barrier Properties in New Copolyamide-Based Nanocomposite Films. *Macrom.,* **39**, 3855-3864 (2006). doi:10.1021/ma052178h

371. Hotchkiss J.H., *Active Food Packaging*, Chapter 18 (Springer, US, 1995).

372. Pasha, I., Saeed, F., Sultan, M. T. & Khan, M. R. Recent Developments in Minimal Processing : A Tool to Retain Nutritional Quality of Food. *Critical Reviews in Food Science and Nutrition.* **54**, 340-351 (2014).

373. Ohlsson T., Bengtsson N. M. *Minimal Processing Technologies in the Food Industry.* (CRC press, Washington, 2002).

374. Farber, J. N., Harris, L. J., Parish, M. E., Beuchat, L. R., Suslow, T. V., Gorney, J. R., Garrett E. H., Busta F. F., Microbiological Safety of Controlled and Modified Atmosphere Packaging of Fresh and Fresh-Cut Produce. *Comprehensive Reviews In Food Science And Food Safety,* **2**, (2003).

375. Xing, Y., Li, X., Xu, Q., Jiang, Y., Yun, J., Li, W. Effects of chitosan-based coating and modi fi ed atmosphere packaging (MAP) on browning and shelf life of fresh-cut lotus root (Nelumbo nucifera Gaerth). *Innov. Food Sci. Emerg. Technol.* **11**, 684–689 (2010).

376. Morris, B. A. *The Science and Technology of Flexible Packaging. Multilayer Films from Resin and Process to End Use;* (Elsevier, Amsterdam, 2016).

377. Wagner, J. R. *Multilayer Flexible Packaging* (Elsevir, Amsterdam, 2000).

378. Ebnesajjad, S. *Plastic Films in Food Packaging—Materials, Technology and Applications* (2013).

379. Dixon, J. Multilayer Pacjaging for Food and Beverages. in *Packaging Materials* (ed. Europe:, I.) (2011).

380. Azeredo, H. M. Nanocomposites for food packaging applications. *Food Res. Int.* **42**, 1240–1253 (2009).

Chapter II
AIM

Packaging represents one of main market sector where plastics are employed; 39% of the entire production is used for food packages and is predicted to increase by an additional 11% in 2021. Polyethylene, polypropylene, poly(ethylene terephthalate), Nylon and polystyrene are the main materials used, due to their good barrier properties, adequate mechanical response and low cost. Despite that, their environmental impact has been deeply discussed from public opinion because of the short shelf-life, non-degradable nature and absence of efficient end-life fate that are causing wide accumulation of plastic waste around the Globe. Moreover, the oil-based nature of monomers is graving on a non-renewable resource. The social pressure and the massive damages caused in natural habitats push both researchers and industries to find a solution. Recycling is one of the main possibilities explored, in fact, since 2017 it is preferred to landfill. Despite that, recycling is encountering substantial issues, hampering the economical suitability of the whole process. Considering the particular nature of packed products, industries are looking for systems with tunable characteristics. In order to better protect the products during transport, improve the shelf-life, hamper chemical/physical contamination and maintain the freshness of products, multilayer materials have conquered the market. Even if these systems boast very good properties, their recycling represents a great challenge. Moreover, the recycling costs are generally high because of problematic separations among layers. Thus, landfill is the preferred choice.

In light of this, a valid solution needs to be found and the new biodegradable and/or bio-based polymers, referred to as bioplastics, are showing encouraging results. Among the different possibilities, the class of biodegradable polyesters is quite promising: the route of synthesis is simple and a large variety of monomers can be used. The different nature of these last confers ad hoc tuning of the final properties in view of the application envisioned. The so-obtained polymers are stable and easy to process, indeed nowadays are conquering the market both in large sector, as packaging, and in high-added value applications, as electronic components or biomedical devices. One example is poly(butylene succinate) (PBS), that is biodegradable and can be completely obtained from renewable sources and is already used for food packaging application, thanks to its high thermal stability and good mechanical properties. Despite that, its stiffness and slow biodegradation rate, due to high crystallinity degree, limits its window

of applicability and substitution of oil-based plastics. Poly(ethylene furanoate), PEF, is another example of bioplastic; it is a fully bio-based polymer with barrier properties much better than the most widely used material for beverage, PET. For this reason, Avantium in collaboration with Coca-Cola, is planning an industrial process to produce of PEF-bottles.

Despite their good properties, bioplastics do not fulfill all the requirements needed for food packaging application. For this reason, in the work presented, different strategies have been tested to synthesize new materials, on one side, and ad hoc modify the properties of well-known biopolyesters, on the other, maintaining the already good characteristics and, concurrently, improving the unsatisfactory ones. In this context, we have acted on the chemical structure as well as on the molecular architecture (random or block distribution of the repeating units).

All the synthetized materials have been completely characterized from chemical, structural and thermal point of view. Moreover, they have been processed in form of film to also test the functional properties, such as mechanical response, surface film hydrophilicity, compostability and barrier performances. Afterwards, a deep structure-property relationship analysis has been carried out. Chemical structure and architecture, in fact, are the starting point for the realization of mono materials in view of an eco-sustainable recycling and, ultimately, of an eco-friendly biodegradation process

An overview of the experimental research conducted is reported here (**Figure 1**).

EXPERIMENTAL ACTIVITY

NEW BIO-BASED POLYMERS

MODIFICATION OF WELL-KNOWN POLYESTERS

PROCESSING

- Compression moulding
- Extrusion

MOLECULAR CHARACTERIZATION

- Nuclear magnetic resonance spectroscopy (^{1}**H-NMR**, ^{13}**C-NMR**)
- Gel permeation chromatography (**GPC**)
- Intrinsic viscosity determination (**IV**)

THERMAL CHARACTERIZATION

- Thermal gravimetric analysis (**TGA**)
- Modulated-temperature thermogravimetric analysis (**MT-TGA**)
- Differential/ Flash scan calorimetry (**DSC/FSC**)

STRUCTURAL CHARACTERIZATION

- Wide-angle X-ray scattering (**WAXS**)
- Infrared spectroscopy (**IR**)

SURFACE CHARACTERIZATION

- Polarized optical microscopy (**POM**)
- Atomic force microscopy (**AFM**)
- Scanning electron microscope of fractured surfaces (**FESEM**)
- Scanning electron microscopy (**SEM**)

MECHANICAL CHARACTERIZATION

- Stress-strain test
- Cyclic measurements

SPECIFIC TESTS

- Water contact angle evaluation (**WCA**)
- Composting test
- Barrier properties measurement

Figure 1*: Schematic representation of the experimental activities*

91
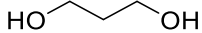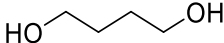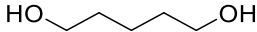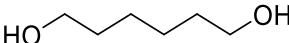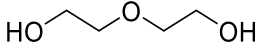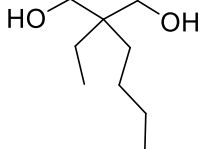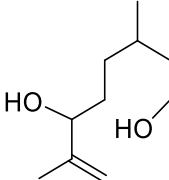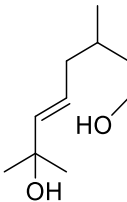
Chapter III
METERIALS AND METHODS

1 MATERIALS

1.1 Electrophilic compounds

Dimethyl succinate (DMS) purchased from Sigma Aldrich (Milan, Italy).	
Pripol 1009 kindly supplied by CRODA (Snaith, UK)	
Dimethyl Isophthalate (DMI) purchased from Sigma Aldrich (Milan, Italy).	
Furandicarboxylic acid (FDCA) Purchased from TCI Europe (Zwijndrecht, Belgium)	
Trans 1,4-cyclohexanedicarboxylic acid (*Trans*-CEDA) purchased from Zentek (Milan, Italy)	
Catechol carbonate (CC) synthetized by Tommaso Tabanelli et al. at the Industrial Chemistry Department "Toso Montanari", University of Bologna	
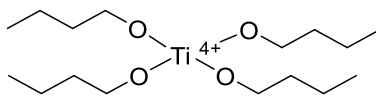
1.2 Diols

1,3-Propanediol (PD) purchased from Sigma Aldrich (Milan, Italy)	HO⌒⌒OH
1,4-Butanediol (BD) purchased from Sigma Aldrich (Milan, Italy)	HO⌒⌒⌒OH
1,5-Pentandiol (Pent) purchased from Sigma Aldrich (Milan, Italy).	HO⌒⌒⌒⌒OH
1,6-Hexandiol (Hex) purchased from Sigma Aldrich (Milan, Italy).	HO⌒⌒⌒⌒⌒OH
Diethylen glycol (DEG) purchased from Sigma Aldrich (Milan, Italy)	HO⌒⌒O⌒⌒OH
2-butyl-2-ethyl propanediol (BEPD) purchased TCI Europe (Zwijndrecht, Belgium)	HO⌒C⌒OH
Diol 4 synthetized by Deianira Lanteri et al. at the Department of Chemistry and Industrial Chemistry, University of Genova	
Diol 5 synthetized by Deianira Lanteri et al. at the Department of Chemistry and Industrial Chemistry, University of Genova	
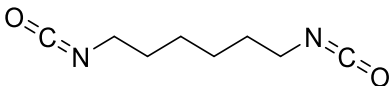
1.3 Diamines

1,4-Butandiammine (BDA) purchased from Sigma Aldrich (Milan, Italy)	H_2N⌒⌒⌒NH_2
1,5-Pentandiammine (PDA) purchased from Sigma Aldrich (Milan, Italy)	H_2N⌒⌒⌒⌒NH_2
1,6-Hexandiammine (HDA) purchased from Sigma Aldrich (Milan, Italy)	H_2N⌒⌒⌒⌒⌒NH_2
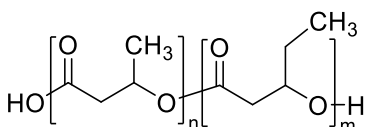
1.4 Catalysts

Titanium(IV) tetrabutoxide (TBT) purchased from Sigma Aldrich (Milan, Italy)	
Titanium(IV) isopropoxide (TIIP) purchased from Sigma Aldrich (Milan, Italy)	

1.5 Chain extenders

Hexamethylene diisocyanate (HDI) purchased from Sigma Aldrich (Milan, Italy)	

1.6 Polymers

Poly(3-hydroxybutyrate-co-3-hydroxyvalerate) (PHBV) purchased Biocycle®, PHB Industrial S.A. (Brazil)	

1.7 Blends

Prepared by Franco Dominici et al. at Civil and Environmental Engineering Department, University of Perugia	Composition		
	TPWF Mol %	PBS Mol %	Co Mol %
Plasticized wheat flour (TPWF)	100	0	0
Poly(butylene succinate) (PBS)	0	100	0
P(BS-co-Pripol) (Co)	0	0	100
70TPWF/30PBS	70	30	0
70TPWF/25PBS/5Co	70	25	5
70TPWF/20PBS/10Co	70	20	10
70TPWF/15PBS/15Co	70	15	15
70TPWF/10PBS/20Co	70	10	20
70TPWF/5PBS/25Co	70	5	25

2   SYNTHESIS

2.1   Monomers

2.1.1   Esterification

The selected diacid sub-unit together with a large mass excess of anhydrous methanol (1:30, w/w) were added into a round-bottom flask. In order to favor the dissolution, the system was heated up to 70°C under reflux. Then, the flask was cooled to room temperature and thionyl chloride was added dropwise, in the same molar amount as the carboxylic end groups of the diacid.

ESTERIFICATION of DICARBOXYLIC ACIDS

HOOC—■—COOH   + CH_3OH ⟶ H_3COOC—■—$COOCH_3$ + H_2O
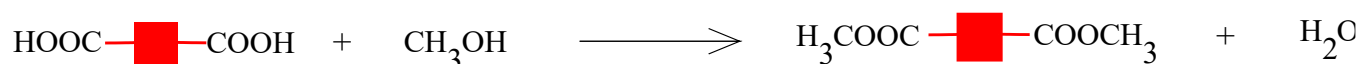
Figure 2.1: Schematic representation of esterification reaction.

The solution obtained was heated again to 70°C under reflux. After 3 hours, the system was cooled to room temperature and precipitation of dimethyl ester, as solid powder, was observed. The product was filtered and washed with anhydrous methanol; a second recrystallization was performed, dissolving the so-obtained dimethyl ester in methanol at 60°C and quenching the solution in ice bath (**Figure 2.1**).

2.2   Polymers

2.2.1   Polycondensation

The following approach was used to synthetize (**Figure 2.2**):

- hydroxyl-terminated prepolymers;
- high molecular weight homopolymers;
- high molecular weight random copolymers.

A defined excess of diol together with the diacid/dimethylester and the catalysts were added in a stirred glass reactor of 250 ml placed into a thermostated molten salts bath (50% w/w KNO_3; 30% w/w $NaNO_2$; 20% w/w $NaNO_3$). In the first stage, the temperature (T^I) was raised to 180-200 °C, keeping the system under N_2 atmosphere until the 90% of the theoretical amount of water/methanol was distilled off. During the second stage, the temperature (T^{II}) was increased slowly to 200-230 °C, and the pressure was gradually reduced to 0.1 mbar in order to facilitate the removal of the excess glycol and promote the

transesterification reactions. The synthesis was carried out until a constant torque was measured. The product of reaction was discharged from the reactor and cooled down to room temperature.
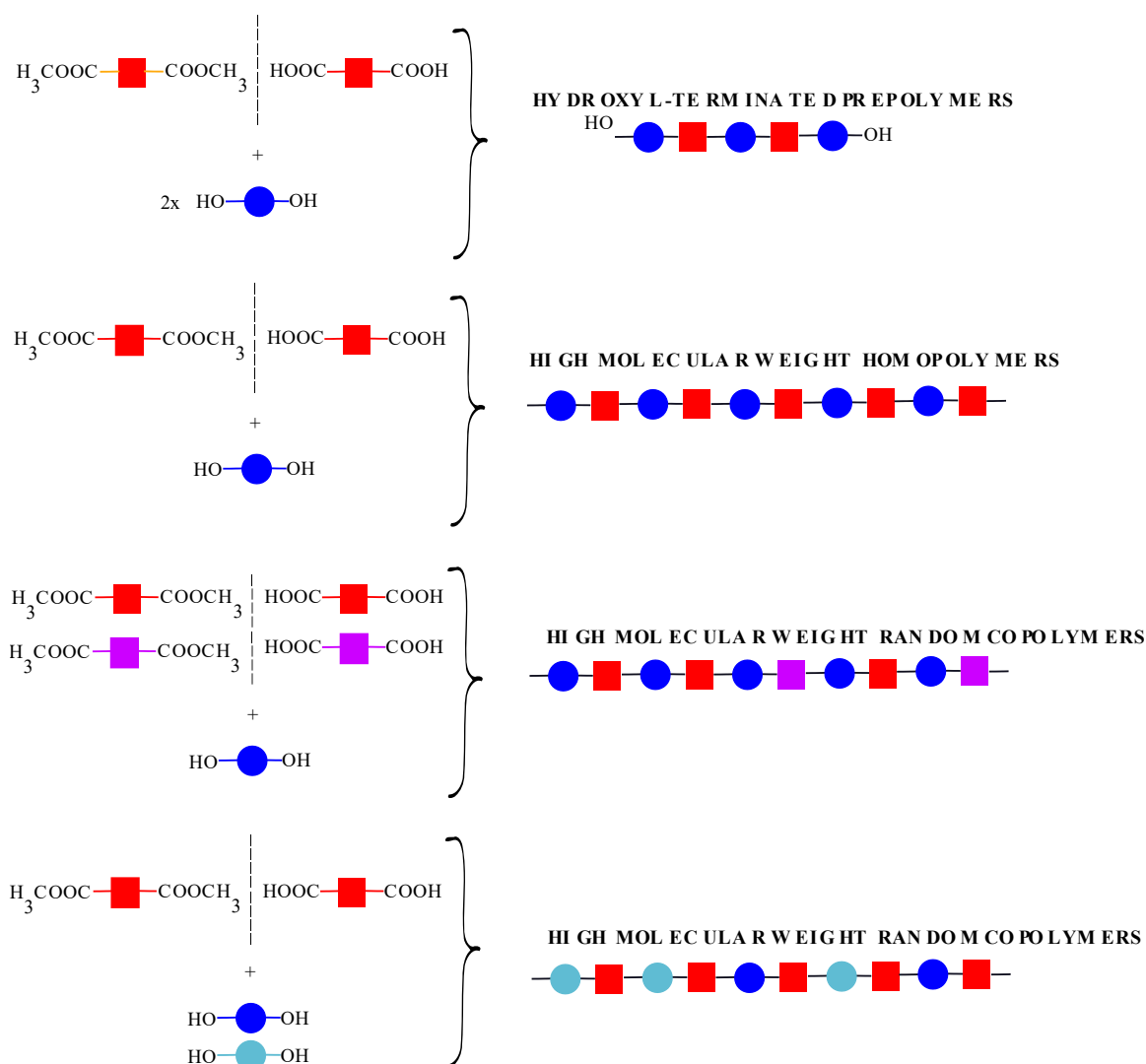
Figure 2.2: Schematic summary of the polycondensation process conducted.

2.2.1.1 Hydroxyl-terminated prepolymers

Detailed information on reagents and conditions for the synthetized prepolymers were summarized in **Table 2.1**. The I step was kept for 120 min while the II step was conducted for 60 min till a constant value of torque was recorded.

Table 2.1: Operation conditions of the hydroxyl-terminated prepolymers prepared.

Hydroxyl-terminated prepolymers	trans-CEDA Mol%	BD Mol%	BEP Mol %	TBT ppm	T^I °C	T^{II} °C
P(BCE$_{70}$BEPCE$_{30}$)-OH	100	140	70	200	180	220

2.2.1.2   High molecular weight homopolymers

Detailed information on reagents and conditions for the synthetized homopolymers were summarized in **Table 2.2**. I step needed 120 min to be completed while II step was kept until a constant value of torque was observed.

Table 2.2: Operation conditions employed for high molecular weight polymers prepared.

High molecular weight homopolymers	Dicarboxylic acid/ester Mol%	Glycol Mol %	Catalyst ppm/kg		T^I °C	T^{II} °C
PBS	DMS 100	BD 130	TBT 200		180	220
PBI	DMI 100	BD 130	TBT 200		200	230
PBF	FDCA 100	BD 300	TBT 200	TIIP 200	180	230
PDEF	FDCA 100	DEG 200	TBT 200	TIIP 200	180	230
PPeF	FDCA 100	Pent 500	TBT 200	TIIP 200	170	220
PPCE	*Trans*-CEDA 100	PD 120	TBT 200		200	220
PBCE	*Trans*-CEDA 100	BD 120	TBT 200		200	220
PPentCe	*Trans*-CEDA 100	Pent 120	TBT 200		200	220
PHexCE	*Trans*-CEDA 100	Hex 120	TBT 200		200	220
Polyurea 4	BDA 100	CC 100	-		110	200
Polyurea 5	PDA 100	CC 100	-		110	200
Polyurea 6	HAD 100	CC 100	-		110	200

2.2.1.3   High molecular weight random copolymers

Detailed information on reagents and conditions for the synthetized random copolymers were summarized in **Table 2.3**. In this case, I step needed 120 min to be completed while II step was kept until a constant value of torque was observed.

Table 2.3: *Operation conditions employed for random copolymers prepared.*

High molecular weight random copolymers	Dicarboxylic acid/ester Mol%		Glycol Mol %		Catalyst ppm/kg		T^I °C	T^{II} °C
P(BS$_{88}$BPripol$_{12}$)	DMS 90	Pripol1009 10	BD 130		TBT 200		180	220
P(BS$_{73}$BPripol$_{27}$)	DMS 80	Pripol1009 20	BD 130		TBT 200		180	220
P(BS$_{59}$BPripol$_{41}$)	DMS 70	Pripol1009 30	BD 130		TBT 200		180	220
P(BS$_{85}$BPripol$_{15}$) Co	DMS 85	Pripol1009 15	BD 130		TBT 200		180	220
Copolymer 6	DMS 100		BD 60	Diol 4 40	TBT 200		180	200
Copolymer 7	DMS 100		BD 70	Diol 4 + Diol 5 30	TBT 200		180	180
P(BF$_{90}$BI$_{10}$)	FDCA 90	DMI 10	BD 700		TBT 200	TIIP 200	180	230
P(BF$_{80}$BI$_{20}$)	FDCA 80	DMI 20	BD 700		TBT 200	TIIP 200	180	230
P(BF$_{70}$BI$_{30}$)	FDCA 70	DMI 30	BD 700		TBT 200	TIIP 200	180	230
P(BF$_{50}$BI$_{50}$)	FDCA 50	DMI 50	BD 700		TBT 200	TIIP 200	180	230
P(BF$_{30}$BI$_{70}$)	FDCA 30	DMI 70	BD 700		TBT 200	TIIP 200	180	230
P(BF$_{20}$BI$_{80}$)	FDCA 20	DMI 80	BD 700		TBT 200	TIIP 200	180	230
P(BF$_{10}$BI$_{90}$)	FDCA 10	DMI 90	BD 700		TBT 200	TIIP 200	180	230
P(BCE$_{90}$BI$_{10}$)	CEDA 90	DMI 10	BD 160		TBT 200		200	230
P(BCE$_{80}$BI$_{20}$)	*Trans*-CEDA 80	DMI 20	BD 160		TBT 200		200	230
P(BCE$_{70}$BI$_{30}$)	*Trans*-CEDA 70	DMI 30	BD 160		TBT 200		200	230
P(BCE$_{50}$BI$_{50}$)	*Trans*-CEDA 50	DMI 50	BD 160		TBT 200		200	230
P(BCE$_{30}$BI$_{70}$)	*Trans*-CEDA 30	DMI 70	BD 160		TBT 200		200	230
P(BCE$_{20}$BI$_{80}$)	*Trans*-CEDA 20	DMI 80	BD 160		TBT 200		200	230
P(BCE$_{10}$BI$_{90}$)	*Trans*-CEDA 10	DMI 90	BD 160		TBT 200		200	230

2.2.2 Depolymerization

HIGH MOLECULAR WEIGHT HOMOPOLYMER

+

HO—OH

HYDROXYL-TERMINATED HOMOPOLYMER

HO—OH
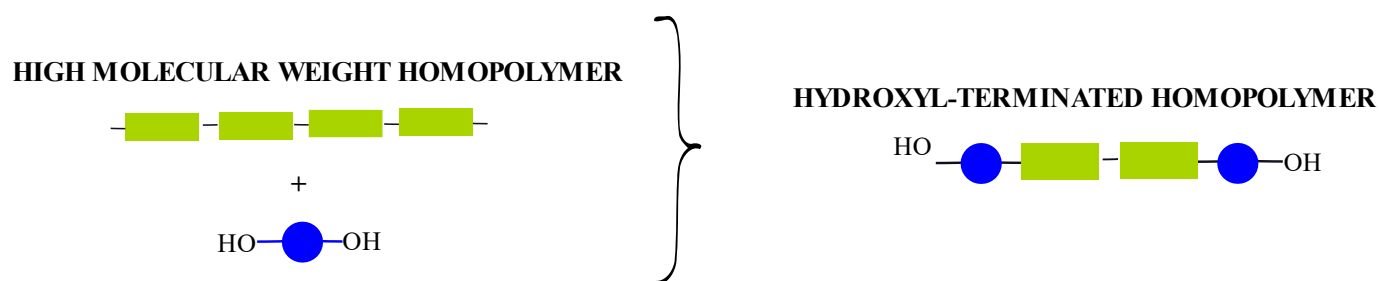
Figure 2.3 Depolymerization process.

The polymeric material, PHB, was added to the glass stirred reactor, kept at 190°C in a thermostated salt bath. Then, glycol was added. The system was stirred under inert atmosphere for 12 minutes, then, the OH-terminated polymer was discharged and allowed cooling. In **Figure 2.3** a graphical representation of the depolymerization process was reported.

Table 2.4: Operation conditions employed for depolymerization process.

Hydroxyl-terminated homopolymer	PHB Mol %	BD Mol %	TBT ppm	T °C	Time min
PHB-OH	100	46	200	190	12

2.2.3 Chain extension

2.2.3.1 Multiblock copolymers

HO—OH
HYDROXYL-TERMINATED HOMOPOLYMER

+

OCN—NCO
CHIAN EXTENDER

+

HO—OH
HYDROXYL-TERMINATED COPOLYMER

MULTYBLOCK COPOLYMER
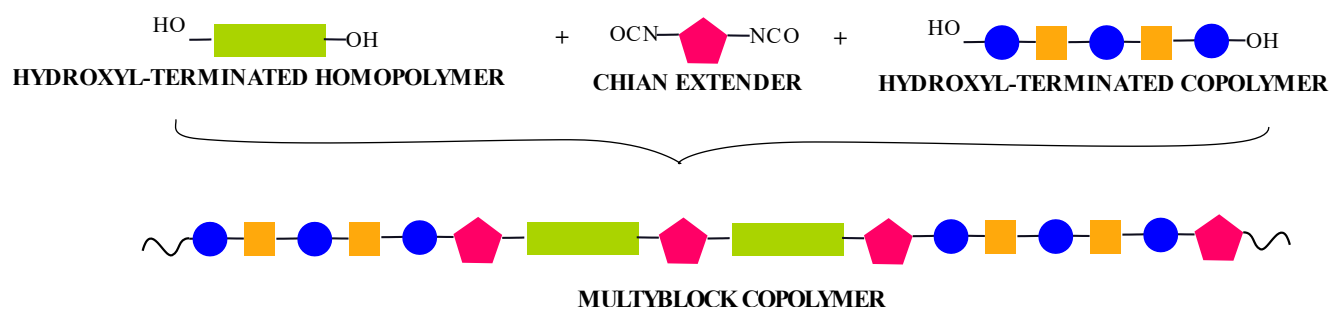
Figure 2.4: Synthesis of multiblock copolymers through chain extension.

Multiblock copolymers were synthetized via chain extension of selected hydroxyl terminated prepolymers. They were added in a stirred glass reactor of 250 ml into a thermostated salt bath, purged by nitrogen flow. Once the two reactants melted, an equimolar amount of HDI with respect to the hydroxyl group present in the prepolymers, was added. The reaction was conducted until a constant

100

torque was measured **(Figure 2.4)**. Detailed information regarding reagents and conditions were reported in **Table 2.5.**

Table 2.5: *Reaction conditions of multiblock copolymers obtained by chain extension.*

Multiblock copolymers	PHB-OH Mol %	P(BCE$_{70}$BEPCE$_{30}$)-OH Mol %	HDI mmol	T °C
PHB$_{50}$-P(BCE$_{70}$BEPCE$_{30}$)$_{50}$	50	50	0.43	160
PHB$_{72}$-P(BCE$_{70}$BEPCE$_{30}$)$_{28}$	75	25	0.45	160

3 METHODS

3.1 Molecular characterization

3.1.1 Nuclear Magnetic Resonance (NMR)

Nuclear Magnetic Resonance spectroscopy is one of the main techniques to collect information about structure of molecules. In the present Thesis, NMR technique was employed to verify the chemical structure of homopolymers and copolymers, and, for these latter, also the real composition and the comonomer sequence distribution.

The samples were prepared dissolving the selected material in $CDCl_3$, containing 0.03 vol.% tetramethylsilane (TMS) as internal standard. If solubility issues were encountered, a mixture of $CDCl_3$ and CF_3COOD (70% v/v) or pure CF_3COOD were used.

The measurements were performed with a Varian Inova 400 MHz (Palo Alto, California, USA). ^{1}H-NMR spectra were recorded at room temperature with a polymer concentration of 0.5 wt%, relaxation delay of 1 s, acquisition time of 1 s and up to 64 repetitions. ^{13}C-NMR spectra were recorded with a polymer concentration of 5 wt% in full decoupling mode with NOE effect, relaxation delay of 2 s, acquisition time of 1 s and up to 512 repetitions.

The molecular architecture of copolymers, defined by the degree of randomness, b, was determined employing ^{1}H-NMR or ^{13}C-NMR, considering the location of the relevant peaks. The degree of randomness has a value close to 0 for physical blends, it is equal to 1 for random copolymers, between 0 and 1 for block copolymers and reach the maximum value of 2 for copolymers with an alternate distribution of comonomeric units.

b was calculated considering the signal of protons or carbon atoms of the common subunit in between the comonomeric ones (X and Y). The degree of randomness can be express as:

$$b = P_{XY} + P_{YX} \qquad\qquad Eqn. 1$$

where P_{XY} represents the probability to find a X unit next to a Y one and P_{YX} is the probability to find a Y unit next to a X one, respectively.

Those probabilities can be defined with the *Eqn.2* and *Eqn.3*.

$$P_{XY} = \frac{\frac{I_{XY}+I_{YX}}{2}}{\frac{I_{XY}+I_{YX}}{2}+I_{XX}} \qquad\qquad Eqn. 2$$

$$P_{YX} = \frac{\frac{I_{YX} + I_{XY}}{2}}{\frac{I_{YX} + I_{XY}}{2} + I_{YY}} \qquad\qquad Eqn.\ 3$$

where I_{XY}, I_{YX}, I_{XX}, I_{YY} represent the integrated intensities of the resonance signals of XY, YX, XX, YY sequences, respectively.

Consequently, the average length of the sequences (L_X and L_Y) can be calculated as follows:

$$L_X = \frac{1}{P_{XY}} \qquad\qquad Eqn.\ 4$$

$$L_Y = \frac{1}{P_{YX}} \qquad\qquad Eqn.\ 5$$

In the case of OH-terminated polymers, NMR analysis also allowed the calculation of the degree of polymerization (DP). DP can be defined considering the normalized areas of the signals of the central (I_{Int}) and terminal (I_{Ext}) units:

$$DP = \left[\frac{I_{Int}}{I_{Ext}}\right] * 2 + 1 \qquad\qquad Eqn.\ 6$$

The polymer molecular weight (M_n) was then calculated according to the following equation:

$$Mn = DP \cdot W_{ru} + W_{glycol} \qquad\qquad Eqn.\ 7$$

where W_{ru} represents the molecular weight of the repeating unit and W_{glycol} is the molecular weight of the glycol.

3.1.2 Gel Permeation Chromatography (GPC)

The molecular weights of the synthetized polymers were investigated by gel-permeation chromatography (GPC). The measurement was conducted at room temperature, using a chromatograph system HP Series 1100 HPLC (Agilent Technologies, Santa Clara, CA, USA) equipped with PL gel 5µm MiniMIX-C (Agilent Technologies, Santa Clara, CA, USA) column and refractive index/UV detector. The chromatograms were collected with HP Chemstation version A.05.04 and analyzed by GPC Calculator 7.6 by General Electric Company. The system was eluted in chloroform at 0.3ml/min. The samples were injected by a loop system, after dissolution and filtration thought a PTFE millipore of 0.3 µm. The samples prepared had a concentration of 2 mg/ml. Calibration curve was obtained using polystyrene standards in the range of 800 – 100000 g/mol.

3.1.3 Intrinsic Viscosity (IV)

Intrinsic viscosity (η) was determined using Ubbelohde type viscosimeter 31 13/Ic (diameter 0.84 mm). The tests were performed in a thermostated bath of water, kept at 30°C. The samples were dissolved in a defined volume of chloroform and filtered. Then, the solution was poured in the viscosimeter. The flowing time of the charged solution was analyzed with an equipped stopwatch. Aliquots of chloroform were added to the solution, until a final concentration of 0.8 g/dl was reached. The measurement was repeated five times for any addition of solvent.

The intrinsic viscosity (η) was extrapolated, considering the following relation:

$$\eta = \frac{ln\frac{t}{t0}}{c} \hspace{5cm} Eqn.\ 8$$

where t_0 is the efflux time of the solvent (s), t is the efflux time of the solution and c is the concentration of the studied solution (g/dl).

3.2   Thermal characterization

3.2.1 Thermogravimetric Analysis (TGA)

3.2.1.1   Perkin Elmer TGA 7

Studies of thermal stability were performed using a Perkin Elmer (Waltham, MA, USA) TGA7 apparatus under nitrogen atmosphere (gas flow: 40 mL/min). The test implied to heat the sample (10 mg) at 10 °C/min from 40°C up to 800 °C.

3.2.1.2   Seiko Exstar 6300

Seiko Exstar 6300 was employed to conduct TGA analysis. The tests started at 30 to 600 °C at 10°C/min under a flow of nitrogen of 250 mL/min.

3.2.1.3   Modulated-Temperature Thermogravimetric Analysis (MT-TGA)

Discovery thermogravimetric analyzer (TA Instruments) was used to investigate thermal degradation process. Nickel and weight standards were employed for calibration. All the measurements were conducted under nitrogen flow of 20 mL/min to prevent oxidative degradation. Starting from room temperature modulated-temperature heating ramps were set, until the temperature of 600°C, using a modulation amplitude of ± 5K and a heating rate of 2K/min with an oscillation period of 60s. The evaluation of activation energy of the main degradation process followed what reported by Blaine et al., and was determined as a function of the conversion using a model-free method[1].

The result obtained was a curve showing the weight loss as a function of temperature. The temperature of maximum weight loss (T_{max}) was calculated as the minimum value of the thermogram derivative, while T_{onset} represents the temperature where the degradation starts. $T_{5\%}$ was determined as the temperature corresponding to the 5% of mass loss.

3.2.2 Differential Scanning Calorimetry (DSC)

Calorimetric analyses were performed using a Perkin Elmer DSC6 (Waltham, MA, USA), Perkin-Elmer DSC 7 (Waltham, MA, USA) equipped with cryogenic cooling accessory CCA 7. The calibration was conducted using high purity standards of indium and cyclohexane. Samples of 6 mg were encapsulated in aluminum pans and place inside the instrument together with the reference (empty aluminum pan). The furnace was purged permanently with dry nitrogen gas.

The general program performed on the samples is reported herein:

- **1st scan**: -70 °C to $T_m + 30$ °C at 20 °C/min
- Isotherm of 5 min at the final temperature
- $T_m + 30$ °C to -70°C at 100 °C/min
- **2nd scan**: -70 °C to $T_m + 30$ °C at 20 °C/min

The thermogram was analyzed, determining the glass-transition temperature (T_g) as the midpoint of the heat capacity increment Δc_p associated to the glass-to-rubber transition; Δc_p was calculated from the vertical distance between the two extrapolated baselines at the glass transition temperature. The cold crystallization temperature (T_{cc}) was determined as the peak minimum of the exothermal transition recorded, and the corresponding heat of crystallization (ΔH_{cc}) was calculated considering the total area of the peak. The melting temperature (T_m) and the related heat of fusion (ΔH_m) were calculated as the maximum and the underlying area of the endothermal peak, respectively.

3.2.3 Fast Scanning Chip Calorimetry (FSC)

Mettler-Toledo Flash DSC 1 in conjunction with a Huber intracooler TC100 was employed. The sample was prepared using a microtome and cutting 10 µm thickness from the 100 µm films; then, the lateral size was reduced to section to about 50 to 100 µm with the aid of a stereomicroscope. According with the instrument operating instructions, the sensor was conditioned and temperature-corrected, then, the as-prepared material was placed onto the chip. The support was located in the furnace, permanently purged with dry nitrogen gas at a flow rate of 35 mL/min.

3.3   Microscopic characterization

3.3.1   Polarized Optical Microscopy (POM)

Polarizing Optical Microscopy, Motic BA41 (Leica, Germany) was used to monitor the spherulitic superstructure of specimens of different aging/crystallization history. The samples were prepared by heating thin sections of polymeric material between two circular plan microscope coverslips of 100 μm thickness each to a temperature of 200°C, using a hot stage Linkam THMS 600. After 3 minutes, the sample was quenched to room temperature.

3.3.2   Scanning Electron Microscopy (SEM)

Scanning electron microscopy (SEM), performed by Phenom Microscope (Amsterdam, The Netherlands), permits to analyze the surface microstructure of the samples. The material was cut and fixed with carbon tape on aluminum stab, then, the system was covered with a gold spattered film.

3.3.3   Scanning Electron Microscope of Fractured Surfaces (FESEM)

225Supra 25-Zeiss microscope was used to analysis the fractured surfaces with an accelerating voltage of 2.5 kV. The fractured surfaces were obtained by cryofracturing in liquid nitrogen. In order to provide adequate electric conductivity, the surfaces were gold-sputtered.

3.3.4   Atomic Force Microscopy (AFM)

Nanometer length-scale semicrystalline morphology was investigated with a Dimension FASTSCAN (Bruker-Nano, USA) operating in peak-force tapping mode and equipped with a silicon nitride sensors SCANASYST-FLUID+ (Bruker, USA), a nominal spring constant of 0.7 N/m and a tip radius of 2 nm, using 0.02 V as set point. The samples analyzed with AFM were cut using a microtome in 10 μm thin sections.

3.4   Structural characterization

3.4.1   Wide-angle X-Ray diffraction (WAXS)

X-ray diffraction patterns were recorded with PAN Analytical X'PertPro diffractometer, equipped with a fast solid state X'Celerator detector (Almelo, the Nederlands), using a copper target ($\lambda = 0.1548$ Å). The interval between 5-60° 2θ (wide angles region) was analyzed, by collecting data for 100 s at each 0.10° step.

Calculating the area of the diffraction profile, crystallinity index (X_c) was calculated as follow:

$$Xc = \frac{Ac}{At}$$ *Eqn. 9*

where, A_c represents the crystalline diffraction area obtained by subtracting the amorphous halo from the total area of the diffraction profile, while A_t is the entire area of the diffraction profile. Employing Scherrer's equation, the average size of the crystalline domains l_c was estimated with *Eqn. 10*[2,3].

$$l_c = \frac{K\,\lambda}{\beta\,\cos\theta}$$ *Eqn. 10*

Where K represents a nondimensional shape factor of 0.89 while λ is the X-rays wavelength (0.154 nm). The Full Width at Half Maximum (FWHM) of the selected crystalline peak is β, and θ is the Bragg's angle. The corresponding crystalline interplanar distance, d, was evaluated with *Eqn. 11*, the Bragg's law:

$$d = \frac{n\,\lambda}{2\,\sin\theta}$$ *Eqn. 11*

Where n is a positive integer.

3.4.2 *Infrared Spectroscopy (IR)*

Infrared spectrometry was performed in the range between 4000 and 450 cm^{-1} (NIR Near Infrared), employing a Perkin Elmer Spectrum One FT-IR spectrometer equipped with the attenuated total reflectance (ATR) element. 64 scans were conducted to acquire the final data.

3.5 Surface wettability

The hydrophilicity/hydrophobicity of polymeric films was studied through evaluation of the static contact angle. The measurement was performed using a KSV CAM101 instrument (Helsinki, Finland) comprised by a camera and syringe placed perpendicularly to a mobile table or employing a standard goniometer (FTA2000, First Ten Angstroms, Inc., Portsmouth, UK) equipped with a camera, and drop shape analyzer (SW21; FTA32 2.0 254 software, First Ten Angstroms, Inc., Portsmouth, UK). Before starting the tests, the polymeric materials were washed with a solution 70/30 v/v ethanol/water and let them dry overnight. The sample was placed on the mobile table and the syringe was charged with deionized water. A drop was deposited on the film by placing it in contact with the polymeric surface using the syringe needle. Side profiles of deionized water drops was recorded for image analysis. In order

to evaluate the reproducibility of the results, images of eight different drops placed in different areas for each film were acquired. The final value of contact angle was reported as the average value ± standard deviation. The data were recorded after 1 second from the deposition of the drop on the surface.

3.6 Sample processing

3.6.1 Purification

The synthetized materials were purified in order to eliminate the possible sub-products of reaction or monomers/catalysts residues. The polymer was solubilized in chloroform or in a solution of chloroform/hexafluoroisopropanol in case of solubility issues. Then, the solution was added dropwise to methanol, whose volume was 5 times higher. The precipitated was filtered off and let dried overnight.

3.6.2 Compression molding

Thin polymeric films were processed by compression molding. Carver Laboratory Press (3851-0) was used: the polymer in form of powder was placed in between two Teflon plates. The system was heated at 40°C higher than the melting point of the processed material. A pressure of 5 tons/m^2 was applied for 2 minutes. Then, the film was let cooling ballistically to room temperature. Prior to further tests, films were stored at room temperature for at least two weeks to reach equilibrium crystallinity.

3.7 Mechanical characterization

3.7.1 Tensile tests

Tensile tests were carried out using an Instron 9965 tensile testing machine (Norwood, MA, USA), equipped with a rubber grip and a 1 KN load cell or employing a universal test machine (Lloyd Instruments, LR30KPlus). The polymeric materials in form of film were cut in a defined rectangular shape (5 mm wide and 20 mm length) and the thickness was evaluated using a Sample Thickness Tester DM-G with a digital dial indicator (MarCartor 1086, Mahr GmbH, Esslingen, Germany) and the associated DM-G software. In 10 different positions of each film, the minimum, maximum, and average value for each reading was measured in triplicates at room temperature. The so obtained sample was fixed with the rubber grips and 10 mm/min crosshead speeds was adopted. During the test, load-displacement curves were recorded, and converted to stress-strain curves. The measurements were repeated on 5 different samples and the final value was reported as average ± standard deviation. Stress-

strain curves allowed to define the elastic modulus (E), determined from the initial linear slope of curve, stress (σ_y) and elongation (ε_y) at yielding and stress (σ_b) and elongation (ε_b) at break.

3.7.2 Cyclic test

Cyclic loading was performed with Instron 9965 tensile testing machine (Norwood, MA, USA), equipped with a rubber grip and a 1 KN load cell. More in detail, film samples were shaped in a rectangular form of 5 mm wide and 20 mm length. The analyzed sample was anchored with the rubber grip and strained up to 50-100%. The load applied was then removed allowing the sample to relax and afterward stretched again. The deformation was repeated for 25 cycles. The stress-strain curves recorded report the cyclic stress amplitude, where the nonlinearity of the stress-strain curves represents the hysteresis loop.

3.8 Composting studies

Square film specimens (20 mm wide, about 0.1 mm thick) were weighed to obtain the initial mass. Then, they were placed in 100ml vessels, surrounded by compost, moisten with 10 ml of deionized water. The glass vessels were located in a system with controlled temperature (58.0 ± 0.1 °C) and humidity (90%). At different time intervals, a selected sample was washed with ethanol aqueous solution (70% vol). After drying over P_2O_5 under vacuum for 2 days, the sample was weighted. In order to follow the degradation process, weight loss was monitored.

$$\% \, weight \, loss = \frac{m_i - m_f}{m_i} \cdot 100 \qquad\qquad Eqn. \, 12$$

where m_f and m_i are the final and the initial sample weight, respectively.

3.9 Gas permeability studies

Permeability tests were performed by a manometric method using a Permeance Testing Device, type GDP-C (Brugger Feinmechanik GmbH), following ASTM 1434-82, DIN 53 536 in compliance with ISO/DIS 15 105-1 and to Gas Permeability Testing Manual of the instrument. The measurements were conducted in the labs of Agri-food Science and Technology Department, University of Bologna, under the supervision of Prof. Valentina Siracusa.

The equipment was constituted of two chambers between which the film was placed. The area of the film samples was 78.5 cm^2 (standard measurement area). Firstly, a preliminary high vacuum was applied, then, the upper chamber was filled with the gas chosen for the test (food grade O_2, CO_2 and N_2 at 23°C,

relative humidity, RH, of 0%, and a gas stream of 100 cm^3/min) at 1 atm. The increasing of gas pressure as a function of time was recorded by a pressure transducer. The gas transmission rate (GTR, expressed as cm^3 cm m^{-2} d^{-1} bar^{-1}) defining the permeability to gasses of the film, was determined studying the increasing of pressure in relation to the volume of the device and time. In some cases, permeability was checked also at different temperatures (5, 10, 15, 35, 38, 40, 45 and 50 °C) and different RH (85% -0% at 23 °C).

Experiments were repeated for three time, providing a final value as average ± standard deviation. Sample temperature was set by an external thermostat HAAKE-Circulator DC10-K15 type (Thermo Fisher Scientific, Waltham, MA, USA)

4 BIBLIOGRAPHY

1. Blaine, R. L., Hahn, B. K. Obtaining Kinetic Parameters by Modulated Thermogravimetry. *J. Therm. Anal. Calorim.* 695–704 (1998). doi:https://doi.org/10.1023/A:1010171315715

2. Holzwarth, U., Gibson, N. The Scherrer equation versus the 'Debye – Scherrer equation'. **6**, 21027 (2011).

3. Alexander, H. Crystallite Size and Lattice Strains from Line Broadening. in *X-Ray Diffraction Procedures for Polycrystalline and Amorphous Materials* (ed. Sons, J. W.) Chapter 9 (1974).

Chapter IV
RESULTS AND DISCUSSION

1 INVESTIGATION OF FULLY RANDOM COPOLYESTERS OF POLY(BUTYLENE SUCCINATE) CONTAINING PRIPOL 1009 MOIETIES

1.1 Introduction

Poly(butylene succinate) (PBS) boasts good thermo-mechanical properties, biocompatibility and biodegradability both in compost and under physiological conditions. It has proved to be a promising material suitable for packaging application[1–3] but also in biomedical field[4–10], as drug release[11–13] or as supports for tissue engineering[4,5,21,11,14–20]. Therefore, PBS is attracting the attention of the scientific community as well as industries[22–28]. Despite that, the main drawbacks, high elastic modulus and low degradation rate, are hampering the massive application of this material. Among the different technique used to mitigate the unsatisfactory properties preserving the good ones, copolymerization[29–32] is one of the most applied. On the basis of this, a new bio-based copolyesters of PBS was successfully synthesized through the introduction of branches and highly flexible co-units into the macromolecular chain. The diacid chosen was a commercially available biobased monomer, Pripol 1009 sold by Croda. Pripol 1009 has been applied with success in adhesives, engineering plastics and elastomers. Solvent free polycondensation allowed to synthesize random copolymers, introducing increased amount of Pripol 1009 (BS/BPripol: 88/12, 73/27 and 59/41) along the PBS macromolecular chain. The materials were easily filmed and tensile tests were performed. Biodegradation was investigated on the films, following the weight loss and the alteration of crystallinity.

1.2 Synthesis and molecular characterization

PBS homopolymer and $P(BS_mBPripol_n)$ random copolymers were synthetized following the procedure described in "Methods and Materials" section. The samples were completely characterized by ^{1}H-NMR and ^{13}C-NMR spectroscopy, determining the chemical structure, composition and degree of randomness. High molecular weight, resulted from GPC analysis, confirmed the appropriate method of synthesis and the good polymerization control. The corresponding data were reported in **Table 1.1**.

Table 1.1: *Molecular characterization data of PBS and P(BS$_m$BPripol$_n$) copolymers.*

Sample	BS mol% feed	BS mol% ^{1}H-NMR	L$_{BS}$	L$_{BPripol}$	W$_{BS}$ g/mol	W$_{BPripol}$ g/mol	b	M$_n$ g/mol	D
PBS	100	100	-	-	55000	-	-	55000	2.0
P(BS$_{88}$BPripol$_{12}$)	90	88	8.3	1.2	1428	704	1.02	46000	2.1
P(BS$_{73}$BPripol$_{27}$)	80	73	4.3	1.4	740	896	0.96	46000	2.1
P(BS$_{59}$BPripol$_{41}$)	70	59	2.5	1.6	430	1024	1.03	39000	2.2

The chemical structure of the synthetized copolymers, with general formula of P(BS$_m$BPripol$_n$), was reported in **Figure 1.1**.
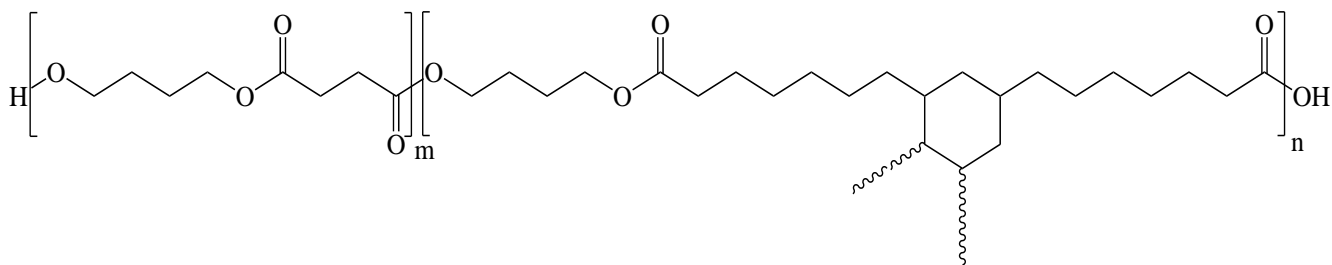
Figure 1.1: *Chemical structure of general P(BS$_m$BPripol$_n$) random copolymers.*

The backbone was constituted by the BS block and the BPripol part, which differ, from the chemical point of view, for the acid sub-units. BS was constituted by a succinic moiety, short and linear, while BPripol co-unit was characterized by quite long PE-like segments containing a six carbons ring with aliphatic side branches bonded to this latter.

In **Figure 1.2** the ^{1}H-NMR spectrum of P(BS$_{59}$BPripol$_{41}$), was reported. The peaks found confirmed the predicted chemical structure. The actual composition reported in **Table 1.1** was calculated considering the integrated areas of *c* and *f* peaks ascribable to the succinic and Pripol sub-units, respectively.

The degree of randomness (b) and the block weight (W) were defined by ^{13}C-NMR (**Figure 1.3**)[33,34], taking into account the carbon atoms of the –OCH$_2$- group (between 64.4 and 63.4 ppm) (**Figure 1.3**).
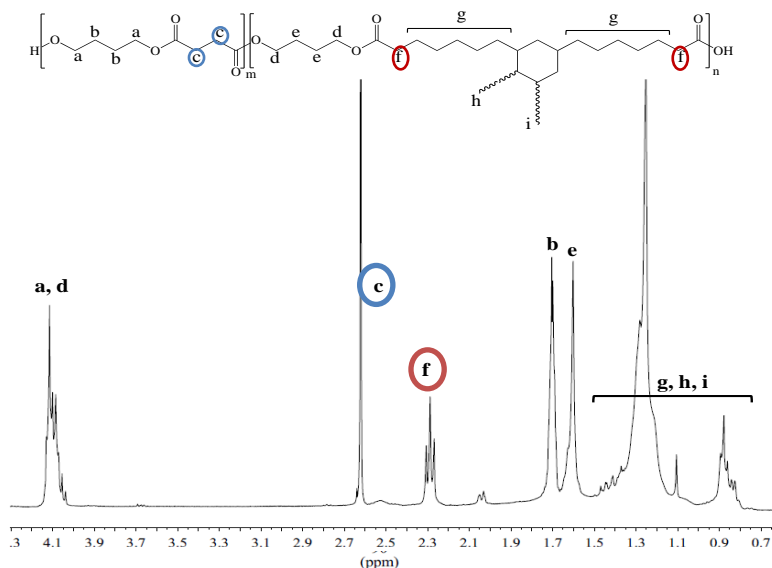
Figure 1.2: *^{1}H-NMR spectrum of P(BS$_{59}$BPripol$_{41}$) with the relative peak assignment.*

The carbons in α-position to the carboxylic oxygen atoms determined four different signals: *k* peak corresponding to Succinic-Butandiol-Succinic triads (S-B-S); the *o* peak due to Pripol-Butandiol-Pripol triads (Pripol-B-Pripol); the *k$_1$* and *o$_1$* peaks related to the Succinic-Butanediol-Pripol triads (S-B-Pripol).
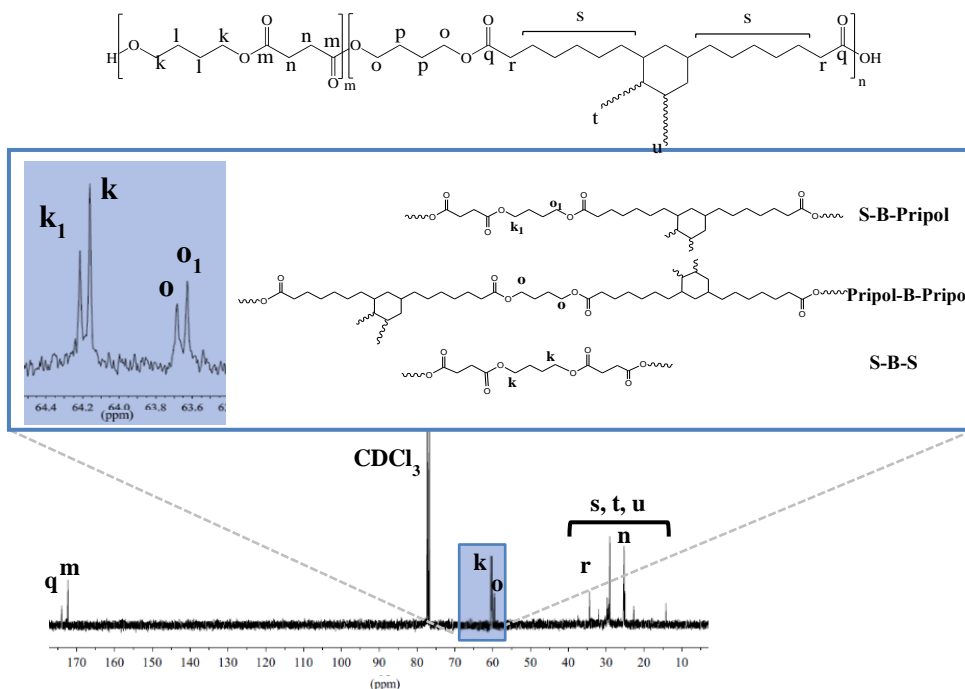
Figure 1.3: *^{13}C-NMR spectrum recorded for P(BS$_{59}$BPripol$_{41}$) with the relative peak assignment. A magnification of the zone 64.6-63.4 ppm is inserted with schematic representation of Succinic-Butandiol-Pripol, Pripol-Butanediol-Pripol and Succinic-Butanediol-Succinic triads.*

114

The degree of randomness, b, was calculated from the relative intensity of these signals, as follows:

$$b = P_{S-Pripol} + P_{Pripol-S} \qquad\qquad Eqn.\ 1$$

where $P_{S-Pripol}$ and $P_{Pripol-S}$ are the probability of finding a succinic subunit, S, next to a Pripol one and the probability of finding a Pripol moiety followed by a S one. $P_{S-Pripol}$ and $P_{Pripol-S}$ can be defined by the following equations:

$$P_{S-Pripol} = \frac{I_{k1}}{I_{k1}+I_k}; \qquad\qquad Eqn.\ 2$$

$$P_{Pripol-S} = \frac{I_{o1}}{I_{o1}+I_o} \qquad\qquad Eqn.\ 3$$

where I_k, I_{k1}, I_{o1}, I_o represent the integrated intensities of the peaks of the S-B-S, S-B-Pripol, Pripol-B-S, Pripol-B-Pripol triads, respectively.

Moreover, it was possible to calculate the length (L) and the average weight of sequence of BS and BPripol (W).

$$L_{BS} = \frac{1}{P_{S-Pripol}} \qquad\qquad Eqn.\ 4$$

$$L_{BPripol} = \frac{1}{P_{Pripol-S}} \qquad\qquad Eqn.\ 5$$

$$W_{BS} = \frac{1}{P_{S-Pripol}} * M_{BS}; \qquad\qquad Eqn.\ 6$$

$$W_{BPripol} = \frac{1}{P_{Pripol-S}} M_{BPripol} \qquad\qquad Eqn.\ 7$$

where M_{BS} and $M_{BPripol}$ are the molecular weights of BS and BPripol repeating units, respectively. The degree of randomness (b) resulted equal to 1 for all the copolymers synthetized. In **Table 1.1** the length and the average weight of the BS and BPripol sequences (L_{BS}, $L_{BPripol}$ and W_{BS}, $W_{BPripol}$) were reported, which resulted directly proportional to the molar amount of the succinic and the Pripol subunits content.

The high values of number molecular weight (M_n) and the polydispersity index (D) close to 2, suggested the good control of the polymerization process.

1.3 Thermal and structural characterization

TGA analysis showed the behavior of the samples during non-isothermal scan, under inert atmosphere.
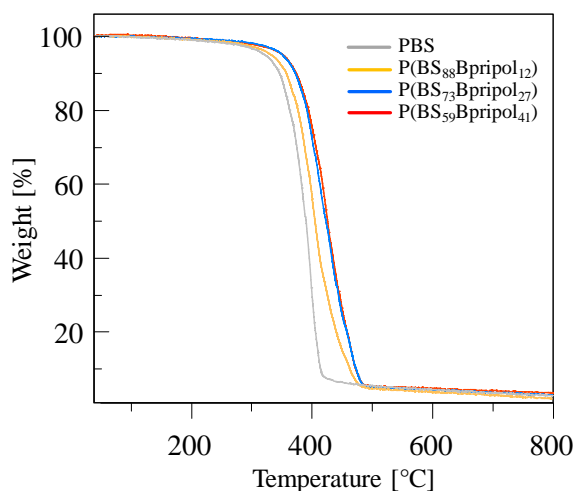
Figure 1.4*: Traces of thermogravimetric analysis conducted on PBS and P(BS$_m$BPripol$_n$) samples obtained by heating at 10°C/min under inert atmosphere.*

The presence of Pripol 1009 increased the thermal stability of the copolymers with respect to PBS. Indeed, from the already high T$_{max}$ values of poly(butylene succinate), the critical temperature of the copolymeric system rose with the amount of Pripol 1009. This effect was explained considering the decreasing of -COOR- groups per unit length. The replacement of the succinic subunit with Pripol one (see **Figure 1.1**), enhanced the thermal stability.
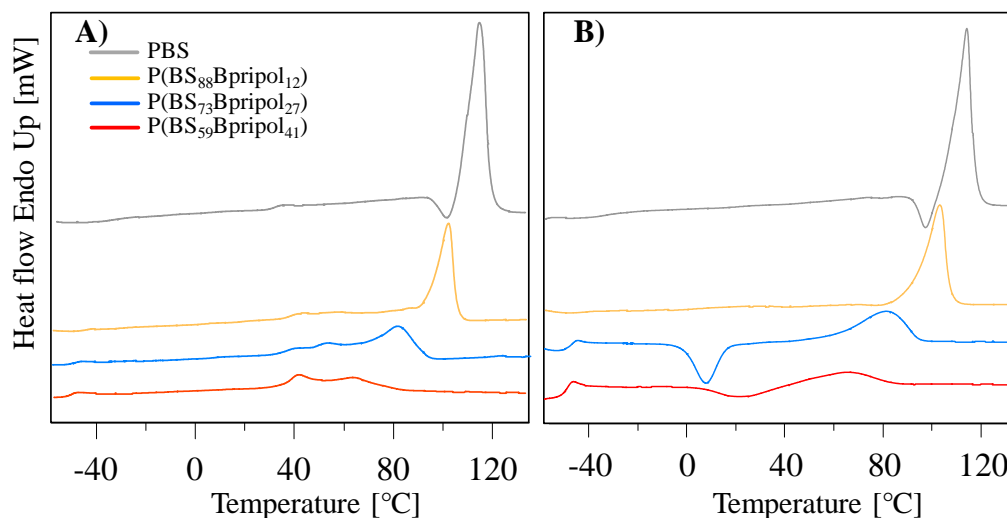
Figure 1.5*: DSC curves recorded during Ist (**A**) and IInd (**B**) scans of PBS and P(BS$_m$BPripol$_n$) copolymeric system. Heating rate: 20 °C/min under nitrogen flow.*

In order to complete the thermal characterization, the filmed materials were subjected to DSC measurements (**Figure 1.5**). First scan analysis showed a semicrystalline nature of all the synthetized polymers, with the characteristic glass transition, at low temperature, and the melting peak clearly present.

As concern the crystalline phase of the polymers, T_m and ΔH_m reduced in line with the decreasing of the average weight of the BS sequences, W_{BS}, as reported in **Table 1.1**. Probably the presence of BPripol hampered the crystallization, disturbing the disposition of the crystallizable sequence BS in the ordered lattice.

The amorphous phase was analyzed considering the IInd heating scan (**Figure 1.5 B**). The very low T_g values, common in all the synthetized materials, allowed them to be in the rubbery state at room temperature. The intrinsic chemical structure of Pripol enhanced chain mobility, with a maximum impact in the case of $P(BS_{59}BPripol_{41})$, where the T_g moved from -35 °C, typical for PBS, to -51°C. Moreover, the melt ability to crystallize was affected by the introduction of the BPripol units. PBS and the copolymer with the higher amount of BS subunit, $P(BS_{88}BPripol_{12})$, were still able to crystallize during cooling, showing a melting peak in the IInd scan trace. The polymeric chains of $P(BS_{73}BPripol_{27})$ resulted partially locked in the amorphous state during cooling from melt; then, a melting phenomenon was found in the IInd scan. Nevertheless, being $\Delta H_c < \Delta H_m$, one can assume the macromolecular chains had not been completely quenched. $P(BS_{59}BPripol_{41})$ copolymer, the lowest Pripol-containing copolymer, had a thermal behavior similar to that of $P(BS_{73}BPripol_{27})$, differing just for lower T_m and ΔH_m. Moreover, it showed $\Delta H_c = \Delta H_m$ demonstrating its macromolecules were quenched during cooling.

Table 1.2: *Thermal and structural characterization data of PBS and P(BSmBPripoln) copolymers.*

Sample	DSC								TGA	WAXS	WCA
	I^{st} scan		IInd scan								
	T_m °C	ΔH_m J/g	T_g °C	Δc_p J/g*°C	T_c °C	ΔH_c J/g	T_m °C	ΔH_m J/g	T_{max} °C	χ_c %	°
PBS	114	50	-35	0.192	/	/	114	51	399	46	89±2
$P(BS_{88}BPripol_{12})$	102	44	-42	0.231	/	/	104	44	414	40	100±2
$P(BS_{73}BPripol_{27})$	82	30	-47	0.360	7	20	82	29	424	28	96±2
$P(BS_{59}BPripol_{41})$	42	20	-51	0.413	22	12	65	13	426	22	95±2

Wide angle X-ray scattering was performed on the compression molded films; the obtained patterns and the calculated crystallinity degree, χ_c, were reported respectively in **Figure 1.6 A** and **Table 1.2**.
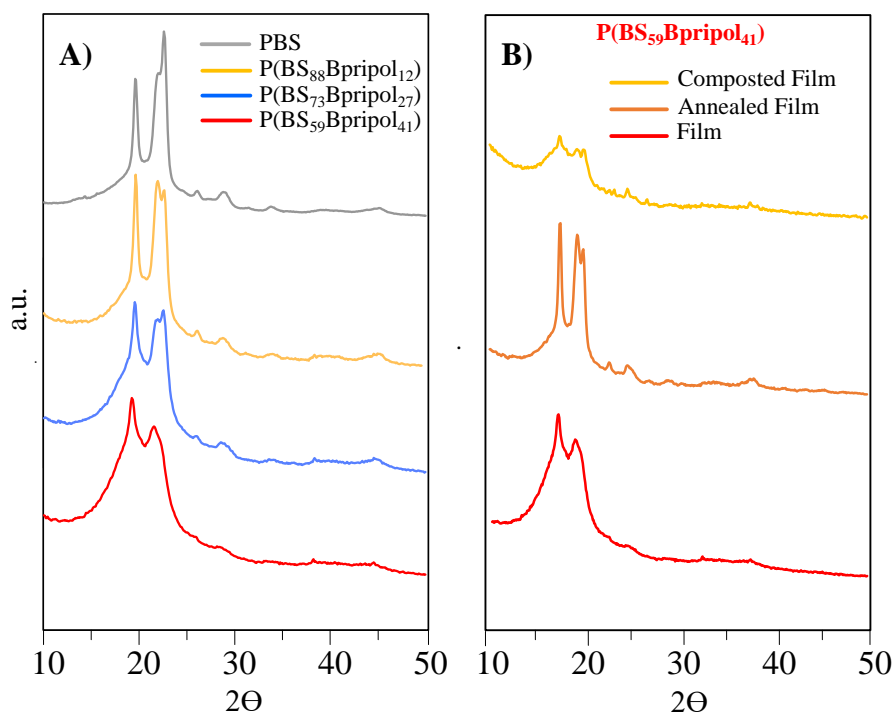
Figure 1.6*: **A)** WAXS spectra of PBS homopolymer and P(PBS$_m$BPriopol$_n$) copolymeric system; **B)** WAXs spectra of P(BS$_{59}$BPripol$_{41}$), from the bottom curve to the top: film; annealed film (incubated at 58 °C); composted film (after 110 days of incubation).*

The diffractograms, in addition to the amorphous halo, presented a series of peaks attributed to α-PBS lattice (main reflections at 19.5 and 22.5 2θ), confirming what was observed by calorimetric analyses. A progressive increase of the area under the bell-shaped background line, directly connected with the amorphous phase fraction, was observed with the increasing of the co-unit content. Moreover, due to the consequent decreasing of the ordered phase, also a reduction of the reflection intensities was observed. As clearly shown from the χ_c values reported in **Table 1.2**, the decrement of the crystallinity degree was directly proportional to the amount of BPripol co-unit. Considering the unchanged position of the peaks in the copolymers, a complete exclusion of BPripol segments from the α-PBS lattice can be supposed. Such result was not surprising considering chemical structure of BPripol was pretty different respect to BS co-units.

Water contact angle, **Figure 1.7**, was measured on the molded films, in order to collect information about their hydrophobic character. The values reported in **Table 1.2** showed an initial increase of the WCA for P(BS$_{88}$BPripol$_{12}$), due to the substitution of succinic subunit with Pripol 1009 moieties. This latter, thanks to the PE-like segments and the aliphatic side chains, increased the hydrophobic character of the chains.

118

Nevertheless, by further enhancing the Pripol 1009 content, WCA value decreased[35]. This peculiar trend can be explained taking into account the presence, in all the materials, of both crystalline phase and amorphous one. This last increases with Pripol content and, consequently, was richer in the more hydrophilic BS segments determining the WCA values reduction.

A) P(BS$_{88}$Bpripol$_{12}$)   **B)**   PBS

(100±2)Θ   (89±2)Θ
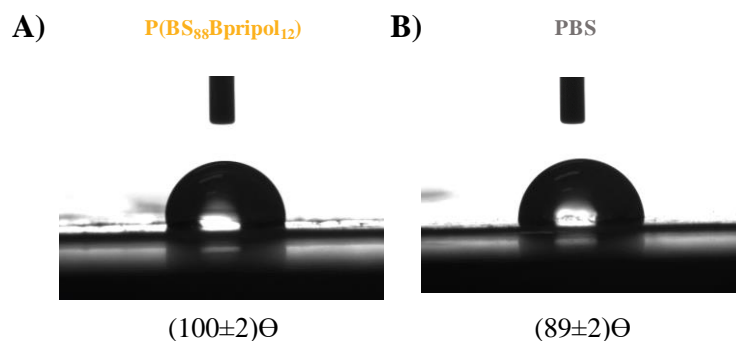
Figure 1.7*: **A)** WCA of P(BS$_{88}$BPripol$_{12}$) and **B)** PBS.*

1.4 Mechanical properties

The results of the mechanical analysis (**Figure 1.8**) collected in **Table 1.3**, suggested a deep impact of BPripol co-units on the tensile response of the copolymers. The PBS homopolymer resulted rigid, with an elastic modulus of 185 MPa, and fragile, reaching the breaking point at 7% of elongation. The introduction of Pripol moiety produced a pronounced decreasing of the elastic modulus (E), as well as tensile strength (σ_b), for all the synthetized copolymers. In details the increment of flexibility was following the increasing content of BPripol, strictly related to the ordered portion in the samples. Indeed, considering the results obtained from calorimetric and diffractometric analyses, the mechanical behavior was attributed to the reduction of crystalline portion in the different copolymers, the elongation at break and the elastic modulus were reaching a maximum in the less crystalline P(BS$_{59}$PBPriol$_{41}$) sample: the higher the content of BPripol, the lower the amount of BS segments that were able to crystallize.

Table 1.3*: Mechanical characterization data of PBS and P(BSmBPripoln) copolymers.*

Sample	E MPa	σ_y MPa	ε_y %	σ_b MPa	ε_b %
PBS	185±42	/	/	11±2	7±2
P(BS$_{88}$BPripol$_{12}$)	130±40	15±2	228±48	14±1	338±22
P(BS$_{73}$PBPripol$_{27}$)	48±4	/	/	7.8±0.5	392±16
P(BS$_{59}$PBPripol$_{41}$)	14±2	/	/	4.6±0.3	460±22
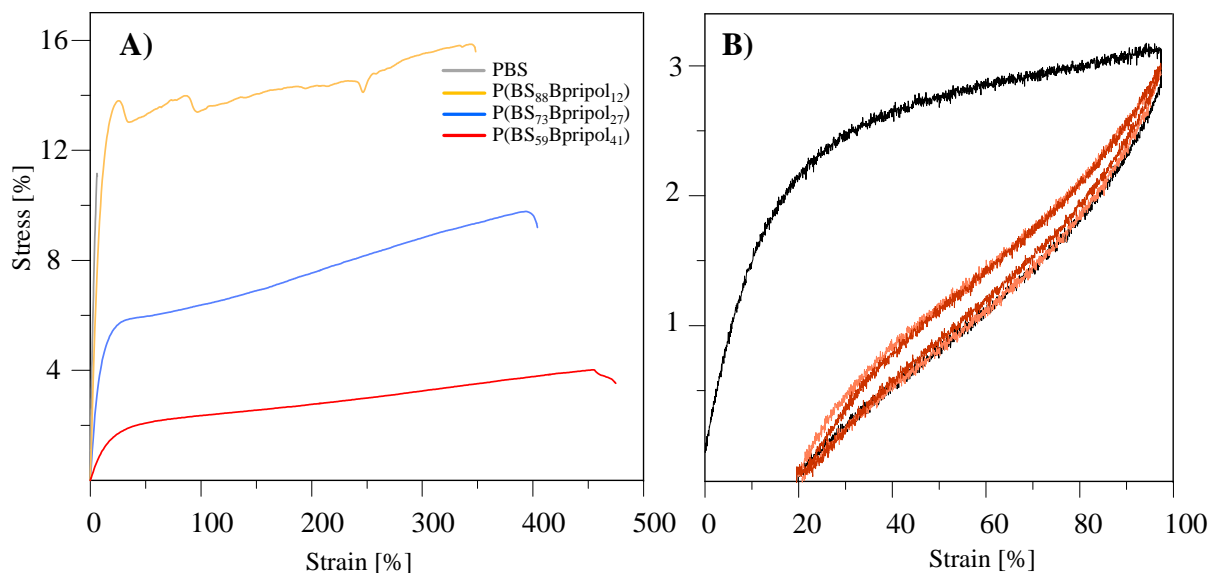
Figure 1.8*: **A)** Stress-strain curves of PBS and P(BS$_m$BPripol$_n$) copolymers; **B)** cyclic mechanical measurement of P(BS$_{59}$BPripol$_{41}$).*

The absence of yielding point for P(BS$_{73}$PBPriol$_{27}$) and P(BS$_{59}$PBPriol$_{41}$) copolymers suggested a thermoplastic elastomer nature of the two samples. On the base of this observation, cyclic tests were conducted on P(BS$_{59}$PBPriol$_{41}$), the highest Pripol-containing copolymer. The measurements were conducted with different elongation (50, 100 and 150%) then the recovery of the stretching was recorded. Twenty cyclic measurements were carried out for each test, and, after 16 hours, the tests were repeated.

The results were summarized in **Table 1.4**, while an example of mechanical loop was reported in **Figure 1.8 B**. The curves show that P(BS$_{59}$PBPriol$_{41}$) was recovering the 86% of the initial 50% elongation which was maintained performing, after 16 hours, the same measurement. This behavior was typical of block copolymeric system, where the amorphous rubbery segments were responsible for high elongation capability and crystallizable parts conferred the elastic return.

Table 1.4*: Cyclic mechanical test results for P(BS$_{59}$BPripol$_{41}$) copolymer: recovery (r %) and corresponding applied elongation (ε %).*

P(BS$_{59}$BPripol$_{41}$)				
ε %	50	50*	100	150
r %	86±2	86±2*	82±3	60±5

* second measurement on the same specimen after 16 h from the previous test.

120

Despite that, as confirmed from ^{13}C-NMR spectroscopy, the copolymer had a random architecture. It was supposed the presence of Pripol moiety, characterized by pretty high molecular weight, acted itself as a block due to its intrinsic structure that was resembling block system. Indeed, as indicated by the average weight of the BS and BPripol units (W_{BS} and $W_{BPripol}$), reported in **Table 1.1**, both the hard segment (BS) and the soft one (BPripol) were quite long. Therefore, the presence of the biobased Pripol subunit permitted to condense the characteristic of random copolymer and block copolymer in just one material.

1.5 Compostability

Biodegradability in compost of PBS and copolymers was tested with the methodology previously reported in "Methods and Materials" section. At different incubation time, the gravimetric weight loss, the resulting copolymer composition and melting (T_m and ΔH_m) were evaluated. As reported in **Figure 1.9**, marked weight loss, proportional to Pripol moieties percentage and time, was observed and clearly confirmed from SEM images collected on the film surfaces after 110 days in compost.
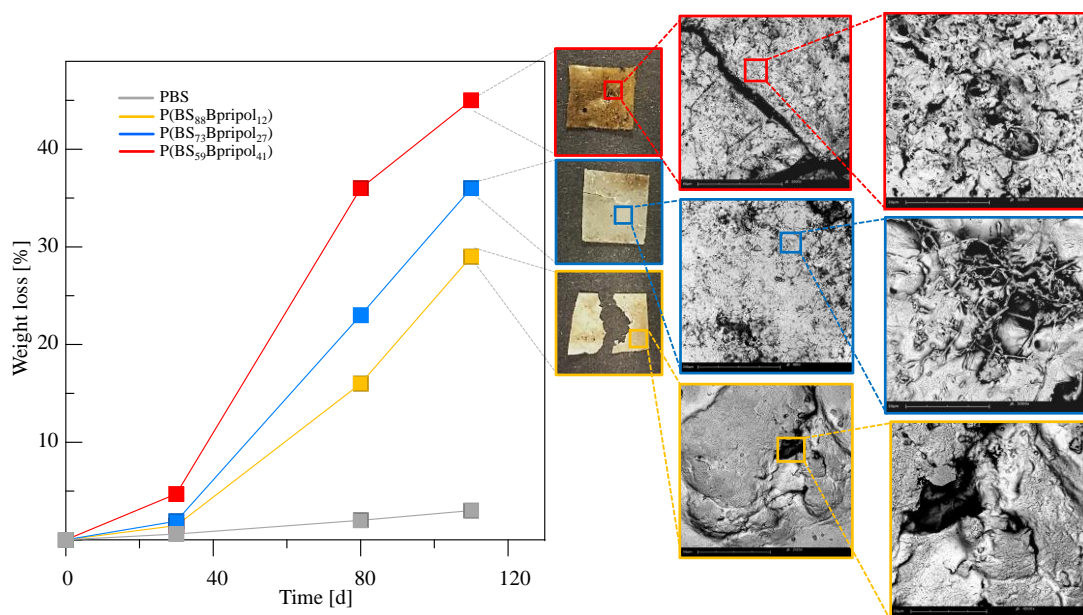
Figure 1.9*: Gravimetric weight loss reported as a function of the time of incubation for PBS and its copolymers. Pictures and SEM images [50x50 and 20x20 μm] of the copolymer films after 110 days in compost.*

Together with the decreasing of the weight, the composition was affected by the degradation process. In detail, H^1-NMR analysis evidenced a progressively enrichment in Pripol content, pointing out a preferential attack to the BS sequence from the bacteria present in compost. Usually, BS parts were less

prone to be degraded, being this former partially locked in crystal lattices, resulting less accessible and mobile.

To explain the experimental results, it was argued that the chemical nature of BPripol had less probability to be subjected to degradation, being the density of -COOR- groups – the most reacting site - lower with respect to PBS homopolymer. Further confirmation on preferential degradation of BS segments was found in DSC analysis where a decreasing of crystalline phase, constituted exclusively by BS segments, was observed. The calorimetric analyses conducted, reported in **Figure 1.10**, showed the thermal transition of the neat films, the copolymer films incubated in compost for 110 days and the films annealed at the composting temperature of 58 °C without compost.
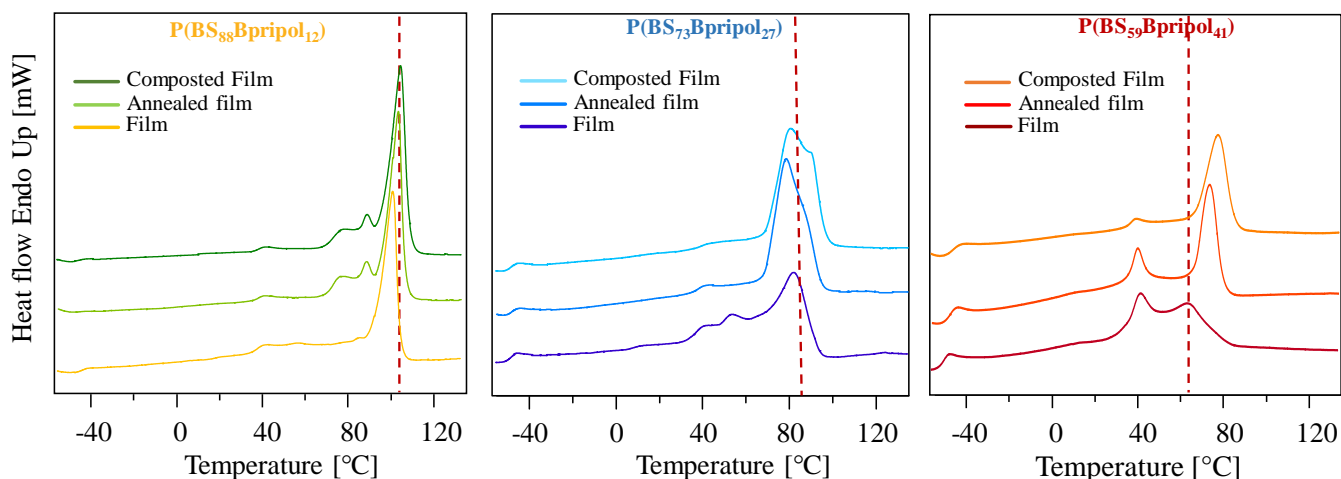
Figure 1.10: *DSC Ist scan of the synthetized copolymers. From the bottom curve to the top: film; annealed film (incubated at 58 °C); composted film (after 110 days of incubation). Heating rate: 20 °C/min.*

These latter samples were useful to evaluate the effect of the temperature without interference of other factors. As it is clearly shown by the DSC curves, keeping the sample at 58°C caused reorganization of the crystalline phase that melted at higher temperature compared to the molded films. Regarding the degraded copolymeric films, further increase of T_m together with the reduction of the endothermic area (ΔH_m) was detected, suggesting a reduction in number of low-melting BS crystals. This effect was also evidenced by WAXS analysis, where, as reported in **Figure 1.6 B**, the diffractograms of P(PBS$_{59}$BPripol$_{41}$) in form of compression molded film, incubated film for 110 days and annealed material were collected, showing a marked reduction of crystalline phase.

1.6 Conclusions

PBS copolymers containing Pripol 1009 subunits were successfully synthesized via eco-friendly solvent free process. The introduction of Pripol moieties conferred higher thermal stability to the copolymers compared to PBS homopolymer. Moreover, also the mechanical behavior was influenced by the presence of BPripol co-units with a significant reduction of Young´s Modulus and an incremented elongation at break, strictly connected to the amount of Pripol. P(BS$_{59}$PBPriol$_{41}$), the copolymer with the highest Pripol amount, showed a mechanical behavior typical of a thermoplastic elastomer with good elastic recovery despite its random composition. The biodegradation of all the synthetized copolymers was tested evidencing promising results. BS sequences appeared to be the co-unit preferentially attacked by the microorganisms. In conclusion, copolymerization confirmed itself as a useful tool to tune the final solid-state properties of a material. Ultimately, the introduction of Pripol 1009 in PBS backbone increased thermal stability, flexibility and degradation rate, making this class of copolymers sustainable for flexible packaging applications.

1.7 Bibliography

1.   Wattanawong, N., Chatchaipaiboon, K., Sreekirin, N. Aht-Ong, D. Migration, physical and antibacterial properties of silver zeolite/poly(butylene succinate) composite films for food packaging applications. *J. Reinf. Plast. Compos.* **39**, 95–110 (2020).

2.   Sapuan, S. M., Nazrin, A., Ilyas, R. A., Sherwani, S. F. K., Syafiq, R. Nanocellulose Reinforced Thermoplastic Starch (TPS), Poly (lactic) Acid (PLA), and Poly (Butylene Succinate)(PBS) for Food Pack-aging Applications. *Front. Chem.* **8**, (2020).

3.   Cornish, K., Vodovotz, Y. Accepted, J. NARROWING THE GAP FOR BIOPLASTIC USE IN FOOD PACKAGING - AN UPDATE. (2020). doi:10.1021/acs.est.9b03755

4.   Ojansivu, M.; Johansson, L.; Vanhatupa, S.; Tamminen, I.; Hannula, M.; Hyttinen, J.; Kellomäki, M.; Miettinen, S. Knitted 3D Scaffolds of Polybutylene Succinate Support Human Mesenchymal Stem Cell Growth and Osteogenesis. **2018**, (2018).

5.   Huang, A. *et al.* Electrospun poly(butylene succinate)/cellulose nanocrystals bio-nanocomposite scaffolds for tissue engineering: Preparation, characterization and in vitro evaluation. *Polym. Test.* **71**, 101–109 (2018).

6.   Domínguez-Robles, J.; Larrañeta, E.; Fong, M. L.; Martin, N. K.; Irwin, N. J.; Mutjé, P.; Tarrés, Q.; Delgado-Aguilar, M. Lignin/poly(butylene succinate) composites with antioxidant and antibacterial properties for potential biomedical applications. *Int. J. Biol. Macromol.* **145**, 92–99 (2020).

7.   Pajoumshariati, S.; Shirali, H.; Yavari, S. K.; Sheikholeslami, S. N.; Lotfi, G.; Mashhadi Abbas, F.; Abbaspourrad, A. GBR membrane of novel poly (butylene succinate-co-glycolate) co-polyester co-polymer for periodontal application. *Sci. Rep.* **8**, 1–16 (2018).

8.   Chen, L.; Cheng, H. H.; Xiong, J.; Zhu, Y. T.; Zhang, H. P.; Xiong, X.; Liu, Y. M.; Yu, J.; Guo, Z. X. Improved Mechanical Properties of Poly(butylene succinate) Membrane by Co-electrospinning with Gelatin. *Chinese J. Polym. Sci. (English Ed.* **36**, 1063–1069 (2018).

9.   Kang, Y. G.; Wei, J.; Kim, J. E.; Wu, Y. R.; Lee, E. J.; Su, J.; Shin, J. W. Characterization and osteogenic evaluation of mesoporous magnesium-calcium silicate/polycaprolactone/polybutylene succinate composite scaffolds fabricated by rapid prototyping. *RSC Adv.* **8**, 33882–33892 (2018).

10.   Tang, X.; Dai, J.; Sun, H.; Nabanita, S.; Petr, S.; Tang, L.; Cheng, Q.; Wang, D.; Wei, J. Copper-doped nano laponite coating on poly(butylene succinate) scaffold with antibacterial properties and cytocompatibility for biomedical application. *J. Nanomater.* **2018**, (2018).

11.   Gigli, M.; Fabbri, M.; Lotti, N.; Gamberini, R.; Rimini, B.; Munari, A. Poly(butylene succinate)-based polyesters for biomedical applications: A review in memory of our beloved colleague and friend Dr. Lara Finelli. *Eur. Polym. J.* **75**, 431–460 (2016).

12.   RS Moraes, N Ricardo, V Saez, F. S. Synthesis of Magnetic Composite of Poly (Butylene Succinate) and Magnetite for the Controlled Release of Meloxicam. **2**, 2–5 (2018).

13.   Zhao, Y., Guo, W., Lu, Q. & Zhang, S. Preparation of poly (butylene succinate) -poly [2- (dimethylamino) ethyl methacrylate] copolymers and their applications as carriers for drug delivery. (2018). doi:10.1002/pi.5559

14.   Shi, M.; Cheng, T.; Zou, H.; Zhang, N.; Huang, J.; Xian, M. The Preparation and Biomedical Application of Biopolyesters. *Mini Rev. Med. Chem.* (2019). doi:10.2174/1389557519666191015211156

15.   Xiaonan Liu, Li Gang, Shuhao Qin. Structure and properties of nano-hydroxyapatite/poly(butylene succinate) porous scaffold for bone tissue engineering prepared by using ethanol as porogen. *J. Biomater. Appl.* **33**, 776–791 (2018).

16.   Cristofaro, F.; Gigli, M.; Bloise, N.; Chen, H.; Bruni, G.; Munari, A.; Moroni, L.; Lotti, N.; Visai, L. Influence of the nanofiber chemistry and orientation of biodegradable poly(butylene succinate)-based scaffolds on osteoblast differentiation for bone tissue regeneration. *Nanoscale* **10**, 8689–8703 (2018).

17.   Chen, H.; Gigli, M.; Gualandi, C.; Truckenmüller, R.; van Blitterswijk, C.; Lotti, N.; Munari, A.; Focarete, M. L.; Moroni, L. Tailoring chemical and physical properties of fibrous scaffolds from block copolyesters containing ether and thio-ether linkages for skeletal differentiation of human mesenchymal stromal cells. *Biomaterials* **76**, 261–272 (2016).

18.   Fabbri, M.; Gigli, M.; Costa, M.; Govoni, M.; Seri, P.; Lotti, N.; Giordano, E.; Munari, A.; Gamberini, R.; Rimini, B. The effect of plasma surface modification on the biodegradation

rate and biocompatibility of a poly(butylene succinate)-based copolymer. *Polym. Degrad. Stab.* **121**, 271–279 (2015).

19. M. Gigli, N. Lotti, M. Gazzano, L. F. and A. M. Synthesis and Characterization of Novel Poly(butylenesuccinate)-Based Copolyesters Designed as Potential Candidates for Soft Tissue Engineering. *POLYM ENG SCI.,* **53**, 491–501 (2013).

20. Gualandi, C.; Soccio, M.; Saino, E.; Focarete, M. L.; Lotti, N.; Munari, A.; Moroni, L.; Visai, L. Easily synthesized novel biodegradable copolyesters with adjustable properties for biomedical applications. *Soft Matter* **8**, 5466–5476 (2012).

21. Gigli, M.; Lotti, N.; Gazzano, M.; Siracusa, V.; Finelli, L.; Munari, A.; Rosa, M. D. Biodegradable aliphatic copolyesters containing PEG-like sequences for sustainable food packaging applications. *Polym. Degrad. Stab.* **105**, 96–106 (2014).

22. Zia, K. M., Noreen, A., Zuber, M., Tabasum, S. Mujahid, M. Recent developments and future prospects on bio-based polyesters derived from renewable resources: A review. *Int. J. Biol. Macromol.* **82**, 1028–1040 (2016).

23. Rameshkumar, S., Shaiju, P., Connor, K. E. O. P, R. B. Bio-based and biodegradable polymers - State-of-the-art, Challenges and Emerging Trends. *Curr. Opin. Green Sustain. Chem.* (2019). doi:10.1016/j.cogsc.2019.12.005

24. Su Shen, Kopitzky Rodion, Tolga Sengül, K. S. Polylactide (PLA) and Its Blends with Poly(butylene succinate) (PBS): A Brief Review. *Polymers (Basel).* 1–21 (2019).

25. Helanto, K., Matikainen, L., Talja, R. Rojas, O. J. Bio-based Polymers for Sustainable Packaging and Biobarriers: A Critical Review. **14**, 4902–4951 (2019).

26. Gumede, T. P., Luyt, A. S. Müller, A. J. Review on PCL , PBS , and PCL / PBS blends containing carbon nanotubes. **12**, 505–529 (2018).

27. Azim, H., Dekhterman, A., Jiang, Z. Gross, R. A. Candida antarctica Lipase B catalyzed synthesis of poly(butylene succinate): Shorter chain building blocks also work. *ACS Symp. Ser.* **999**, 285–293 (2008).

28. Xu, J. Guo, B. H. Poly(butylene succinate) and its copolymers: Research, development and industrialization. *Biotechnol. J.* **5**, 1149–1163 (2010).

29. Techniques, F., Lin, S., Wang, H., Wang, J. Wu, T. Enzymatic Degradation of Acrylic Acid-Grafted. (2020).

30. Sonseca, A.; Sahay, R.; Stepien, K.; Bukala, J.; Wcislek, A.; McClain, A.; Sobolewski, P.; Sui, X. M.; Puskas, J. E.; Kohn, J. Architectured helically coiled scaffolds from elastomeric poly(butylene succinate) (PBS) copolyester via wet electrospinning. *Mater. Sci. Eng. C* **108**, 110505 (2020).

31. Śmigiel-Gac, N., Pamuła, E., Krok-Borkowicz, M., Smola-Dmochowska, A. & Dobrzyński, P. Synthesis and properties of bioresorbable block copolymers of l-lactide, glycolide, butyl succinate and butyl citrate. *Polymers (Basel).* **12**, (2020).

32.   Bi, T., Qiu, Z. Synthesis, thermal and mechanical properties of fully biobased poly(butylene-co-propylene 2,5-furandicarboxylate) copolyesters with low contents of propylene 2,5-furandicarboxylate units. *Polymer (Guildf).* **186**, 122053 (2020).

33.   Soccio, M.; Lotti, N.; Gazzano, M.; Govoni, M.; Giordano, E.; Munari, A. Molecular architecture and solid-state properties of novel biocompatible PBS-based copolyesters containing sulphur atoms. *React. Funct. Polym.* **72**, 856–867 (2012).

34.   Chen, M. S.; Chang, S. J.; Chang, R. S.; Kuo, W. F.; Tsai, H. B. Copolyesters. I. Sequence distribution of poly(butylene terephthalate-co-adipate) copolyesters determined by 400 MHz NMR. *J . Appl. Polym.* **40**, 1053–1057 (1990).

35.   Areias, A. C.; Ribeiro, C.; Sencadas, V.; Garcia-Giralt, N.; Diez-Perez, A.; Gómez Ribelles, J. L.; Lanceros-Méndez, S.Influence of crystallinity and fiber orientation on hydrophobicity and biological response of poly(l-lactide) electrospun mats. *Soft Matter* **8**, 5818–5825 (2012).

2 BIOBASED COPOLYESTERS FROM REGIOSELECTIVE PHOTOOXIDATION OF CITRONELLOL

2.1 Introduction

Among the different hydrocarbon-rich biomass sources, terpenes and terpenoids have been employed in an increasing number of researches in science[1,2,11,3–10]. Indeed, a renovate interest is growing around this organic feedstock for the generation of green plastics and composites due to their low cost and natural abundance[12,13]. In the last years, new approaches of functionalization were developed in order to synthetize more competitive polymers[14]. In our specific case, the syntheses of bio-based copolyesters were conducted employing a new polyoxygenated compound, derived from citronellol substrates. The principles of green chemistry were followed during the synthesis of the diols, where air, visible light and zeolite supported-photosensitizer (Thionine-NaY) were employed, as well as for the preparation of the copolymers, obtained via two step solvent free polycondensation. In particular, citronellol derivates were copolymerized in presence of succinic acid and 1,4-butanediol, two 100% bio-based monomers, usually employed with success in the synthesis of PBS. This latter ecofriendly polymer, characterized by outstanding physical and mechanical properties, good processability, low cost and biodegradability, results suitable for a wide range of different applications, from biomedical field[15–21] to food packaging[22–24]. The main disadvantage that is hampering the conquer of the market, is found in its rigidity. With the aim of increasing its flexibility without compromising the biobased nature, PBS was copolymerized with citronellol derivates. Moreover, the possibility to post-functionalize the new citronellol-based copolyester via thiol-ene click reaction [25,26] was proven.

2.2 Synthesis of the monomer 4 and 5

The diols 4 and 5, derived from citronellol, were obtained thanks the scientific collaboration with the Department of Chemistry and Industrial Chemistry (DCC) of the University of Genova. The schematic representation of the synthesis of diol 4 and 5 was reported in **Figure 2.1**.
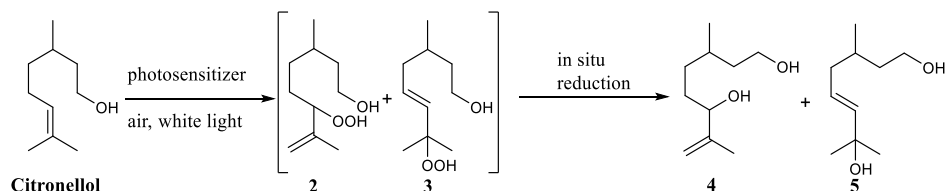
Figure 2.1: Schematic representation of the steps conducted to obtain diol 4 and 5.

2.3 Synthesis and molecular characterization of copolyester 6 and copolyester 7

The synthesis of copolyester 6 and copolyester 7 was conducted as solvent free two step polycondensation (**Figure 2.2**). The details were reported "Methods and Materials" section. The chemical structures were verified by means ^{1}H-NMR spectroscopy.
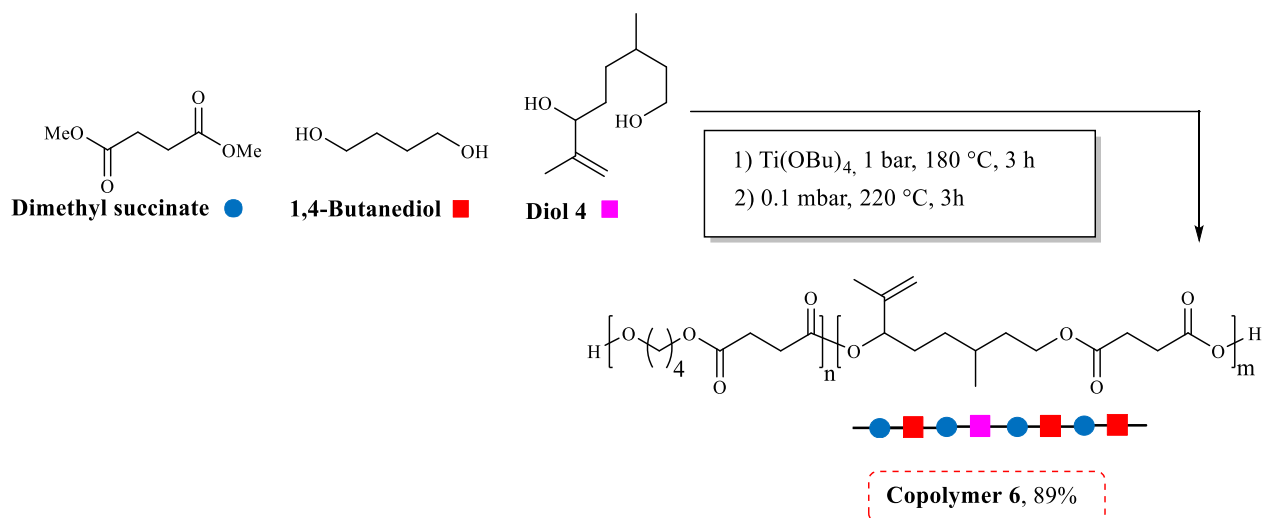
Figure 2.2: *Schematic representation of the synthesis of copolymer 6.*

As concerns copolymer 6, the predicted structure was confirmed by the spectrum reported in **Figure 2.3**. No unexpected peaks were detected evidencing an adequate and controllable polycondensation process.

The clear triplet at 5.13 ppm could be assigned to proton 4, α located respect to the double bond. The two protons $H_2C=$, identified as 6, were instead resonating at 5.93 ppm. Moreover, $-OCH_2-$ of the butandiol and diol 4 subunits (1 and 12) were overlapped at 4.10 ppm. The signal at 2.64 ppm was attributed to methylene protons of the succinic subunits, bonded to both butanediol and diol 4. The signals of $-CH_3$ (5) and $-CH_2-$ (2) were again overlapped at 1.75 ppm. The $-CH_3$ labeled as 10 could be found at 0.89 ppm. The remaining signals, 7, 8, 9 and 11, were ascribed to the hydrogen atoms of diol 4.

128
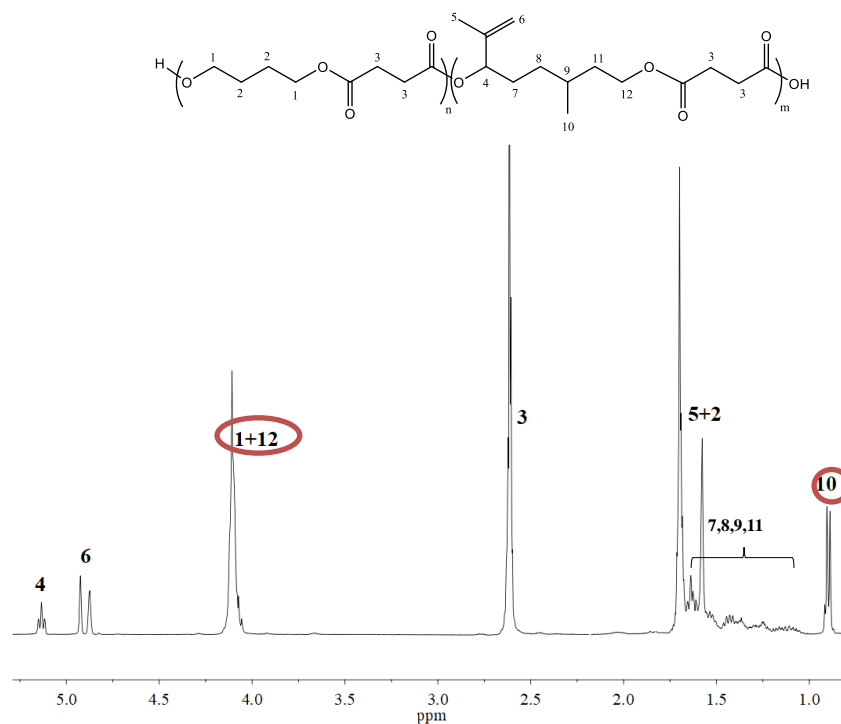
Copolymer 6

Figure 2.3: ^{1}H-NMR spectrum of copolymer 6 with the relative peak assignment.

The chemical composition was calculated from the integrals recorded by ^{1}H-NMR. In detail, the percentage of BS co-units was calculated considering the signal at 4.10 ppm, where was placed the peak of -OCH$_2$- (1+12) for both the subunits, subtracting the normalized area of the signal 10, at 0.89 ppm, ascribed to diol 4. The so-obtained results of composition were reported in **Table 2.1**.

Table 2.1: Molecular characterization data of PBS, copolymer 6, copolymer 7 and 8.

Sample	BD %	Diol 4 %	Diol 4+5 %	Yield %	I.V dL/g
PBS	100	/	/	96	1.48
Copolymer 6	75	25	/	89	0.79
Copolymer 7	65	/	35	63	1.06
Copolymer 8	73	27	/	75	0.67

As well as copolymer 6, also copolymer 7 -synthetized employing a mixture of diol 4 and diol 5- **Figure 2.4**, was characterized by ^{1}H-NMR. The spectrum was reported, with the relative assignment, in **Figure 2.5**.
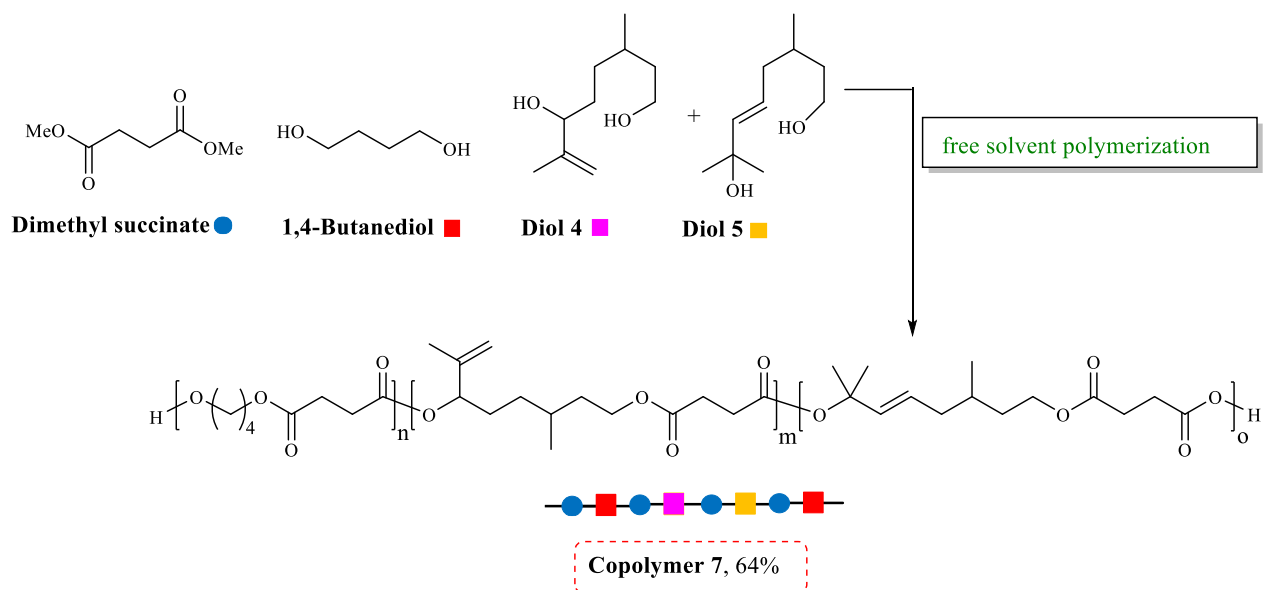
Figure 2.4: Representation of synthesis of copolymer 7.

The spectrum presented the expected signals: the ones already assigned together with the peaks ascribable to the diol 5 moiety.
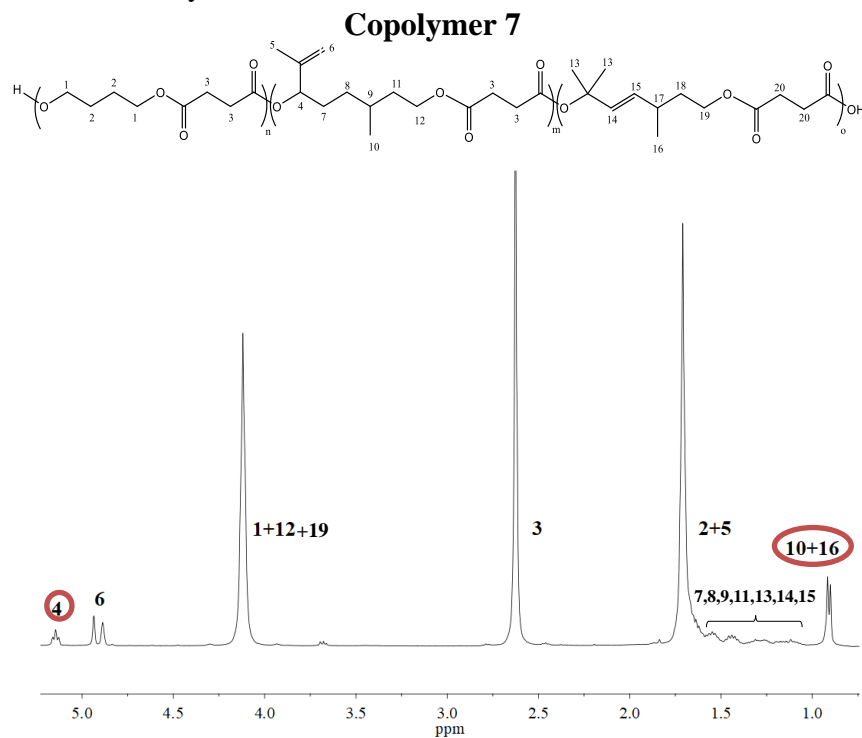
Figure 2.5: ^{1}H-NMR spectrum of Copolymer 7 with the relative peak assignment.

While protons 4 and 6 were clearly appreciable, -CH$_2$ in diol 5, numbered as 19, were overlapped with proton 1 and 12. No differences were recorder for the two hydrogens proper of the succinic

130

subunit and the signal at 1.75 ppm, identified as protons 2 and 5. At 1.75 ppm, protons 10 and 16, coming from diol 5, were observed. The zone in between 1.5 and 1.0 ppm was populated from the signals of the remaining protons of the copolymer. The amount of BS co-units in copolymer 7, was defined considering the normalized signal at 4.10 ppm, where were still placed the -OCH$_2$ peak (1+12+19) for all the three different glycolic subunits, and subtracting the intensity of the signal 10+16, at 0.90 ppm, ascribed to the methyl groups of diol 4 and diol 5. The percentage of diol 4 with respect to diol 5, was calculated subtracting the intensity of protons 4 at 5.10 ppm, to the signal of hydrogens 10+16. The results were summarized in **Table 2.1**.

The absence of byproducts clearly evidenced by ^{1}H-NMR spectroscopy suggested side reaction were not occurring. Moreover, from the good yields obtained, the process of synthesis could be considered optimized.

2.4   Thermal characterization

Further analyses were conducted on copolymer 6 and 7 in order to define the thermal stability. In details, thermogravimetric analysis (TGA) was performed acquiring the curves as reported in "Methods and Materials" section.
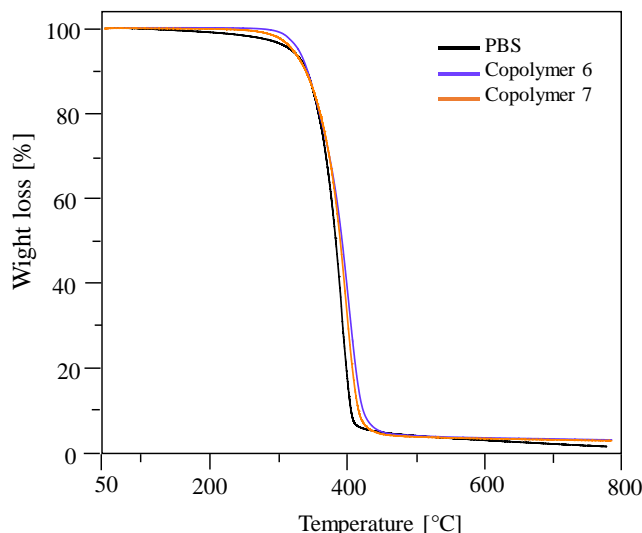
Figure 2.6*: TGA traces of PBS homopolymer, copolymer 6 and copolymer 7, recorded under inert atmosphere with a heating rate of 10°C/min.*

The two synthetized materials were compared with PBS homopolymer, considered as reference. For all the samples studied, the degradation proceeded with a one-step weight loss with maximum

degradation rate at high temperature. The derived data were reported in **Table 2.2**. It was evident that the introduction of both diol 4 and diol 5, carried out via copolymerization of PBS, had not compromised the high thermal stability of the neat homopolymer. Indeed, the T_{max} recorded for copolymer 6 and 7 were even higher than the T_{max} observed for PBS.

The differential scanning calorimetry (DSC) heating curves were recorded for the compression molded films (Ist scan) and the same materials after melt quenching (IInd scan). The traces obtained were reported in **Figure 2.7**, while the data were collected in **Table 2.2**.

Table 2.2: Thermal characterization of PBS, copolymer 6, copolymer 7 and copolymer 8.

Sample	DSC								TGA
	Ist scan		IInd scan						T_{max}
	T_m	ΔH_m	T_g	ΔC_p	T_c	ΔH_c	T_m	ΔH_m	°C
	°C	J/g	°C	J/g*°C	°C	J/g	°C	J/g	
PBS	115	81	-34	0.212	/	/	115	62	399
Copolymer 6	53	30	-33	0.481	/	/	/	/	409
Copolymer 7	85	45	-34	0.223	23.1	12	85	40	404
Copolymer 8	51	15	-16	0.573	/	/	/	/	259,396

Both the scans showed semicrystalline nature of the materials. As concerns the first heating scan, the glass transition step followed by an endothermic peak, due to the melting of crystals, could be clearly observed. The effect of the copolymerization was particularly evident in melting phenomenon. As a matter of fact, a decrease of the melting temperature and the associated heat was observed in copolymer 6 and 7 with respect to PBS. The double melting peak of copolymer 6 in the Ist scan (**Figure 2.7 A**) could be attributed to the presence of two different population of crystals: more perfect lattices melting at higher temperature, while the defected crystals started the process at lower temperature. Alternatively, a process of melting-crystallization-remelting could be responsible of a multiple endotherm, as well. As regards copolymer 7, it presented a low melting peak, almost coincident with the lower peak of melting of copolymer 6, at which a defective crystal phase, the same observed for copolymer 6, started melting. Then, the main process was located at 85 °C. The difference between the two copolymers was both in the temperature and enthalpy of melting, copolymer 6 needing lower energy to melt its crystals with respect to copolymer 7. Moreover, the crystalline phase formed in copolymer 7 was not only more perfect, but the

population was also more abundant. For this reason, the impact of the copolymeric subunit seemed to be related only to the amount, not to its chemical nature. In case of copolymer 6, diol 4 was 35%mol, and T_m and ΔH_m were lower respect to copolymer 7, constituted by two different co-units (20 and 5 mol% of diol 4 and 5, respectively). This result let us suppose a complete exclusion of the diols added from the crystalline phase, probably constituted by pure BS sequences while the comonomeric units were rejected in the amorphous phase.
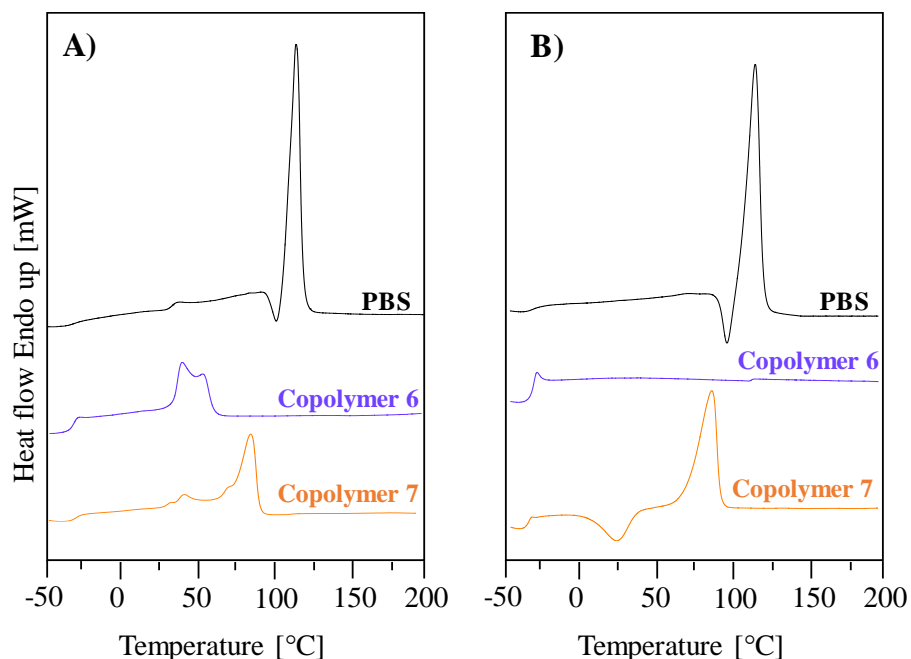
Figure 2.7: *A) DSC Ist scan of PBS, copolymer 6 and copolymer 7 as purified films; **B**) DSC IInd scan after quenching of the melt; Heating scans were acquired at 20°C/min in inert atmosphere.*

The amount of co-units added in PBS homopolymer had a different impact on crystallization behavior, as reported from the IInd calorimetric traces in **Figure 2.7 B**. The good ability to crystallize of the homopolymer was affected by the insertion of the different co-units; **Table 2.2** reported a reduced enthalpy of melting for copolymer 7, containing 25% of diols, and the complete absence of this phenomenon for copolymer 6, composed by 35% of diol 4. Moreover, copolymer 7 showed more accentuated glass transition confirming higher amount of amorphous phase. The crystallization of copolymer 7 was occurring both during heating scan (as cold crystallization at 23°C) and during cooling rate, since ΔH_m was higher than ΔH_c. Regarding copolymer 6, as described above, the introduction of 35% of diol 4 suppressed completely the crystallization behavior, leading to a complete amorphous material after quenching. Indeed, only glass transition

was appreciable. Besides that, keeping into account the value of T_g, constant for all the samples, the insertion of diol 4 and diol 5 was not affecting the chain mobility.

2.5   Wide angle X-ray scattering

The purified powders were filmed employing a compression molding process. The resulting films were analyzed with WAXS in order to investigate the crystal lattice. The X-ray diffractograms and the calculated crystallinity degree (χ_c) were reported respectively in **Figure 2.8** and **Table 2.3**.
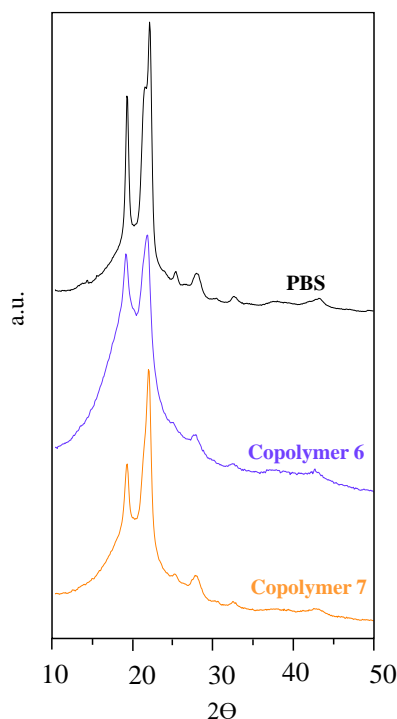
Figure 2.8: *WAXS spectra of compression molded film of PBS, copolymer 6 and copolymer 7.*

It was possible to individuate an amorphous halo overlapped with sharp signals, proper of the crystalline parts, confirming the semicrystalline nature of the samples. All the peaks observed for copolymer 6 and 7 at 19.6, 22.5, 21.7, 25 and 45 2Ө, matching the diffractogram of PBS homopolymer, could be attributed to α-PBS lattice, confirming that the crystalline phase was constituted just from BS sequences, hypothesis formulated during thermal analysis. The characteristic peaks of α crystalline phase of PBS did not change in position by copolymerization. Since, as supposed before, the comonomeric units were relegated in the amorphous phase. Considering the crystallinity degree, the results were in line with the values recorded for ΔH_m, in particular, the higher the amount of diol introduced, the lower the crystalline domains.

2.6 Mechanical properties

The compression molded films was subjected to mechanical analysis (**Figure 2.9**). In particular, stress-strain measurements were conducted. The results were collected in **Table 2.3**.

Table 2.3*: Mechanical characterization and crystallinity degree data of PBS, copolymer 6, copolymer 7 and 8.*

Sample	σ_{max} MPa	ε_{max} %	E MPa	Xc %
PBS	337±27	4±1	301±2	40
Copolymer 6	2.3±0.2	22±1	26±5	16
Copolymer 7	7±1	5±1	147±16	27
Copolymer 8	/	/	/	11

For both the copolymers, elastic modulus (E) and tensile strength (σ_b) were reduced. Considering the data collected for PBS, E was halved in copolymer 7 and was five times lower for copolymer 6.
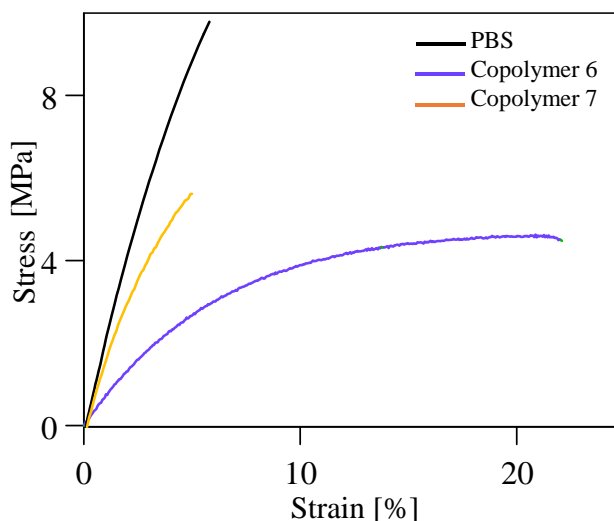
Figure 2.9*: Mechanical characterization of PBS and copolymer 6 and 7.*

The trend observed was strictly related to the presence of crystalline domain, indeed E and σ_b were directly dependent on the amount amorphous/crystal phases. A reduction of ordered regions decreased the elastic modulus and tensile strength. Regarding the elongation at break (ε_b), an increase from 4% for PBS film to 22% in the less crystalline copolyester 6 was observed.

Differently, no significant effect was observed for copolymer 7, showing a similar elongation at break of the homopolymer.

2.7 Functionalization of copolymer 6 in copolymer 8

The possibility to functionalize the unsaturated copolyester 6 employing a thiol–ene coupling reaction (**Figure 2.10**), was explored. Copolymer 8 was obtained at the Department of Chemistry and Industrial Chemistry (DCC) of the University of Genova and characterized by us.
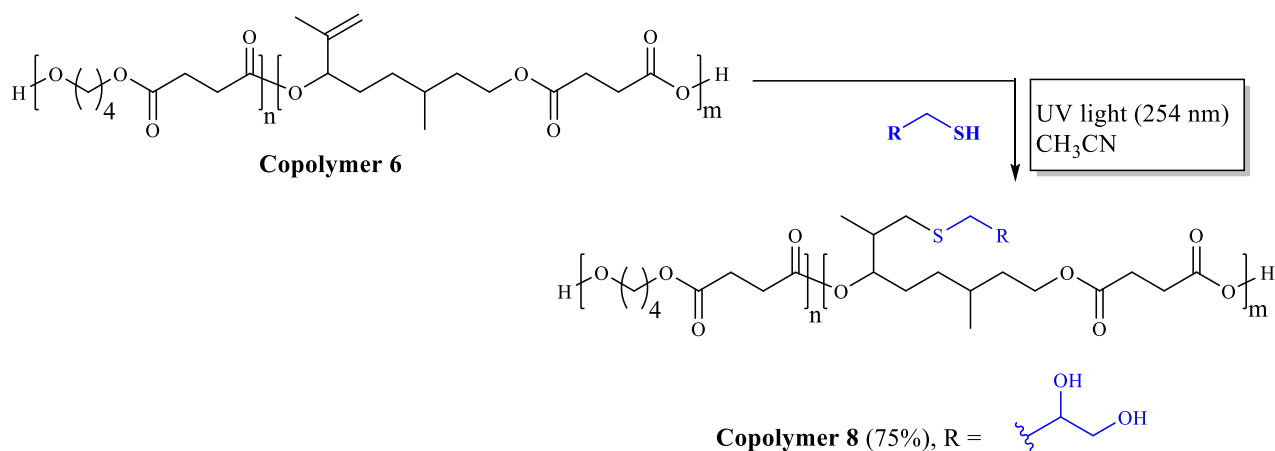
Figure 2.10: Schematic representation of functionalization pathway of Copolymer 6.

The molecular characterization of copolymer 8 was listed in **Table 2.1**; as one can see, the intrinsic viscosity decreased of 15% compared to the starting material, copolymer 6. Despite that the I.V. value, proportional to the polymer molar mass, resulted still quite high. TGA analysis (**Table 2.2**) showed a good thermal stability, with a degradation proceeding via two-step process: the first weight loss appeared around 259 °C and was related to co-units degradation, while second step was observed at 395 °C, ascribable to the BS sequences degradation. Calorimetric measurements were reported in **Table 2.2** and underlined further reduction of the crystalline portion, indeed ΔH_m decreased while ΔC_p increased with the introduction of -SR branch. The observation was confirmed also from WAXS measurements, where the crystallinity degree decreased, as reported in **Table 2.3**. Moreover, -SR branch added in copolymer 8 determined a reduction of chain mobility as indicated by the rise of T_g.

2.8 Conclusions

In the present work, dye-sensitized photooxidation reaction was applied to obtain a sustainable route for the regioselective conversion of citronellol, a naturally terpenoid, into diol 4 and diol 5. The so-obtained glycols were employed to synthetize two copolyesters of poly(butylene succinate), copolymer 6 and copolymer 7, leading to two new bio-based flexible materials where the presence of the C=C double bond made them functionalizable. Copolymerization proved to be an efficient way to tune the final polymer properties, such as crystallinity, elasticity, and eventually, bioactivity. As a proof of concept, the C=C has been functionalized using thiolene click reaction employing UV light.

2.9 Bibliography

1. Thomsett, M. R., Moore, J. C., Buchard, A., Stockman, R. A., Howdle, S. M. New renewably-sourced polyesters from limonene-derived monomers. *Green Chem.* **21**, 149–156 (2019).

2. Stamm, A.; Tengdelius, M.; Schmidt, B.; Engström, J.; Syrén, P. O.; Fogelström, L.; Malmström, E. Chemo-enzymatic pathways toward pinene-based renewable materials. *Green Chem.* **21**, 2720–2731 (2019).

3. Parrino, F.; Fidalgo, A.; Palmisano, L.; Ilharco, L. M.; Pagliaro, M.; Ciriminna, R. Polymers of Limonene Oxide and Carbon Dioxide: Polycarbonates of the Solar Economy. *ACS Omega* **3**, 4884–4890 (2018).

4. Ogawa, K., Stafford, J. A., Rothstein, S. D., Tallman, D. E., Rasmussen, S. C. Nitrogen-functionalized polythiophenes: Potential routes to new low band gap materials. in *Synthetic Metals* **152**, 137–140 (2005).

5. Byrne, C. M., Allen, S. D., Lobkovsky, E. B. & Coates, G. W. Alternating copolymerization of limonene oxide and carbon dioxide. *J. Am. Chem. Soc.* **126**, 11404–11405 (2004).

6. Hauenstein, O., Reiter, M., Agarwal, S., Rieger, B., Greiner, A. Bio-based polycarbonate from limonene oxide and CO2 with high molecular weight, excellent thermal resistance, hardness and transparency. *Green Chem.* **18**, 760–770 (2016).

7. Firdaus, M., Meier, M. A. R. Renewable polyamides and polyurethanes derived from limonene. *Green Chem.* **15**, 370–380 (2013).

8. Firdaus, M., Montero De Espinosa, L. Meier, M. A. R. Terpene-based renewable monomers and polymers via thiol-ene additions. *Macromolecules* **44**, 7253–7262 (2011).

9. Chen, Y. Z., Wu, L. Z., Zhang, L. P. Tung, C. H. Confined space-controlled hydroperoxidation of trisubstituted alkenes adsorbed on pentasil zeolites. *J. Org. Chem.* **70**, 4676–4681 (2005).

10. Lowe, A. B. Thiol-ene 'click' reactions and recent applications in polymer and materials synthesis: A first update. *Polym. Chem.* **5**, 4820–4870 (2014).

11. Kobayashi, S., Lu, C., Hoye, T. R. Hillmyer, M. A. Controlled polymerization of a cyclic diene prepared from the ring-closing metathesis of a naturally occurring monoterpene. *J. Am. Chem. Soc.* **131**, 7960–7961 (2009).

12. Wilbon, P. A., Chu, F., Tang, C. Progress in renewable polymers from natural terpenes, terpenoids, and rosin. *Macromol. Rapid Commun.* **34**, 8–37 (2013).

13. Winnacker, M., Rieger, B. Recent Progress in Sustainable Polymers Obtained from Cyclic Terpenes: Synthesis, Properties, and Application Potential. *ChemSusChem* **8**, 2455–2471 (2015).

14. Thomsett, M. R., Storr, T. E., Monaghan, O. R., Stockman, R. A., Howdle, S. M. Progress in the synthesis of sustainable polymers from terpenes and terpenoids. *Green Mater.* **4**, 115–134 (2016).

15. Ojansivu, M.; Johansson, L.; Vanhatupa, S.; Tamminen, I.; Hannula, M.; Hyttinen, J.; Kellomäki, M.; Miettinen, S. Knitted 3D Scaffolds of Polybutylene Succinate Support Human Mesenchymal Stem Cell Growth and Osteogenesis. **2018**, (2018).

16. Huang, A.; Peng, X.; Geng, L.; Zhang, L.; Huang, K.; Chen, B. Electrospun poly(butylene succinate)/cellulose nanocrystals bio- nanocomposite scaffolds for tissue engineering: Preparation, characterization and in vitro evaluation. *Polym. Test.* **71**, 101–109 (2018).

17. Domínguez-Robles, J.; Larrañeta, E.; Fong, M. L.; Martin, N. K.; Irwin, N. J.; Mutjé, P.; Tarrés, Q.; Delgado-Aguilar, M. Lignin/poly(butylene succinate) composites with antioxidant and antibacterial properties for potential biomedical applications. *Int. J. Biol. Macromol.* **145**, 92–99 (2020).

18. Pajoumshariati, S.; Shirali, H.; Yavari, S. K.; Sheikholeslami, S. N.; Lotfi, G.; Mashhadi Abbas, F.; Abbaspourrad, A. GBR membrane of novel poly (butylene succinate-co-glycolate) co-polyester co-polymer for periodontal application. *Sci. Rep.* **8**, 1–16 (2018).

19. Chen, L.; Cheng, H. H.; Xiong, J.; Zhu, Y. T.; Zhang, H. P.; Xiong, X.; Liu, Y. M.; Yu, J.; Guo, Z. X. Improved Mechanical Properties of Poly(butylene succinate) Membrane by Co-electrospinning with Gelatin. *Chinese J. Polym. Sci. (English Ed.* **36**, 1063–1069 (2018).

20. Kang, Y. G.; Wei, J.; Kim, J. E.; Wu, Y. R.; Lee, E. J.; Su, J.; Shin, J. W. Characterization and osteogenic evaluation of mesoporous magnesium-calcium silicate/polycaprolactone/polybutylene succinate composite scaffolds fabricated by rapid prototyping. *RSC Adv.* **8**, 33882–33892 (2018).

21. Tang, X.; Dai, J.; Sun, H.; Nabanita, S.; Petr, S.; Tang, L.; Cheng, Q.; Wang, D.; Wei, J. Copper-doped nano laponite coating on poly(butylene succinate) scaffold with antibacterial properties and cytocompatibility for biomedical application. *J. Nanomater.* **2018**, (2018).

22. Wattanawong, N., Chatchaipaiboon, K., Sreekirin, N. & Aht-Ong, D. Migration, physical and antibacterial properties of silver zeolite/poly(butylene succinate) composite films for food packaging applications. *J. Reinf. Plast. Compos.* **39**, 95–110 (2020).

23. Sapuan, S. M., Nazrin, A., Ilyas, R. A., Sherwani, S. F. K., & Syafiq, R. Nanocellulose Reinforced Thermoplastic Starch (TPS), Poly (lactic) Acid (PLA), and Poly (Butylene Succinate)(PBS) for Food Pack-aging Applications. *Front. Chem.* **8**, (2020).

24. Cornish, K., Vodovotz, Y. & Accepted, J. NARROWING THE GAP FOR BIOPLASTIC USE IN FOOD PACKAGING - AN UPDATE. (2020). doi:10.1021/acs.est.9b03755

25. Dondoni, A. The emergence of thiol-ene coupling as a click process for materials and bioorganic chemistry. *Angew. Chemie - Int. Ed.* **47**, 8995–8997 (2008).

26. Hoyle, C. E. & Bowman, C. N. Polymer Chemistry Thiol – Ene Click Chemistry ** Angewandte. 1540–1573 (2010). doi:10.1002/anie.200903924

3 PBS BASED COPOLYMER AS COMPATIBILIZER IN THERMOPLASTIC FLOUR/POLY(BUTYLENE SUCCINATE) BLENDS

3.1 Introduction

Despite the great benefits apported to our life, plastic materials have a negative impact on the environment. The products have generally a short life and the derived wastes are not subjected to an efficient recycling process, since the manufacts remain dispersed in the environment, leading to serious implications for human health and the natural habitats. The transition to eco-friendly plastics is an urgent need: scientific community, industries and public politics are working to find a solution for this alarming situation. Among the different strategies, the use of modified natural polymers, defined as natural polymers subjected to chemical modification to obtain new functional properties, is a promising option. Modified proteins, cellulose acetate and starch are representative examples.

In particular, modified starch also known as thermoplastic starch (TPS), is obtained by heating the material in presence of plasticizer or gelatinization agent[1]. Wheat, rice, corn, potato, pea, and cassava are natural and low cost sources for starch, characteristic that, together with biodegradable and compostable nature, are increasing the interest on TPS class[2–4]. Despite that, brittleness, high degradation rate and great sensibility to moisture content, make TPS difficult to be directly used. Blending methodology has been successfully operated, resulting a rapid, and cheap method to obtain new materials with enhanced properties with respect to TPS[4–6]. Traditional fossil-based polymers have been mixed with TPS, polyethylene (PE)[7,8], polypropylene (PP)[9], and polyamide (PA)[10,11], but also biodegradable polymers have been tested, leading to 100% bio-based and compostable material[12,13].

Among biopolymers, the systems based on poly(butylene succinate) (PBS) have attracted the interest of the scientific community: PBS is obtainable from renewable resources, has mechanical responses comparable with LDPE ones and a wide workability window. Indeed, different studies are carried out testing the miscibility of starch with PBS, with poor results without previous plasticization or chemical modification of the polymer[14–16]. For this reason, different strategies of

compatibilization have been conducted. The use of NCO-terminated PBS, defined as reactive PBS, leads to blends characterized by improved tensile strength[17]. Also grafting the polymer with starch, through a single step process, bring good results[18].

Besides that, the effect of plant oil (0.5 % wt.)[19] and of different flours as rice[20] and corn[21,22], has been also reported.

Despite the different factors investigated, the impact on the final properties of amylose or amylopectin starch content, has not been deeply evaluated[22,23]. Just a few papers report thermoplastic corn starch, waxy (0% amylose, WTPS) and normal (26% amylose, NTPS), during preparation of PBS blands, and to the best of our knowledge, there are also just few publications dealing with plasticized flours with significant contents of proteins[24].

In the present work, high amount of plasticized wheat flour (TPWF) was blended with PBS homopolymer and PBS-based copolymer, thanks to the collaboration with the Civil and Environmental Engineering Department of the University of Perugia.

Low cost cereal flours not suitable for food preparation, due to presence of fungi or infested by insects, was employed to prepare the blends. In particular, several mixtures of PBS homopolymer/PBS-based copolymer and TPWF were tested. In detail, in the copolymer the succinic acid subunit, was partially replaced by Pripol 1009 moiety, produced by Croda. The diacid was constituted by aliphatic 6 carbon atoms ring, with long side chains, and bound to -COOR groups through PE-like segments (**Figure 3.1**).
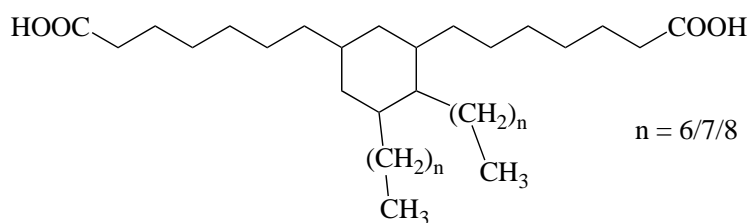
Figure 3.1: Chemical structure of Pripol 1009.

The aliphatic ring bearer by Pripol moieties resembled the flour starch structure, enhancing the TPWF/polymer compatibility. Moreover, as previously observed by us, the PE-like sequences connected to the ring and the side branches favored the macromolecular mobility and decreased the elastic modulus compared to PBS homopolymer.

3.2 Preparation of TPWF based formulations

Thermoplastic plasticized flour-based films (TPF) were produced by using a twin-screw microextruder: plasticizer wheat flour (70%wt.) was mixed with homopolymer/copolymer (PBS/Co) in different weight amounts. The composition and the aspect of the so obtained films were reported respectively in **Table 3.1** and **Figure 3.2**.

Table 3.1: Final composition of TPWF based films and the related code.

	TPWF wt%	PBS wt%	Co wt%
TPWF	100	0	0
PBS	0	100	0
Co	0	0	100
70TPWF/30PBS	70	30	0
70TPWF/25PBS/5Co	70	25	5
70TPWF/20PBS/10Co	70	20	10
70TPWF/15PBS/15Co	70	15	15
70TPWF/10PBS/20Co	70	10	20
70TPWF/5PBS/25Co	70	5	25
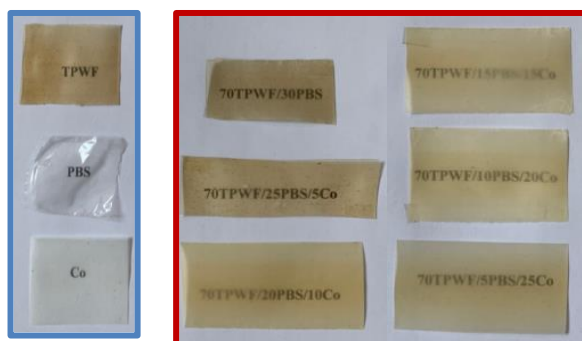
Figure 3.2: Extruded films obtained and related code.

3.3 Homopolymer and copolymer characterization

The synthesis of PBS homopolymer and P(BS85BPripol15) copolymer (namely Co), were conducted as explained before, via solvent free two step polycondensation. The so-obtained polymers appeared as colored solids.

PBS
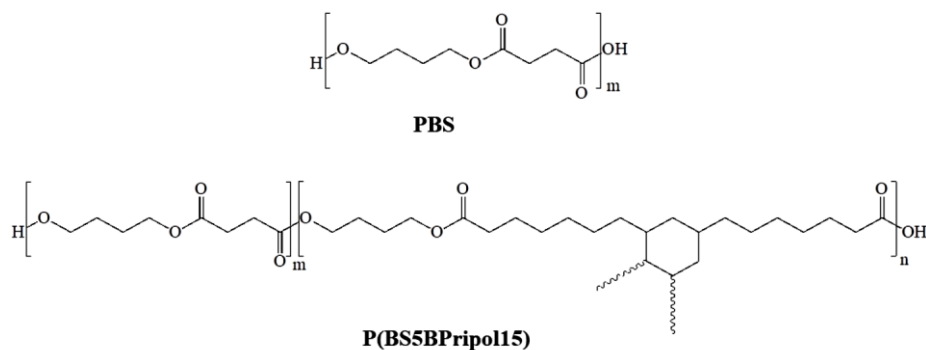
P(BS5BPripol15)

Figure 3.3: Chemical structure of PBS homopolymer and P(BS85BPripol15) copolymer (Co).

^{1}H-NMR spectroscopy was employed to verify the molecular structure (**Figure 3.3**). Regarding PBS, the polymer peaks appeared at the following ^{1}H-NMR chemical shifts: δ 4.2 ppm (t, 4H); δ 2.6 ppm (s, 4H); δ 1.7 ppm (t, 4H). ^{1}H-NMR and ^{13}C-NMR spectra recorded for Co were presented in **Figure 3.4 A** and **B**. Where, together with the characteristic peaks of the butylene-succinate, BS, subunits, signals from the butylene-Pripol1009 part, BPripol, were observed. No additional peaks were detected, excluding the occurrence of side reactions.

The chemical composition was calculated analyzing the signal recorded by ^{1}H-NMR spectroscopy, while degree of randomness (b) and the block length (L) were evaluated considering the ^{13}C-NMR spectrum (**Figure 3.4 B**), in particular the region in between 64.4 and 63.5 ppm, where –OCH$_2$- group were resonating. The data collected were reported in **Table 3.2**.

Table 3.2: Chemical characterization of the synthesized materials.

Sample	BS mol% feed	BS mol% ^{1}H-NMR	L_{BS}	$L_{BPripol}$	W_{BS} g/mol	$W_{BPripol}$ g/mol	b	M_n g/mol	D
PBS	100	100	-	-	55000	-	-	55000	2.0
P(BS$_{85}$BPripol$_{15}$)	85	82	8.3	1.2	1428	704	1.0	46000	2.1

The value of b resulted pretty close to 1, confirming the random nature of the synthetized copolymer. The average block length of the BS and BPripol sequences, L_{BS} and $L_{BPripol}$, were strictly related to the molar amount of two diacid subunits constituting the polymeric chains.
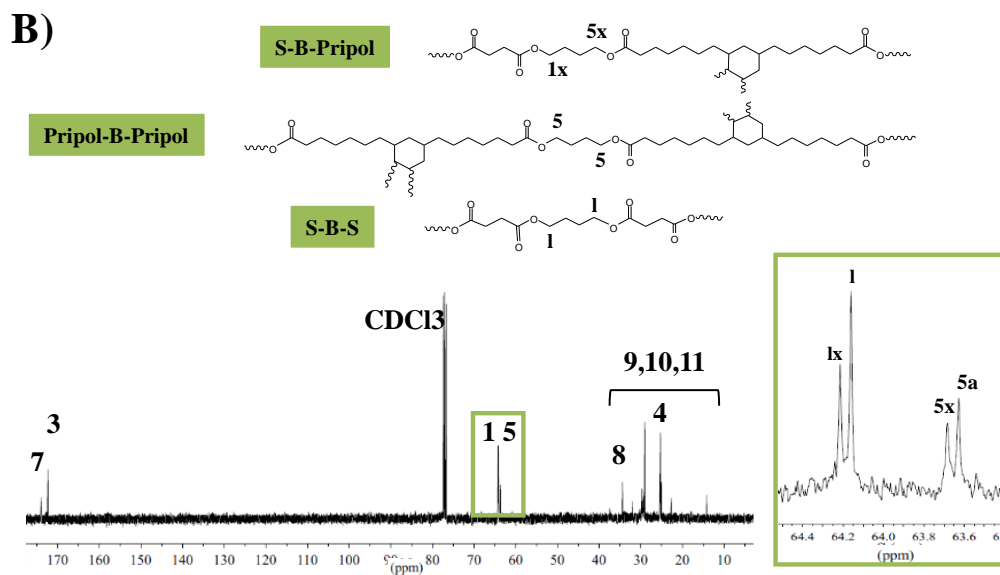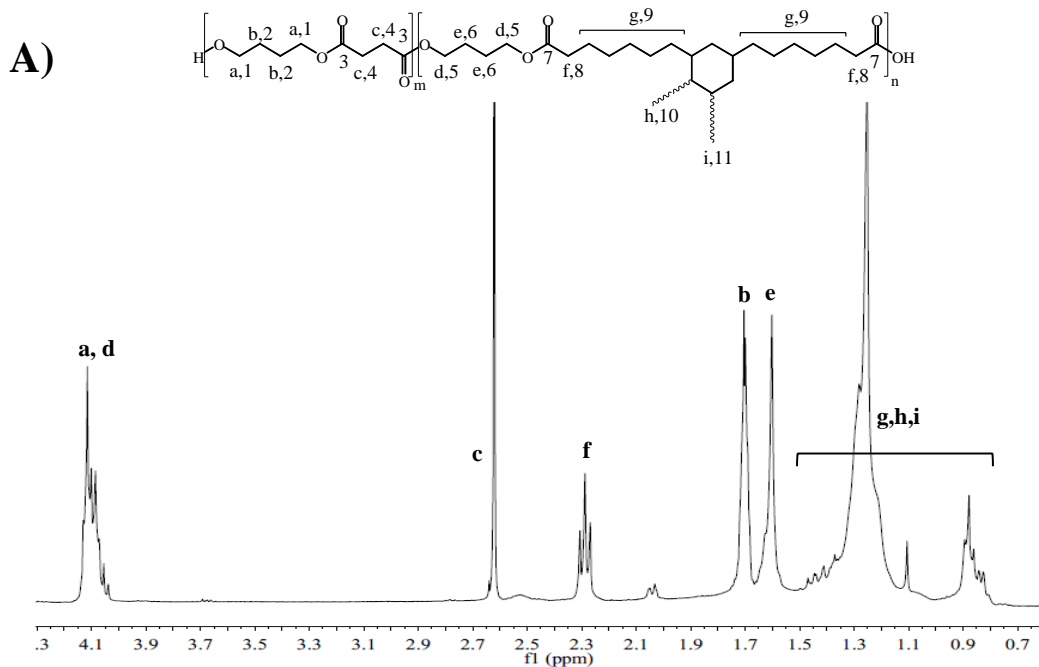
Figure 3.4: *A)* ^{13}C-NMR and *B)* ^{13}C-NMR spectrum of P(BS85BPripol15) (Co) with peak assignment.

Table 3.2 reported GPC data. The molecular weight (M_n), high and comparable for both the synthetized polymers and the polydispersity indices confirmed the suitability of the synthetic method adopted.

3.4 Morphological properties of TPWF based formulation

FESEM was employed to analyse the morphology of fractured surfaces for TPWF/polymer blends (**Figure 3.5**).
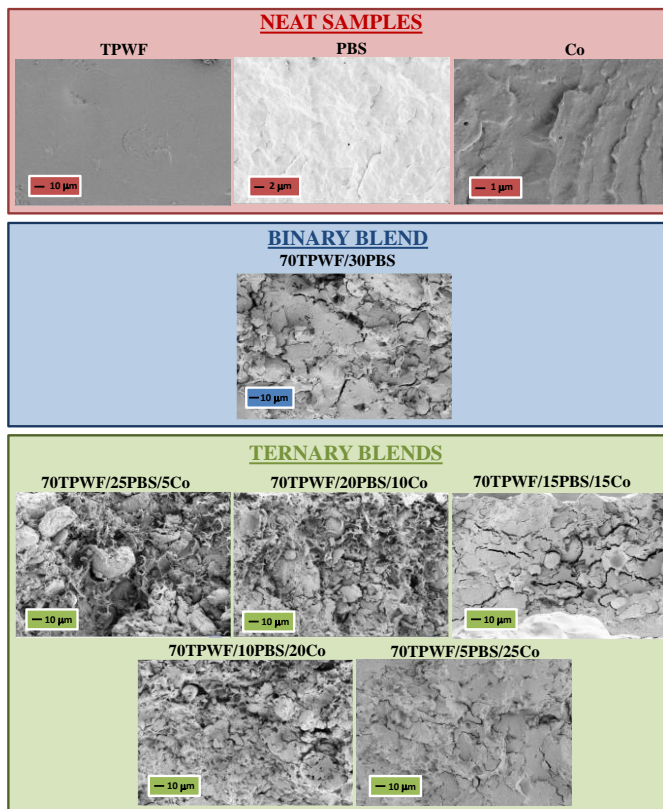
Figure 3.5: *FESEM images of TPWF, PBS, Co and TPWF based films.*

Starting the analysis from the neat materials, TPWF PBS and Co, different characteristics could be evidenced. TPWF, broken with fragile behaviour, presented homogeneous and continuous surface; differently, PBS and Co, after semi-ductile fracture, were characterized by a rough surface. The observed morphological variations were associated to the different viscosity of PBS, Co and TPWF. Analysing the fractured surface of TPWF polymer blends, different interaction between polymeric phase and plasticized flour caused different roughness profiles. In details, 70TPWF/30PBS and 70TPWF/25PBS/5Co showed incompatible ''sea island'' bi-phase structure. Indeed, microcavities were observed at the filler-matrix interface, suggesting poor compatibility between the components of the mixture. With the increasing of Co amount, the matrix fibrillation disappeared from the fracture surface, the conglomerates were reduced, and a general better dispersion of the starchy particles was observed. The results suggested Co, used in higher amount

then 5%, explicated a compatibilizer effect; further confirmation came from the absence of clear delamination of the polymer matrix. The compatibilizer role of Co was supposed to lead to positive impact on stiffness of the final materials.

3.5   Thermal analysis of TPWF based formulations

Thermogravimetric analysis of the blends was carried out to evaluate the thermal stability of the mixtures. In **Figure 3.6 A** the curves of neat PBS and random copolymer Co, processed at different temperature (135 and 145°C) were reported, while **Figure 3.6 C** showed the data collected for TPWF polymer blends.

BINARY BLEND and TERNARY BLENDS
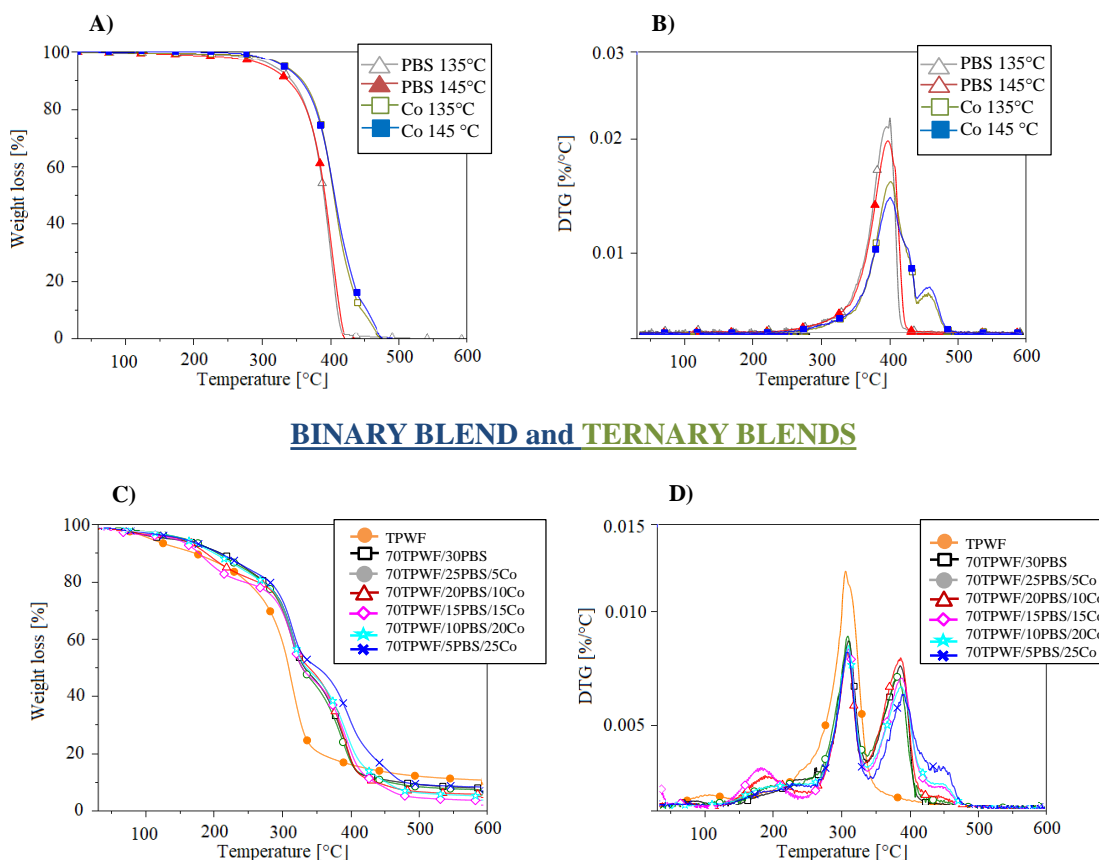
Figure 3.6: A) Weight loss and B) derivative mass loss curves of PBS homopolymer and Co processed at 135 °C and 145 °C; C) weight loss and D) derivative mass loss of TPWF and blends.

Thermal degradation of PBS agreed with the data reported in literature, with a single step process starting around 300°C, while the complete degradation was reached at 430°C. The first weight loss was related to the volatilization of low mass compounds as succinic acid and butylene glycol. Then, the major thermal degradation occurred on PBS chains, with random scission of ester bonds

146

and formation of carboxylic and vinyl end groups[25,26]. P(BS85BPripol15), Co, showed higher stability compared to PBS homopolymer. The mechanism of degradation was evolving in two different steps: the first one proportional to the amount of BS content followed by a second step, related to BPripol sequences. The introduction of Pripol subunit in the homopolymeric chain enhanced the thermal stability, due to the replacement of thermally degradable ester groups with long PE-like segments. For both the polymers, changing the extrusion temperature, from 135 °C to 145°C, had a negligible effect on the final stability of PBS and Co, being no differences in the curves recorded after the different processing.

As concern the blends, TGA curves reported three distinct regions. The first weight loss, occurring between the range 90–230°C, was due to the volatilization of small molecules, as water and glycerol; then, thermal degradation of starch was occurring, starting at about 300°C. The final stage was identified with the main degradation of PBS and Co, above 400°C. Comparing these curves with the neat TPWF, a general increasing of thermal stability due to blending with PBS or Co was observed.

In order to evaluate the changing in thermal transitions, DSC analysis have been conducted. In **Figure 3.7** the calorimetric traces of the extruded TPWF and PBS and Co, were reported (panel **A**, **B**, **C**).

As regards TPWF, the first scan showed a wide endothermic peak attributed to water evaporation. In the subsequent cooling and heating scan, no thermal transitions were taking place indeed the calorimetric trace reported absence of signals. Differently, PBS and Co showed the typical behaviour of semicrystalline material, with glass to rubber transition step at low temperature followed by an endothermic peak due to melting process. In details, PBS had a glass transition temperature located at -35°C, then a little sharp exothermic peak just before melting, around 90°C, attributed to the crystallization phenomenon. The melting temperature, T_m, was identified at 114°C. The thermal transitions were affected by copolymerization process, indeed in case of Co the glass transition temperature was located at -42°C due to the increased mobility of polymeric chains conferred by the PE-like segments of Pripol moiety and to the branches on its aliphatic ring. Together with the glass transition temperature, also the melting phenomenon was subjected to shift, being the copolymer melting at 97°C, indicating a lower perfection of the formed crystals. As well as T_m, enthalpy of melting, ΔH_m, was decreased indicating a lower amount of crystals

respect to PBS sample. Moreover, the exothermic crystallization peak observed for PBS at 90°C was suppressed in case of Co.

NEAT SAMPLES

BINARY BLEND and TERNARY BLENDS
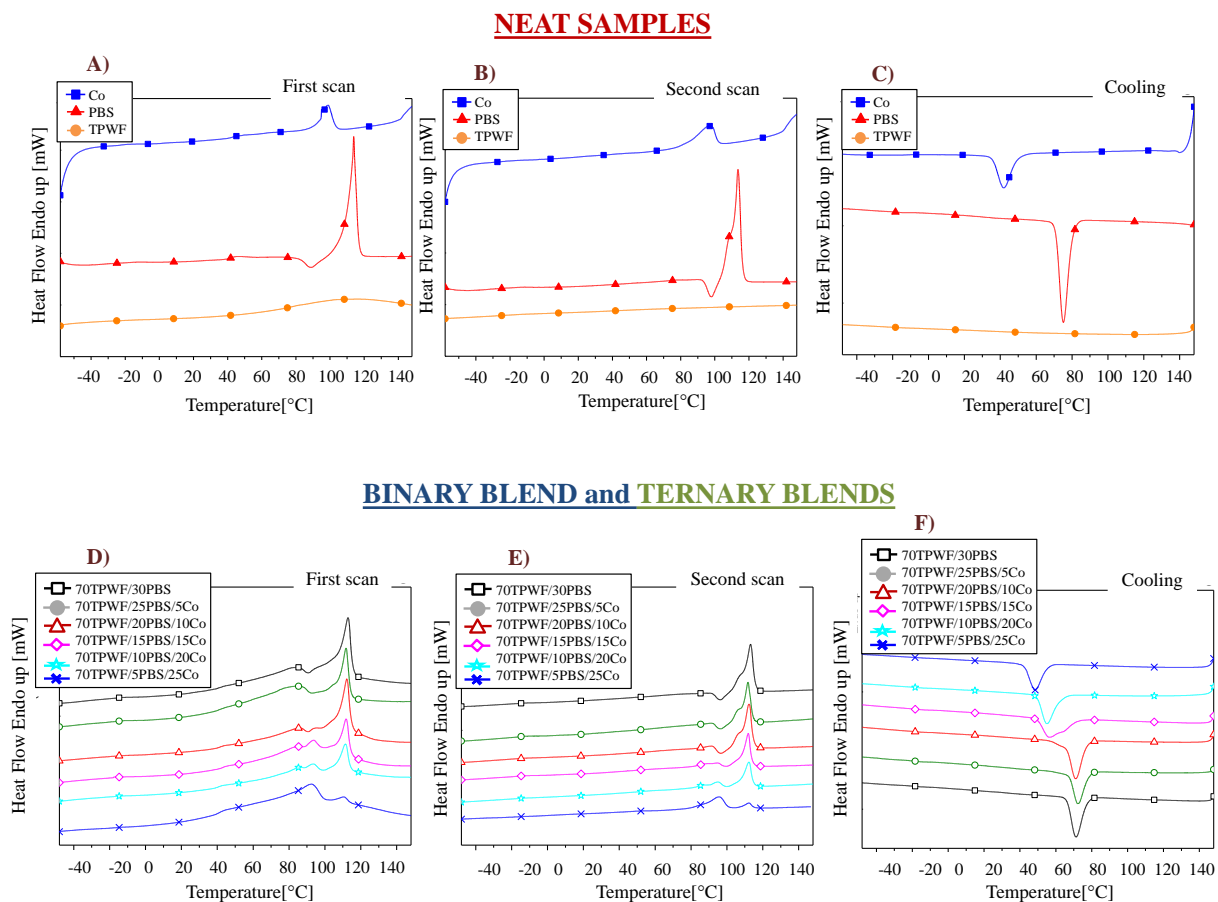
Figure 3.7: A) First heating scan, B) second heating scan and C) cooling scan recorded for TPWF, PBS and Co films. D) First heating scan, E) second heating scan and F) cooling scan measured for the different composition of TPWF based films.

The equilibrium melts were cooled down (10°C/min), resulting in the calorimetric traces reported in **Figure 3.7 C**. As one can see, PBS was crystallizing at 75°C while for Co the corresponding exothermic peak was observed at 44°C. As expected, the crystallization process was slowed down due to the co-unit introduction. The followed heating scan, **Figure 3.7 B**, for PBS retraced the first scan conducted. Differently, Co was subjected to a decrease of crystalline perfection during the cooling step; as a consequence, slight shift at lower temperature and enlargement of the endothermic peak was detected.

As concern, DCS analysis of TPWF blends the calorimetric traces were reported in the bottom part of **Figure 3.7.** For each sample, peaks related to the different components in the blend could be

observed and the intensity was proportional to the amount. The first scans recorded, panel **D**, were similar to the second scans, panel **E**; an endothermic peak, due to water release from TPWF, was overlapping the melting peaks, for this reason the evaluation of the characteristic temperature (T_c, T_m) and the related enthalpies (ΔH_c, ΔH_m), was carried out after water removal, in the second scan.

In **Figure 3.7 F**, the crystallization capability could be evaluated: the presence of TPWF was not affecting the crystallization process, being all the blends characterized by comparable crystallization enthalpy values, as reported in **Table 3.3**. Despite that, from 70TPWF/30PBS, crystallizing at 71°C, to 70TPWF/5PBS/25Co that presented the endothermic peak at 48°C, a general shift of the crystallization process to lower temperature could be observed. Moreover, 70TPWF/15PBS/15Co blend was subjected to crystallization of BS sequence, located in the homopolymer but also of the copolymer Co, causing an overlapping of exothermic phenomena.

The second heating scans, reported in **Figure 3.7 E**, as mentioned before, retraced the first scans, just the water evaporation peak was suppressed. The glass transition temperature decreased due to the presence of TPWF, confirming its plasticizers effect. PBS-rich blends showed a crystallization peak around 97°C, as PBS homopolymer, then a double melting process was occurring: at 105°C less perfect crystal fractions melted, then at 112°C the remaining crystal phase was melting. With the increasing of Co content in the blends, the exothermic transition at 97°C was replaced by an endothermic peak, observed just some Celsius before, at 94°C. This was attributed to the melting of Co crystalline phase.

Table 3.3: Thermal characterization data of ternary blends (cooling step from the melt and subsequent heating scan).

Sample	Cooling		IInd heating					
	T_c °C	ΔH_c Jg^{-1}	T_g °C	Δc_p Jg^{-1}K^{-1}	T_{cc} °C	ΔH_{cc} Jg^{-1}	T_m °C	ΔH_m Jg^{-1}
70TPWF/30PBS	71	21	-48		97	4	113	24
70TPWF/25PBS5Co	71	16	-49		97	3	112	22
70TPWF/20PBS10Co	70	22	-49		96	3	112	20
70TPWF/15PBS15Co	56	18	-49		-	-	94 112	2 14
70TPWF/10PBS20Co	55	16	-50		-	-	94 112	4 11
70TPWF/5PBSCo	48	15	-50		-	-	94 112	14 4

3.6 Tensile behavior of TPWF based formulations

The mechanical behaviour of PBS, Co and TPWF as neat material, as well as the one of the ternary blends, was studied. The results were reported in **Table 3.4** and **Figure 3.8**.

Table 3.4: *Young´s modulus (E), stress at break (σ_b), strain at break (ε_b) for the neat materials together with the TPWF based films.*

Sample	E MPa	σ_b MPa	ε_b %
TPWF	4.71 ± 0.07	0.32 ± 0.02	48.4 ± 4.7
PBS	402 ± 23	22.6 ± 1.6	10.8 ± 2.8
Co	120 ± 5	12.2 ± 3.5	253 ± 34
70TPWF/30PBS	83.2 ± 7.6	3.48 ± 0.04	8.91 ± 1.67
70TPWF/25PBS/5Co	72.0 ± 7.3	2.79 ± 0.35	8.22 ± 0.62
70TPWF/20PBS/10Co	69.9 ± 8.6	2.63 ± 0.34	7.55 ± 0.52
70TPWF/15PBS/15Co	62.2 ± 3.0	2.62 ± 0.20	11.12 ± 0.13
70TPWF/10PBS/20Co	56.2 ± 3.9	2.97 ± 0.28	13.00 ± 1.25
70TPWF/5PBS/25Co	37.4 ± 2.6	2.52 ± 0.17	20.95 ± 1.10

PBS homopolymer showed a brittle fracture accompanied by modest deformation and high elastic modulus; differently, TPWF sample presented poor mechanical performance in terms of tensile strength and modulus, but higher deformation at break, lengthening 5 times more than the PBS. Considering PBS and TPWF presented pretty different mechanical performance, low compatibility could be supposed, as already mentioned. The mechanical behaviour of Co was collocated in between TPWF and PBS, with good Young's modulus and stress resistance values, tough behaviour and high elongation at break. Indeed, if the prevalent use of TPWF maintained the system economically affordable and the presence of PBS made the material eco-sustainable, the introduction of Co enhanced the TPWF/PBS chemico-physical compatibility. The PBS/Co ratio of the so-obtained ternary mixture was correlated with the mechanical behavior and summarized in **Table 3.4**.

The addition of 30% wt. of PBS in TPWF significantly increased the resistance, considering the mechanical behavior of neat material but, despite that, the deformation value was still low. As regard the ternary blends, the use of 5-10% wt. of Co in the mixture in 70TPWF/25PBS/5Co and 70TPWF/20PBS/10Co blends, did not affect the final elongation at break that still low, even if

caused a reduction of modulus and final resistance. The blends composed by 15% and 20% wt. of Co, 70TPWF/15PBS/15Co and 70TPWF/10PBS/20Co, preserved good elastic modulus and value of stress at break, with an increasing of deformation. The maximum of deformation at break was observed for the sample with the maximum amount of Co, 70TPWF/5PBS/25Co; despite that, a slight reduction in strength was reported.

The tests conducted defined the role of the component used in the mixture. PBS conferred rigidity and strength to the mixture while Co acted both as a reinforcement and toughener, linking the rigid and fragile nature of PBS with the low resistance and plastic deformation response to stress of TPWF.
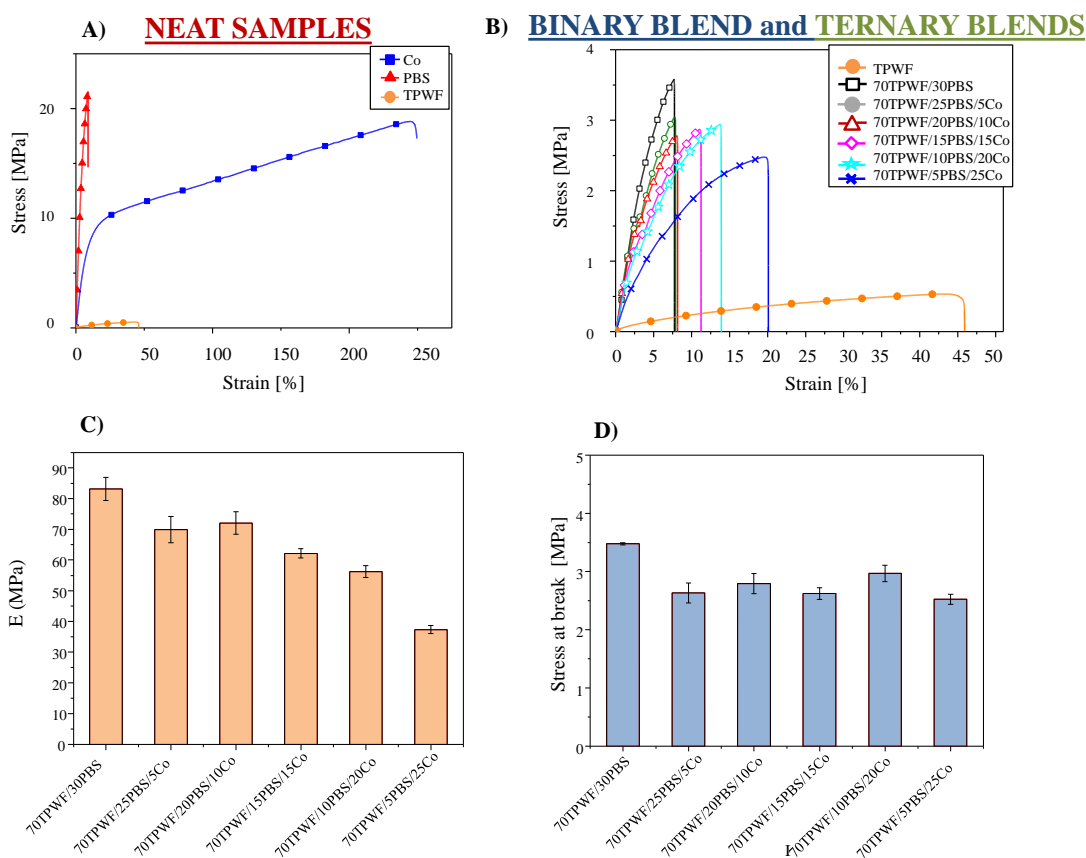
Figure 3.8: *Recorded stress-strain curves for **A**) TPWF, PBS and Co films and **B**) TPWF based series of extruded films. **C**) Young's modulus and **D**) stress at break are reported for each blend.*

3.7   Disintegration in compost

The compostability of the extruded blends was tested, according to the EN ISO 20200:2015, (EN ISO 20200:2015). The initial state of the materials and their conditions after incubation was

reported in **Figure 3.9**; the gravimetric weight loss as a function of time spent in compost, was plotted in **Figure 3.10**. Just after the first few days, shape and color changed. In details, neat TPWF film and TPWF based formulations were the most affected, due to the hydrophilic nature of the flour that favored the water attack; indeed, after 3 days of incubation TPWF film appeared completely fractured.

Incubation time	Start	Day 3	Day 7	Day 10	Day14	Day 21	Day 28	Day 42	Day 56	Day 77	Day 90
TPWF											
PBS											
Co											
70TPWF/30PBS											
70TPWF/25PBS/5Co											
70TPWF/25PBS/10Co											
70TPWF/15PBS/15Co											
70TPWF/10PBS/20Co											
70TPWF/5PBS/25Co											
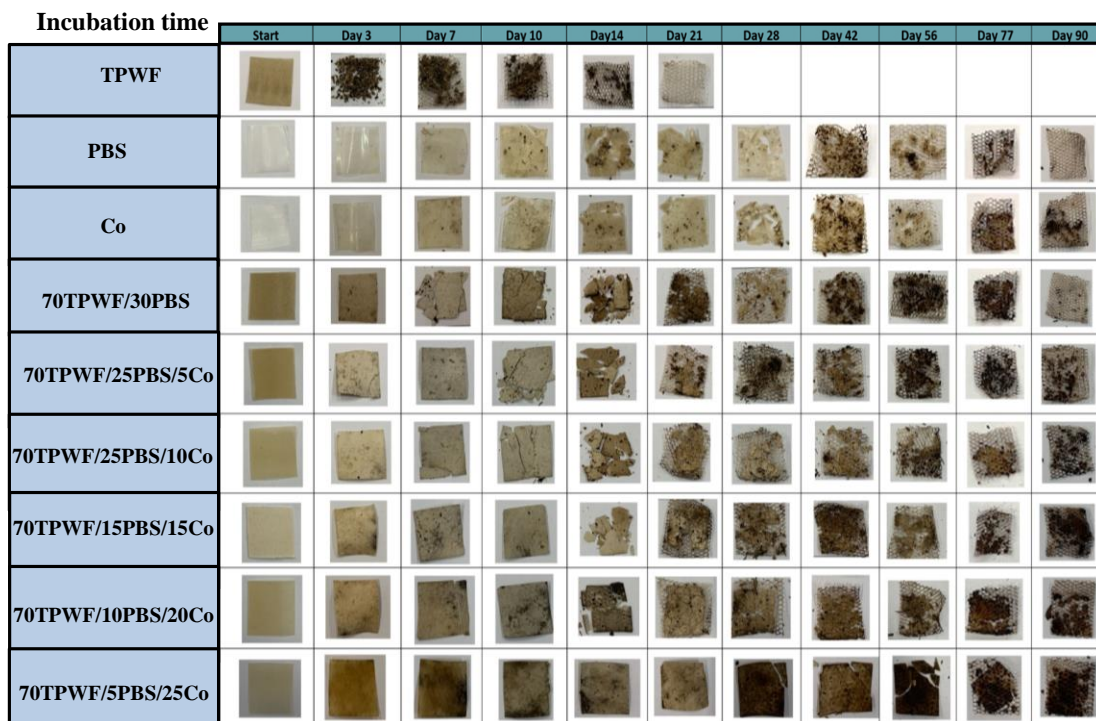
Figure 3.9: *Visual changing of TPWF, PBS homopolymer, Co copolymer and TPWF based extruded films after composting at different times.*

PBS and Co films degraded with a kinetics completely different, in general lower, if compared to neat TPWF. In general, binary and ternary blends, decomposed faster than PBS and Co. The predominant presence of TPWF, 70% wt., with its hydrophilic groups enhanced the adsorption of water and microorganisms from the compost, for degradation in polymer matrix. In this way, the hydrolysis in these samples occurred faster than in the neat polymers, PBS and Co[27]. After 14 days in compost, PBS lost 6% of its initial weigh, Co 4% while, after the same time of incubation.

The disintegration of PBS phase was proceeding essentially through the hydrolysis of amorphous parts, being the attack of microorganisms and fungi easer in this zone[27,28]. Despite the higher amount of amorphous fraction, Co presented a lower disintegration value compared to neat PBS, due to the intrinsic structure of the copolymer, where the replacement of 18 mol% of succinic

moieties with Pripol ones, made the hydrolysable -COOR- groups less frequent in the copolymeric backbone. As confirmation, the Co sample incubated showed an increased value of BPripol sequence, in agreement with previous studies[29]. On the base of the latter observation, increasing the amount of Co in the formulation led to a decreasing of the disintegrability values. TPWF, PBS, 70TPWF/30PBS and 70TPWF/25PBS/5Co were almost completely fractured, with a disintegrability values close to 90%, within 90 days. As regarding Co neat film, the degradation at the end of incubation period reached a value of 58%; while the ternary blends 70TPWF/20PBS/10Co, 70TPWF/15PBS/15Co, 70TPWF/10PBS/20Co and 70TPWF/5PBS/25Co, where the Co amount was progressively increased, the final results were 87%, 85%, 76% and 62% of disintegration, respectively.
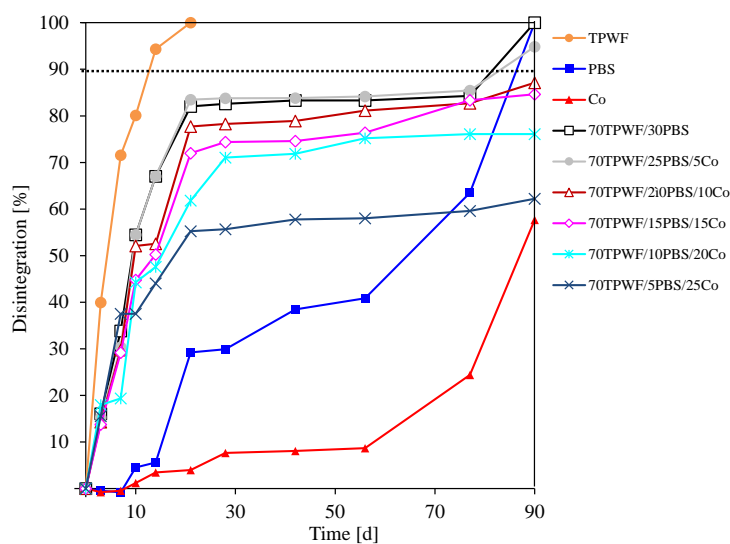
Figure 3.10: *Disintegration values of composted samples of TPWF, PBS, Co and TPWF based blends at different time of incubation.*

3.8 Morphological analysis of disintegrated samples

FESEM was employed to analyze the degraded surfaces of the extruded blends after composting test. The images collected were shown in **Figure 3.11.** At time 0, the surface of Co resulted smooth and homogeneous, with absence of pores or cracks, as described for plasticized flours[30]. As already mentioned, PBS was poorly miscible with thermoplastic starch[31] and the introduction of Co in the mixtures, with amount up to 15% wt., determined the formation of a matrix-dispersed phase of TPWF/PBS. Despite that, reaching higher amount of Co, not-perfectly plasticized granules appeared as small surface asperities[23,32]

Surfaces- time 0

Co | 70TPWF/25PBS/5Co | 70TPWF/20PBS/10Co

70TPWF/15PBS/15Co | 70TPWF/10PBS/20Co | 70TPWF/5PBS/25Co

Surfaces – 21 days

Co | 70TPWF/25PBS/5Co | 70TPWF/20PBS/10Co

70TPWF/15PBS/15Co | 70TPWF/10PBS/20Co | 70TPWF/5PBS/25Co

Surfaces – 56 days

Co | 70TPWF/25PBS/5Co | 70TPWF/20PBS/10Co

70TPWF/15PBS/15Co | 70TPWF/10PBS/20Co | 70TPWF/5PBS/25Co

Surfaces – 90 days

Co | 70TPWF/25PBS/5Co | 70TPWF/20PBS/10Co

70TPWF/15PBS/15Co | 70TPWF/10PBS/20Co | 70TPWF/5PBS/25Co

Figure 3.11: *FESEM images of Co and extruded films surface recorded on samples before the test and after 21, 56 and 90 days in composting conditions.*

154

In the case of 70TPWF/25PBS/5Co and 70TPWF/20PBS/10Co samples, after 21 and 56 days in compost, the surface showed holes with sharp boundaries, deriving from fast degradation of TPWF in presence of slow degrading PBS. With the passing of incubation time, the holes increased their dimensions becoming deeper and, after 90 days in compost, pores were formed[33]. As regard 70TPWF/15PBS/15Co, 70TPWF/10PBS/20Co and 70TPWF/5PBS/25Co the rate of degradation was slow since the formation of holes/porosity was less evident and the surface remains smoother, in line with the disintegration profile of neat Co[34]. These observations agreed with the weight loss experiments, which showed the disintegration of TPWF/PBS blends slowing down with Co content.

3.9   Water contact angle of TPWF based formulations

Water contact angle (WCA) data for TPWF/PBS samples were reported in **Table 3.5**. TPWF showed a value of 55°, confirming previous observation[35,36]. As concerns PBS, the reported WCA value showed higher hydrophobic character of this polymer compared to TPWF, as expected considering the chemical structure of the two compounds. In case of Co, the presence of Pripol, a non-polar moiety, in the repeating unit rose the angle value from 59° to 63°, since increased the hydrophobicity.

Table 3.5: Water contact angle for the TPWF based films.

	WAC (°)
TPWF	54.74 ± 1.37
PBS	58.90 ± 1.87
Co	63.48 ± 0.77
70TPWF/30PBS	60.55 ± 1.23
70TPWF/25PBS/5Co	79.16 ± 1.57
70TPWF/20PBS/10Co	79.87 ± 1.88
70TPWF/15PBS/15Co	72.27 ± 0.81
70TPWF/10PBS/20Co	76.89 ± 1.72
70TPWF/5PBS/25Co	70.38 ± 1.90

WCA recorded for TPWF-based blends showed a complex trend. Two different effects had to be considered, eventually acting in opposition: *i)* the amount of Co, the most hydrophobic component and *ii)* the rheological characteristics of the blends, since rheology of the melt influenced the

solidification dynamics, therefore the morphology of the films. The surface texture of the final material was indeed deeply affected by processing[37]. In this case, the surface roughness degree, with different asperities in terms of quantity and size, influenced the final value of WCA[38].

The 70TPWF/30PBS system showed a contact angle of 60°, value similar to PBS, due to role of the homopolymer in the blend. Consequently, the final surface of the film was smooth and the resulting crystalline phase was similar to neat PBS. 70TPWF/25PBS/5Co and 70TPWF/20PBS/10Co, characterized by small adding of Co, reported values up to 79-80° of contact angle, strictly related to both the intrinsic hydrophobicity of Co structure and the surface roughness, due to the presence of conglomerates derived from the ability of Co to bind with particles of the plasticized flour. The starchy conglomerates formed were appreciable not only on the surfaces (**Figure 3.11**, time 0) but also through the section of the films (**Figure 3.5**). As forecasted from Wenzel model, the surface roughness increased the wettability character of the neat surface: the hydrophilic ones becoming more hydrophilic, the hydrophobic surface more hydrophobic[39]. Due to the low presence of Co in these formulation, 5% wt. and 10% wt., this component was not acting as a proper plasticizer. Instead, reaching a value of 15% wt., as in case of 70TPWF/15PBS/15Co, the plasticizing effect of Co was evident by the reduction of starchy conglomerates size, as reported in see **Figure 3.11.** The resulting surface appeared with rounded asperities, leading to a reduction of WCA to 72° despite the increased amount in the blend of the most hydrophobic component (Co). In case of 70TPWF/10PBS/20Co blend the conglomerates reduced their dimensions and starchy particles were better dispersed, therefore the surface presented few rounded asperities, as one could see in **Figure 3.10**, time 0, where many small asperities of the "deconglomerated" particles could be observed. The increased amount of Co together with this morphology rose the water contact angle to 77°. As concern 70TPWF/5PBS/25Co blend, WCA dropped to 70°; in this case the amount of Co determined better dispersion of starchy particles with consequent formation of uniform and smooth surface.

The mechanical tests confirmed the relation found between contact angle, morphology of surfaces and sections. In case of ternary mixture, a progressive decrease in the Young's modulus was observed with the rise of content of Co. This trend agreed with the observation on morphologies presented by the samples. The Co content was also affecting the maximum stress that decreased with the increasing of the amount of copolymer used in the formulation. In this case, a relative

maximum for 70TPWF/15PBS/20Co was observed, traced back to the good dispersion and compatibilization of the small starch particles that acted as reinforcement, improving the strength. The upper limit of Co used, 70TPWF/5PBS/25Co, led to an excessive plasticization of the particles and prevented their reinforcement function, lowering the mechanical strength.

3.10 Conclusions

In order to realize the passage from linear economy, responsible of large quantities of plastic waste with consequent severe environmental problems, to a circular one, the replacement of the oil-based non-biodegradable traditional plastics with bioplastics is fundamental. Nowadays, these latter are delaying their entrance in the global market due to high costs and poor properties with respect to classical commodities. The present work represents a step forward closer to the affirmation of bioplastics.

A low-cost series of blends obtained with eco-friendly technological process were tested. The mixtures were constituted by 70% in weight of plasticized wheat flour and different ratio of PBS and its derived copolymer, Co, a 100% bio-based polyester, containing aliphatic six carbon ring moieties. This latter component acted as compatibilizer, as proven by the mechanical tests conducted, without losing the characteristic compostability of wheat flour. The mixtures with 15% wt. and 20% wt. of copolymer reported the best mechanical performances: film deformation improved, and a good value of elastic modulus and stress were preserved. The results evidenced how the PBS/Co ratio had a key role in modulating the properties of the final material.

3.11 Bibliography

1.   Luo, X., Li, J., Lin, X. Effect of gelatinization and additives on morphology and thermal behavior of corn starch/PVA blend films. *Carbohydr. Polym.* **90**, 1595–1600 (2012).

2.   Moad, G. Chemical modification of starch by reactive extrusion. *Prog. Polym. Sci.* **36**, 218–237 (2011).

3.   Pereira, A. G. B.; Paulino, A. T.; Nakamura, C. V.; Britta, E. A.; Rubira, A. F.; Muniz, E. C. Effect of starch type on miscibility in poly(ethylene oxide) (PEO)/starch blends and cytotoxicity assays. *Mater. Sci. Eng. C* **31**, 443–451 (2011).

4.   Zullo, R., Iannace, S. The effects of different starch sources and plasticizers on film blowing of thermoplastic starch: Correlation among process, elongational properties and macromolecular structure. *Carbohydr. Polym.* **77**, 376–383 (2009).

5. Yu, L., Dean, K., Li, L. Polymer blends and composites from renewable resources. *Prog. Polym. Sci.* **31**, 576–602 (2006).

6. Xie, F., Halley, P. J., Avérous, L. Rheology to understand and optimize processibility, structures and properties of starch polymeric materials. *Prog. Polym. Sci.* **37**, 595–623 (2012).

7. Pedroso, A. G, Rosa, D. S. Mechanical, thermal and morphological characterization of recycled LDPE/corn starch blends. *Carbohydr. Polym.* **59**, 1–9 (2005).

8. Shujun, W., Jiugao, Y., Jinglin, Y. Preparation and characterization of compatible thermoplastic starch/polyethylene blends. *Polym. Degrad. Stab.* **87**, 395–401 (2005).

9. Ramis, X.; Cadenato, A.; Salla, J. M.; Morancho, J. M.; Vallés, A.; Contat, L.; Ribes, A. Thermal degradation of polypropylene/starch-based materials with enhanced biodegradability. *Polym. Degrad. Stab.* **86**, 483–491 (2004).

10. Teyssandier, F., Cassagnau, P., Gérard, J. F., Mignard, N., Mélis, F. Morphology and mechanical properties of PA12/plasticized starch blends prepared by high-shear extrusion. *Mater. Chem. Phys.* **133**, 913–923 (2012).

11. Teyssandier, F., Cassagnau, P., Gérard, J. F., Mignard, N. Reactive compatibilization of PA12/plasticized starch blends: Towards improved mechanical properties. *Eur. Polym. J.* **47**, 2361–2371 (2011).

12. Ma, X., Chang, P. R., Yu, J. Wang, N. Preparation and properties of biodegradable poly(propylene carbonate)/thermoplastic dried starch composites. *Carbohydr. Polym.* **71**, 229–234 (2008).

13. Wang, N., Yu, J., Chang, P. R. Ma, X. Influence of citric acid on the properties of glycerol-plasticized dry starch (DTPS) and DTPS/poly(lactic acid) blends. *Starch/Staerke* **59**, 409–417 (2007).

14. Ni, Hong Kai, Biao Yang, Hui Sun, and G. Z. X. Wet Blending of Pregelatinized Starch and Poly(butylene Succinate). *Adv. Mater. Res.* **557–559**, 1121–1126 (2012).

15. Lai, S. M., Huang, C. K., Shen, H. F. Preparation and properties of biodegradable poly(butylene succinate)/starch blends. *J. Appl. Polym. Sci.* **97**, 257–264 (2005).

16. Wang, W., Zhang, G., Zhang, W., Guo, W., Wang, J. Processing and Thermal Behaviors of Poly (Butylene Succinate) Blends with Highly-Filled Starch and Glycerol. *J. Polym. Environ.* **21**, 46–53 (2013).

17. Zeng, J. B.; Jiao, L.; Li, Y. D.; Srinivasan, M.; Li, T.; Wang, Y. Z. Bio-based blends of starch and poly(butylene succinate) with improved miscibility, mechanical properties, and reduced water absorption. *Carbohydr. Polym.* **83**, 762–768 (2011).

18. Suchao-In, K., Koombhongse, P., Chirachanchai, S. Starch grafted poly(butylene succinate) via conjugating reaction and its role on enhancing the compatibility. *Carbohydr. Polym.* **102**, 95–102 (2014).

19. Piotr Tynski, Justyna Ostrowska, Magdalena Paluch, W. S. Properties of biodegradable films based on thermoplastic starch and poly(butylene succinate) with plant oil additives. in *Proceedings of the 2nd International Scientific Conference «Chemical Technology and Engineering»* 257–261 (2019).

20. Kim, H. S., Kim, H. J., Lee, J. W., Choi, I. G. Biodegradability of bio-flour filled biodegradable poly(butylene succinate) bio-composites in natural and compost soil. *Polym. Degrad. Stab.* **91**, 1117–1127 (2006).

21. Lee, T. O. Effect of aliphatic isocyanates (HDI and LDI) as coupling agents on the properties of eco-composites from biodegradable polymers and corn starch. *J. Adhes. Sci. Technol.* **18**, 905–924 (2004).

22. Ku-marsilla, K. I.; Verbeek, C. J. R. Effect of modified tapioca starch on mechanical, thermal, and morphological properties of PBS blends for food packaging. *Polymers (Basel).* **10**, (2018).

23. Li, J., Luo, X., Lin, X., Zhou, Y. Comparative study on the blends of PBS/thermoplastic starch prepared from waxy and normal corn starches. *Starch/Staerke* **65**, 831–839 (2013).

24. Ku-marsilla, K. I., Verbeek, C. J. R. Compatibilization of protein thermoplastics and polybutylene succinate blends. *Macromol. Mater. Eng.* **300**, 161–171 (2015).

25. Chrissafis, K., Paraskevopoulos, K. M., Bikiaris, D. N. Thermal degradation mechanism of poly(ethylene succinate) and poly(butylene succinate): Comparative study. *Thermochim. Acta* **435**, 142–150 (2005).

26. Gan, Z., Abe, H., Kurokawa, H., Doi, Y. Solid-state microstructures, thermal properties, and crystallization of biodegradable poly(butylene succinate) (PBS) and its copolyesters. *Biomacromolecules* **2**, 605–613 (2001).

27. Huang, Z.; Qian, L.; Yin, Q.; Yu, N.; Liu, T.; Tian, D. Biodegradability studies of poly(butylene succinate) composites filled with sugarcane rind fiber. *Polym. Test.* **66**, 319–326 (2018).

28. Thellen, C.; Orroth, C.; Froio, D.; Ziegler, D.; Lucciarini, J.; Farrell, R.; D'Souza, N. A.; Ratto, J. A. Influence of montmorillonite layered silicate on plasticized poly(l-lactide) blown films. *Polymer (Guildf).* **46**, 11716–11727 (2005).

29. Quattrosoldi, S.; Soccio, M.; Gazzano, M.; Lotti, N. Fully biobased, elastomeric and compostable random copolyesters of poly(butylene succinate) containing Pripol 1009 moieties: structure-property relationship. *Pol Deg Stab Accept.* (2020).

30. Sreekumar, P. A., Leblanc, N., Saiter, J. M. Effect of Glycerol on the Properties of 100 % Biodegradable Thermoplastic Based on Wheat Flour. *J. Polym. Environ.* **21**, 388–394 (2013).

31. Garalde, R. A., Thipmanee, R., Jariyasakoolroj, P. & Sane, A. The effects of blend ratio and storage time on thermoplastic starch/poly(butylene adipate-co-terephthalate) films. *Heliyon* **5**, e01251 (2019).

32. Imre, B., García, L., Puglia, D., Vilaplana, F. Reactive compatibilization of plant polysaccharides and biobased polymers: Review on current strategies, expectations and reality. *Carbohydr. Polym.* **209**, 20–37 (2019).

33. Bai, Z., Liu, Y., Su, T., Wang, Z. Effect of hydroxyl monomers on the Enzymatic degradation of poly(ethylene succinate), poly(butylene succinate), and poly(hexylene succinate). *Polymers (Basel).* **10**, (2018).

34. Bulatović, V.O., Grgić, D.K., Slouf, M. Biodegradability of blends based on aliphatic polyester and thermoplastic starch. *Chem. Pap.* **73**, 1121–1134 (2019).

35. Averous, L., Fauconnier, N., Moro, L., Fringant, C. Blends of Thermoplastic Starch and Polyesteramide: Processing and Properties. *J. Appl. Polym. Sci.* **76**, 1117–1128 (2000).

36. Mahieu, A., Terrié, C., Agoulon, A., Leblanc, N., Youssef, B. Thermoplastic starch and poly(ε-caprolactone) blends: Morphology and mechanical properties as a function of relative humidity. *J. Polym. Res.* **20**, (2013).

37. Garrido, T., Etxabide, A., Peñalba, M., De La Caba, K., Guerrero, P. Preparation and characterization of soy protein thin films: Processing-properties correlation. *Mater. Lett.* **105**, 110–112 (2013).

38. Lin F.Y.H., Li D. Effect of Surface Roughness on the Dependence of Contact Angles on Drop Size,. *J. Colloid Interface Sci.* **159**, 86–95 (1993).

39. Kwangseok Seo, M. K. Re-derivation of Young's Equation, Wenzel Equation, and Cassie-Baxter Equation Based on Energy Minimization. in *Surface Energy* (ed. Aliofkhazraei, M.) (2015). doi:10.5772/61066

4 POLY(DIETHYLENE 2,5-FURANOATE) (PDEF) VS. POLY(PENTAMETYLENE 2,5-FURANOATE) (PPEF) OR POLY(BUTYLENE FURANOATE) (PBF): THE EFFECT OF INSERTION OF AN ETHER-OXYGEN ATOM ON THE FINAL PROPERTIES OF THE MATERIAL

4.1 Introduction

The constant increasing of world plastic production is the signal that these materials are going to play a crucial role also in the future[1]. Indeed, plastics are continuing to be the only materials with unique combination of light-weight, durability and other intrinsic properties. However, challenges related to end-of-life of plastics waste and the possibility to employ just renewable resources for plastic production must be investigated in order to build a new circular economy. Despite recycling is becoming a suitable option[2], plastics employed for food packaging are encountering different criticisms, mainly due to organic matter contamination. Moreover, multilayer structures are employed to ensure high food safety, making the recycling expensive and difficult[3]. In this view, compostable materials represent a suitable solution to produce mono-materials, compostable, characterized by smart mechanical and barrier properties.

In this context, a new 100% biobased polyester was synthesized from 2,5-furandicarboxylic acid and diethylene glycol, obtaining poly(diethylene 2,5-furaoate) (PDEF). The polymer was processed in form of film and compared with poly(pentametylene 2,5-furanoate) (PPeF) and poly(butylene 2,5-furanoate) (PBF), in order to evaluate the effect of insertion of an ether-oxygen atom or methylene group substitution with an ether-oxygen atom, in the glycol sub-unit. The polyesters were deeply characterized from the molecular, thermal and mechanical point of view. Moreover, lab-scale composting experiments were carried out at 58°C. Barrier performance to oxygen and carbon dioxide were investigated at two different temperatures (23 and 38 °C). The effect of relative humidity at 23°C was also studied.

4.2 Molecular characterization

Three different solvent free polycondensations were set as reported in "Method and Materials" section in order to obtain the three polymers, reported in **Figure 4.1**. All the polyesters chosen presented a furan ring in the acid subunit, while the difference was beard in the glycolic moiety.

In case of poly(butylene 2,5-furanoate) (PBF) four methylene groups were present; poly(diethylene 2,5-furaoate) (PDEF) had the same number of methylene groups, but an oxygen atom in between. This latter was replaced by a methylene group in case of poly(pentametylene 2,5-furanoate) (PPeF).

PDEF could be considered as derived, on one side from PBF by the insertion of a central O atom in the glycol moiety and, on the other, from PPeF by the substitution of the central -CH$_2$- group with an ether oxygen.

Poly(butylene 2,5-furanoate) (PBF)   Poly(diethylene 2,5-furaoate) (PDEF)   Poly(pentametylene 2,5-furanoate) (PPeF).
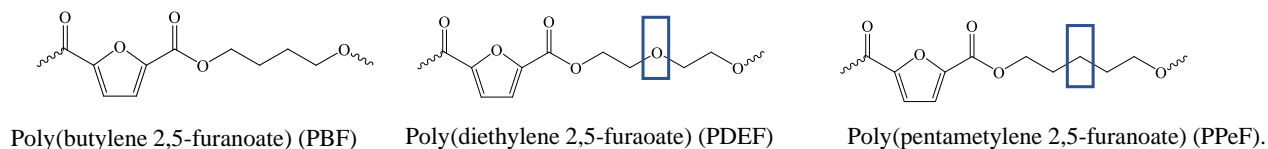
Figure 4.1: *Molecular structure of the prepared samples.*

As one can see, the expected structures were confirmed by ^{1}H NMR spectroscopy (**Figure 4.2**).
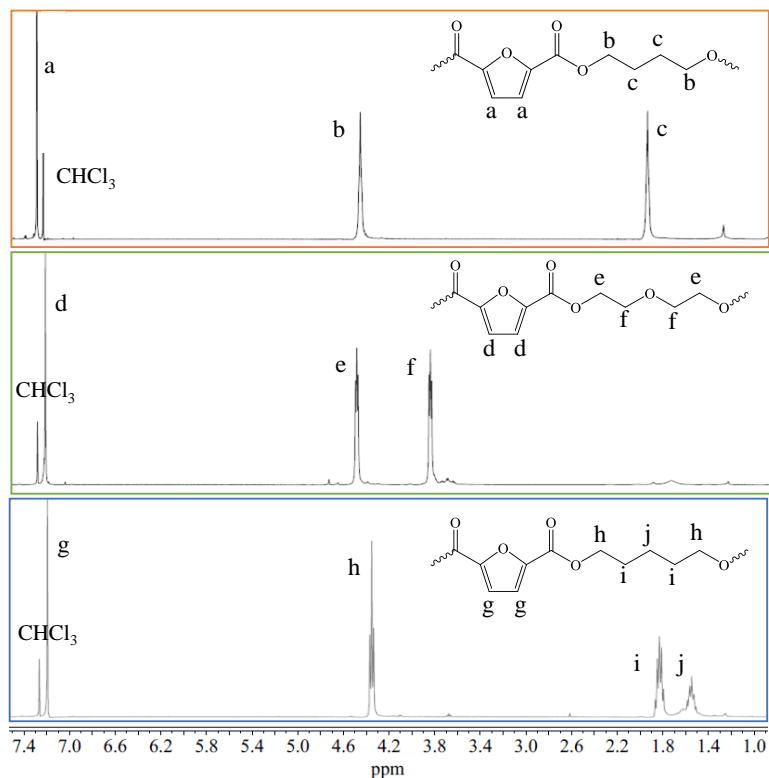
Figure 4.2*: ^{1}H-NMR spectra of PBF, PDEF, PPeF with the relative peak assignment.*

162

In details, as regards PBF, the -CH$_2$- groups of the glycolic unit were resonating at 4.5 (b) and 2.0 ppm (c), while the two protons proper of the furanic ring were located at 7.25 ppm (a). PBF and PDEF showed the same signal at 7.25 ppm (d), then the methylene groups of the diethylene subunit could be observed at 3.82 (f) and 4.45 ppm (e). PPeF, beside the furan ring signal, presented three different peaks due to the three methylene hydrogen atoms at 4.35 (h), 1.84 (i) and 1.55 ppm (j). The molecular weight was evaluated by means of GPC. The high molecular weights obtained and reported in **Table 4.1** confirmed the good control of the synthetic routes. Moreover, the polydispersity index (D) resulted close to 2 as expected for a polycondensation process.

4.3   Thermal characterization

TGA analysis showed the behaviour of the three synthetized samples during heating scan under inert atmosphere. The thermogravimetric curves were reported in **Figure 4.3** while the data were listed in **Table 4.1**. As one can see, the degradation of PBF, PDEF and PPeF was proceeding via one step mechanism with a final char residue of around 10%.
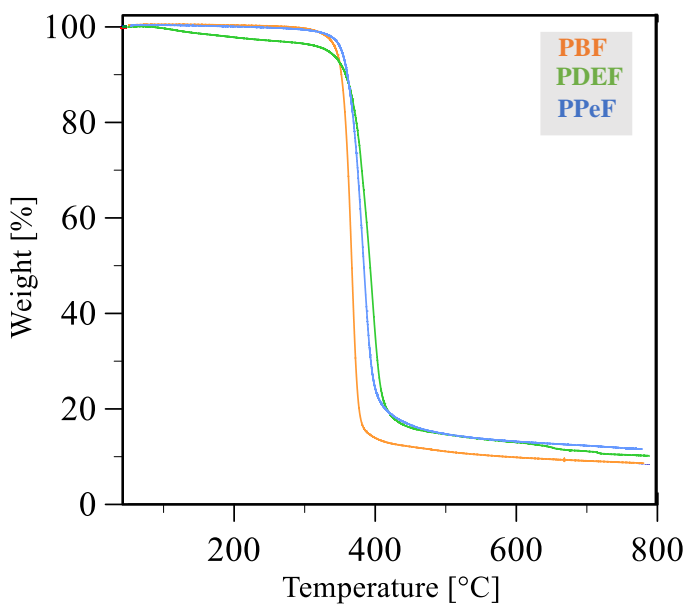
Figure 4.3*: Traces of thermogravimetric analysis conducted on PBF, PDEF and PPeF samples obtained by heating at 10°C/min under inert atmosphere (nitrogen).*

As one can see, PBF degraded faster compared with the other two samples, reaching the maximum degradation rate at 366°C. Differently, PDEF had the highest stability despite an initial weight loss of 4% located at 100°C. The presence of heteroatoms as oxygen along the glycolic subunit, in fact,

increased the tendency of the material to absorb polar molecules as water. In this view, the evaporation of H_2O molecules was likely responsible for this initial weight loss step in PDEF.

Table 4.1: Molecular and thermal characterization data of the prepared polymers.

			PBF	PDEF	PPeF
GPC		M_n [g/mol]	36100	21400	29600
TGA		T_{MAX} [°C]	366	396	390
DSC	Iˢᵗ SCAN	T_g [°C]	35	24	16
		ΔCp [J/g*°C]	0.19	0.445	0.341
		T_c [°C]	87	/	/
		ΔH_c [J/g]	17	/	/
		T_m [°C]	164	/	/
		ΔH_m [J/g]	32	/	/
	IIⁿᵈ SCAN	T_g [°C]	35	24	16
		ΔCp [J/g*°C]	0.311	0.465	0.432
		T_c [°C]	104	/	/
		ΔH_c [J/g]	28	/	/
		T_m [°C]	164	/	/
		ΔH_m [J/g]	32	/	/
WAXS		Xc [%]	12	/	/
Tensile test		σ_b [MPa]	21 ± 4	7,2 ± 0,9	6 ± 1
		ε_b [%]	157 ± 28	502 ± 100	1050 ± 200
		E [MPa]	1289 ± 127	673 ± 76	9 ± 1
WCA		Θ [°]	92 ± 2	74 ± 1	93 ± 3
Barrier properties		O_2-TR [cm^3 cm / m^2 d atm]	0.10	0.0022	0.0016
		CO_2-TR [cm^3 cm / m^2 d atm]	0.19	0.0018	0.0014

Moreover, T_{max} was reached at higher temperature compared to PBF, due to the higher stability of the C-O-C bond, presented in the diethylene moieties that was less subjected to random scission compared with C-C link, proper of PBF. Another important aspect was related to the formation of inter-chain hydrogen bonds as schematized in **Figure 4.4**. These interactions could enhance the final thermal stability of the material.

PBF   PDEF
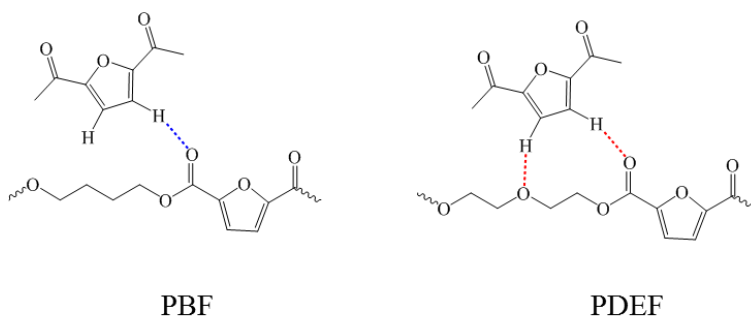
Figure 4.4: H-bonds formed among chains, in PBF and PDEF

A similar phenomenon could be observed for PPeF, that presented thermal stability slightly lower than PDEF.

The lower stability of PBF could be ascribed to its higher T_g, i.e. lower molecular mobility, with respect to PDEF and PPeF. In particular, one could hypothesize the glassy state of PBF limited the establishment of H-bonds interactions.

Calorimetric analyses were performed in order to define the thermal transition proper of the three samples subjected to compression moulding. The experimental details were reported in "Method and Materials" section, while below in **Figure 4.5** the traces were collected; the derived data were listened in **Table 4.1.**

PBF film presented a melting temperature of 164°C and a crystallization process located at 87°C; despite that, $\Delta H_m > \Delta H_c$ therefore the polyester could be considered as semicrystalline material. As confirmation of this observation, WAXS measurements evidenced a crystallinity degree of 12%, as reported in **Table 4.1**. PDEF and PPeF did not present any melting peaks, evidencing no capability of organizing their macromolecules in crystalline structure after-moulding cooling. Just a glass transition step, respectively at 24°C and 16°C, was observed; in both cases, the values recorded were lower than PBF one. PDEF and PPeF were characterized by longer glycolic subunits

(PDEF: 4 -CH_2- + 1 -O-; PPeF= 5 -CH_2-) compared with PBF, and, even if the nature of the atoms changes, the mobility of the macromolecules was favoured moving T_g towards lower temperature. In this context, also the just mentioned semicrystalline nature of PBF was playing an important role; the crystalline phase was acting as knot for the macromolecules, hampering the movement of the amorphous phase and increasing the glass transition temperature as actually happen for PBF (T_g = 35°C).

Due to their common fully amorphous nature, PDEF could be compared with PPeF in terms of glass transition. As one can see, $T_{g,PDEF} > T_{g,PPeF}$, the difference probably was due to the presence of heteroatoms in the glycolic unit of PDEF. Indeed, despite the comparable length, the highly electronegative oxygen of the glycolic portion of PDEF promoted inter-chain interactions (hydrogen bonds as well as Van der Walls interactions). In this way, the motion of the chains was hampered (i.e. glass transition temperature increases).
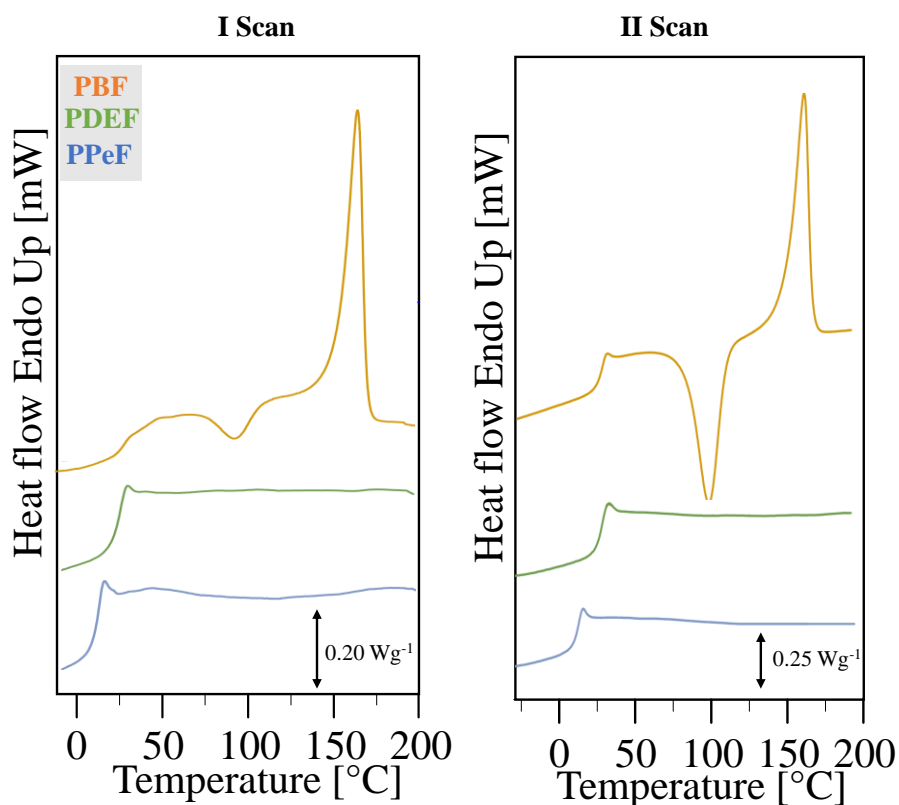
Figure 4.5: *Calorimetric traces obtained by DSC analysis (I and I scans) on PBF, PDEF, PPeF in form of films.*

The three molten samples were subjected to fast cooling in the DSC and analysed in a second heating measurement. As expected, PDEF and PPeF resulted completely amorphous. As concern

PBF, a major polymer fraction could be locked in the amorphous phase thanks to the high cooling rate, nevertheless once T_g was exceeded, it was able to fold in an ordered structure at 104 °C $(\Delta H_c = 28 \text{ J/g})$ then melted at higher temperature $(T_m = 164°C; \Delta H_m = 28 \text{ J/g})$.

4.4 Mechanical characterization

Stress-strain measurements were conducted on the three filmed materials, adequately shaped. The obtained curves were reported in **Figure 4.6,** while the related data were in **Table 4.1**. In details, PBF confirmed its semicrystalline state that, together with the T_g above room temperature, led to high elastic modulus and stress at break, and quite low deformation at break. Differently, thanks to its amorphous nature and a T_g below room temperature, PPeF showed an elastic modulus reduced by two orders of magnitude together with an outstanding elongation at break (more than 1000 %). Moreover, as previously reported[4], PPeF was able to recover its initial shape thanks to a supramolecular 2D structure springing from interchain hydrogen bonds established in the matrix[5]. PDEF had a mechanical behavior intermediate between a semicrystalline material, as PBF, and a fully amorphous polymer, as PPeF. In particular, the lack of crystallites produced a reduction of E and σ_b, nevertheless the decrement was contained by the interactions among different chains, thanks to the oxygen atom of the glycolic subunit, which helped keeping the elastic modulus and the strain at break quite high. At the same time, the higher chain mobility of PDEF with respect to PBF (lower T_g), coming from the introduction of O atom, allowed reaching a 500% ε_b.
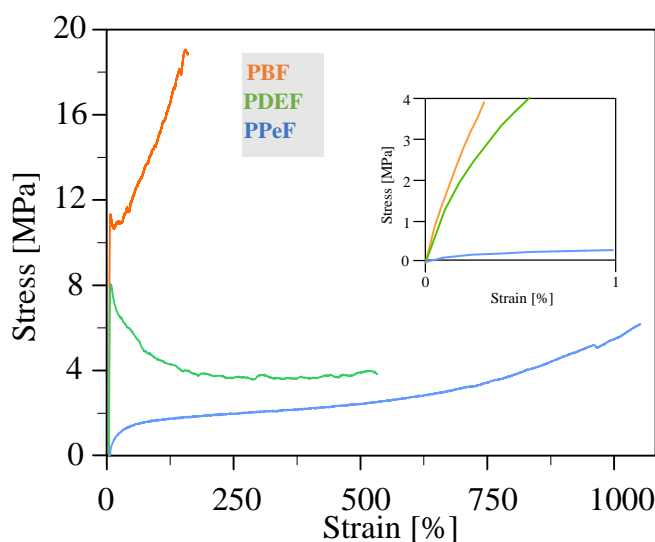
Figure 4.6*: Stress/strain measurements conducted on PBF, PDEF and PPeF films.*

4.5 Water contact angle

In order to evaluate the hydrophilicity character of these materials, the interaction between film and water was investigated through water contact angle measurements.
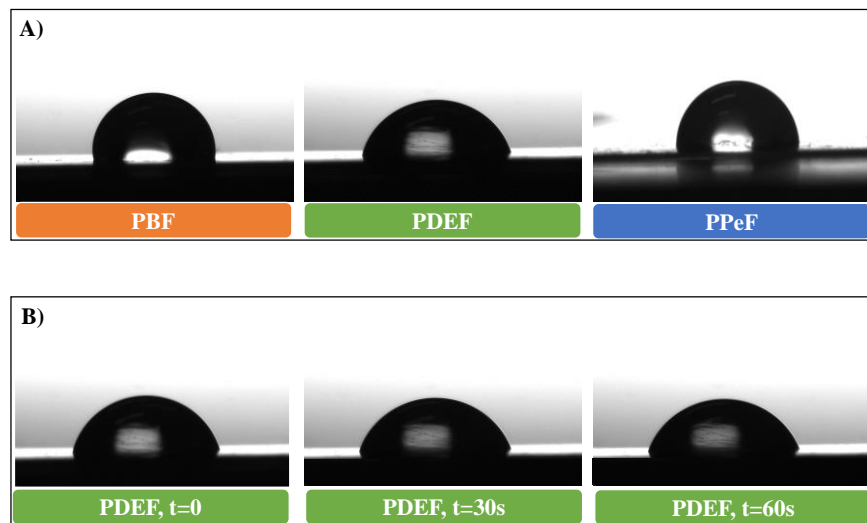
Figure 4.7: A) Images of water drops deposited on PBF, PDEF and PPeF films; B) water drop on PDEF 0, 30 and 60 s after deposition.

As it was clearly visible from **Figure 4.7 A**, PDEF resulted more hydrophilic than PBF, being the PDEF WCA value 18° lower, due to the introduction of ether-oxygen in the repeating unit that increased the final polarity of the material. The high compatibility with water was in line with the TGA results obtained for PDEF, in particular, with the initial weight loss during thermogravimetric analysis, due to the release of the humidity absorbed from the environment. Changing the oxygen atom of the glycolic subunit with a non-polar -CH_2- group, made the resulting material, PPeF, more hydrophobic with a WCA value similar to PBF, despite the higher length of aliphatic portion (4 -CH_2- for PBF *vs* 5 -CH_2- for PPeF).

In **Figure 4.7 B**, the profile changing of the drop located on PDEF as a function of time was reported. A clear difference in contact angle could be observed just after 30 s from the release of the water drop. Opposite behaviour was observed for PPeF and PBF, for which no evolution of the drop shape with time was detected.

4.6 Composting test

In order to evaluate the end-of-life process of PBF, PDEF and PPeF, composting tests were conducted. For each sample, square shaped films were incubated in adequately prepared compost and maintained under controlled atmosphere (58°C, 90% relative humidity); then, several withdrawals were operated at different times. More experimental details were reported in "Method and Materials" section. As regards PBF, after 62 days in compost, no changes on the film surface nor in the gravimetric weight were observed.
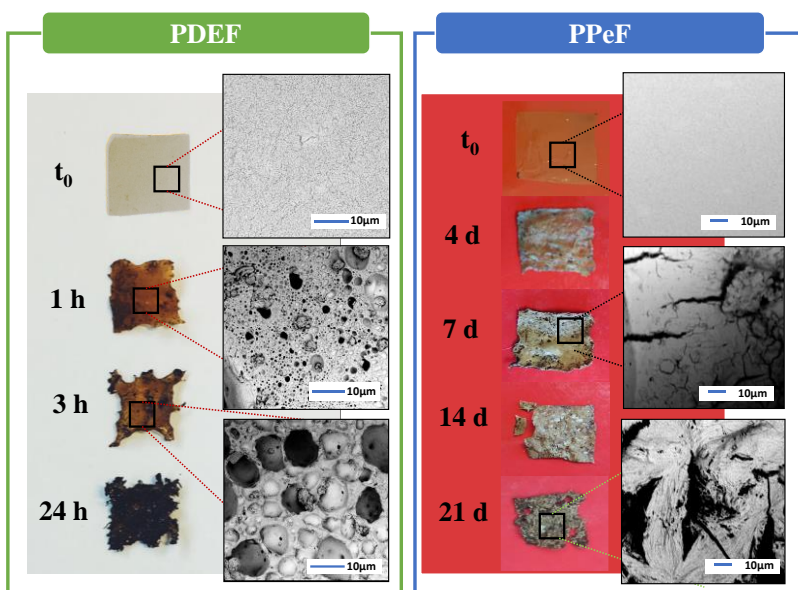
Figure 4.8: Images collected at different times of composting tests: macroscopic view (on the left) with SEM images (on the right).

A deeply different behaviour was observed for PDEF, that underwent degradation as soon as incubated (**Figure 4.8**). Indeed, just after 1 hour the film changed in colour and dimension; from the microscopic point of view, holes and cracks were clearly observed with SEM. In particular, the holes increased in dimension with the time of incubation, and after just 3 hours the surface was almost completely covered of holes. After 24 hours of incubation, the film was wholly incorporated in compost. The high tendency to degrade directly came from the high hydrophilicity of PDEF given by the oxygen atoms inserted in the glycolic subunit but also from the rubbery state of the polymer under the experimental conditions, both these features favouring the water molecules diffusion and hydrolytic attack. It is worth noting that PDEF film did not undergo solubilization, as confirmed by additional experiments carried out in neat water that evidenced no

changes in PDEF film both at micro- and macroscopic level even after months. As concerns PPeF, its degradation proceeded very fast as well, but at lower extent compared with PDEF. Even if also in this case $T_{incubation} > T_g$, PPeF degradation was slowed down likely because of its lower hydrophilicity. Anyway, after 4 days macroscopical changing on the film surface could be seen and, after 7 days, cracks and holes could be observed microscopically via SEM analysis; in 21 days the film was deeply compromised by degradation process both at micro- and macroscopical level (**Figure 4.8**). Given the compost contamination of the incubated PDEF and PPEF films, it was not possible to perform weight loss measurements.

4.7 Barrier properties

As well known, barrier properties were deeply influenced by several factors that can have different impact on the final performances. As a general trend, elements that increased free volume among chains worsened barrier properties. A pertinent example was the flexibility of the macromolecules, correlated to T_g; the lower the glass transition temperature the higher were the unoccupied spaces between chains, rising the gas transmission rate, GTR, of the material. Differently, the presence of ordered phases in the polymer matrix hampered the passage of gases through the film. In this view, PBF, PDEF and PPeF was analysed.

The permeability performances to two different gases, O_2 and CO_2, were evaluated on compression moulded films. In **Figure 4.9** the results, expressed as gas transmission rate (GTR), were reported. The experiments was conducted sequentially, one after the other, as follows:

1: temperature of 23°C, relative humidity (RH) of 0%

2: temperature of 23°C, RH 85%

3: temperature of 23°C, RH 0

From the first test conducted at 23°C with 0% RH, it was clear that PBF presented the highest values of GTR among the series, despite its higher glass transition temperature and semicrystalline nature. Differently, PDEF and PPeF, even though amorphous and with T_g values around the temperature of measuring, resulted very outstanding. An explanation could be found, as mentioned before, in the presence of particular macromolecular arrangement that blocked the passage of gases through the materials. In the case of PPeF, as previously reported[4], 2D-ordered domains developed during compression moulding with consequent improvement of gas barrier performances. This

peculiar microstructure originated from inter-chain hydrogen bonds, also present, and to a greater extent, in the PDEF. The presence of ether-oxygen atom in PDEF repeating unit enhanced the number of H-bonds favouring the inter-molecular forces, these last leading to a compact array that hampered the gas molecules passage, but, at the same time, their high number limited the formation of an ordered structure as for PPeF.

Afterwards, the three films were subjected to permeability tests at 85% RH, keeping the temperature constant at 23°C. In case of PDEF and PBF, an improvement of barrier performance was observed. The result was quite surprising considering the usually observed plasticizing effect of water, which, enhancing the chain mobility, determined an increment of the free volume. On the other side, the same plasticizing effect detected for PPeF, caused a slight increase of GTR values under humid conditions. To explain the behaviour of PDEF and PBF films, it was supposed that water enhanced the inter-chain interactions occupying the empty sites at the oxygen atoms of the furan ring and, in case of PDEF, also at the oxygen of the glycolic subunit. Hence, a more compact and dense new structure was formed, responsible of the decreasing of the GTR values. In case of PPeF, also containing furan O atoms, the longer glycolic part compared to PBF, decreased the density of furan ring per unit length. In this case, the plasticising effect of water prevailed on that due to the more compact microstrucure due to hydrogen bonds. In PDEF, characterized by repeating unit length comparable to PPeF, the presence of the oxygen instead of methylene group explained the different behaviour in wet environment between the two polymers.

In the third experiment, the films were firstly subjected to vacuum in order to remove the moisture residues and then, a new test was performed at 23°C and 0% RH. PBF and PDEF maintained the same good performances reached under humid conditions: probably the vacuum applied was not affecting the new hydrogen bonds formed among water and furan/ether oxygen; for PPeF, it could be hypothesized the free molecules of water trapped inside the material and acting as plasticizer, were removed by vacuum, while those forming H-bonds with the furan ring remained inside the material making GTR values decreased.

Another aspect to consider was the different perm-selectivity ratio exhibited by the three samples, which was an indication of the barrier performance towards the two different gases. It should be remembered that oxygen was a small and apolar molecule characterized by a lower diffusion rate than the larger carbon dioxide containing polar C-O covalent bonds. Consequently, usually the

171

perm-selectively ratio, defined as ratio between GTR_{CO_2}/GTR_{O_2} was higher than 1. More in detail, two factors have to be taken into consideration: solubility and diffusivity of the two gas molecules. Specifically, the higher the affinity with polymer, the higher the solubility and the residence time of gas inside the film (GTR lowering); differently, as regards diffusivity, the gas molecular size played the key role: the larger the molecule, the higher the diffusion rate (molecular diameter of $CO_2 = 3.4$ Å, molecular diameter of $O_2 = 2.9$ Å[6]). Since, as mentioned above, in polyesters, usually, $GTR_{CO2} > GTR_{O2}$, this means the molecular size contribution prevailed over the interactions with the materials; carbon dioxide passed through the films easily thanks to its higher diameter compared with O_2. In the furan-based polyesters, a peculiar behaviour with particularly low GTR values for CO_2 had been documented[4,7–9]. This evidence was ascribed to the presence of permanent dipoles in CO_2 interacting with the polar groups of polymer matrix (furan ring as well as ester groups) thus increasing CO_2 solubility. The final result was a GTR_{CO_2}/GTR_{O_2} ratio close to 1.

Considering the three-step experiment reported in **Figure 4.9**, a different effect of humidity conditions on perm-selectivity ratio could be found for PBF, PDEF and PPeF films.
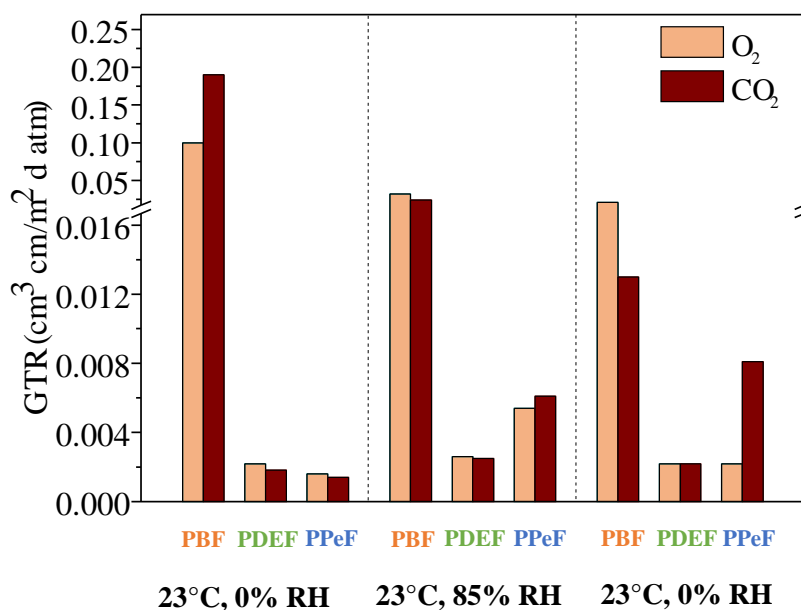
Figure 4.9*: Gas transmission rates (GTR) for three subsequent experiments conducted at 23°C in different conditions of humidity.*

As concerns PBF, in the first test conducted, the driving force was the dimension of the molecules. Operating at 85% RH, new polar interactions between water molecules and polymer matrix formed, favouring CO_2 solubility. The effect kept constant even returning to dry environment.

In case of PDEF, its higher polarity due to the O atom insertion in the PBF backbone, helped to maintain the GTR_{CO_2}/GTR_{O_2} ratio always closed to 1. As regards PPeF, the trend observed was different: humidity determined an increment of perm-selectivity ratio, which further increased after removing free water molecules by vacuum. This trend could be explained considering H_2O first acted as plasticizer enhancing polymer chain mobility and then left vacancies after vacuum was applied. Both these effects increased the free volume favouring the passage of CO_2 molecules that, in turn, were less soluble in PPeF than in PBF and mainly in PDEF films.

PDEF and PPeF were also tested at 38°C to simulate hot weather conditions. As one can see from **Figure 4.10**, despite at this higher temperature macromolecular chains of both polymers were in a complete mobile state, barrier properties did not change. This experiment confirmed, one more time, the presence of supramolecular structures originated from hydrogen bonds among the chains. As evident, these compact structures were not affected by the increasing of temperature and consequently the polymers maintain their performances. Differently, the increase of temperature in case of common polyesters led to higher free volume among the macromolecules favouring gas permeation.
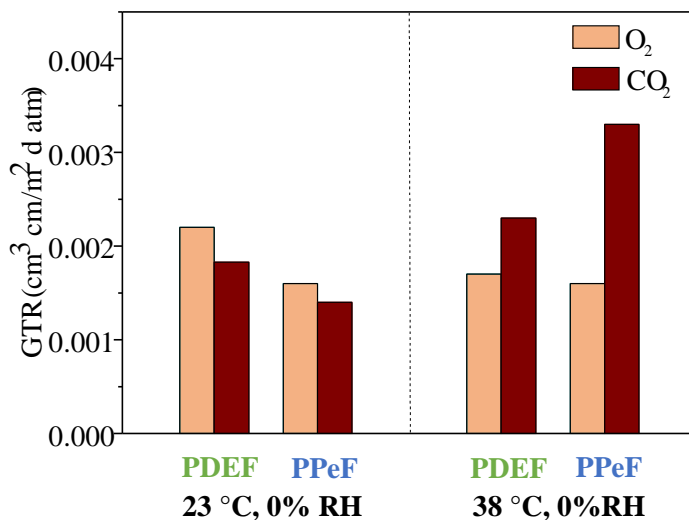
Figure 4.10: *Gas transmission rates (GTR) to O_2 and CO_2 for PDEF and PPeF at 23 and 38°C.*

Anyway, a clear increase of CO_2 gas transmission rate was detected with increasing temperature. As already mentioned, the gas passage depended on both solubility and diffusivity. As well known, this latter generally rose with temperature, the effect being more intense for the gas molecules

characterized by the most chaotic motions, such as the large CO_2 molecules. As a matter of fact, in both cases, the performances to O_2 at 23°C and 38°C were constant, while GTR_{CO_2} values increase.

In **Figure 4.11**, a comparison of the analysed materials, PBF PDEF and PPeF, with other furan-based polyesters was reported. As one can see, PDEF and PPeF had GTR values much lower than the other materials.
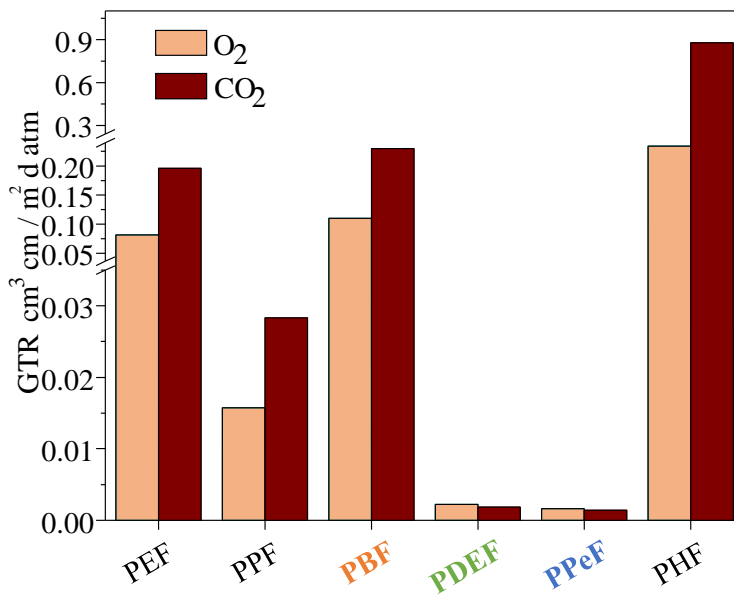
Figure 4.11: GTR value of CO_2 and O_2 tested on different furan based polyesters (PEF[7], PPF[9],PHF[4]).

In addition, an odd/even effect could be observed: the materials with odd number of -CH_2- groups resulted more performant compared to the even numbered -CH_2- containing ones. Conversely from what usually happened for traditional polymers, PPeF and PDEF presented a GTR values lower than PPF, despite their lower T_g ($T_{g,PPeF}$ = 16°C; $T_{g,PDEF}$ = 24°C; $T_{g,PPF}$ = 52°C). As previously reported, the deviating behaviour of PPeF and PDEF could be attributed to the supramolecular compact phase coming from the H-bond formation, this last being favoured in rubbery amorphous furan-polyesters, as PPeF and PDEF.

As regard the materials containing an even number of -CH_2- groups, PEF, PBF and PHF, they had comparable performances.

Our previous studies reported the presence of mesophase also in PHF[8], but differently from what happened for PPeF, this 2D ordered phase looked like worsening the barrier performances, indeed $GTR_{PBF}<GTR_{PHF}$. This effect was explained with the concomitant presence in PHF not only of 2D

ordered domains and the amorphous zone but also of a 3D crystalline phase. As a consequence, higher density of disclinations, channels through which gas molecules could more easily diffuse, were formed and the barrier values of PHF exceeded the GTR values of PBF. Another factor to take into account was the lower free volume fraction in PBF compared with PHF ($T_{g,PHF} > T_{g,PBF}$).

4.8 Conclusions

Three 100% biobased homopolyesters, PBF, PDEF and PPeF, obtained from the reaction of 2,5-furandicarboxylic acid with different glycols, was successfully synthesized by two step solvent-free polycondensation process. PDEF could be considered as derived, on one side from PBF by the insertion of an O atom in the centre of glycol moiety and, on the other, from PPeF by the substitution of the central -CH_2- group with an ether oxygen. A complete and deep analysis was conducted, investigating the effect of chemical modification on the structural as well as functional characteristics. Molecular characterization confirmed the chemical structures of the three samples revealing high molecular weights; moreover, PDEF and PPeF showed better thermal stability compared with PBF. The three materials were filmed via compression moulding and the thermal transition, investigated with DSC measurements, showed a semicrystalline behaviour for PBF and a complete amorphous state for PDEF and PPeF. As concern mechanical characterization, the different polymer chemical structure for the three samples brought distinct response, proving that this characteristic is an efficient tool to tune the final properties of the materials in accordance with the final application envisioned. Composting tests indicated a different behaviour of PBF respect the other two samples: indeed both PDEF and PPeF were easily degraded in compost. Then, precise studies were conducted on barrier properties. The filmed materials were tested in different condition of temperature, humidity, employing CO_2 and O_2. The results had shown the chemical structures of PDEF and PPeF allowed particular supramolecular organization that strongly impacts on the final properties. Summarizing, PPeF and PDEF showed really good barrier performances, that, together with the high rate of degradation, candidate the two samples to become a real alternative to the traditional materials for flexible packaging application.

4.9 Bibliography

1. Association of Plastics manifacturors. Plastics -The facts 2018. *Plast. Eur.* 1–57 (2018). doi:10.1016/j.marpolbul.2013.01.015

2. Kale, G., Kijchavengkul, T., Auras, R., Rubino, M., Selke, S. E., Singh, S. P. Compostability of bioplastic packaging materials: An overview. *Macromol. Biosci.* **7**, 255–277 (2007).

3. Morris, B. A. *The Science and Technology of Flexible Packaging. Multilayer Films from Resin and Process to End Use;* (Elsevier, 2016).

4. Guidotti, G., Soccio, M., García-Gutiérrez, M. C., Ezquerra, T., Siracusa, V., Gutiérrez-Fernández, E., Lotti, N. Fully Biobased Superpolymers of 2,5-Furandicarboxylic Acid with Different Functional Properties: From Rigid to Flexible, High Performant Packaging Materials. *ACS Sustain. Chem. Eng.* **8**, 9558–9568 (2020).

5. Guidotti, G., Soccio, M., García-Gutiérrez, M. C., Gutiérrez-Fernández, E., Ezquerra, T. A., Siracusa, V., Lotti, N.. Evidence of a 2D-Ordered Structure in Biobased Poly(pentamethylene furanoate) Responsible for Its Outstanding Barrier and Mechanical Properties. *ACS Sustain. Chem. Eng.* **7**, 17863–17871 (2019).

6. Schawe, J. E. K. Mobile amorphous, rigid amorphous and crystalline fractions in isotactic polypropylene during fast cooling. *J. Therm. Anal. Calorim.* **127**, 931–937 (2017).

7. Burgess, S. K., Kriegel, R. M., Koros, W. J. Carbon dioxide sorption and transport in amorphous poly(ethylene furanoate). *Macromolecules* **48**, 2184–2193 (2015).

8. Guidotti, G., Genovese, L., Soccio, M., Gigli, M., Munari, A., Siracusa, V., Lotti, N.Block copolyesters containing 2,5-furan and trans-1,4-cyclohexane subunits with outstanding gas barrier properties. *Int. J. Mol. Sci.* **20**, 1–15 (2019).

9. Guidotti, G., Soccio, M., Lotti, N., Gazzano, M., Siracusa, V., Munari, A. Poly(propylene 2,5-thiophenedicarboxylate) vs. Poly(propylene 2,5-furandicarboxylate): Two examples of high gas barrier bio-based polyesters. *Polymers (Basel).* **10**, (2018).

5 INVESTIGATION OF ENTHALPY RELAXATION, CRYSTAL NUCLEATION AND GROWTH OF A PROMISING BIOPLASTIC, POLY(BUTYLENE ISOPHTHALATE)

5.1 Introduction

In Europe during 2018, 64 Mt of plastics have been entered in the market. Most of them were synthetized employing no renewable sources[1]. Packaging sector is, in terms of volumes produced and short life of most the devices, one of the most environment impacting field. The low density of these materials favors the dispersion in the marine as well as terrestrial environment, causing pollution problems. In order to reduce the environmental impact and the exploitation of finite fossil resources, new bio-based plastics have been proposed. Promising results have been obtained with polymers derived from isophthalic acid (IPA), synthetized directly via fermentation of biomasses or cycloaddition of bio-isoprene units and bio-acrylic acid[2–4]. IPA can be polymerized in presence of 1,4-butanediol via two step polycondensation process[5–7], obtaining a completely bio-based homopolymer, poly(butylene isophthalate) (PBI). As described in Paragraph 2.2.2.3 Chapter I, this polyester has T_g around room temperature[8,9] and shows good mechanical properties, together with easy melt-processability[10]. Nevertheless, its crystallization rate is too slow in view of its commercial production and application. In this context, the present work had the aim to investigate crystallization rate and lamellar crystals formation for PBI. Then, more specific studies were conducted on crystal nuclei at high supercooling from the melt and in glassy state, as alternatives to the traditional method utilizing heterogeneous nucleators[11,12]. Lastly, glass relaxation and crystal nucleation at temperatures slightly below T_g were investigated.

5.2 Synthesis and molecular characterization

The solvent free two step polycondensation synthesis of PBI homopolymer was described in detail in Paragraph 2.2.1.1, Chapter II. The so-obtained polymer was studied by mean ^{1}H-NMR, confirming the expected chemical structure. As one can see from **Figure 5.1** the spectrum recorded was not presenting unexpected signals, consequently, the method of synthesis could be considered well set.

At a 4.43 and 1.95 ppm, one could find the signals referred to the methylene protons of the glycolic subunit, *d* and *e*, respectively. The remaining signals were ascribed to the aromatic protons of the

isophthalic ring: at 8.68 ppm the hydrogen located between the two carbonyl group was observed (*a*); at 8.22 ppm proton *b* was located and at 7.52 ppm the last aromatic hydrogen *c* was recognized.
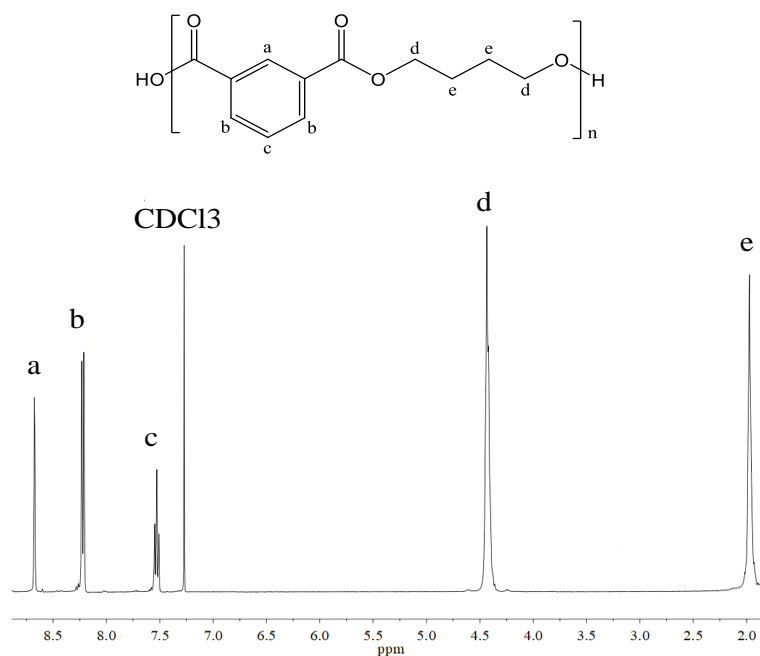
Figure 5.1: ^{1}H-NMR spectrum of PBI with the relative peak assignment.

Gel permeation chromatography was conducted to evaluate the molecular weight and the polydisperisty of the polyester. The results showed a high-weight polymer, with an M_n of 33150 Da and D equal to 2.0 as expected for a polycondensation product.

5.3 Spherulite and gross crystallization rates of PBI

Figure 5.2 A reported the characteristic times of crystallization in PBI as a function of temperature, obtained employing FSC and DSC analysis. In details, FSC points (blue squares) were obtained stopping the isothermal crystallization after predefined crystallization times. Then, a heating scan was performed to analyze the enthalpy of melting. This latter value was plotted as a function of crystallization time (up to 10,000 s) then the halftime of crystallization was extrapolated. As concern DSC data (red circles), they were obtained studying the crystallization peak-times, which, resulted close to the FSC crystallization halftimes. The so-obtained data revealed the maximum rate of crystallization at 85–90°C, with crystallization halftime around 3000 s. Some researches regarding temperature dependency of the crystallization rate, reported different values of the temperature of maximum crystallization rate as 60°C[13], 85°C[14], 100°C[15] and with a related

178

minimum crystallization halftimes of around 12,000 s, 210 s and 456 s, respectively. These values could be attributed to the different polymer molecular weight, due to various synthetic routes.
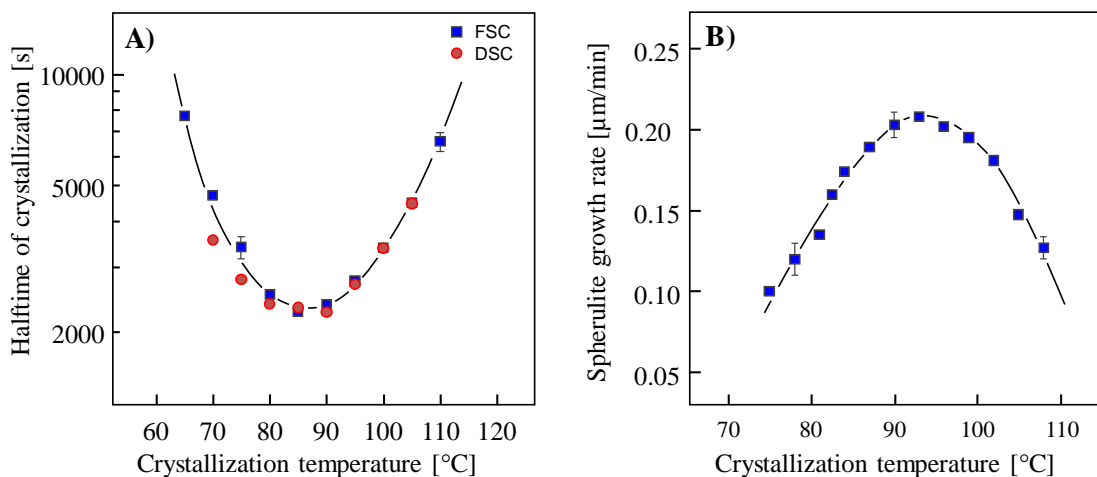
Figure 5.2: Characteristic times of crystallization as a function of crystallization temperature A) evaluated with FSC and DSC measurements; B) spherulitic grow rate.

The spherulitic growth rate of PBI as a function of temperature, was reported in **Figure 5.2 B.** As one could see, a maximum rate of around 200 nm/min was reached at 95°C, suggesting that the low total crystallization rate of PBI could be due not only to low nucleation rate but also to the slow secondary crystallization.

5.4 Analysis of crystal nucleation using Tammann's two-stage crystal nuclei development method

5.4.1 Optical microscopy measurements

Semi-quantitative analysis was used to study the crystal nuclei formation of PBI. In **Figure 5.3** the temperature-time profile adopted for the tests was reported. The method involved a ballistic quenching of the equilibrated melt to a temperature between 22 and 50°C; afterwards, the sample was subjected to annealing up for 200 min (light blue segment), in order to favor nucleation. Then, the development-stage temperature of 100°C (orange segment), to allow the growing of the nuclei formed, was reached by heating. After 20 minutes, a rapid cooling was applied in order to freeze the system and POM images were recorded. These last were reported in **Figure 5.3 A,** as a function of nucleation time and temperature. As one can see, the increasing of the annealing time and temperature, until 50 min and 50°C, respectively, favored the formation of spherulites/crystal

nuclei. In case of PCL, PLLA, or PA, this phenomenon was interpreted considering the homogeneous crystal nucleation rate was reaching a maximum slightly above T_{g}. As a matter of fact, in case of PBI, 50°C was just above the glass transition.

The analysis conducted was possible thanks the slow crystallizing nature of PBI; similar results were obtained with PET[16] and PLLA[17]. Differently, with fast crystallizing polymers, the nuclei density would be too high to permit the growth of spherulite, leading to nodular domains analyzable just with higher resolution microscopic techniques[18–20].
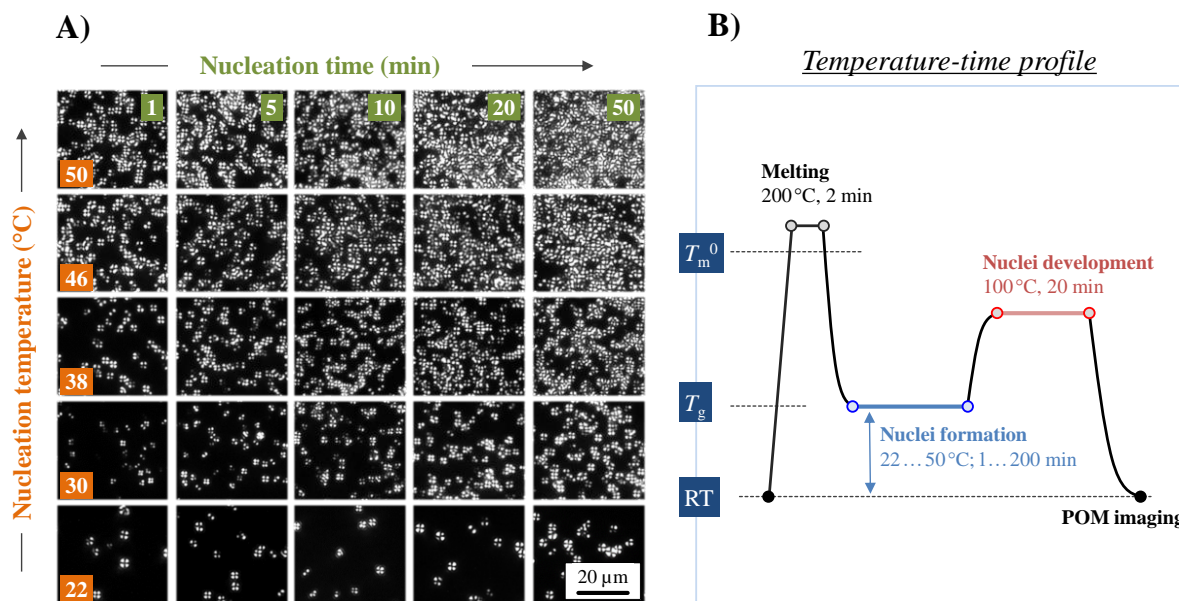
Figure 5.3: A) *POM images reported during Tammann's two-stage crystal nuclei development method as temperature-time profile;* **B)** *Tammann's two-stage crystal nuclei development method experimental profile.*

5.4.2 Calorimetry

Calorimetric analyses were employed to evaluate the relation between temperature and nucleation kinetics. A set of FSC curves, heat-flow rate as a function of temperature, reported (**Figure 5.4 A**) the results obtained after the application of Tammann's nuclei development method on PBI samples. In the specific case reported, 45°C was selected as nucleation temperature and the nucleation time was varied between 1s (light blue curve) and 10,000 s (orange curve). Then, the sample was heated (1000 K/s) reaching the growth-stage at 85°C, where the growing of nuclei was allowed for 1000 s. Subsequent heating permitted to detect the as-formed crystals analyzing the resulting enthalpy of melting. **Figure 5.4 A** showed an endothermic peak at 125°C, whose area

was proportional to the number of nuclei formed and reflecting the fraction of crystals obtained during the Tammann's experiment. These nuclei were forming during different moments as initial cooling of the melt, nucleation stage, and during heating of the sample from nucleation stage to the growth stage, and also during isothermal growth step. To overcome this problem, during the experiments all the parameters were kept constant, except the annealing time. As a consequence, the changing of enthalpy could be attributed just to this parameter. Melting enthalpy as a function of annealing time was reported in the inset in **Figure 5.4 B**, where the non-zero ground state was representing the nuclei not formed during the annealing. These nuclei were observed also in the non-annealed sample.

Annealing experiments were conducted at temperatures in the range between 25 and 55°C. At 25°C, the nucleation process was too slow to be detected with 10,000 s of analysis; while, at 55°C, the growth of spherulites was not observed yet in the nucleation stage, as one can see also in **Figure 5.2**. The onset time of nuclei formation, reported in **Figure 5.4 B**, reached a maximum at 50-55°C. Moreover, the maximum rate of nucleation was detected at $T_g + 25$ K.
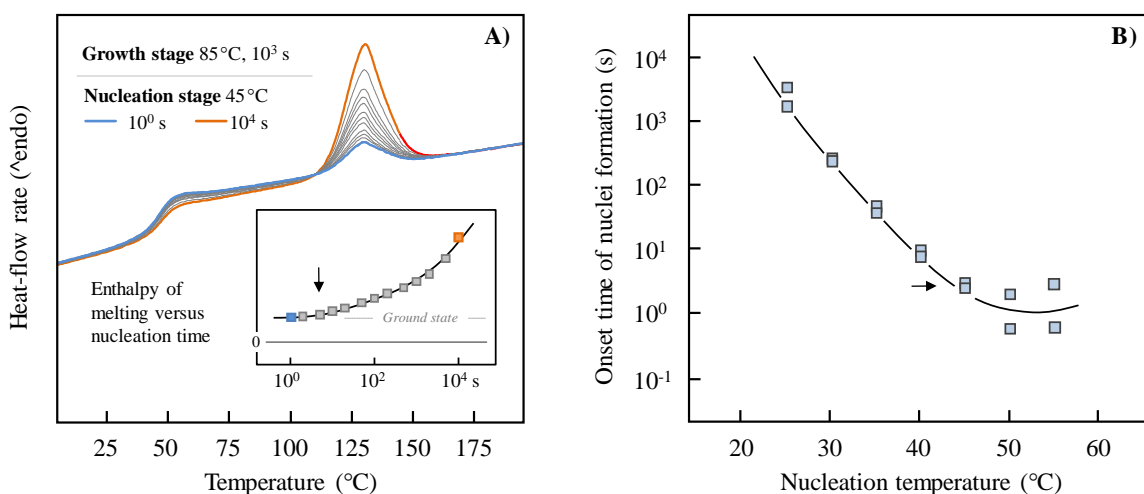
Figure 5.4*: **A)** heat-flow rate as a function of temperature obtained by FSC on PBI, collected after Tammann's nuclei development method. The temperature of nucleation was 45°C and the nucleation time was ranging between 1 s (light blue line) and 10,000 s (orange line). The growth-stage was performed at 85°C for 1000 s, respectively. **B)** onset time of nuclei formation is reported as a function of nucleation temperature.*

181

5.5 Semicrystalline morphology after melt- and cold-crystallization

The semicrystalline nature of PBI could be easily tailored varying the nucleation pathway. In **Figure 5.5**, the morphology of the structures developed by melt- and cold-crystallization at 100°C was reported. The images were collected via POM and showed the spherulitic superstructures obtained by direct melt-crystallization (**A1** image), or by cold-crystallization (**A2** image). From the experimental point of view, the sample subjected to melt-crystallization was obtained quenching the equilibrium melt to 100°C, at which an isothermal stage, in order to allow crystallization, was conducted; in case of cold-crystallization, PBI was kept at 22°C for more than 12 hours and then crystallization was allowed at 100°C. In this latter case, the superstructures obtained were much finer, with a spherulite size in the order of magnitude of 2 µm. On the contrary, the spherulites obtained after melt-crystallization, were around 10 µm. This evident difference directly impacted on the characteristic of the final material, such as mechanical properties[21–23].
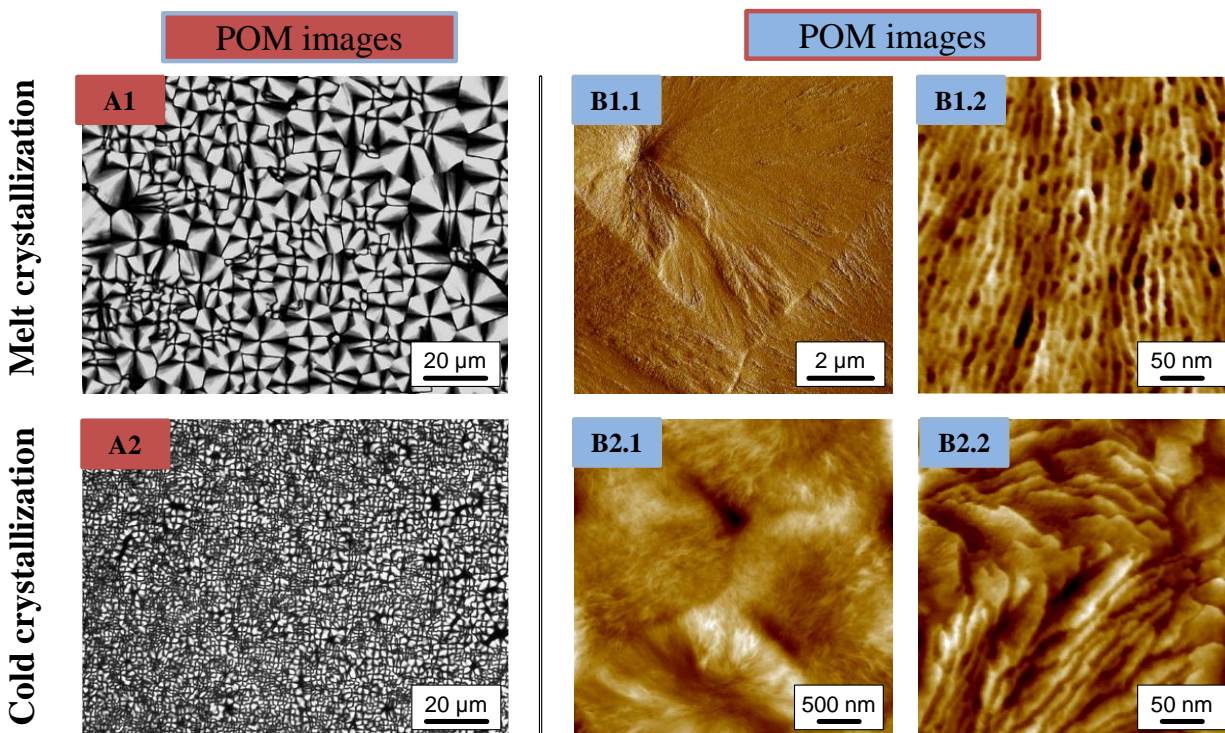
Figure 5.5: *Images collected with POM of PBI (left); **A1)** was obtained directly by cooling the melt; **A2)** the sample was prepared via cold crystallization. AFM images (right) of PBI, crystallized from the melt **B1.1/B1.2)** and via cold crystallization **B2.1/B2.2)**.*

The specimens previously analyzed by POM, were investigated also by means of AFM. Two representative images obtained were reported in **Figure 5.5 B**. The different sizes of the spherulites

were here confirmed. **Figure 5.5 B1.1)** was recorded on cold-crystallized PBI, showing a spherulite with a radius of about 6 µm. In **Figure 5.5 B1.2)**, four spherulites with a radius of about 1 µm were detected. Beside this difference, the lamellar structure of the spherulite was common in both cases, melt- and cold-crystallization. In detail, they were oriented parallel to the spherulite radius presenting a 10 nm lamellar thickness.

5.6 Kinetics of enthalpy relaxation

PBI was cooled down from 180°C at 1000 K/s by FSC, in order to get a fully amorphous sample, that was subsequently annealed at different temperatures (between -20°C and 25°C) for different times (0.001 s to 10,000 s). Then, the sample was heated up at 1000 K/s, and the so-obtained calorimetric trace was reported in **Figure 5.6 A**. Samples annealed for the minimum time (0.001 s) showed heat-capacity step at about 42°C. Due to the short time spent in the glassy state, the enthalpy recovery-peak detected was really low.

In the further experiments the annealing time was increased, and the relaxation of the glass could occur, as a consequence the enthalpy-recovery peak was increasing. Evaluating the annealing time as a function of the area of the enthalpy-recovery peak, quantitative analysis of the relaxation kinetics could be carried out. **Figure 5.6 B** collected experimental data obtained between 15 and 27.5°C, while **Figure 5.6 C** contained data of annealing experiments conducted in the range between -20 to 15°C. The relaxation-enthalpy was derived integrating all the set of curves obtained in a range of temperature, subtracting the value of enthalpy of the sample annealed for 0.001 s.

Considering the experimental results obtained in the range slightly below T_g region, between 20 and 27.5 °C, the relaxation process was completed in 10,000 s as suggested by the constant value of relaxation enthalpy. As expected, the time needed to reach the metastable structure/enthalpy-value increased by decreasing the annealing temperature. At the same time, the maximum relaxation strength, defined as the maximum enthalpy change[24] increased, as well.

For temperature below 20°C, the time necessary to reach a stationary structural state was higher than 10,000 s and further decreasing of temperature below 15°C, as reported in **Figure 5.6 B**, made the relaxation slowing down. For example, at 15°C the relaxation started after 0.05 s while at -20°C, the process started after 1 s; moreover the collected data showed, together with a decreasing of the annealing temperature, a marked decrease of the slope of the curves.
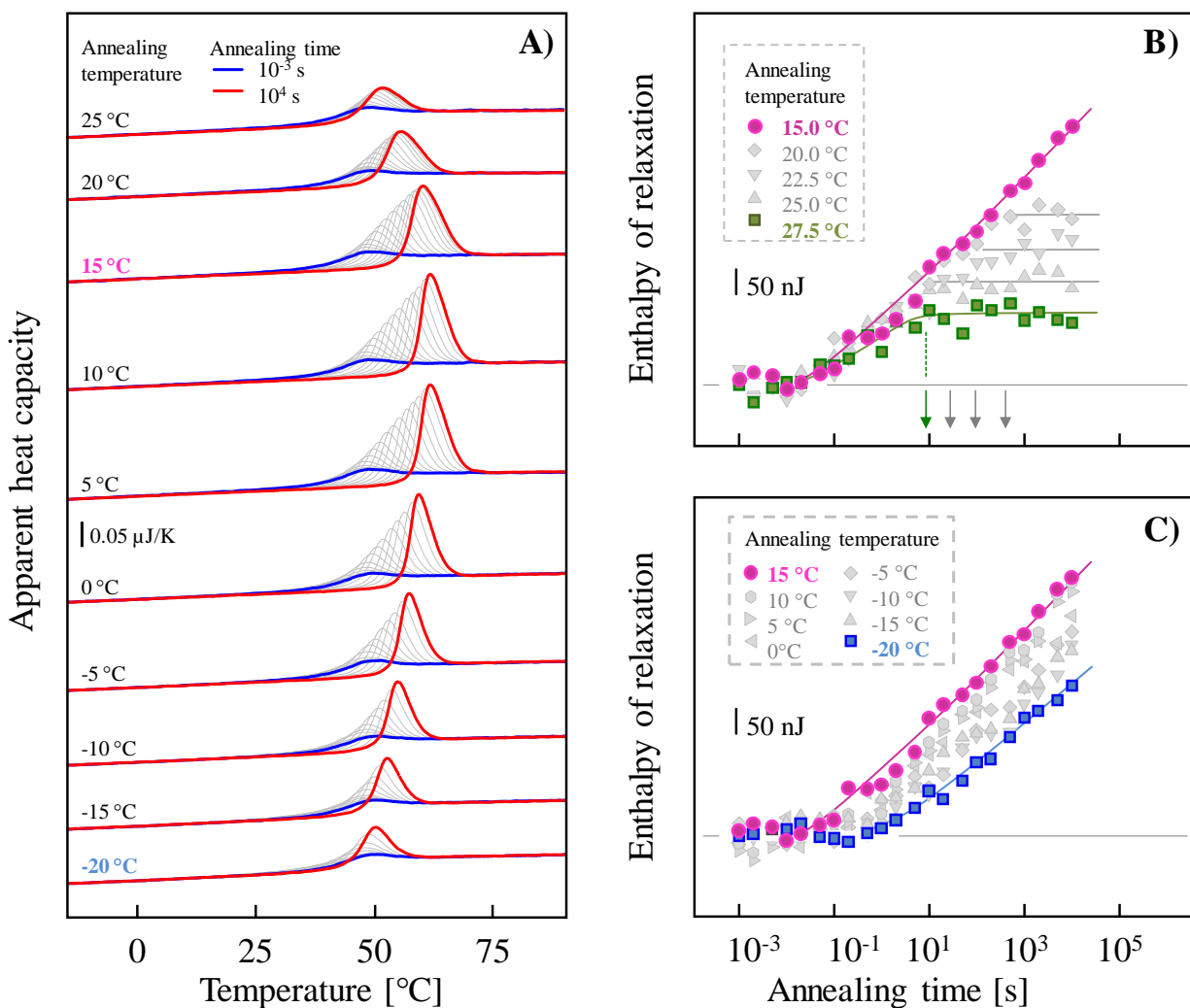
Figure 5.6: A) heating scans, recorded with FSC, of samples annealed at different temperatures between -20°C and 25°C for different time (0.001 s - blue line ; 10,000s - red line). B) Enthalpy of relaxation as a function of annealing time at temperatures between 15 and 27.5°C C), and between -20 and 15°C.

The time needed to complete the process of relaxation of PBI, was then estimated. During enthalpy relaxation, cooperative rearrangements of segments took place until nuclei of supercritical size were formed. As a consequence, considering the data reported in **Figure 5.6 B**, at temperatures of 20, 22.5, 25, and 27.5°C the crystal nucleation started after 7, 25, 100 and 500 s, respectively.

A brief summary of the information collected about crystal nucleation and crystal growth of PBI was reported in **Figure 5.7**. In detail, the time of completion of enthalpy relaxation (blue line),

onset time of nuclei formation (green line), and halftime of crystallization of PBI (red line) were reported as a function of temperature.
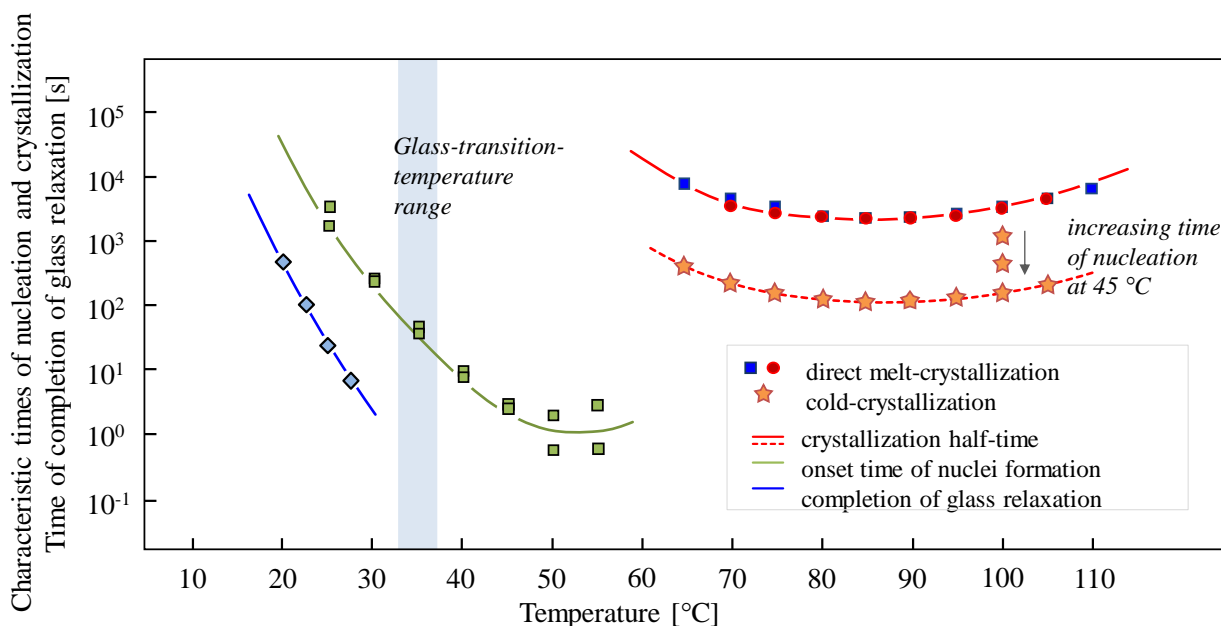
Figure 5.7: Time to complete enthalpy relaxation process (blue line), onset time for nuclei formation (green line), and halftime of crystallization (red line) as a function of temperature. Crystallization halftimes has been evaluated via direct melt-crystallization and via cold-crystallization (star points).

The halftimes of crystallization were studied employing direct melt-crystallization (see also **Figure 5.2**, squares and circles). Further experiments were performed after nucleation at 45°C for a few hours; the so obtained data were reported as star symbols in the plot. The heating rate used to bring the nuclei from 45°C to the crystallization temperature of 100°C was 50 K/min. As for the results of the previous experiments, a sample subjected to cold-crystallization at 100°C, after annealing at 45°C for less than 5 hours, crystallized faster than through melt-crystallization process performed at the same temperature.

5.7 Conclusions

Calorimetric and microscopic techniques were employed to study the crystallization behavior of poly(butylene isophthalate) (PBI). This material showed the capability to develop lamellar crystals and rather large spherulites. Then, Tammann's two-stage crystal nuclei development method was applied with success, obtaining an acceleration of the crystallization process. Crystal nuclei formation was observed after annealing near the glass transition temperature (T_g), which grow to

crystals. In this case, the crystals produced were much finer compared to the structure obtained after direct melt-crystallization. As well as other slowly crystallizing polymers like poly(ethylene terephthalate) or poly(L-lactic acid), low-temperature crystal-nuclei formation at a timescale of hours/days was too slow to allow non-spherulitic crystallization at elevated temperature.

5.8 Bibliography

1.   Association of Plastics manifacturors. Plastics -The facts 2018. *Plast. Eur.* 1–57 (2018). doi:10.1016/j.marpolbul.2013.01.015

2.   Frost, J. W. Synthesis of biobased and substituted terephthalic acids and isophthalic acids. 5–6 (2016).

3.   He, Y. C., Wu, Y. D., Pan, X. H., Ma, C. L. Biosynthesis of terephthalic acid, isophthalic acid and their derivatives from the corresponding dinitriles by tetrachloroterephthalonitrile-induced Rhodococcus sp. *Biotechnol. Lett.* **36**, 341–347 (2014).

4.   Yim, H., Haselbeck, R., Niu, W., Pujol-Baxley, C., Burgard, A., Boldt, J., Khandurina, J., Trawick, J.D., Osterhout, R.E., , Stephen, R., Estadilla, J., Teisan, S., Schreyer, H. B., Andrae, S., Hoon Yang, T., Yup Lee, S. Metabolic engineering of Escherichia coli for direct production of 1,4-butanediol. *Nat. Chem. Biol.* **7**, 445–452 (2011).

5.   Bechthold, I., Bretz, K., Kabasci, S., Kopitzky, R., Springer, A. Succinic acid: A new platform chemical for biobased polymers from renewable resources. *Chem. Eng. Technol.* **31**, 647–654 (2008).

6.   Liu, H., Lu, T. Autonomous production of 1,4-butanediol via a de novo biosynthesis pathway in engineered Escherichia coli. *Metab. Eng.* **29**, 135–141 (2015).

7.   Burgard, A., Burk, M. J., Osterhout, R., Van Dien, S., Yim, H. Development of a commercial scale process for production of 1,4-butanediol from sugar. *Curr. Opin. Biotechnol.* **42**, 118–125 (2016).

8.   Gilbert, M., Hybart, F. J. Effect of chemical structure on crystallization rates and melting of polymers: 2. Aliphatic polyesters. *Polymer (Guildf).* **15**, 407–412 (1974).

9.   Castles, J. L., Vallance, M. A., McKenna, J. M., Cooper, S. L. Thermal and Mechanical Properties of Short-Segment Block Copolyesters and Copolyether-Esters. *J. Polym. Sci. Part A-2, Polym. Phys.* **23**, 2119–2147 (1985).

10.   Wang, Z., Li, W., Zhao, X., Zhu, D., You, J. Self-segregation behavior of n-ethyl-pentadecafluorooctanamide-terminated polybutylene isophthalate and its effects on film morphology and wettability. *J. Phys. Chem. B* **113**, 15204–15211 (2009).

11.   Binsbergen, F. L. Natural and artificial heterogeneous nucleation in polymer crystallization. *J. Polym. Sci. Polym. Symp.* **59**, 11–29 (1977).

12.   Chatterjee, A. M., Price, F. P., Newman, S. Heterogeneous nucleation of crystallization of

high polymers from the melt. III. Nucleation kinetics and interfacial energies. *Phys. J. Polym. Sci. Polym.* **13**, 2391–2400 (1975).

13. Gilbert, M.; Hybart, F. J. Effect of chemical structure on crystallization rates and melting of polymers: Part 1. Aromatic polyesters. *Polymer (Guildf).* **13**, 327–332 (1972).

14. Finelli, L., Lotti, N., Munari, A. Influence of branching on the thermal behavior of poly(butylene isophthalate). *J. Appl. Polym. Sci.* **84**, 2001–2010 (2002).

15. Righetti, M. C., Pizzoli, M., Lotti, N., Munari, A. Crystallization kinetics and melting behavior of poly(butylene adipate), poly(butylene isophthalate) and their copolymers. *Macromol. Chem. Phys.* **199**, 2063–2070 (1998).

16. Illers, K. H. Geordnete Strukturen in „amorphem" Polyäthylenterephthalat. *Kolloid-Zeitschrift und Zeitschrift für Polym.* **245**, 393−398 (1971).

17. Androsch, R., Di Lorenzo, M. L. Crystal nucleation in glassy poly(l -lactic acid). *Macromolecules* **46**, 6048–6056 (2013).

18. Schick, C., Androsch, R. Nucleation-controlled semicrystalline morphology of bulk polymers. *Polym. Cryst.* **1**, (2018).

19. Androsch, R., Di Lorenzo, M.L., Schick, C. Optical microscopy to study crystal nucleation in polymers using a fast scanning chip calorimeter for precise control of the nucleation pathway. *Macromol. Chem. Phys.* **219**, (2018).

20. Zhang, R., Zhuravlev, E., Androsch, R., Schick, C. Visualization of Polymer Crystallization by In Situ Combination of Atomic Force Microscopy and Fast Scanning Calorimetry. *Polymers (Basel).* **11**, 890 (2019).

21. Starkweather, H.W., Brooks, R. E. Effect of spherulites on the mechanical properties of nylon 66. *J. Appl. Polym. Sci.* **1**, 236–239 (1959).

22. Way, J.L., Atkinson, J.R., Nutting, J. The effect of spherulite size on the fracture morphology of polypropylene. *J. Mater. Sci.* **9**, 293–299 (1974).

23. Perkins, W.G. Polymer toughness and impact resistance. *Polym. Eng. Sci.* **39**, 2445–2460 (1999).

24. Hodge, I. Enthalpy relaxation and recovery in amorphous materials. *J. Non-Cryst. Sol.* **169**, 211–266 (1994).

6 STUDY ON THE STABILITY OF NUCLEI OF POLY(BUTYLENE ISOPHTHALATE) FORMED NEAR GLASS TRANSITION TEMPERATURE

6.1 Introduction

Poly(butylene isophthalate) (PBI) is the isomer of the well-known poly(butylene terephthalate) (PBT)[1], in which the two ester groups are in meta-position, while in PBT they are located in para-position. This chemical architecture causes different behavior in crystallization capability affecting the potential applications. Indeed, PBT results a rather fast crystallizing polymer, allowing the generation of semicrystalline products in typical processing routes as injection molding[2–4]. PBI has a glass transition temperature similar to PBT[5,6]; despite that, the crystal phase is melting at lower temperature. Considering what was observed in Paragraph 4 of Chapter 4, PBI presents the fastest melt crystallization process in the range of 80°C-100°C with crystallization halftime of several minutes[7,8]. Its nature of slow crystallizing material limits its commercial application. As a consequence, some attempt to control crystallization rate and semicrystalline morphology of PBI has already been tested[9]. In details, low temperature annealing favored the formation of homogenous crystal nuclei, able to grow in spherulite morphology at higher temperature and leading to a finer structure than that observed after direct melt crystallization. This information was collected employing Tammann's two-stage crystal nuclei development method[10–13], to solve the problem of limited direct detection of homogenous nuclei by calorimetric methods or imaging. These initial studies on PBI crystallization[9] were deepened in order to collect more information on the effects of growth temperature and transfer-heating rate in Tammann's experiment.

6.2 Critical rates to prevent non-isothermal crystal nucleation and growth

Controlling the non-isothermal formation of nuclei was one of the most important pre-requisites for the analysis of crystal nucleation. Firstly, it was important to find a cooling rate from the melt, where no nucleation nor crystallization were allowed. The specimens of PBI were subjected to temperature-time profile reported in **Figure 6.1 A**, in order to define the critical cooling rate necessary to avoid crystallization. In detail, PBI was subjected to cooling process with rate between 0.01K/s to 1000K/s; the presence of crystals was evaluated considering the enthalpy of melting derived from the consequent heating scan. The cooling rate was applied up to 120°C to reduce the interval of time where the sample was molten and control polymer degradation.

188

Moreover, from -20°C down, a temperature well below T_g, it was assumed that the cooperative movements of the chains were negligible. In **Figure 6.1 B,** heating scans recorded after the different cooling rates were reported. As one can see, cooling rates higher than 0.02 K/s suppressed crystallization processes, indeed only the glass transition phenomenon, around 50°C, was observed. Lowering the cooling rate favors crystallization, as it can be concluded considering the increasing of the area of endothermic peaks recorded.
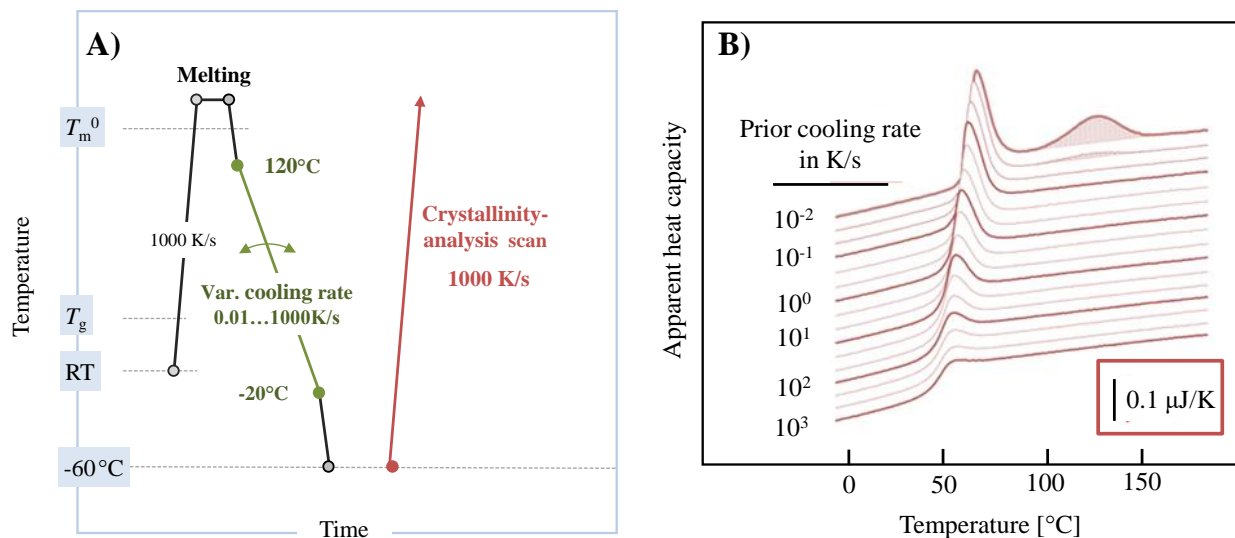
Figure 6.1*: **A)** Profile of time/temperature used for analysis of the cooling-rate dependence in PBI crystallization; **B)** FSC heating scans after cooling at different rates.*

The possibility to suppress not only crystallization but also nucleation during cooling and heating was investigated. In **Figure 6.2 A** the temperature-time profile applied to the sample was reported. In detail, the equilibrium melt was cooled from 120 to -20°C, the relevant temperature range; then, the sample was heated up to 85°C. Cooling/heating rates were varied in the range of 0.01 - 10,000 K/s (green segment). At 85°C the specimen, after applying defined cooling/heating rate, was annealed for 1000 s to grow the formed nuclei (blue segment). The so-obtained crystals were evaluated considering the enthalpy of melting detected during the second heating scan (red segment). In **Figure 6.2 B** the enthalpies recorded were shown as a function of cooling rate (reported in abscissa) and heating rate (reported in the legend). The experiments conducted, resembled Tammann's method for separate nucleation and growth steps. An increased number of nuclei could be observed reducing the cooling/heating rate, despite, as it was reported in **Figure 6.2 B**, using a minimum rate of 0.1 K/s, absence of crystal growth was assured. The fraction of

crystal growing at the pre-defined condition was dependent on the number of nuclei formed during cooling/heating process.

Employing fast heating of 10,000 K/s, as reported in **Figure 6.2 B** by pentagons, allowed formation of crystal nuclei during the cooling, employing rate comprise between 0.01 to 20 K/s. Cooling rates lower than 20 K/s, made the enthalpy of crystallization larger than the ground level (gray horizontal line), identified by the value of enthalpy recorded for a sample crystallized at 85°C for 1000 s. Consequently, cooling the equilibrium melt at 20 K/s or with lower rates, favored the formation of nuclei during cooling and the crystallization at 85°C. With infinitely fast cooling (10,000 K/s) nuclei formation was not allowed and if the heating rate was lower than 50 K/s (red arrow and red data reported in **Figure 6.2 B**), an increase of the crystallinity was detected. To summarize, the performed experiments showed that applying a cooling/heating rate lower than 20 K/s no crystal nuclei could be formed.
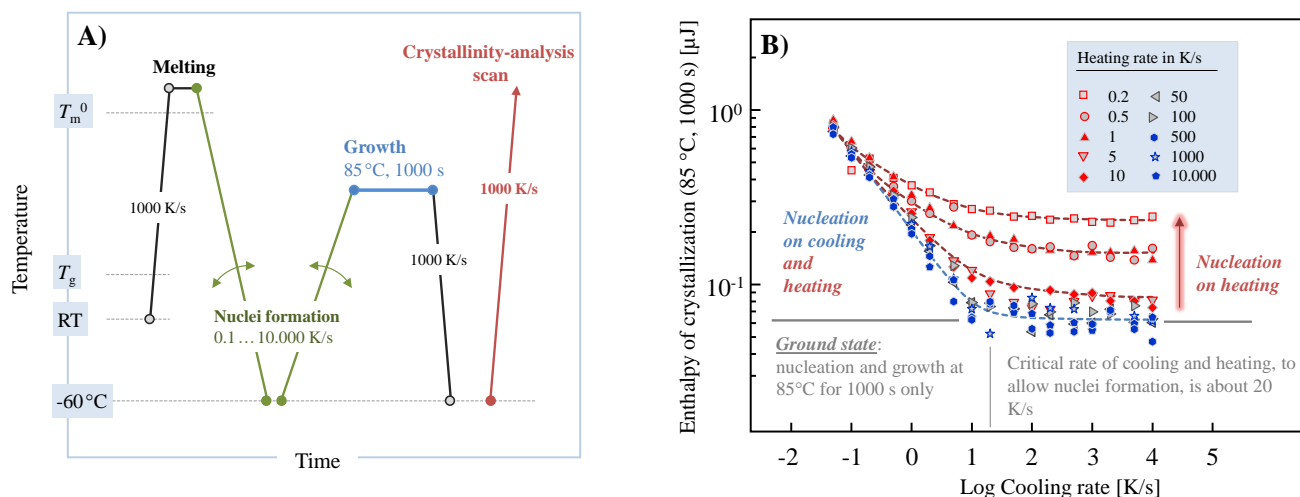
Figure 6.2*: **A)** Profile of the analysis conducted as a function of time/temperature, used for cooling- and heating-rate dependencies of crystal nucleation of PBI; **B)** enthalpies of crystallization (85°C, 1000 s) after different cooling and heating histories.*

6.3 Investigation of thermal stability of nuclei formed close to glass transition temperature

Our previously study regarding PBI showed a maximum rate of crystallization around 50°C[9]; in order to investigate the variation of cluster-size distribution, different nucleation times were tested, as reported in **Figure 6.3 A**. The stability of the so-obtained nuclei was evaluated, heating at 1000

K/s the sample to spike temperatures between 85 and 140°C (pink segments); then, the nuclei remained were grown at 85°C for 1000 s. During this experiment, the nuclei formed at 50°C, without prior stabilization/growth, disappeared on heating to above a nucleus-size dependent critical temperature. Increasing the spike temperature, the number of nuclei surviving and growing at fixed condition, decreased. In the section below, the assumption of absence of nuclei-reorganization with heating rate of 1000 K/s was discussed. In **Figure 6.3 B**, the FSC curves obtained after treating the specimen at 50°C for 5000 s (nucleation), then heating to a spike temperature in the range comprise between 85 and 140°C, were reported. The remained nuclei were developed in crystals by annealing at 85°C for 1000 s. The resulting crystalline phase was evaluated by the heating scan represented by the red colored segment in **Figure 6.3 A**. As one can see, the heat-capacity of glass transition, superimposed with a small enthalpy-recovery peak, was incrementing. Moreover, melting phenomena decreased with the increasing of the spike temperature reached. In detail, nuclei directly transferred to the growth temperature of 85°C led to a largest melting peak, which was smaller for the experiments testing higher temperature till to a spike temperature of 140°C.
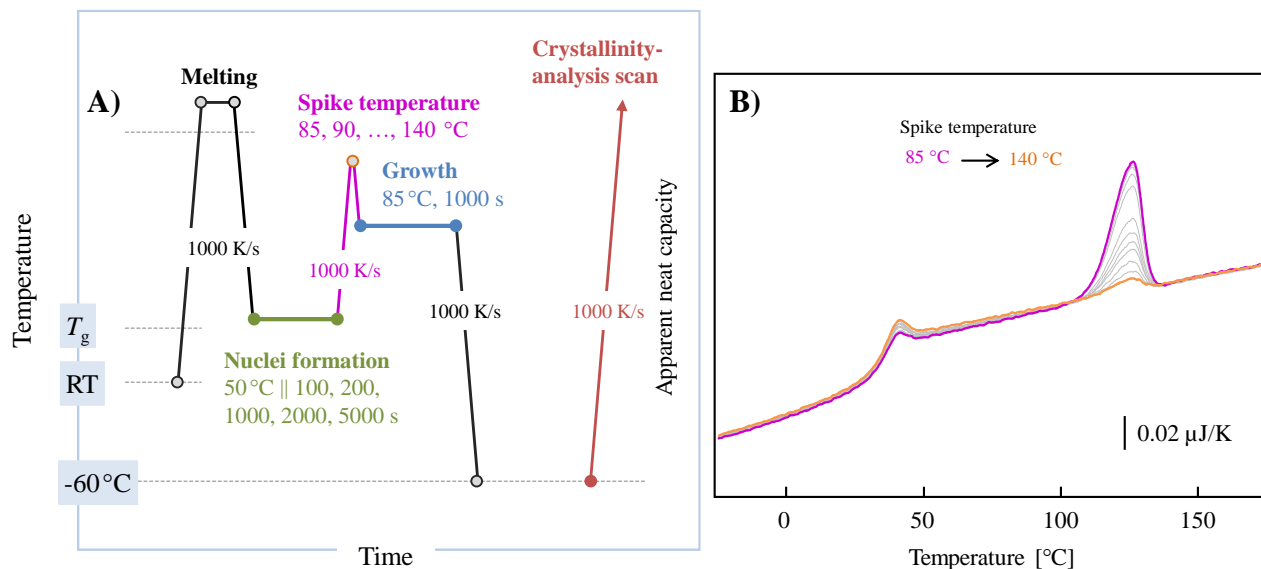
Figure 6.3*: **A)** Profile of the analysis conducted as a function of time/temperature employed; **B)** FSC heating curves obtained following the route reported.*

The data of crystallization enthalpy of PBI after annealing at 85°C for 1000 s as function of the spike temperature, were shown in **Figure 6.4**. As reported in the legend, the data sets represented

different nucleation time. Firstly, the enthalpy of crystallization increased with the time of nucleation, due to the higher number formed; as a matter of fact, the gray vertical line at 85°C, clearly indicated the crystallization enthalpy progressively increased from 100 s (black square) to 5000 s (orange diamond).
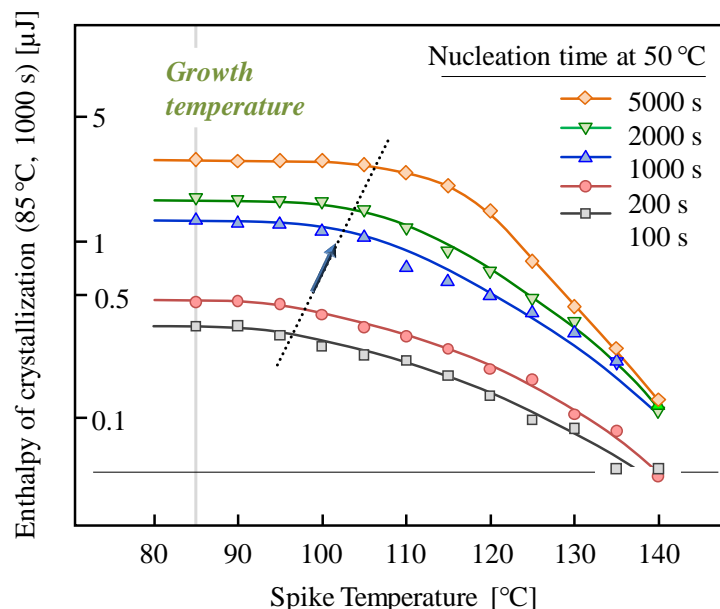
Figure 6.4: *Enthalpy of crystallization of PBI (85°C, 1000 s) reported as a function of the spike temperature. PBI samples were subjected to nucleation at 50°C for different times and nuclei-transfer-heating rate of 1000 K/s*

Besides that, the data set could be read as function of spike temperature. The crystallization enthalpy was still constant, reaching an upper plateau, then was decreasing to a critical value. Considering PBI treated at 50°C for 5000s (diamonds), the population of nuclei survived to the spike temperature of 105°C, but when heated to higher temperature, part of them were reduced because of the sub-critical size of the nuclei at the respective spike temperature. At 140°C the abatement of the largest amount of nuclei formed at 50°C, was almost complete. Finally, **Figure 6.4** proved that the nucleation time was affecting the nuclei-size distribution. In fact, longer nucleation time was not only responsible of higher number of nuclei, but also of an increased fraction of larger nuclei, as one can see following the dot line with arrow, indicating a shifting of the downturn of the curves to higher spike temperature, as a function of nucleation time.

6.4 Crystal-nuclei reorganization with different transfer-heating rate

The experiment performed before, was modified in order to study the effect of transfer-heating rate on crystal nuclei (between 1 and 10,000 K/s), from 50°C, temperature of their formation, up to different spike temperatures. A growth step was applied, keeping the sample at 85°C for 1000 s then the crystals survived were evaluated from the melting enthalpy recorded in the subsequent heating scan. **Figure 6.5 B** reported the FSC set scans recorded for different spike temperatures. In details, the red curve represented the low limit of transfer-heating rates, 1 K/s, while the blue one, the curve for the highest transfer-heating rates used, 1000 K/s. As evidenced by FSC curves, negligible effect of the transfer-heating rate was recorded on the number of crystal nuclei for spike temperatures lower than 100 °C. While employing higher temperature than 100°C, determined an effect of the transfer rate, indeed nuclei number decreased with increasing heating rate. Furthermore, even if slow heating allowed nuclei reorganization, a lowering of nuclei number was observed by increasing spike temperature. The temperatures of 150 °C destroyed indeed almost all nuclei.
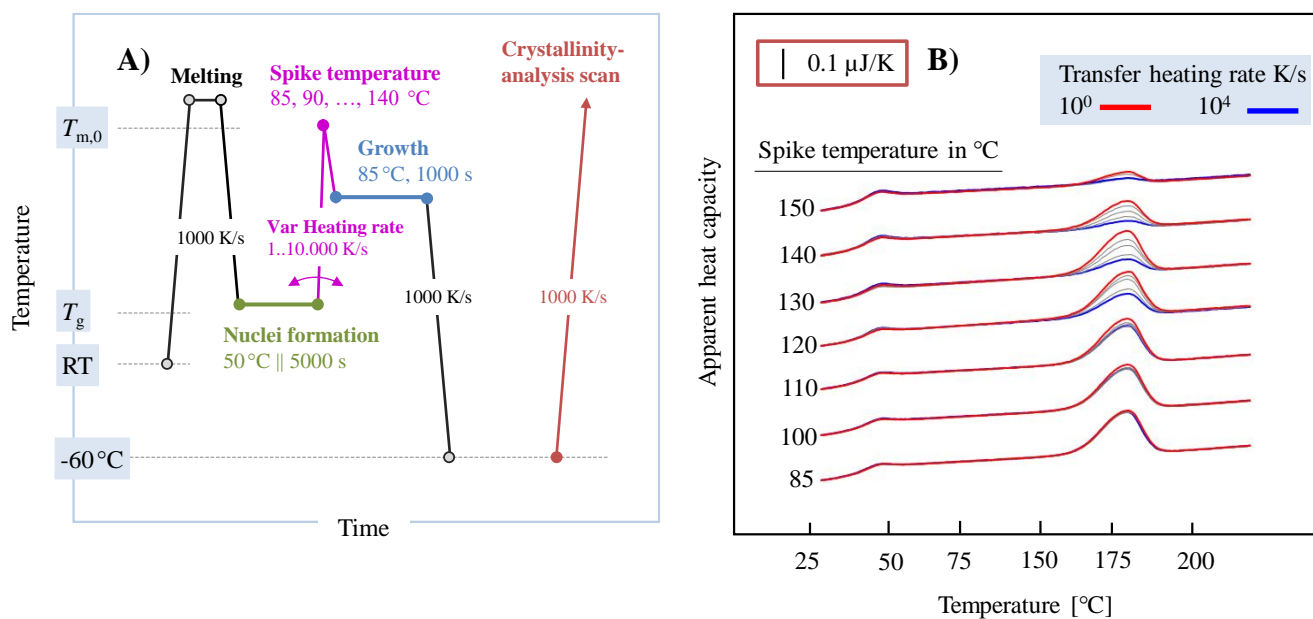
Figure 6.5: ***A)*** *Profile of the analysis conducted as a function of time/temperature employed for analysis of the effect of the nuclei-transfer-heating rate and spike temperature on nuclei stabilization;* ***B)*** *FSC heating curves after subjecting PBI to nucleation (50°C,5000 s), followed by heating to a spike temperature at different rates (1 K/s, red curves; 10,000 K/s, blue curves), and final growth of nuclei to crystals (85°C, 1000 s).*

After exposing the system to different maximum temperatures, quantitative data regarding the dependence of nuclei number formed at the growth-stage, on different transfer-heating rate, were collected and reported in **Figure 6.6**. The specimens of PBI were subjected to the thermal profile reported in **Figure 6.5 A**. The derived enthalpies of melting in the subsequent FSC heating scan were plotted vs transfer-heating rate and reported in **Figure 6.6** where data sets represented samples subjected to different spike temperature. As reported before, at the growth-stage temperature of 85°C, no significant crystallization was occurring after a previous suppression of crystal nuclei formation. Since a no-zero value of enthalpy of crystallization at growth stage was observed (see **Figure 6.5 A**), crystal nuclei were formed before the growth stage in the nucleation step. Crystal nuclei developed at 50°C for 5000 s have been heated up at different rates to the growth stage and a large number of nuclei were formed with the critical size corresponding to the growth stage temperature of 85°C. No influence of the different heating rates was detected.

Crystal-nuclei populations formed at 50 and 85°C presented a no relevant differences for spike temperature lower than 110°C. Just a minor decrease of enthalpy of crystallization was observed. This result agreed with orange colored data points reported in **Figure 6.4**, referring to specimens subjected to the same nucleation history (50°C, 5000 s). The transfer-heating rate of 1000 K/s was reported in **Figure 6.6** with similar orange-color.
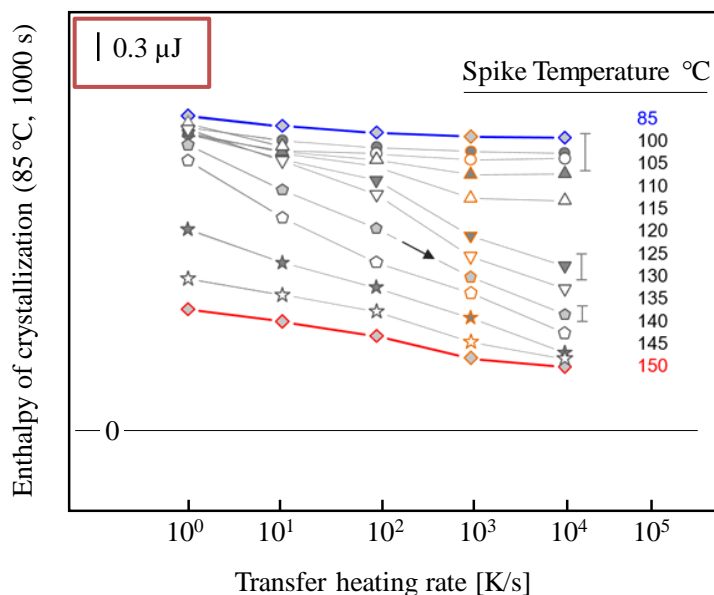
Figure 6.6: *Enthalpy of crystallization of PBI samples kept at 85°C for 1000 s as a function of heating rate of the crystal nuclei formed at 50°C (5000 s) to different spike temperatures, as*

The number of nuclei was not significantly reduced by heating to slightly above 100°C and no effect of the transfer-heating rate was observed. Using a spike temperature higher than 110°C, the number of nuclei was depending on transfer-heating rate. A lower plateau was reached for spike temperature up to 115°C, open upward triangles, on heating faster (1000 K/s). In particular, the decrease of nuclei number with the increasing of heating rate was due to the suppression of their reorganization. The crystallization enthalpies observed at high transfer-heating rate were ascribed to the presence of nuclei with a size equal or larger than the critical size at the spike temperature. On the other side, by applying a slow heating, low number of nuclei with a smaller size than their critical one at the spike temperature were formed and their growth was allowed. For example, with a spike temperature of 135°C, the number of nuclei at 50°C with a dimension larger than the critical size was negligible. Moreover, slow heating of 1 K/s allowed growth of a large number of nuclei of initially subcritical dimension, leading to the same melting enthalpy obtained with direct heating to 85°C.

6.5   Conclusions

The test performed allowed us to investigate the thermal behavior of homogenous crystal nuclei in PBI. Crystal nuclei formed at low temperature of different size could melt during heating to critical temperature, or could grow to develop a spherulite, applying a selected thermal protocol. As well as for crystals, heating rate was controlling melting process/reorganization of nuclei. In detail, Tammann's two-stage nuclei development method was applied in order to obtain quantitative information. Nuclei were formed at 50°C, and their number was studied as a function of the transfer-conditions (maximum temperature, heating rate) by developing crystal fraction with a defined growth stage at 85°C. Nucleation time controls the different nuclei size distribution, and a distinct reduction of nuclei number was observed during heating to a temperature higher than 90°C. An increased fraction of larger nuclei was developed by increasing nucleation time. Applying a heating rate of 1000 K/s to 140 - 150°C determined the melting also of the most stable nuclei formed. Besides that, the transfer process of crystal from 50°C (nucleation stage) to 85°C (growth stage) showed negligible effect of the transfer-heating rate.

In conclusion, quantitative information about the characteristics of crystal nuclei of PBI was provided and the importance of a proper design of Tammann's nuclei development experiment for analysis of nuclei numbers was proven.

6.6 Bibliography

1. Radusch, H. J. Poly(butylene terephthalate). in *Handbook of Thermoplastic Polyesters* (389–419, ed. Wiley-VCH: Weinheim, G., 2001).

2. Ludwig, H. J., Eyerer, P. Influence of the processing conditions on morphology and deformation behavior of poly (butylene terephthalate)(PBT). *Polym. Eng. Sci.* **28**, 143–146 (1988).

3. Shibaya, M., Ishihara, H., Yamashita, K., Yoshihara, N., Nonomura, C. Effect of mold temperature on structure and property variations of PBT injection moldings in the thickness direction. *Int. Polym. Proc.* **19**, 303–307 (2004).

4. Rhoades, A. M., Williams, J.L., Wonderling, N., Androsch, R., Guo, J. Skin/core crystallinity of injection-molded poly (butylene terephthalate) as revealed by microfocus X-ray diffraction and fast scanning chip calorimetry. *J. Therm. Anal. Calor.* **127**, 939–946 (2017).

5. Gilbert, M., Hybart, F. J. Effect of chemical structure on crystallization rates and melting of polymers: 2. Aliphatic polyesters. *Polymer (Guildf).* **15**, 407–412 (1974).

6. Castles, J.L., Vallance, MA., McKenna, J.M., Cooper, S. L. Thermal and Mechanical Properties of Short-Segment Block Copolyesters and Copolyether-Esters. *J. Polym. Sci., Polym. Phys.* **23**, 2119–2147 (1985).

7. Finelli, L., Lotti, N., Munari, A. Influence of branching on the thermal behavior of poly(butylene isophthalate). *J. Appl. Polym. Sci.* **84**, 2001–2010 (2002).

8. Finelli, L., Lotti, N., Munari, A. Crystallization kinetics and melting behavior of poly(butylene isophthalate/terephthalate) random copolyesters. *Eur. Polym. J.* **37**, 2039–2046 (2001).

9. Quattrosoldi, S., Androsch, R., Janke, A., Soccio, M., Lotti, N. Enthalpy Relaxation, Crystal Nucleation and Crystal Growth of Biobased Poly (butylene Isophthalate). *Polymers (Basel).* **12**, 235 (2020).

10. Davis, M. J. Effect of the Growth Treatment on Two-Stage Nucleation Experiments. *J. Am Ceram. Soc.* **84**, 492–496 (2001).

11. Deubener, J., Montazerian, M., Krüger, S., Peitl, O., Zanotto, E. D. Heating rate effects in time-dependent homogeneous nucleation in glasses. *J. Non-Crystalline Sol.* **474**, 1–8 (2017).

12. Zhuravlev, E., Schmelzer, J. W. P., Androsch, R., Schick, C. Experimental test of

tammann's nuclei development approach in crystallization of macromolecules. *Int. Polym. Process.* **31**, 628–637 (2016).

13. Androsch, R., Iqbal, H. N., Schick, C. Non-isothermal crystal nucleation of poly (L-lactic acid). *Polymer (Guildf).* **81**, 151–158 (2015).

7 RETHINKING PLASTIC PACKAGING WITH A NEW BIO-BASED COPOLYMERIC SYSTEM OF POLY(BUTYLENE ISOPHTHALATE) AND POLY(BUTYLENE FURANOATE) WITH SMART BARRIER PROPERTIES

7.1 Introduction

Among the different fields of application, food packaging is one of the main categories where plastic materials are applied[1]. The characteristic self-life of the envelopes is really short, since the rate of production of waste and the total amount are high. These volumes of plastic are increasing the pollutants in the environment, because, due to the properties of floating and durability, wastes can easily spread around the environment. In particular, the oceans are collecting huge amounts of polymeric wastes, accumulating and converging in the subtropical gyres[2]. Despite that, the environmental impact of plastics is not only due to their end-life fate, but also the resources from which the monomers are obtained have an important role. Nowadays, most of the plastic materials used are oil-based and derive from finite fossil resources[3]. Given this complex scenario, affordable solutions for decrease the environmental impact of plastics are among the most important challenges facing the scientific community. Bioplastics are promising candidates as substitutes of non-degradable oil-based polymers. In particular, polymers derived isophthalic acid, IPA, and 2,5-furan dicarboxylic acid, FDCA, are capturing the attention from both academic researchers and industry. In details, IPA, an isomer of the well-known terephthalic acid, can be synthetized starting from bio-acrylic acid and bio-isoprene or directly from biomass (fermentation process)[4,5]. The polyester derived from IPA and 1,4-butanediol, Poly(butylene isophthalate), (PBI), can be considered in total agreement with the principles of "green chemistry" , being this polyester obtainable via two step solvent free polycondensation employing monomers totally bio-based[6–8]. As well as IPA, FDCA monomer is obtainable from dehydrogenation of glucose or fructose[9,10]. Among the different derivatives, poly(butylene furanoate), PBF, is really promising for its good mechanical, barrier properties and thermal stability, despite that its high stiffness is hampering the application in flexible food packaging[11–14]. In order to modify the unsatisfying characteristic of PBF, maintaining the good ones, the material was copolymerized. In detail, different amounts of isophthalic acid were added in presence of 2,5-furan dicarboxylic acid and 1,4 butanediol, in order to obtain a 100% biobased copolymeric system, $P(BF_mBI_n)$.

7.2 Synthesis and molecular characterization

PBF, PBI homopolymer and $P(BF_mBI_n)$ random copolymers were synthetized via one-pot synthetic approach, i.e. two step melt polycondensation, as explained in "Methods and Materials" section. The chemical structure of all the polymers synthesized and, in case of copolymers, the real composition, the sequence distribution and length were evaluated by ^{1}H-NMR and ^{13}C-NMR spectroscopy. The spectra agreed with the predicted ones, confirming the chemical structure of polymers under investigation. This result indicated an appropriate method of synthesis that was used with a good polymerization control. As example, the ^{1}H-NMR spectrum for $P(BF_{70}BI_{30})$ was reported with related peak assignations, (**Figure 7.1**).
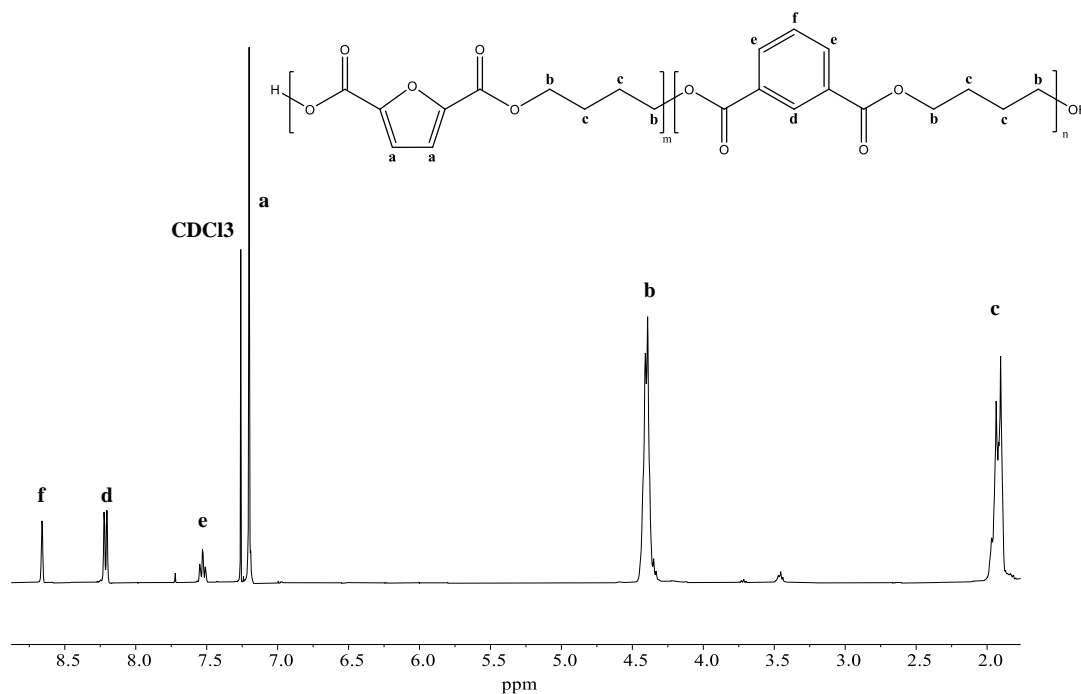
Figure 7.1*: ^{1}H-NMR spectrum of P(BF$_{70}$BI$_{30}$) with the relative peak assignments.*

The signals at 1.95 and 4.43 ppm were referred to the methylene protons of the glycolic subunit, *b* and *c*, respectively, while, at 7.20 the two hydrogens of the furan ring were resonating (a). The remaining signals were ascribed to the aromatic protons of the isophthalic ring: specifically, at 8.68 ppm the hydrogen located between the two carbonyl groups was observed; proton d was located at 8.22 ppm, whereas at 7.52 ppm the two last aromatic hydrogens, e, were recognized. ^{1}H-NMR spectra were also employed to evaluate the actual chemical composition of the synthetized copolymers. In detail, the integrals of the signals ascribed to the two aromatic subunits,

furan and isophthalic rings, respectively at 7.20 ppm (a) and 8.22 ppm (d), was considered. The results were collected in **Table 7.1**

Table 7.1: *Molecular characterization data of PBF, PBI homopolymer and P(BF$_m$BI$_n$)copolymeric system.*

Sample	mol% BF by ^{1}H-NMR	b	L$_{BF}$	L$_{BI}$	M$_n$[a] g/mol	D[a]
PBF	100	/	/	/	27300	2.3
P(BF$_{90}$BI$_{10}$)	88	0.96	8.93	1.25	25700	2.5
P(BF$_{80}$BI$_{20}$)	76	0.96	5.00	1.36	30600	2.4
P(BF$_{70}$BI$_{30}$)	69	0.95	3.53	1.51	48300	2.5
P(BF$_{50}$BI$_{50}$)	50	1.0	2.0	2.0	49000	2.6
P(BF$_{30}$BI$_{70}$)	30	1.0	1.44	2.96	47900	2.6
P(BF$_{20}$BI$_{80}$)	20	0.95	1.36	5.10	39700	2.2
P(BF$_{10}$BI$_{90}$)	9	0.95	1.19	8.93	40100	2.4
PBI	0	/	/	/	33150	2.0

a) Obtained from GPC analysis

The distribution of comonomeric units along macromolecular chain were determined via ^{13}C-NMR spectroscopy. As reported in **Figure 7.2** for P(BF$_{70}$BI$_{30}$), the inner methylenic carbons, proper of the glycolic subunit bonded to the isophthalic moieties, 4, and to the furan one, 10, were resonating at 24.8 ppm, while the outer methylene carbons of the glycolic subunit 5 and 11 were observed at 64.8 ppm. The furan-ring carbons were, instead, visible at higher chemical shift: carbon 1 at 119.3 ppm, carbon 2 at 147 ppm. The signal of the carbonyl moiety, 3, was located at 168.9 ppm. The carbons of the isophthalic ring, 9, 8 and 7, were resonating at 128.5 ppm, 130.5 ppm and 134.9, respectively. Lastly, the carbonyl group bonded to the isophthalic ring (6) was recorded at 156 ppm.

Considering the signals attributed to the methylene carbons in α position respect to the carbonyl groups at 64,8 ppm, a multiple class of peaks could be observed. It was due to the possible triads, F-B-F, F-B-I, I-B-F e I-B-I, where the glycolic subunit (Butandiol: B) could be bonded to two different acid subunits, (furan: F and isophtalic one: I). Analyzing the mentioned signals, it was possible to calculate the randomness degree, b, for the copolymer series.
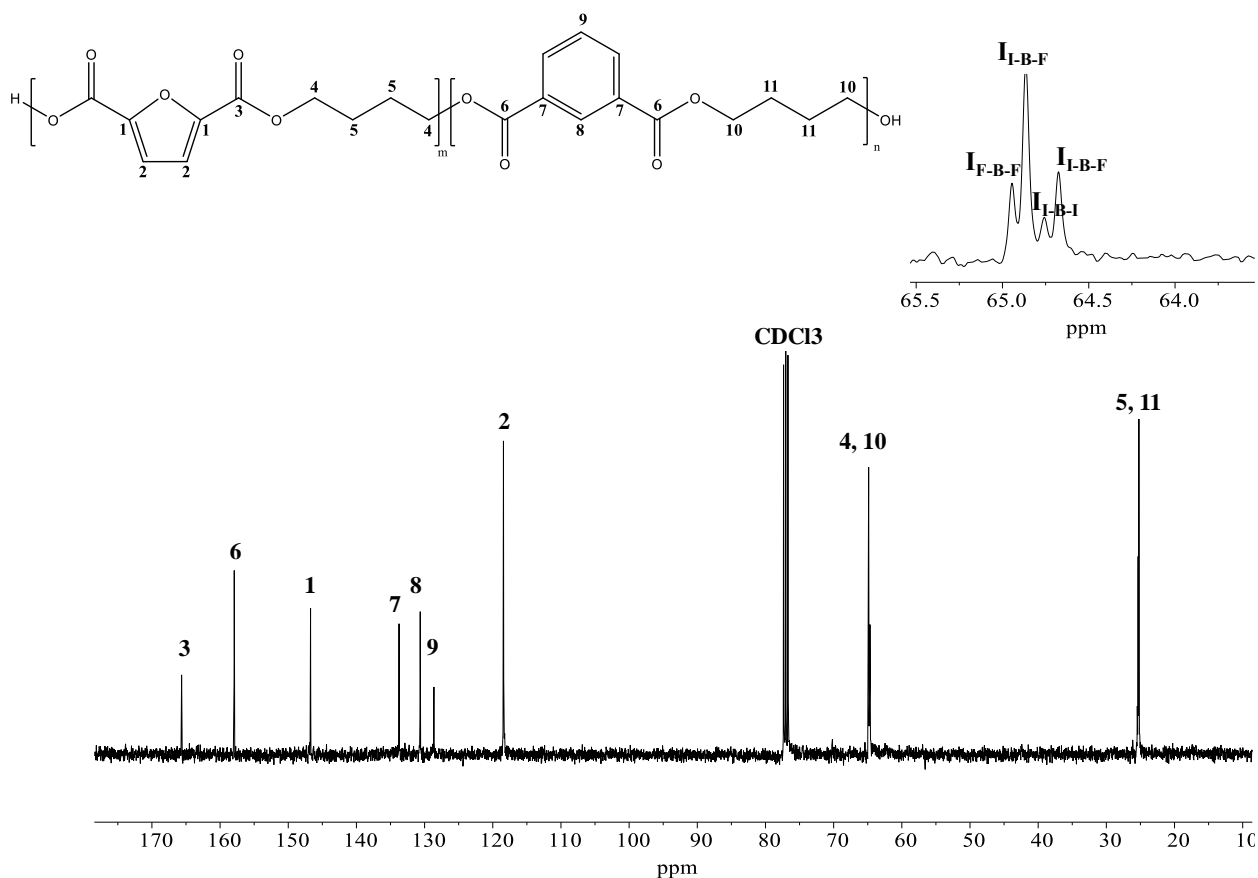
Figure 7.2: *^{13}C-NMR spectrum of P(BF$_{70}$BI$_{30}$) with the relative peak assignment. In the insert, magnification of the 65.5-63.4 ppm region and schematic representation of I-B-F, F-B-F and I-B-I triads.*

This parameter was given by the sum of two probabilities, the one related to a glycolic subunit bonded to the furan and the isophthalic moiety (P$_{F\_I}$) and the other representing the glycolic subunit bonded to the isophthalic and furanic one (P$_{I\_F}$).

$$b = P_{F-B-I} + P_{I-B-F} \qquad\qquad Eqn.\ 1$$

$$P_{F\_I} = \frac{(I_{F-B-I}+I_{I-B-F})/2}{(I_{F-B-I}+I_{F-B-I})/2+I_{F-B-F}} \qquad\qquad Eqn.\ 2$$

$$P_{I\_F} = \frac{(I_{F-B-I}+I_{I-B-F})/2}{(I_{F-B-I}+I_{I-B-F})/2+I_{I-B-I}} \qquad\qquad Eqn.\ 3$$

Where I$_{F\_I}$, I$_{I\_F}$, I$_{F\_F}$ e I$_{I\_I}$ rapresented the integrals of the peaks related to the triads, F-B-I, I-B-F, F-B-F e I-B-I.

As well known, randomness degree assumed a value from 0 to 1 for block copolymers, was equal to 1 for random copolymers and 2 for altering structures. In this specific case, b resulted ranging from 0.95 and 1 for all the synthetized copolymers, confirming their random nature (**Table 7.1**).

The molecular weight and the polydispersity, evaluated by means of GPC analysis, were also collected in **Table 7.1**. As it could be noted, high and similar values of M_n were found with D values close to 2, as expected for polyester polycondensation synthetic process. It is worth noting that the measured molecular weight values were comparable to those found by Morales-Huerta et al[15]., that synthesized the samples under investigation through ROP of cyclic oligomers. The synthetic approach adopted in the present paper was simpler and employs as catalytic system a Titanium alkoxide mixture, which was characterized by high activity towards polyesterification, environmentally safe nature and availability at acceptable costs for performing low-cost industrial processes.

7.3   Thermal characterization

Thermal stability of the samples was evaluated through thermogravimetric analysis. The tests were conducted applying a non-isothermal scan of temperatures under inert atmosphere. In **Table 7.2**, the experimental results for the homopolymers, PBF and PBI, and for the copolymers, $P(BF_mBI_n)$, had collected.

Table 7.2: Thermogravimetric data of PBF and PBI, and their random copolymers

Sample	T_{onset} °C	$T_{95\%}$ °C	T_{max} °C
PBF	353	343	366
$P(BF_{90}BI_{10})$	362	344	387
$P(BF_{80}BI_{20})$	364	351	386
$P(BF_{70}BI_{30})$	367	355	389
$P(BF_{50}BI_{50})$	371	358	395
$P(BF_{30}BI_{70})$	377	364	409
$P(BF_{20}BI_{80})$	382	365	414
$P(BF_{10}BI_{90})$	382	372	406
PBI	382	375	404

As shown in **Figure 7.3**, gravimetric weight loss of PBI was taking place in one step and led almost 100% degradation. Differently, PBF TGA curve, after degradation, was characterized by a char

residue of 10/12%. PBI was more thermally stable respect to PBF, despite both were aromatic polymers. The lower thermal stability of PBF could be explained on the basis of the lower resonance energy of stabilization of the furan ring, due to the high electronegativity of the oxygen atom present in the heterocyclic ring, which obstacle π electronic delocalization, ($E_{res,furan}=11$ Kcal/mol *vs* $E_{res,isophthalic}=36$ Kcal/mol). The data collected for the copolymers showed an intermediate thermal stability, which appeared to be dependent on their own composition. In detail, as presumable, the higher the amount of BI co-unit, the higher the thermal stability. A residual char was present in random copolymers too and also in this case, as expected, was found to increase with BF amount. The thermal stability could be anyway considered very good for all the analyzed samples, the T_{max} values being always superior to 350°C.

Lastly, it was worth noting the results obtained were in line with those previously obtained by Morales-Huerta et al[15].
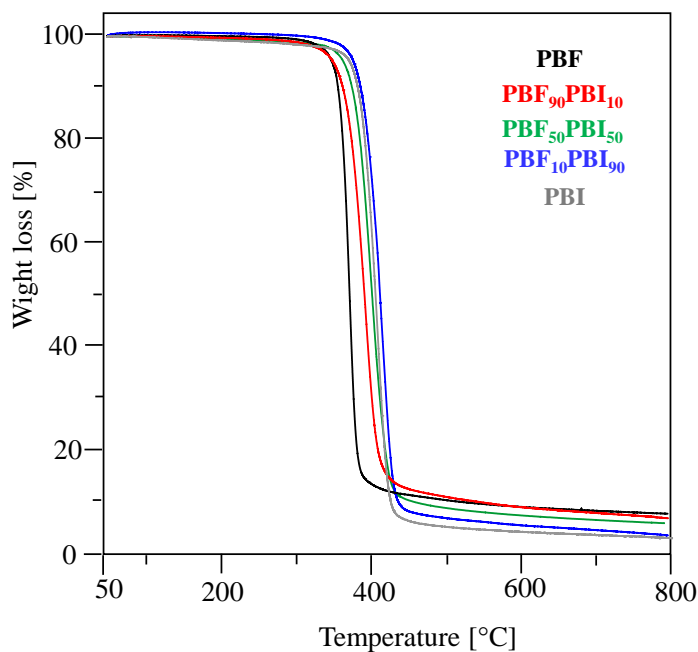
Figure 7.3*: TGA traces of PBF, PBI and P(BF$_{90}$BI$_{10}$), P(BF$_{50}$BI$_{50}$) and P(BF$_{10}$BI$_{90}$) under inert atmosphere (heating rate 10°C/min)*

The purified powders of the synthetized materials were thermally characterized via differential scanning calorimetry, in order to study their thermal transitions, the phase behavior and crystallizing ability under non-isothermal conditions. Ist scan DSC traces of purified PBI, PBF and P(BF$_m$BI$_n$) copolymers were reported in **Figure 7.4 A**, while the calorimetric results were collected in **Table 7.3**. All the analyzed powders were semi-crystalline materials, the corresponding

calorimetric scans being characterized by the glass transition and melting phenomena, occurring at higher temperature. This result indicated that the phase behavior was the same for all the powders investigated. As highlighted from **Table 7.3** and from **Figure 7.4 A**, PBF was characterized by a higher melting temperature (T_m) than PBI. Despite the non-linear and asymmetrical aromatic structure of both acid moieties present in PBF and PBI, the electronegativity of the oxygen atom in the furan ring favored inter chain hydrogen bonds, besides the possible π-π dipolar interactions occurring in both polyesters. Therefore, PBF chains could resulted better packed, consequentially, melting at higher temperature. On the contrary, the enthalpy of fusion was higher in PBI sample, indicating its higher tendency to crystallize respect to PBF. Such difference could be ascribed to the higher chain flexibility of PBI, which facilitated polymer chain folding occurring during polymer crystallization.

Table 7.3: *Thermal characterization data of PBF, PBI and P(BF$_m$BI$_n$) random copolymers in form of powders.*

Sample	Ist scan		IInd scan					
	T_m	ΔH_m	T_g	ΔCp	T_c	ΔH_c	T_m	ΔH_m
	°C	J/g	°C	J/°C·g	°C	J/g	°C	J/g
PBF	163	45	35	0.311	104	28	164	32
P(BF$_{90}$BI$_{10}$)	154	39	34	0.397	117	4	151	5
P(BF$_{80}$BI$_{20}$)	77-143	3-26	33	0.379	111	2	143	2
P(BF$_{70}$BI$_{30}$)	79-126	7-19	31	0.326	/	/	/	/
P(BF$_{50}$BI$_{50}$)	73	24	30	0.370	/	/	/	/
P(BF$_{30}$BI$_{70}$)	101	28	28	0.376	/	/	/	/
P(BF$_{20}$BI$_{80}$)	113	33	27	0.404	/	/	/	/
P(BF$_{10}$BI$_{90}$)	125	40	26	0.320	/	/	/	/
PBI	147	62	25	0.326	/	/	/	/

Regarding the copolymers, as reported in **Table 7.3** and shown in **Figure 7.4 A** and **B**, the melting temperature changed according to copolymer composition. Most of the copolymers under study were characterized by a multiple melting behavior: for P(BF$_{80}$BI$_{20}$), P(BF$_{70}$BI$_{30}$) and P(BF$_{50}$BI$_{50}$), it was interesting to note the presence of a low melting peak around 80°C, attributed to the fusion of PBF crystallites characterized by a low degree of perfection. In the copolymer containing equimolar amount of the two comonomeric units, the two melting peaks were overlapped because of the significant decrement in temperature of the endothermic peak at higher temperature. As far as the copolymers rich in BI co-units, (P(BF$_{20}$BI$_{80}$) and P(BF$_{30}$BI$_{70}$), the endothermic process was

characterized by the presence of a shoulder on the low temperature side, whose intensity increased with the amount of BF co-units, due to crystallization-melting-recrystallization processes occurring during the heating scan, which were typical of polyesters. P(BF$_{50}$BI$_{50}$) resulted the least crystalline among all the samples investigated, as evidenced by the lowest heat of fusion measured for this sample.
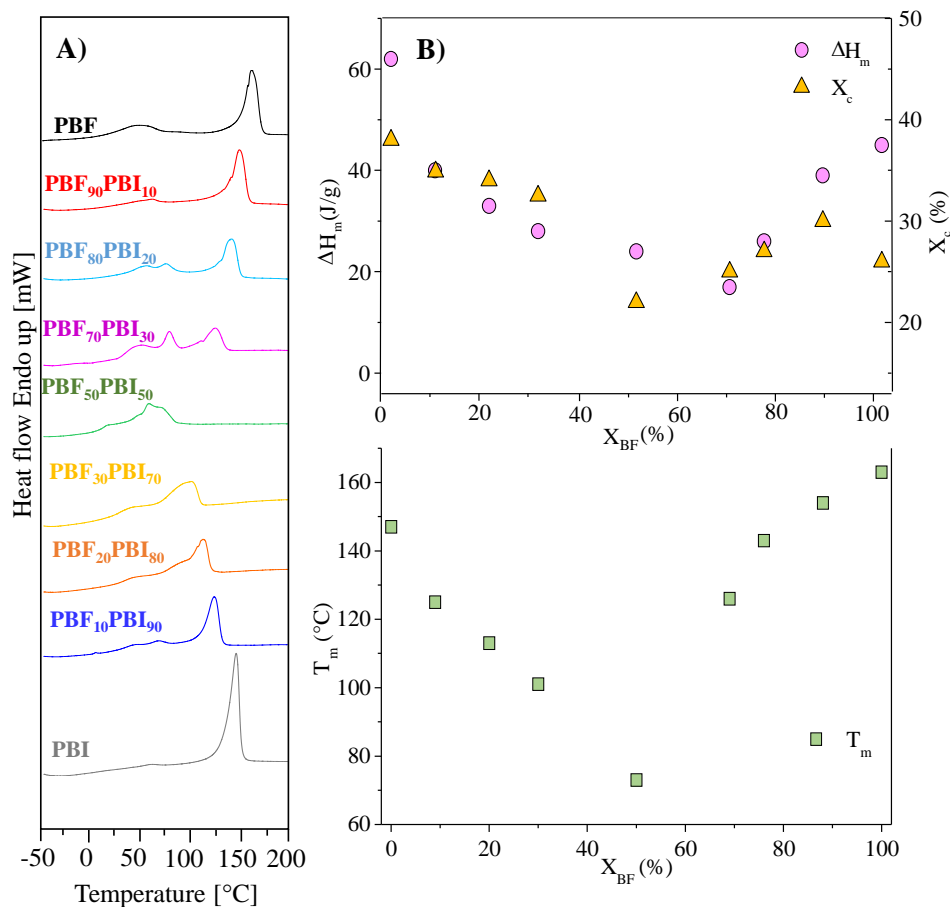
Figure 7.4: *DSC traces of PBF, PBI and P(BF$_m$BI$_n$) random copolymers as powders: a) Ist scan (heating rate: 20 °C/min) and b) melting temperature (■), heat of fusion (●) and crystallinity degree (▲) as a function copolymer composition, expressed as % molar fraction of BF.*

The values of T$_m$ and ΔH$_m$ were plotted as a function of molar fraction of BF co-unit (X$_{BF}$) in **Figure 7.4 B**. As one can see, the heat of fusion (pink circle) was characterized by a trend with a minimum at 50 mol% of BF co-unit. Differently, melting temperatures, green squares, presented a trend, describable by two independent branches. Such a trend was usual for random copolymers with both comonomer units able to crystallize, where just one, normally the more abundant co-unit, develops a crystal lattice. The non-crystallizing co-units could be included or excluded from the formed crystalline phase. In the latter case, melting point trend could be described with

exclusion model (Baur's equation). On the basis of the observed trend, it could be hypothesized that the samples rich in BF co-units crystallized according to PBF crystal structure, the BI ones being rejected in the amorphous phase. The *viceversa* occurred in case of copolymers richer in BI co-units. With the increasing of non-crystallizing co-unit percentage, in both cases, the crystalline fraction decreased (lower ΔH_m) and, at the same time, crystal perfection was missed (lower T_m).

Before checking the applicability of Baur´s equation to copolymer melting temperatures, the crystalline phase present in powder samples had been investigated by means of X-ray diffractometric analysis. **Figure 7.5** showed the diffractometric profiles of PBF, PBI and P(BF$_m$BI$_n$) copolymers.
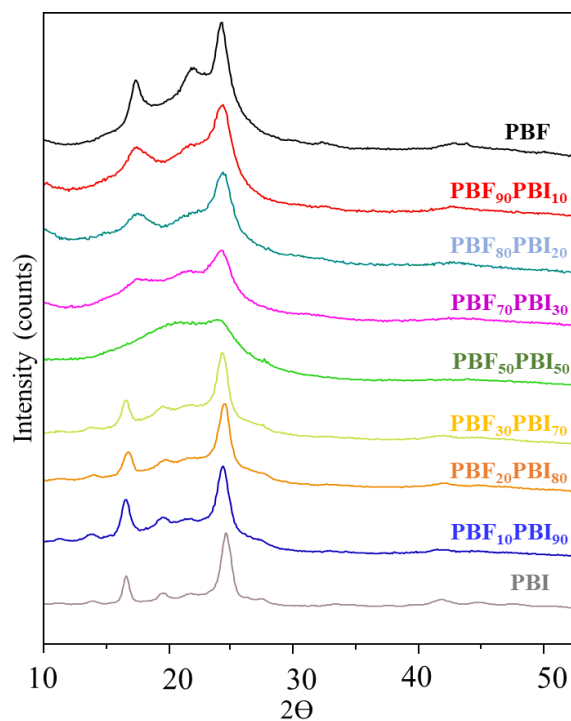
Figure 7.5*: WAXS patterns of powder PBF, PBI and P(BF$_m$BI$_n$) random copolymers.*

All the WAXS spectra were typical of semi-crystalline samples, presenting some reflections due to the crystalline fraction, superimposed on a bell-shaped halo, characteristic of the amorphous phase. As regards the two homopolymers, the WAXS spectra were in agreement with those previously determined[11,15,16]. In particular, the PBF profile was characterized by the two strong reflections (010) and (100) at 2θ values of 17.6° and 24.5°, respectively, and another one due to diagonal planes is at 22.4°[14]. PBI pattern also showed several reflections: among the others, the

two most intense were at 16.8° and 24.8°. The spectra of copolymers could be divided into two groups according to copolymer composition: in the samples rich in BF co-units (0-70 mol%), PBF-like patterns were appreciated as single crystal phase, whereas in case of those rich in BI co-units (0-70 mol%), the profile was very similar to PBI homopolymer. In all cases, diffraction peak position was invariant respect to the copolymer composition, proving the total exclusion of the amorphous co-units from the crystalline phase of PBF or PBI. On the contrary, peak width, which roughly indicated the crystal perfection (narrower the peak, higher the crystal perfection), showed an increment as the content of co-unit rose, as evidenced by **Table 7.4**.

Table 7.4*: Crystallinity index and peak width of PBF, PBI and P(BF$_m$BI$_n$) random copolymers in form of powders from XRD analysis.*

Sample	Xc %	FWHM °
PBF	24 ±2	0.9
P(BF$_{90}$BI$_{10}$)	23 ±2	1.8
P(BF$_{80}$BI$_{20}$)	21 ±2	1.9
P(BF$_{70}$BI$_{30}$)	15 ±2	2.3
P(BF$_{50}$BI$_{50}$)	8 ±2	n.d.
P(BF$_{30}$BI$_{70}$)	24 ±2	0.8
P(BF$_{20}$BI$_{80}$)	26 ±2	0.8
P(BF$_{10}$BI$_{90}$)	29 ±3	0.8
PBI	44 ±3	0.6

This broadening effect was more pronounced in samples belonging to the PBF-crystal phase set, which were also generally less crystalline respect to those belonging to PBI-crystal set containing the same amount of crystallizable co-units. P(BF$_{50}$BI$_{50}$) copolymer showed a low crystallinity that could not be easily ascribable to a specific crystal phase, since the position of the low intense and broad reflection equally fitted with the position of main peak of PBF or PBI.

WAXS data suggested the crystal phase developed in the copolymers was always unique, with the monomer units not belonging to the crystal phase remaining in the disordered phase and hampering the crystallite formation. Such disturbing effect was stronger for PBF-rich samples, in total agreement with the calorimetric results. Furthermore, the copolymer P(BF$_{50}$BI$_{50}$) turned out to be the least crystalline material of the series, as also evidenced by DSC results. From WAXS analysis the degree of crystallinity was estimated: the resulting values were collected in **Table 7.4** and plotted in **Figure 7.4 B** as a function of copolymer composition expressed as BF molar percentage.

It was interesting to note that the values of X_c were characterized by a trend similar to the fusion heats. Lastly, WAXS analysis confirmed the crystalline phase developed by each copolymer was pure, supporting exclusion model.

It was therefore expected that the melting temperature data of the copolymers were well interpolated from the Baur equation (*Eq.4*):

$$\frac{1}{T_{m,co}} = \frac{1}{T_m^0} - \left(\frac{R}{\Delta H_m^0}\right)(\ln x_c - 2x_c(1-x_c)) \qquad\qquad Eqn.\ 4$$

where $T_{m,co}$ is the experimental melting temperature of the copolymer with mole fraction x_c of the crystallizable comonomer C, T_m^0 is the equilibrium melting temperature, ΔH_m^0 is the equilibrium melting enthalpy of the homopolymer (in this case PBF or PBI), and R is the gas constant.

In **Figure 7.6**, the inverse of T_m was plotted against $-[\ln x_c - 2x_c (1-x_c)]$, where x_c is the molar fraction of the crystallizable co-unit. In panel **A**, we considered the copolymers rich in BI co-units, while in panel **B**, the inverse of melting temperatures of copolymers rich in BF co-units, together with the values of poly(butylene furanoate/diglycolate) random copolymers previously investigated were reported[11].
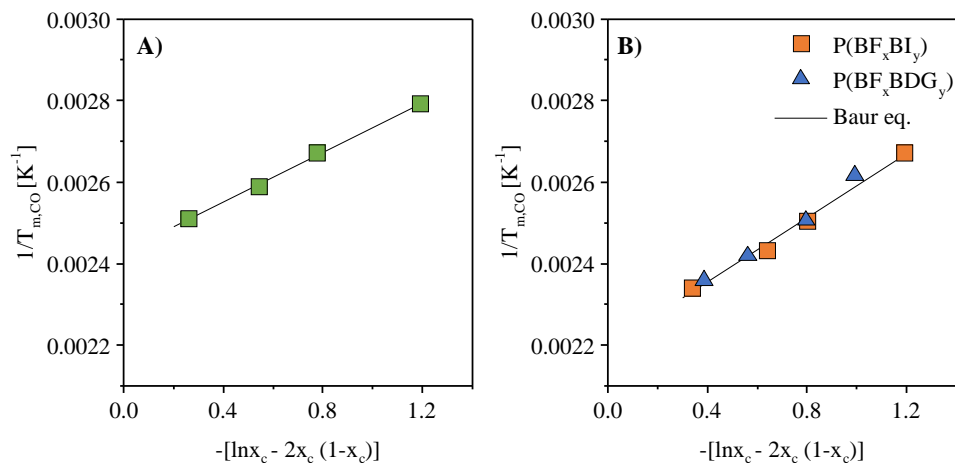
Figure 7.6: *$1/T_{m,co}$ vs. $-[\ln x_c - 2x_c (1-x_c)]$ according to Baur´s equation for **A**) PBI and **B**) and PBF.*

In both cases, the experimental data were well described by Baur´s equation (black line), confirming the exclusion model as well as the randomness nature of the synthetized copolymers. As was known, through this equation, the ΔH_m^0 and T_m^0 of PBI and of PBF could be extrapolated;

regarding PBI, T^0_m resulted 144°C while ΔH^0_m 99 J/g, in accordance with the values reported in literature[17]. In case of PBF, T^0_m was 184.5°C and ΔH^0_m 129 J/g, in good agreement with the previously reported data (T^0_m 182°C e ΔH^0_m 101 J/g)[12].

All samples were subjected to melt quenching in order to avoid development of crystals during cooling step, which affected the glass transition temperature value, acting as physical constraints. That was particularly important to investigate the trend of glass transition temperature with copolymer composition. The subsequent second DSC scans were reported in **Figure 7.7 A**.
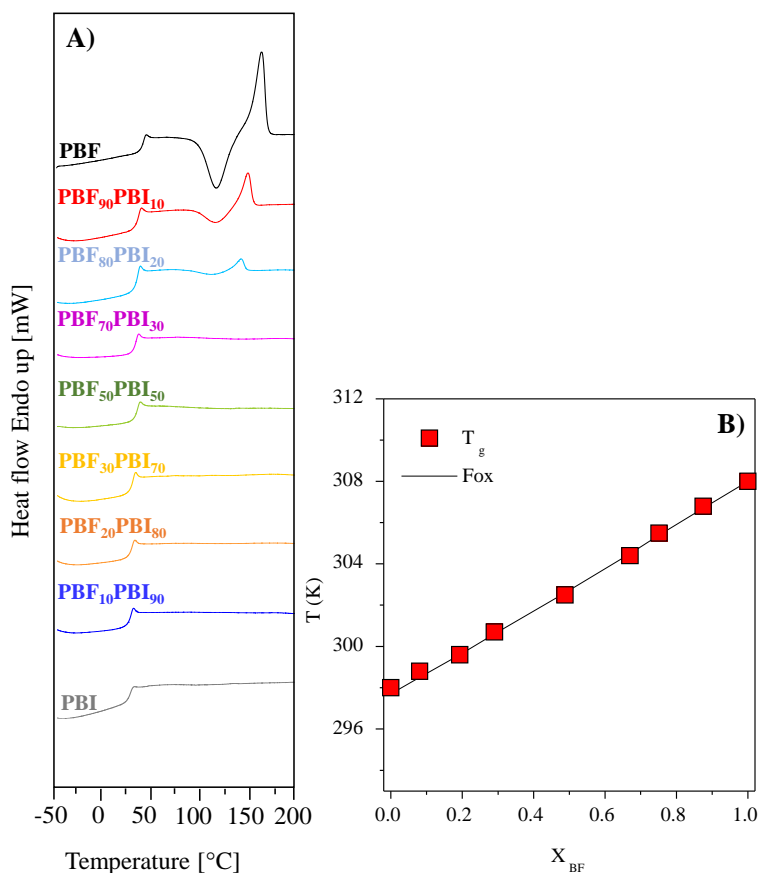
Figure 7.7*: **A)** IInd DSC scan after melt quenching for PBF, PBI and their random copolymers; **B)** T_g as a function of X_{BF} for $P(BF_mBI_n)$ random copolymers. Black line represents the theoretical Fox´s equation.*

The DSC trace of PBF homopolymer showed a cold crystallization process at around 164 °C, followed by melting phenomena at higher temperature. ΔH_c was anyway lower than ΔH_m, indicating that PBF preserved its semicrystalline nature also after melt quenching. Even $P(BF_{90}BI_{10})$ and $P(BF_{80}BI_{20})$ DSC traces showed a crystallization process during heating scan.

However, in these cases, $\Delta H_m = \Delta H_c$, indicating all the crystals melting at T_m were formed during cold crystallization. Such a behavior was typical of amorphous samples. The capability to crystallize during heating scan was further decreased with $P(BF_{70}BI_{30})$, due to the increased amount of BI co-units. The remaining samples were characterized by DSC curves showing just endothermic baseline deviation associated to the glass transition, to indicate the amorphous nature of these polymers as well as their inability to crystallize during heating scan.

The glass transition temperature value of copolymers was comprised between the T_g values of parent homopolymers, 25°C and 35°C. In particular, as evidenced by **Table 7.3**, the values of T_g decreased with increasing amount of BI co-units, which conferred higher mobility to the polymeric chains.

As known, several equations were proposed in literatures to describe the T_g trend with copolymer composition, the most simple being Fox´s equation. In **Figure 7.7 A** the values of T_g recorded during IInd scan, were plotted as a function of copolymer composition expressed as BF molar fraction (X_{BF}): as clearly shown by the **Figure 7.7 B**, Fox´s equation fitted very well the experimental data.

Lastly, compression molded films were also investigated by means of DSC and WAXS analysis (**Figure 7.8**). The resulted I^{st} DSC curves were typical of complete amorphous materials, with exception of PBF homopolymer. In detail, in most samples (PBI and copolymers containing up to 70% in mol of BF co-units) just the endothermic jump of glass transition phenomenon was observed. In case of PBF and the copolymers containing 10% and 20% of BI co-units, DSC traces showed an exothermic peak due to cold crystallization process and an endothermic one related to melting process beside glass transition phenomenon. In case of PBF, $\Delta H_c < \Delta H_m$ indicating its semicrystalline nature, while, for the two copolymers, $\Delta H_c \cong \Delta H_m$, proving the films were completely amorphous.

As regards WAXS analysis, all samples showed a no linear background due to an amorphous phase, whereas the contribution of crystalline material to the overall diffraction was evident only in PBF, in total agreement with calorimetric results.
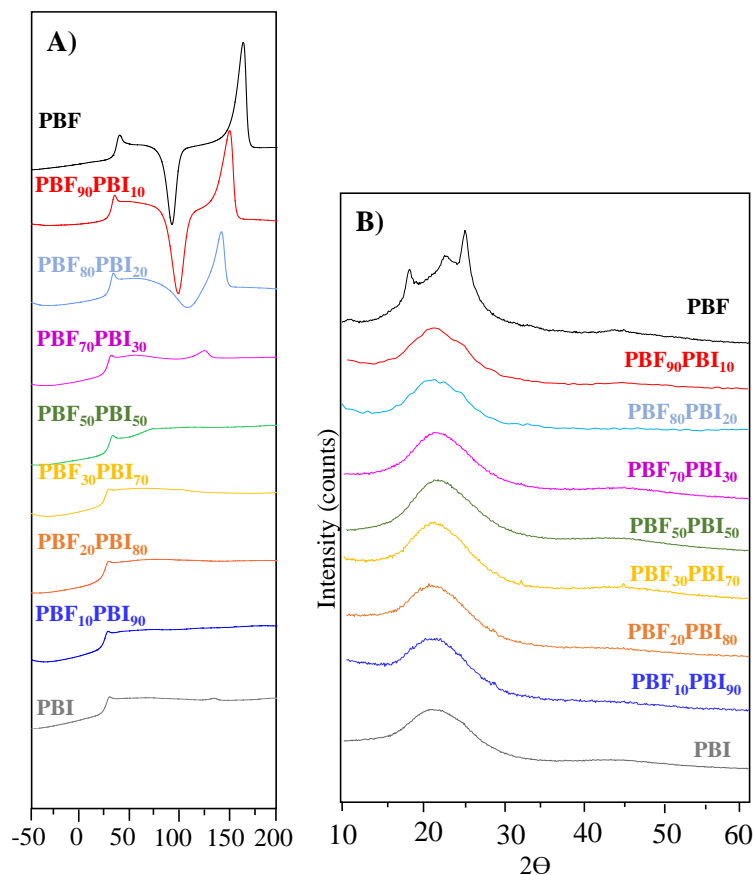
Figure 7.8: a) Ist DSC scan; b) WAXS profiles of PBF, PBI and their random copolymer compression molded films.

7.4 Mechanical properties

Mechanical performance of PBI, PBF and P(BF$_m$BI$_n$) random copolymers was evaluated subjecting rectangular shaped films to stress-strain measurements. **Table 7.5** reported the corresponding values of stress and strain at yield, σ_y e ε_y, strain at break, ε_{max} and elastic modulus, E, these last also plotted in **Figure 7.9 B**. In **Figure 7.9 A** the stress-strain curves for some samples were shown as examples.

PBF presented higher elastic modulus and lower strain at break respect to PBI, due to its crystalline nature. Specifically, PBF was a semicrystalline material with an amorphous phase in the glassy state (T$_g$= 35°C), while PBI was completely amorphous and presented a lower T$_g$ around room temperature (25°C), which implied higher chain mobility. Moreover, in case of PBF, the inter chain hydrogen bonds, due to the oxygen present in the furan ring, hampered even more the mobility of the macromolecules.

211

Table 7.5: *Mechanical characterization data of PBF, PBI homopolymers and P(BF_mBI_n)copolymers.*

Sample	σ_y MPa	ε_y %	ε_{max} %	E MPa
PBF	17±5	4±1	157±28	1289±127
P(BF$_{90}$BI$_{10}$)	66±4	4.7±0.1	80±31	1908±76
P(BF$_{80}$BI$_{20}$)	48±5	3.9±0.7	200±2	1643±147
P(BF$_{70}$BI$_{30}$)	48±4	4.0±0.5	559±18	1666±186
P(BF$_{50}$BI$_{50}$)	34±7	3±1	502±140	1386±351
P(BF$_{30}$BI$_{70}$)	20±2	2.9±0.3	668±58	1190±117
P(BF$_{20}$BI$_{80}$)	16±2	2.9±0.2	777±72	1051±102
P(BF$_{10}$BI$_{90}$)	16±2	2.6±0.1	747±53	1060±123
PBI	4.3±0.5	3.9±0.8	795±38	426
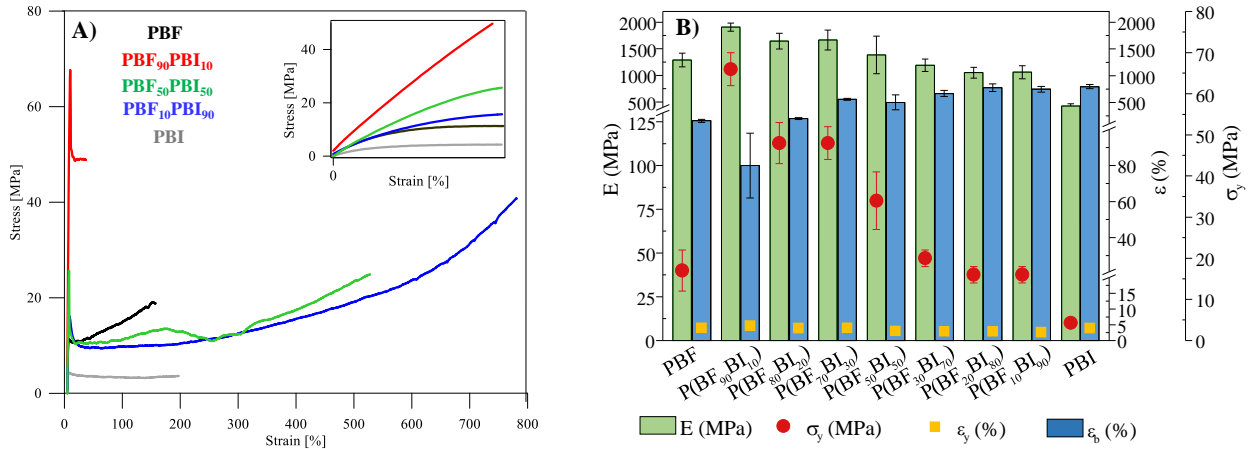
Figure 7.9: A) *Stress-strain curve of PBF (black), PBI (grey), P(BF$_{90}$BI$_{10}$) (red), P(BF$_{50}$BI$_{50}$) (green) and P(BF$_{10}$BI$_{90}$)(blu);* **B)** *mechanical data for PBF, PBI and their random copolymers*

As regarding the copolymer system P(BF$_m$BI$_n$), we observed an increasing of E and a decreasing of ε_{max} with increasing BF co-unit content, as expected on the basis of the lower flexibility of butylene furanoate comonomeric units. In detail, σ_y and E were reaching the highest values for P(BF$_{90}$BI$_{10}$) copolymer, 66 MPa e 1900 MPa respectively, while ε_{max} resulted the lowest recorded for the series. PBF homopolymer deviated from the trend observed, the elastic modulus measured being 1289 MPa and the elongation at break 157%. Such peculiar result could be explained as due to the presence in PBF of a liquid crystal phase beside the amorphous and the crystalline ones, characterized by a 2D-order and consisting of layers of partially ordered furan rings formed during compression molding and favored by the alignment of the intermolecular C−H···O bonds already present in the as-synthesized material[16]. In conclusion, copolymerization revealed to be an

efficient tool to properly tune mechanical response, simply playing on copolymer composition: it was worth noting that the presence of BI comonomeric units along PBF macromolecules chains ensured good elastic modulus and stress resistance values with improved tough behaviour and high deformation capability.

7.5 Barrier properties

The permeability tests were conducted at 23°C using both dry and humid gases (O_2 and CO_2). The experimental data were collected as Gas Transmission Rate (GTR), in **Table 7.6**, and reported in **Figure 7.10 A** and **B** for PBI and PBF homopolymers and for some copolymers.

Table 7.6: GTR values for PBF, PBI homopolymers and for some $P(BF_mBI_n)$ copolymers.

Sample	GTR 23 °C; 0%RH cm^3 cm/m^2 d atm		GTR 23 °C; 85%RH cm^3 cm/m^2 d atm	
	O_2	CO_2	O_2	CO_2
PBF	0.1	0.19	0.032	0.024
$P(BF_{90}BI_{10})$	0.22	0.36	0.0028	0.0069
$P(BF_{80}BI_{20})$	0.30	0.28	0.0025	0.0025
$P(BF_{50}BI_{50})$	0.34	0.62	0.002	0.007
$P(BF_{20}BI_{80})$	0.08	0.070	0.0025	0.0023
$P(BF_{10}BI_{90})$	0.0042	0.0043	0.0019	0.0025
PBI	0.0029	0.0038	0.03	0.028

PBF as well as PBI were characterized by very low GTR values to both gases (oxygen and carbon dioxide), in dry and humid conditions. Such very good performances could be surely correlated in both cases to the hindering of ring flipping and the limited subglass local dynamics evidenced by structural and dynamical studies[18–21]. Moreover, it was worth noting in both polyesters the presence of stiff units, as furan ring in PBF and isophthalic one in PBI, alternated to a flexible moiety. The alternation of rigid segments, acting as mesogenic units, and flexible ones was the necessary requirement for possible formation of 1D/2D ordered phase, so called mesophase, characteristic of polymeric liquid crystals, which, as known, were the most gas barrier performant polymers, among those currently used. As to furan-based polyesters, mesophase's existence was experimentally proved[16,22], while in case of PBI such phase, arising presumably from the π-π

213

stacking of aromatic rings were not detected by any technique so far. However, comparing the gas barrier performances of the two homopolymers, one can see PBI boasted a permeability to the oxygen and carbon dioxide, respectively 34 and 51 times lower respect those of PBF. Considering the amorphous semimobile nature of PBI (its T_g was indeed recorded at 25°C), on one side, and the semicrystalline and glassy state of PBF, on the other, the result was pretty surprising and unexpected. However, it was well known that interphases (so called disclinations) between meso- and crystal phases represented channels for the preferential passage of gases. The result could be therefore explained considering the presence in PBF of higher disclination content. Lastly, studies carried out during the PhD Thesis at laboratories of Halle University under the supervision of Dr. Androsch (see Paragraph 5.6 of Chapter IV) showed the occurrence in PBI of a fast densification process of amorphous phase at 25°C (note that T_g of PBI was located at room temperature), which brought to a reduction of its free volume and consequently to outstanding gas barrier properties.

From the data collected in **Table 7.6** and reported in **Figure 7.10 A** and **B**, it could be noted how gas barrier performances of PBI and PBF changed differently due to humidity (85% RH). As well know, H_2O molecules dispersed in a polymer matrix could exert two main effects: on one side, water had a plasticizing action, on the other, depending on the macromolecular structure, it could also physically interact with the polymer chains by H-bonds. Under humid conditions, PBF gas barrier properties improved by about a factor 10, thus, it could be supposed water molecules strengthen the hydrogen bonds present among the macromolecular chains, which favor the mesophase formation. On the contrary, in case of PBI, the plasticizing effect prevailed, causing a worsening of barrier performance as indicated by the increasing of gas permeability (of one order of magnitude).

As far as copolymers were concerned, the observed trend could be explained dividing the copolymers into two groups, the first formed by copolymers with BF co-unit content ranging from 90 to 50 mol%, the second by those rich in BI co-units (P(BF$_{10}$BI$_{90}$) and P(BF$_{20}$BI$_{80}$)).

Regarding the first group, no dramatic worsening of the barrier performances respect to PBF homopolymer was observed. The slight increase in GTR values with the increment of BI unit content could be ascribed to two main reasons: *i)* amorphous nature of the copolymers (PBF was on the contrary semicrystalline); *ii)* copolymer amorphous phase characterized by an increased free volume fraction (in fact, T_g regularly decreased with increasing BI co-unit content). Passing

214

from the PBF homopolymer to the copolymer containing equimolar quantities of the two comonomeric units, in fact, about tripled permeability values were measured. In the case of the two copolymers rich in BI co-units, it had noted that $P(BF_{10}BI_{90})$ copolymer was characterized by gas barrier properties similar to those of PBI, while $P(BF_{20}BI_{80})$ copolymer was markedly more permeable to both gases (GTR values increased by one order of magnitude). An increase in T_g value was indeed observed as the amount of BF present in macromolecular chain increases, which made the densification process kinetically slower. As proof of this, the gas barrier performances of the equimolar copolymer ($P(BF_{50}BI_{50})$) were the worst among the samples studied
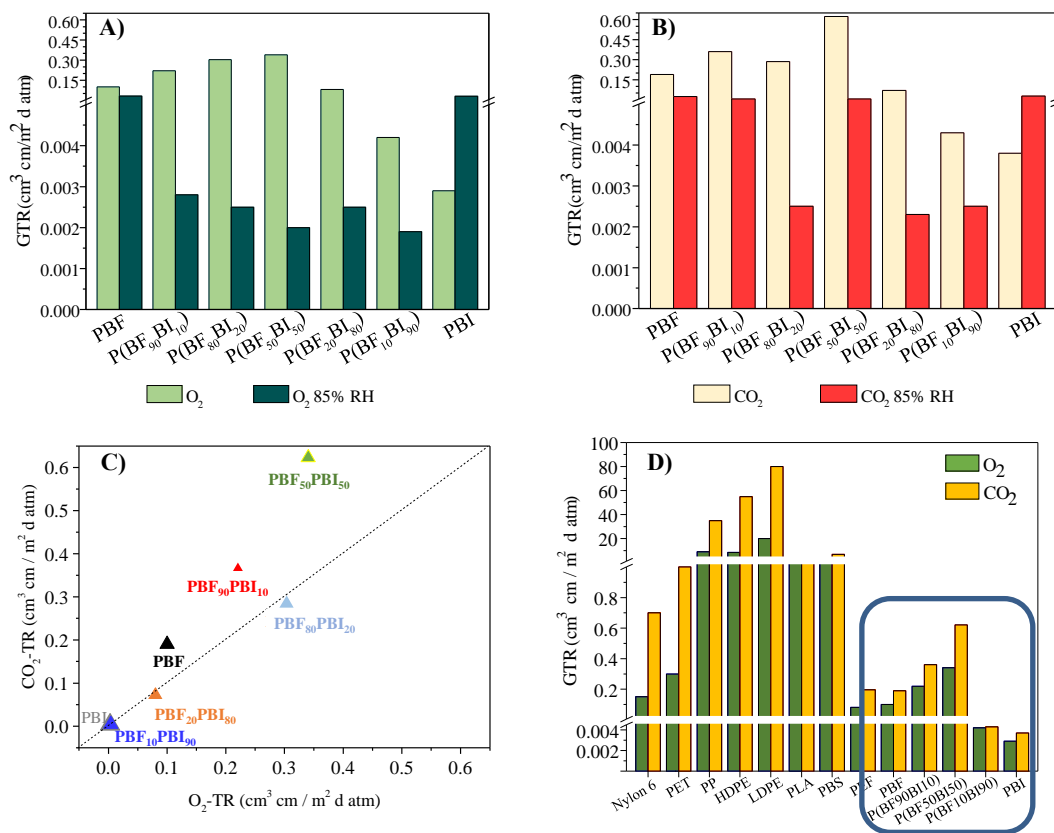
Figure 7.10: ***A)*** *GTR values for PBI, PBF and some of their random copolymers to dry and humid (85% RH) oxygen and **B)** to dry and humid (85% RH) carbon dioxide; **C)** perm-selectivity ratio for PBI, PBF and some of their random copolymers; **D)** comparison among GTR values of the most common polymers used for food packaging applications, and those of PBI and PBF homopolymers and $P(BF_{90}BI_{10})$, $P(BF_{50}BI_{50})$ and $P(BF_{10}BI_{90})$ random copolymers.*

As regards the effect of humidity on gas barrier performances of copolymers, in all cases, a behavior similar to PBF was observed, with the exception of the copolymer containing the lowest

amount of BF co-units (P(BF$_{10}$BI$_{90}$)). The presence of the furan ring up to 20 mol% guaranteed the formation of hydrogen bonds, strengthened by the water molecules that were arranged as a bridge between the polymeric chains, significantly improving (up to two orders of magnitude) the barrier properties to both gases. In the copolymer containing only 10 mol% of BF co-units, the barrier properties remained practically constant, due probably to low amount of H-bonds.

In **Figure 10 C** GTR values to carbon dioxide were shown as a function of GTR data to oxygen in order to evaluate the perm-selectivity ratio. For all the samples under investigation, the perm-selectivity ratio was found close to 1, indicating a good solubility of carbon dioxide in polymer matrix, which counterbalances the higher diffusion rate of CO_2 gas molecules with respect to oxygen ones, due to their larger size. The P(BF$_{50}$BI$_{50}$) copolymer deviated from the observed trend, being characterized by a doubled perm-selectivity ratio ($\approx$ 1.8). Such result was probably correlated to its worst barrier properties that determined the faster passage of the gas with the highest diffusion rate (carbon dioxide).

Lastly, as shown in **Figure 7.10 D**, the GTRs of the studied samples have been compared to those of the most common fossil-based commercial materials employed in food packaging, such as PET, polyolefins and Nylon; the comparison was extended to some bioplastics, including PLA, PBS and PEF. As you can see, all the investigated polymers presented significantly better performances with respect to traditional polymers as well as some bioplastics (PLA and PBS). In particular, PBI and P(BF$_{10}$BI$_{90}$) boasted also lower GTR values compared to PEF, the most investigated, also from the industrial companies, furan-based polyester for sustainable food packaging.

7.6   Conclusions

The copolymeric system object of the present study represented a smart solution to minimize the production of plastic waste produced by food packaging - hardly recyclable due to contamination by organic matter and film multilayer structure- and to reduce the consumption of raw materials. All the material synthesized were characterized by high thermal stability, crucial property during polymer processing. Moreover, suitable mechanical properties for the realization of flexible films and outstanding barrier properties to both oxygen and carbon dioxide, which were maintained even in presence of humidity, were observed.

Copolymerization revealed to be a winning strategy to optimize the final polymer properties, since permitted to prepare a wide plethora of new 100% bio-based polymers with properties finely adjustable simply by changing copolymer composition, starting from two fully bio-based polyesters with outstanding mechanical and barrier properties.

7.7 Bibliography

1. Association of Plastics manifacturors. Plastics -The facts 2018. *Plast. Eur.* 1–57 (2018). doi:10.1016/j.marpolbul.2013.01.015

2. Andrady, A. L. Microplastics in the marine environment. *Mar. Pollut. Bull.* **62**, 1596–1605 (2011).

3. Kohli, K., Prajapati, R., Sharma, B. K. Bio-based chemicals from renewable biomass for integrated biorefineries. *Energies* **12**, (2019).

4. He, Y. C., Wu, Y. D., Pan, X. H., Ma, C. L. Biosynthesis of terephthalic acid, isophthalic acid and their derivatives from the corresponding dinitriles by tetrachloroterephthalonitrile-induced Rhodococcus sp. *Biotechnol. Lett.* **36**, 341–347 (2014).

5. Frost, J. W. Synthesis of biobased and substituted terephthalic acids and isophthalic acids. 5–6 (2016).

6. Harry Yim, Robert Haselbeck, Wei Niu, Catherine Pujol-Baxley, Anthony Burgard, Jeff Boldt, Julia Khandurina, John D Trawick, Robin E Osterhout, Rosary Stephen, Jazell Estadilla, Sy Teisan, H Brett Schreyer, Stefan Andrae, Tae Hoon Yang, Sang Yup Lee, M. J. B Metabolic engineering of Escherichia coli for direct production of 1,4-butanediol. *Nat. Chem. Biol.* **7**, 445–452 (2011).

7. Forte, A., Zucaro, A., Basosi, R., Fierro, A. LCA of 1,4-butanediol produced via direct fermentation of sugars from wheat straw feedstock within a territorial biorefinery. *Materials (Basel).* **9**, 1–22 (2016).

8. Burgard, A., Burk, M. J., Osterhout, R., Van Dien, S., Yim, H. Development of a commercial scale process for production of 1,4-butanediol from sugar. *Curr. Opin. Biotechnol.* **42**, 118–125 (2016).

9. Gandini, A. The irruption of polymers from renewable resources on the scene of macromolecular science and technology. *Green Chem* **13**, (2011).

10. Gomes M., Gandini, A. Synthesis and characterization of poly(2,5-furan dicarboxylate)s based on a variety of diol,". *J. Polym. Sci. Part APolymer Chem.* **49**, 3759–3768 (2011).

11. Soccio, M.; Costa, M.; Lotti, N.; Gazzano, M.; Siracusa, V.; Salatelli, E.; Manaresi, P.; Munari, A. Novel fully biobased poly(butylene 2,5-furanoate/diglycolate) copolymers containing ether linkages: Structure-property relationships. *Eur. Polym. J.* **81**, 397–412 (2016).

12. P apageorgiou, G. Z.; Tsanaktsis, V.; Papageorgiou, D. G.; Exarhopoulos, S.; Papageorgiou, M.; Bikiaris, D. N.. Evaluation of polyesters from renewable resources as alternatives to the current fossil-based polymers. Phase transitions of poly(butylene 2,5-furan-dicarboxylate). *Polymer (Guildf).* **55**, 3846–3858 (2014).

13. Ma, J., Yu, X., Xu, J., Pang, Y. Synthesis and crystallinity of poly(butylene 2,5-furandicarboxylate). *Polymer (Guildf).* **53**, 4145–4151 (2012).

14. Zhu, J.; Cai, J.; Xie, W.; Chen, P. H.; Gazzano, M.; Scandola, M.; Gross, R. A. Poly(butylene 2,5-furan dicarboxylate), a biobased alternative to PBT: Synthesis, physical properties, and crystal structure. *Macromolecules* **46**, 796–804 (2013).

15. Morales-Huerta, J. C., de Ilarduya, A. M., Muñoz-Guerra, S. Partially renewable poly(butylene 2,5-furandicarboxylate-co-isophthalate) copolyesters obtained by ROP. *Polymers (Basel).* **10**, (2018).

16. Guidotti, G.; Soccio, M.; García-Gutiérrez, M. C.; Ezquerra, T.; Siracusa, V.; Gutiérrez-Fernández, E.; Munari, A.; Lotti, N. Fully Biobased Superpolymers of 2,5-Furandicarboxylic Acid with Different Functional Properties: From Rigid to Flexible, High Performant Packaging Materials. *ACS Sustain. Chem. Eng.* **8**, 9558–9568 (2020).

17. Lotti, N., Finelli, L., Munari, A., Siracusa, V. Melting behavior and crystallization kinetics of sulfonated poly(butylene isophthalate). *Polym. Eng. Sci.* **42**, 1590–1599 (2002).

18. Soccio, M.; Martínez-Tong, D. E.; Guidotti, G.; Robles-Hernández, B.; Munari, A.; Lotti, N.; Alegria, A. Broadband dielectric spectroscopy study of biobased poly(alkylene 2,5-furanoate)s' molecular dynamics. *Polymers (Basel).* **12**, 1–16 (2020).

19. Kotek, R., Pang, K., Schmidt, B., Tonelli, A. Synthesis and gas barrier characterization of poly(ethylene isophthalate). *J. Polym. Sci. Part B Polym. Phys.* **42**, 4247–4254 (2004).

20. Soccio, M., Martínez-Tong, D. E., Alegría, A., Munari, A., Lotti, N. Molecular dynamics of fully biobased poly(butylene 2,5-furanoate) as revealed by broadband dielectric spectroscopy. *Polymer (Guildf).* **128**, 24–30 (2017).

21. Genovese, L.; Soccio, M.; Lotti, N.; Munari, A.; Szymczyk, A.; Paszkiewicz, S.; Linares, A.; Nogales, A.; Ezquerra, T. A. Effect of chemical structure on the subglass relaxation dynamics of biobased polyesters as revealed by dielectric spectroscopy: 2,5-furandicarboxylic acid vs. trans -1,4-cyclohexanedicarboxylic acid. *Phys. Chem. Chem. Phys.* **20**, 15696–15706 (2018).

22. Guidotti, G.; Soccio, M.; García-Gutiérrez, M. C.; Gutiérrez-Fernández, E.; Ezquerra, T. A.; Siracusa, V.; Munari, A.; Lotti, N. Evidence of a 2D-Ordered Structure in Biobased Poly(pentamethylene furanoate) Responsible for Its Outstanding Barrier and Mechanical Properties. *ACS Sustain. Chem. Eng.* **7**, 17863–17871 (2019).

8 SYNTHESIS AND CHARACTERIZATION OF POLY(ALKYLENE1,4-CYCLOHEXANEDICARBOXYLATE): INFLUENCE OF THE GLYCOL LENGTH ON BIODEGRADABILITY, MECHANICAL AND BARRIER PROPERTIES

8.1 Introduction

In the last years, the interest around poly(alkylene 1,4-cyclohexanedicarboxilate)s has increasing due to the possibility to avoid the use of not degradable terephthalic-based polymers, produced from fossil sources. In order to increase the knowledge on this family, the present research was focused on the synthesis and characterization of four homopolymers obtained from 1,4-cyclohexane dicarboxylic acid and diols with different length:

- ➢ PPCE: Poly(propylene 1,4-cyclohexanedicarboxylate)
- ➢ PBCE: Poly(butylene1,4-cyclohexanedicarboxylate)
- ➢ PPeCE: Poly(pentamethylene 1,4-cyclohexanedicarboxylate)
- ➢ PHCE: Poly(hexamethylene 1,4-cyclohexanedicarboxylate)

Currently, 1,4-cyclohexane dicarboxylic acid is derived from petroleum sources, but different studies report the possibility to produce it by reduction of bio-based terephthalic acid, starting from limonene and other terpenes[1]; while the diols employed are obtainable from biomass, such as corn. As a consequence, poly(alkylene 1,4-cyclohexanedicarboxilate)s can be considered as fully sustainable materials. Some of the poly(alkylene 1,4-cyclohexanedicarboxilate)s investigated, in particular, poly(propylene 1,4-cyclohexanedicarboxylate) (PPCE) and poly(butylene-1,4-cyclohexanedicarboxylate (PBCE) have already been studied from our research group[2–6].

In the present work, they were compared with two new homopolymers poly(pentamethylene 1,4-cyclohexanedicarboxylate) (PPeCE) and poly(hexamethylene 1,4-cyclohexanedicarboxylate) (PHCE). These were fully characterized from the molecular (^{1}H-NMR, GPC), thermal (MT-TGA, DSC, FSC) and structural (WAXS) point of view. In details, MT-TGA and FSC measurements were conducted with the collaboration of Professor Antonella Esposito, of the University of Rouen (FR); the so-obtained thermal data were employed to make detailed investigation on the thermal behaviour of the synthetized materials. Moreover, mechanical performance and barrier properties of all the series were studied to test their suitability for packaging applications. Lastly, composting

experiments were carried out, to check their potential biodegradability. The so-obtained results were correlated to chemical structure, i.e. to glycol sub-unit length, to establish structure-property relationship.

8.2 Molecular characterization

The synthesized materials were firstly checked by ^{1}H-NMR spectroscopy in order to verify the chemical structure and the *cis* isomer content. The spectra reported just the expected signals, suggesting no side reactions occurred during polycondensation process. In **Figure 8.1**, as example, the ^{1}H-NMR spectrum of PHCE with the relative peak assignments was shown.
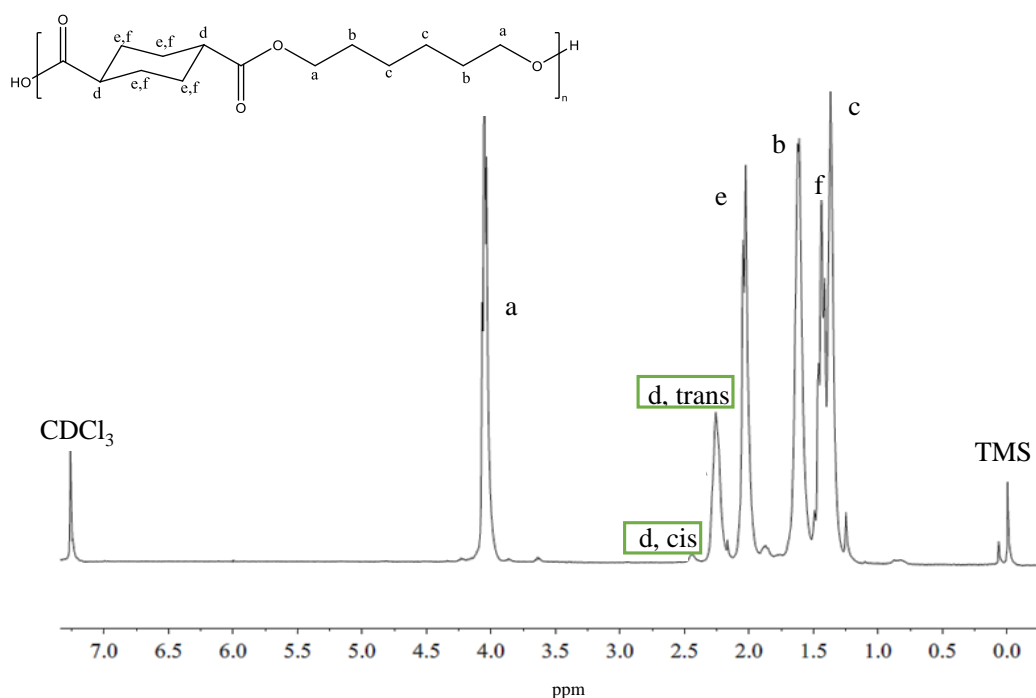
Figure 8.1:^{1}H-NMR spectrum of PHCE and the relative peak assignment.

At 4.05, 1.62 and 1.43 ppm a, b and c protons of glycol subunit, respectively, were resonating. As concerns the cyclohexane ring, the axial and equatorial protons, e and f, were located at 2.05 and 1.40 ppm, respectively. Moreover, d protons were represented by two different signals ascribed to the two possible isomeric forms: the peak at 2.28 ppm was due to the *trans* isomer, and the second one at 2.44 ppm, was attributed to the *cis* isomer.

^{1}H-NMR spectra recorded for the other poly(alkylene 1,4-cyclohexanedicarboxylates)s synthesized agreed with the predicted structure. The characteristic peaks were listed here below.

220

PPCE ^{1}H-NMR (CDCl$_3$, 400MHz, ppm): 4.10 (4H, m); 2.30 (2H, s); 2.05 (4H, m); 1.43 (4H, m); 1.90 (2H, m); 1.47 (4H, m).

PBCE ^{1}H-NMR (CDCl$_3$, 400MHz, ppm): 4.10 (4H, m); 2.28 (2H, s); 2.05 (4H, m); 1.60 (4H, m); 1.43 (4H, m).

PPeCE ^{1}H-NMR (CDCl$_3$, 400MHz, ppm): 4.10 (4H, m); 2.28 (2H, s); 2.05 (4H, m); 1.60 (4H, m); 1.47 (2H, m); 1.40 (4H, m).

The relative integral of *cis* d protons and *trans* d protons were employed to evaluate the abundance of the isomers. The results were reported in **Table 8.1**, where a slight increase of *cis* isomer compared with the feed (4 mol%) was observed and attributed to the high temperatures employed during polycondensation necessary for obtaining high molecular weight polymers, but also causing a certain degree of isomerization. The *cis/trans* ratio had a strong impact on the final properties of the material, for example barrier performance and mechanical behavior were deeply influenced by this factor. Thus, the control of the relative amount of the two isomers was crucial to obtain the performance wanted.

In **Table 8.1** the molecular weight (M_n) and polydispersity index (D) for all the synthetized polyesters were reported. As one can see, the high values of M_n accompanied by D indexes close to 2 resulted from GPC analysis, suggested a good control of the overall polymerization process.

Table 8.1: Molecular characterization data of the synthetized polyesters.

Sample	*cis* %	M_n Da	D
PPCE	10	46200	1.8
PBCE	11	57100	2.3
PPeCE	8	34000	2.1
PHCE	6	50700	2.3

8.3 Thermal characterization

8.3.1 Modulated-Temperature Thermogravimetric Analysis (MT-TGA)

Figure 8.2 A illustrated the degradation process recorded with MT-TGA, where mass loss was reported as a function of temperature. Here, the specific thermal stability was estimated by considering the temperature at which 5% of weight loss was reached, $T_{95\%}$, while the temperature

of maximum rate of degradation, T_{max}, associated with the maximum mass loss[7–9], was reported in **Figure 8.2 B** as the maximum of the derivative peak.
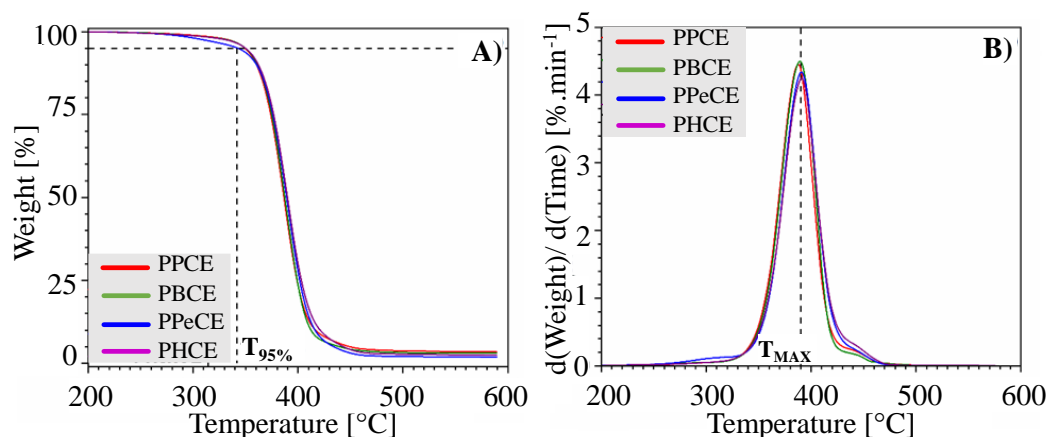
Figure 8.2*: **A)** Curves recorded by MT-TGA from room temperature to 600°C (modulation amplitude of ± 5K, heating rate of 2 K min⁻¹ and an oscillation period of 60s) for each sample. $T_{95\%}$ is the temperature at which a weight loss of 5% is occurring; **B)** derivative MT-TGA curves evidending the temperature of maximum rate of weight loss (T_{max}). Up to 200 °C no appreciable variations have been detected.*

The values obtained were listed in **Table 8.1.** showing that, under the measuring conditions, the CEDA-based polyesters with different linear diols presented one main degradation step and had a similar thermal stability, since this parameter was not affected by different lengths of the linear alkyl segment in the repeating unit. This was an unexpected results considering the literature, where one can find several examples of polyesters presenting thermal stability dependent on the length of the glycolic subunit[10,11]. The data reported in **Table 8.2** were also employed to calculate the activation energy of the main degradation process using a model-free method[7,10]. The value obtained were similar and in line with the T_{max} results, with no influence of the chemical structure of the repeating unit.

Table 8.2*: Parameters obtained by MT-TGA analysis associated with thermal degradation.*

Sample	$T_{95\%}$ °C	T_{max} °C	E_a kJ mol⁻¹
PPCE	349 ± 1	388 ± 1	187 ± 4
PBCE	350 ± 1	389 ± 1	183 ± 6
PPeCE	342 ± 1	390 ± 1	183 ± 10
PHCE	350 ± 1	391 ± 1	182 ± 7

8.3.2 Differential Scanning Calorimetry (DSC)

DSC analysis was conducted in order to evaluate the thermal behavior of the filmed samples. At a first sight, all the synthetized samples resulted semicrystalline materials, due to the presence of melting phenomenon above glass transition.

More in detail, in the Ist scan (**Figure 8.3 A**), PPCE showed an endothermic baseline deviation around 10 °C due to the glass to rubber transition followed by two endothermic peaks at higher temperature, attributed to melting of crystalline phase.
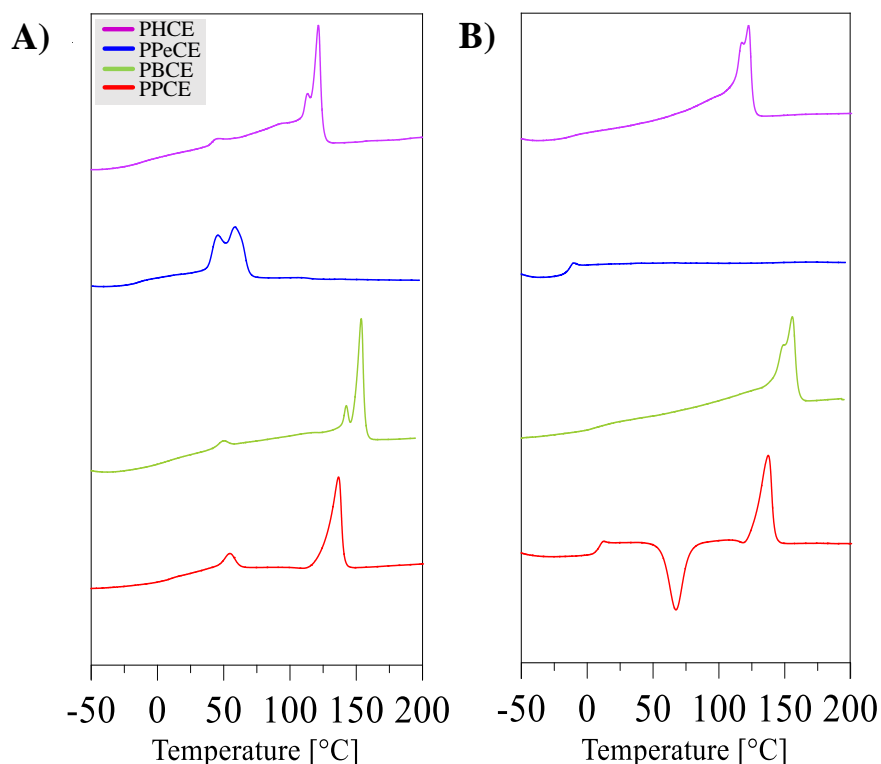
Figure 8.3. A) DSC scans recorded upon heating at 20 K/min; DSC scan at 20 K/min after cooling at 100 K/min.

After quenching (**Figure 8.3 B**), the glass transition was located at 9°C; then an exothermic inflection of the trace was observed at 68°C, corresponding to a cold crystallization, and a sharp endothermic peak at 137°C was observed, due to the PPCE crystal melting. Being $\Delta H_{cc} \approx \Delta H_m$, PPCE could be considered in a fully amorphous state. As concern PBCE and PHCE, the DSC curves obtained in Ist and IInd scan were pretty similar, being both characterized by the presence of a double endothermic peak attributed to the melting of crystalline phase. Glass transition was beardly visible, due to the high crystallinity degree that persisted even after rapid cooling from the

melt. This result indicated the higher crystallization rate of PBCE and PHCE with respect to PPCE. In case of PPeCE, the Ist scan showed, together with the glass to rubber transition step, a double endothermic peak corresponding to the melting of crystalline phase. This multiple melting peak was located at low temperature (around 50°C), indicating a defective crystalline population. The multiple melting peaks usually observed in polyesters could be correlated to *i)* melting-crystallization-remelting processes occurring during the heating scan and/or *ii)* presence of different ordered phases. Further analyses were necessary to clarify the origin of the phenomenon observed in our samples. After quenching, just an endothermic baseline deviation corresponding to glass transition could be observed for PPeCE. As happened for PPCE, fast cooling allowed to avoid crystallization obtaining a 100% amorphous material, as confirmed by the IInd scan (**Figure 8.3 B**).

A comparison of the thermal properties of the polymers under study was made in order to evaluate the effect of glycol sub-unit length on their thermal behaviour. The samples containing even number of methylene groups in the glycol sub-unit were characterized by a melting peak located at higher temperature. A more perfect and, considering the higher energy to complete the melting, more abundant crystalline phase could be supposed for PBCE and PHCE compared with PPCE and PPeCE, these last containing an odd number of -CH$_2$- groups in the glycol sub-unit. Moreover, the melting process position evidenced an odd-even effect on the crystallizing ability. In case of methylene odd numbered samples, as PPCE and PPeCE, the cooling rate of 100 K/min led to a completely amorphous material, since their ability to crystalize could be more easily inhibited. Differently, PBCE and PHCE were able to arrange in crystal structures during cooling, as confirmed by **Figure 8.3 B**.

Table 8.3: *Thermal and structural characterization data derived from DSC and WAXS analyses on the synthetized samples.*

Samples	WAXS	DSC							
		Ist SCAN				IInd SCAN			
	χ_c %	T_m °C	ΔH_m J g^{-1}	T_g °C	ΔC_p J g^{-1}K^{-1}	T_{cc} °C	ΔH_{cc} J g^{-1}	T_m °C	ΔH_m J g^{-1}
PPCE	20	136	30	8	0.294	68	27	137	28
PBCE	30	157	36	7	0.209	-	-	156	36
PPeCE	18	58	28	-13	0.236	-	-	-	-
PHCE	36	119	45	-12	0.158	-	-	120	40

As regards T_g, a decreasing trend, ranging from 10°C for PPCE to -12°C for PHCE, was reported (see **Table 8.3**). In particular, T_g progressively reduced with the number of -CH$_2$- groups per repeat unit: such trend could be explained on the basis of an increment of chain flexibility. As a matter of fact, the higher the number of methylene groups in the polymeric chain, the lower the concentration of the stiffer ester groups (-CO-OR-). In this way, the polymeric chain was more flexible and thus T_g decreased. Looking into more detail the data, PPCE and PBCE on one side and PPeCE and PHCE on the other, had the same T_g value, but one must consider the latter polymer of each pair was semicrystalline and, as well known, crystallites acted as physical crosslinks moving T_g towards higher temperature with respect to the fully amorphous sample.

8.3.3 Fast Scanning Calorimetry (FSC)

Considering the results obtained with DSC, FSC measurements (**Figure 8.4**) were employed to completely quench crystallization process of PBCE and PHCE. This technique allowed to obtain completely amorphous samples, thanks to the higher cooling rates allowed, applied on much smaller and thinner samples[12].
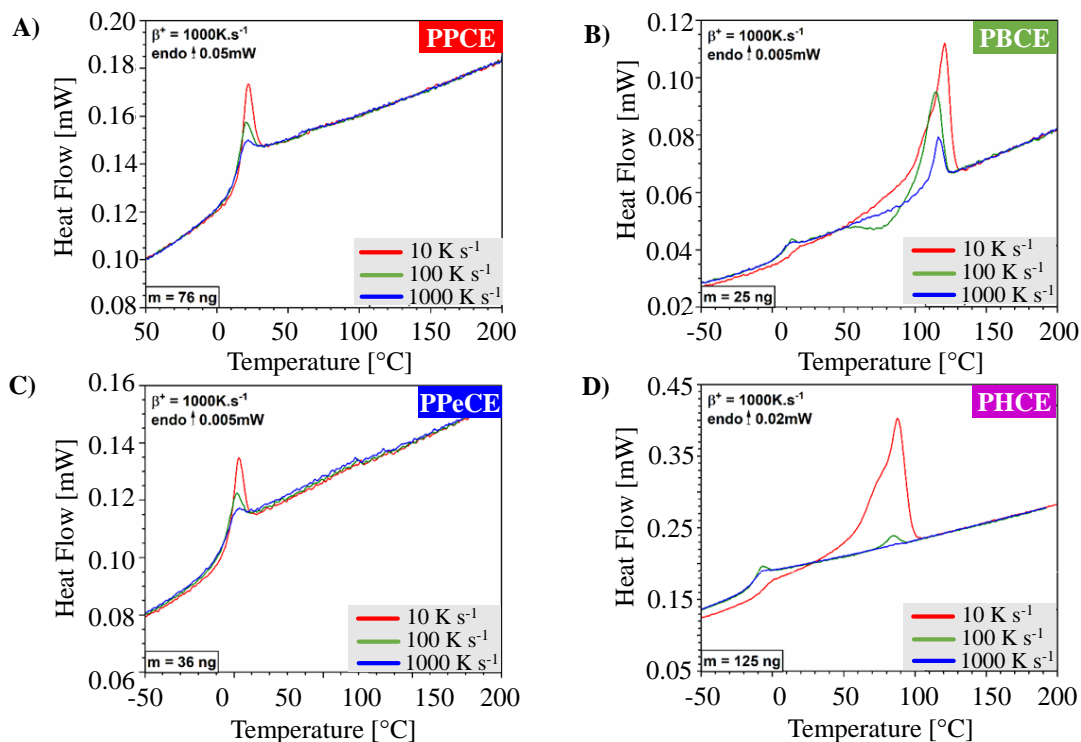
Figure 8.4*: FSC curves recorded for each sample with a heating rate of 1000 K/s after quenching at different cooling rates (10 K/s, 100 K/s, 1000 K s).*

During the test, the samples were heated until melting at 1000 K/s, then different cooling rates, from 10 to 10 000 K/s, were applied. In case of PPCE and PPeCE (**Figure 8.4 A** and **Figure 8.4 C**) the experiments were also conducted for confirmation; indeed, for these samples, a cooling rate of 10 K/s led to complete suppression of the crystalline phase. Also, the increasing of heating scan rate (1000 K/s) for both the samples avoided endothermic and/or exothermic processes, above the glass transition temperature, suggesting a suppression of the cold-crystallization and the subsequent melting processes. Different was the behavior for the samples containing an even number of methylene units. In case of PHCE (**Figure 8.4 D**) a fully amorphous nature was reached with the highest cooling rate; while PBCE (**Figure 8.4 B**), even at 10000 K/s, was still able to crystallize during cooling.

Therefore, a different test was conducted on PBCE in order to reach the amorphous status; by cooling at 1000 K/s and subsequently heating at 3000 K/s, it was possible to suppress the formation of crystalline phase, as showed in **Figure 8.5**.

The different behavior reported for PPCE, PBCE, PPeCE and PHCE, underlined the importance of controlling the cooling rate in order to obtain materials with different molecular mobility, microstructure and aptitude to crystallize, (maximum crystallinity degree and crystallization kinetics).
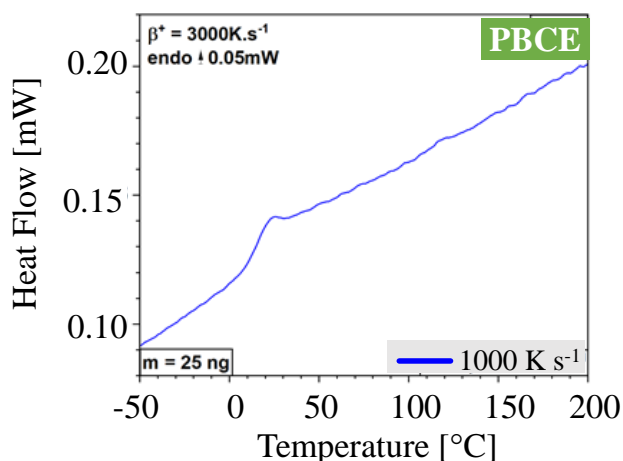
Figure 8.5*: FSC curve for PBCE (heating rate of 3000 K s^{-1}) after cooling at 1000 K s^{-1}.*

8.4 Structural characterization

Wide angle X-ray scattering, WAXS, was conducted as reported in "Method and Materials" section. The obtained profiles of PPCE, PBCE, PPeCE and PHCE polymers were reported in **Figure 8.6**, while the relative values of crystallinity degree, χ_c, were reported in **Table 8.3**.
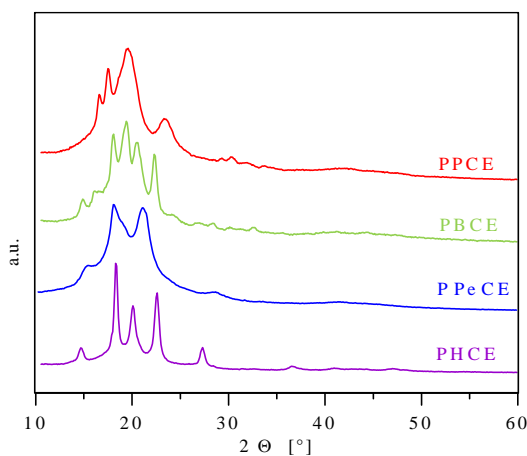
Figure 8.6: Diffraction profile recorded for the poly(alkylene 1,4-cyclohexanedicarboxylate)s synthetized.

As regards PPCE and PPeCE, constituted by an odd number of methylene units, the WAXS patterns were characterized by broad peaks, due to small and defective crystalline phase. On the other hand, the samples with an even number of methylene units, PBCE and PHCE, boasted sharp signals, suggesting more extended and regular crystalline domains. This evidence agreed with the χ_c value calculated but also with Ist scan recorded at DSC, **Figure 8.3** and **Table 8.2**, where PBCE and PHCE were characterized by higher melting temperature and enthalpy compared with PPCE and PPeCE. The odd/even trend was deeply investigated and confirmed by our group in systems previously investigated[13]. In particular, it was reported that samples with even number of -CH$_2$- are able to more readily assemble in ordered structures.

More in details, peak position, intensity and width could be evaluated by deconvolution procedure, as shown in **Figure 8.7**. Due to the lack of information about crystalline structure lattice, it was hard to find direct relationship between the peaks of the different poly(alkylene 1,4-cyclohexanedicarboxylate)s; anyway previous studies reported PBCE diffraction profile and its modifications were analyzed[4,14]. On the basis of that, the signals at 16.2° and 19.4° were ascribed to a different second phase formed just with specific crystallization conditions and usually not present in copolymers. If these two peaks were excluded, PBCE and PHCE patterns showed a

correspondence of the main diffraction peaks suggesting an isomorphous crystal phase for the two polymers. Considering the number and position of diffraction peaks recorded for PPCE and PPeCE, no common shared crystal phase could be supposed and a different crystalline form should be expected.
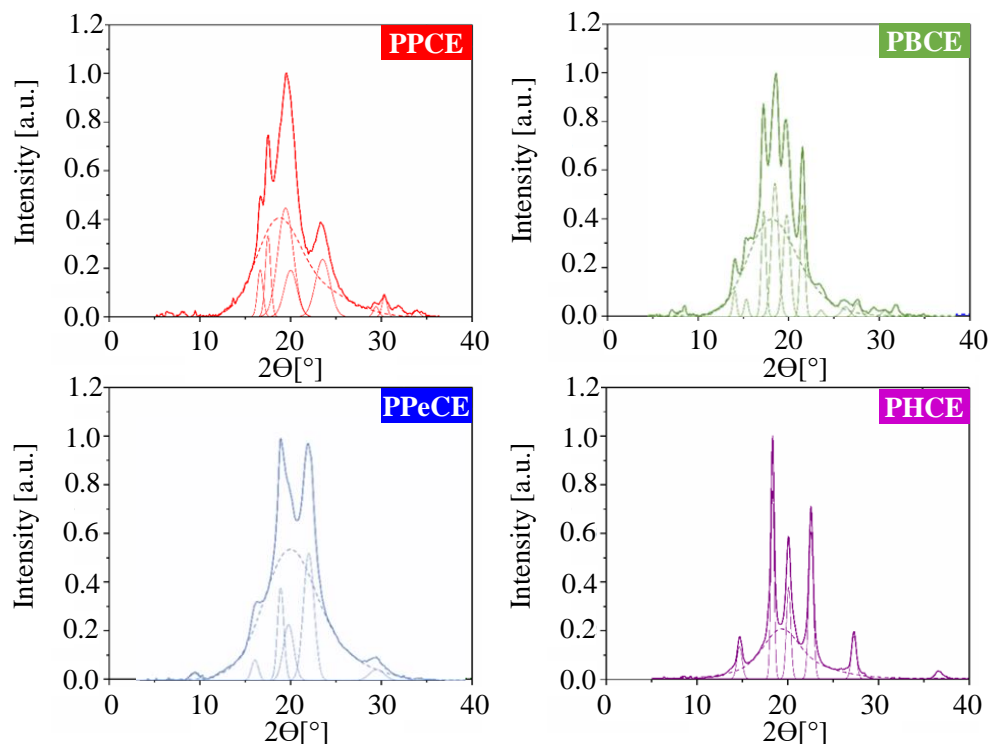
Figure 8.7*: Deconvolution of the WAXS spectra recorded for the synthetized samples.*

The deconvolution reported in **Figure 8.7** was analysed in order to define the mean size of the crystalline domains, l_c, applying Scherrer´s equation, and the crystalline inter-planar distance, d, obtained with Bragg´s equation (**Table 8.4**). The l_c values collected in **Table 8.4** confirmed the previous observations; PBCE and PHCE samples had bigger crystalline domains with more perfect crystalline lamellae, compared with PPCE and PPeCE ones**.**

On the basis of Scherrer´s equation, the full width at half height, FWHM, of X-rays diffraction peaks represented the average size of the crystalline domains. In this view PBCE and PHCE were analysed as follows: from the diffraction peaks at 18.0° and 18.3°, respectively, the crystalline domains derived were around 18 nm for PBCE and 22 nm for PHCE. This kind of approach was more difficult in case of PPCE and PPeCE, due to the overlapping and spreading of the diffraction peaks; despite that, it could be supposed a smaller size of the crystalline domains.

Table 8.4: *Mean size of the crystalline domains (l_c) and inter-planar distance (d) obtained for the poly(alkylene 1,4-cyclohexanedicarboxylate) samples employing Scherrer´s equation and Bragg´s equation; w represents the width of the peaks; 2θ is the peak angle position (from c1 to c5).*

PPCE / X_c = 20%						
Peak	c1	c2	c3	c4	c5	
w (°)	0.6	0.6	1.69	1.41	0.15	
2θ (°)	16.6	17.5	19.5	20.0	23.5	
l_c (nm)	11	11	4	5	4	
d (nm)	0.53	0.51	0.45	0.44	0.38	
PBCE / X_c = 30%						
Peak	c1	c2	c3	c4	c5	c6
w (°)	0.41	0.44	0.50	0.78	0.78	0.49
2θ (°)	14,9	16,2	18,1	19,3	20,6	22,3
l_c (nm)	16	15	13	9	9	14
d (nm)	0,59	0,55	0,49	0,47	0,43	0,40
PPeCE / X_c = 18%						
Peak	c1	c2	c3	c4	c5	
w (°)	0.77	0.71	1.15	1.19	1.6	
2θ (°)	15.2	18.1	19.0	21.2	28.7	
l_c (nm)	9	10	6	6	4	
d (nm)	0.58	0.49	0.47	0.42	0.31	
PHCE / X_c = 36%						
Peak	c1	c2	c3	c4	c5	
w (°)	0.58	0.38	0.48	0.51	0.55	
2θ (°)	14.7	18.3	20.1	22.6	27.3	
l_c (nm)	12	18	14	13	13	
d (nm)	0.60	0.48	0.44	0.39	0.33	

8.5 Mechanical characterization

Mechanical characterization was performed via tensile tests, on PPCE, PBCE, PPeCE and PHCE. The obtained stress–strain curves were reported in **Figure 8.8** while the derived data (Young modulus E, stress and strain at break, σ_{break} and ε_{break}) were shown in the **Table 8.5.** Considering the results obtained, it was clear the influence of glycol length on the mechanical properties of the material. PPCE and PBCE presented the highest and comparable elastic moduli among the synthetized polymers. The observations regarding E values agreed with the diffractometric and calorimetric results, where PPCE and PBCE showed similar crystallinity degree and comparable T_g (i.e. macromolecular mobility). The elastic modulus of PHCE had a lower value compared with

PPCE and PBCE, due to the enhanced chain flexibility, evidenced by the lower T_g, that contrasted the higher crystallinity degree and led a decrease of E value. PPeCE had the lowest E value in line with the low T_g and χ_c values (**Table 8.5**).

Table 8.5: Mechanical characterization data collected during tensile test on PPCE, PBCE, PPeCE and PHCE.

Sample	E MPa	σ_{break} MPa	ε_{break} %
PPCE	537 ± 23	8 ± 1	2.0 ± 0.3
PBCE	528 ± 45	23 ± 3	16 ± 4
PPeCE	252 ± 37	7 ± 1	10 ± 3
PHCE	473 ± 47	21 ± 3	12 ± 1

The crystallinity degree, consequence of the previously discussed odd/even effect due to the nature of the glycol, had an important role also to explain the stress at break of the samples. As concern the stress at break, PBCE and PHCE, presenting the highest crystalline phase amount, also showed σ_{break} values higher than the less crystalline homopolymers, PPCE and PPeCE. Finally, considering elongation at break, negligible differences were reported, ranging from 3 to 15% for all the studied samples.
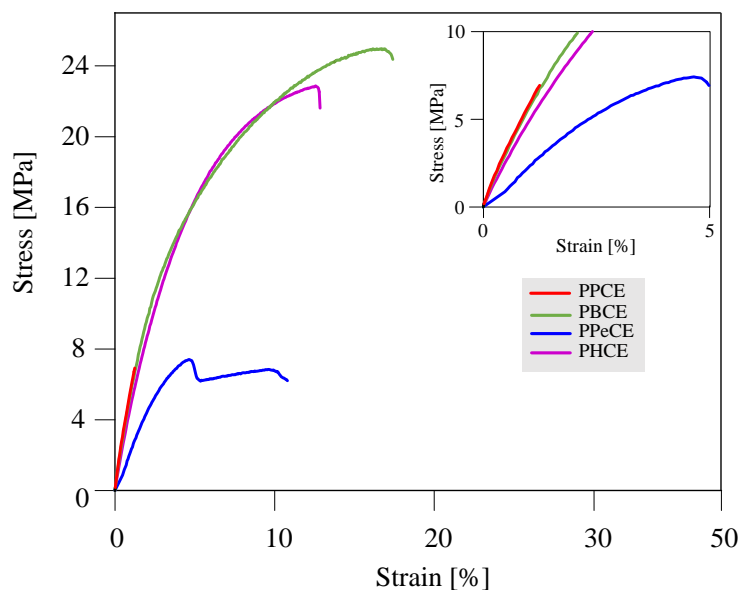
Figure 8.8: Stress-strain curves of the synthetized polyesters.

8.6 Barrier properties

Compression molded films were subjected to permeability test, according to the procedure reported in "Method and Materials". The results were shown as GTR values to O_2 and CO_2 in **Figure 8.9**. In order to interpret them, several factors had to be considered. In details, free volume fraction played an important role, and was lower when T_g rises. Moreover, the amount and the perfection of ordered phases, defined by $\chi_c/\Delta H_m$ and T_m, could change the performance of the materials. In details, the lower the free volume fraction the higher the portion of ordered phases, these last being more effective in blocking the passage of gases. Regarding PBCE, this material showed the best performance compared with the other samples, indeed its GTR values were the lowest. The explanation could be found in the highest melting temperature and crystallinity degree accompanied with the lowest free volume fraction (highest T_g) together with PPCE, observed among the series (**Table 8.3**). In case of PPCE, a slight increase of GTR values compared with PBCE was observed and referred to the presence of lower amount and less perfect crystalline phase, as suggested by T_m and ΔH_m values. On the basis of the latter observations, higher permeability for PPeCE was expected considering its less crystalline (lower χ_c and ΔH_m) and more flexible (lower T_g) nature respect to PPCE and PBCE. Comparing PPeCE with PHCE, despite the higher crystallinity degree and perfection of the lattice of this latter, $GTR_{PPeCE} < GTR_{PHCE}$.
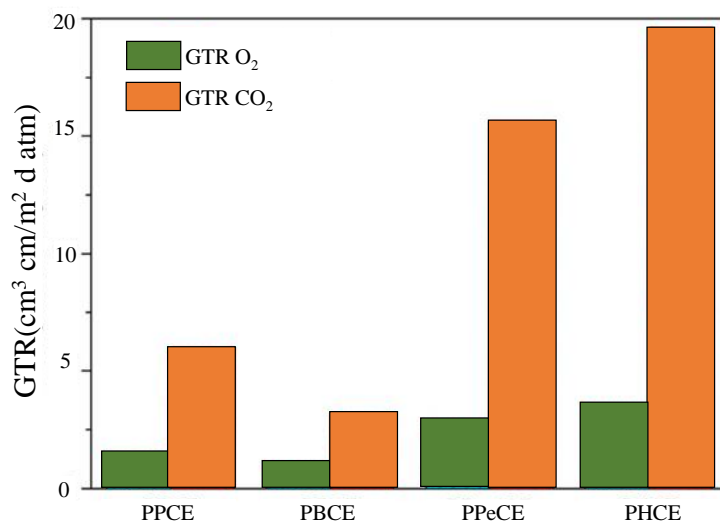
Figure 8.9: *GTR evaluated with CO_2 (orange) and O_2 (green) for PPCE, PBCE, PPeCE, PHCE.*

The obtained results were unexpected and unpredictable on the basis of overmentioned factors. Recently, Guidotti et al. attributed the smart barrier performance of a random PBCE-based

copolymer, to the presence of 2D-ordered domains, mesophase, coming from the disposition of cyclohexane moieties in very compact conformation[15]. Indeed, cyclohexane ring was included in the so called "mesogenic groups". Additionally, as reported before, presence of crystalline domains inhibited mesophase formation[16]. The chemical structure of PPeCE, with higher frequency of mesogenic group, cyclohexene ring, per chain length and the lesser presence of crystals compared with PHCE, favored the formation of mesophase.

As general observation, packing of aliphatic cyclohexane rings hampered the flowing of gas through the materials, conferring good barrier properties to the cyclohexane-containing polymers under study.

Moreover, all the copolyesters analysed presented GRT values to O_2 lower than to CO_2, due to the higher diffusivity of a large molecule, as CO_2, compared with a small one, as O_2.

The GTR values of PPCE, PBCE, PPeCE, PHCE were reported together with the GTR data of plastics generally used in packaging applications, both common fossil-based materials and bio-based and biodegradable polymers, as PLA and PBS (see **Figure 8.10**).
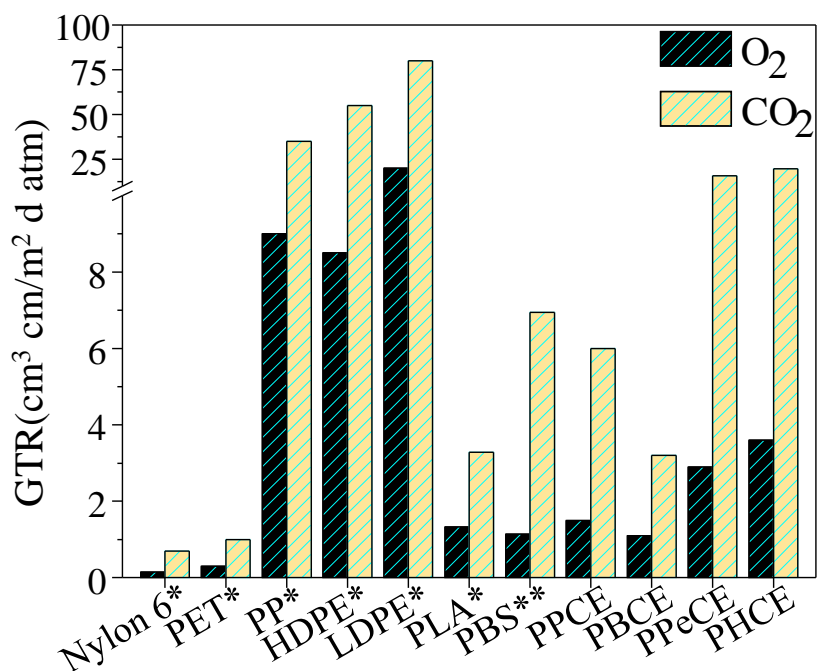
Figure 8.10*: GTRs to CO_2 and O_2 for the polymers under study and for some petrochemical-based materials and biopolymers (PLA and PBS) used in polymeric packaging(*[17] ;**[19]).*

The polymers under study showed superior barrier properties with respect to polyolefins for both the tested gases. In particular, in case of PPCE and PBCE, performances comparable to PBS and PLA were reported.

8.7 Composting test

The biodegradability of the prepared samples was evaluated through composting tests. The results for PPCE and PBCE, previously reported by us[18], showed a negligible weight loss even after six months of incubation in compost. Regarding PPeCE and PHCE, the behavior was pretty different, as one can see from surface SEM images collected and the weight loss recorded at different incubation times (**Figure 8.11**). The proceeding of the degradation was evidenced by the presence of cracks and holes on the surface of both PPeCE and PHCE films, shown in **Figure 8.11 A,** and was also connected to weight loss (**Figure 8.11 B**). In details, PHCE was five times slower in degradation compared to PPeCE; indeed, the former sample lost around 4% after 90 days in compost, while the latter, PPeCE, reached 20% in the same period of incubation.
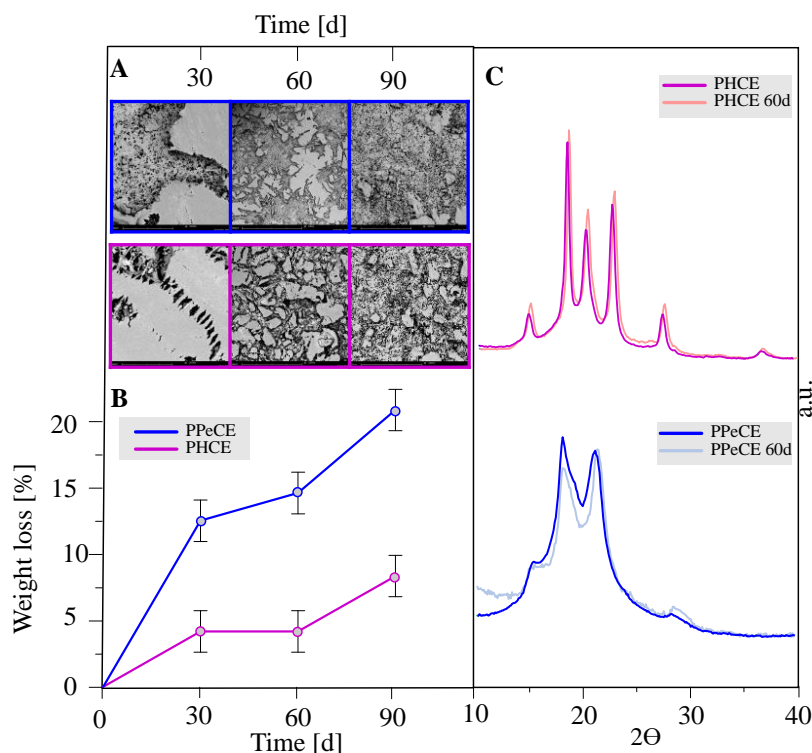
***Figure 8.11: A)** SEM images of PPeCE and PHCE film surface at 30, 60, 90 days of incubation [2000x]; **B)** Weight loss of PPeCE and PHCE as a function of incubation time; **C)** WAXS analysis of PHCE and PPeCE, neat polymers and the specimens incubated for 60 days in compost.*

233

As well known, the degradation processes started in the amorphous region, more easily reached by bacteria and fungi with respect to crystalline zone. On the basis of that, the behavior of PPeCE and PHCE could be interpreted. Indeed, as evidenced by the data in **Table 8.3**, PPeCE was less crystalline than PHCE and consequently the degradation process was favored. Moreover, the temperature of the composting chamber was 58°C, i.e. in correspondence of the melting point of PPeCE. As a consequence, the macromolecules were more mobile and easily reached by bacteria and fungi. With the preferential attack of the amorphous regions, an increasing of relative amount of crystal portion should be observed. Indeed, as reported in **Figure 8.11 C**, WAXS patterns of neat PPeCE and PHCE films resulted less sharp compared with the spectra of the two materials incubated for 60 days, which were subjected to a relative increase in intensity that, in turn, led to an increase of χ_c.

8.8   Conclusions

Poly(propylene 1,4-cyclohexanedicarboxylate) (PPCE), poly(butylene-1,4-cyclohexanedicarboxylate (PBCE), poly(pentylene 1,4-cyclohexanedicarboxylate) (PPeCE) and poly(hexylene 1,4-cyclohexanedicarboxylate) (PHCE) were successfully synthetized via solvent free two steps polycondensation. The molecular characterization conducted via H^1-NMR confirmed the expected chemical structures with no by-products. Then, the materials were fully characterized. TGA analysis showed good thermal stability due to the presence of the cyclohexane ring along the polymer backbone. The activation energy needed for the degradation process was evaluated and resulted independent from the glycol length. Differently, functional features as mechanical, thermal and barrier properties, were affected by changing the repeating unit structure. In details, in case of thermal properties a strong effect was recorded: melting temperature and ability to crystallize followed an even-odd trend already observed in poly(alkylene dicarboxylate)s, whereas glass transition temperature decreased with the increase of the glycol length. The mechanical properties were affected, as well, by glycolic subunits length, changing the behaviour of final material. Considering the barrier performances, PPCE and PBCE showed the smartest behaviours, being comparable to PLA and PBS, two well-known commercialized bioplastics. PPeCE, despite its low amount of crystal phase with low degree of perfection, presented interesting barrier performance, superior to polyolefins. This unexpected result could be explained considering the formation of mesophase, originating from the stacking of the aliphatic

rings mainly in this polymer than in the other samples under study (PPCE, PBCE and PHCE), for its low amount of crystals that let space for the formation of this particular ordered phase. Also, the composting kinetics changed as a function of glycol length. Indeed, PPeCE and PHCE degraded faster.

In conclusion, changing of glycol length resulted a suitable tool to tune the final properties of materials. The poly(alkylene 1,4-cyclohexanedicarboxilate)s family synthetized revealed to be a good option for the realization of short-life flexible packaging films.

8.9 Bibliography

1.   C. Berti, E. Binassi, M. Colonna, M. Fiorini, G. Kannan, S. Karanam, M. M. and I. O. BioBased Terephthalate Polyesters. (2010).

2.   Gigli, M., Lotti, N., Vercellino, M., Visai, L. Munari, A. Novel ether-linkages containing aliphatic copolyesters of poly(butylene 1,4-cyclohexanedicarboxylate) as promising candidates for biomedical applications. *Mater. Sci. Eng. C* **34**, 86–97 (2014).

3.   Genovese L., Lotti N., Gazzano M., Finelli L., Munari A. New eco-friendly random copolyesters based on poly(propylene cyclohexanedicarboxylate): Structure-properties relationships. *Express Polym. Lett.* **9**, 972–983 (2015).

4.   Gigli, M., Lotti, N., Siracusa, V., Gazzano, M., Munari, A., Dalla Rosa, M. Effect of molecular architecture and chemical structure on solid-state and barrier properties of heteroatom-containing aliphatic polyesters. *Eur. Polym. J.* **78**, 314–325 (2016).

5.   Gigli, M., Lotti, N., Gazzano, M., Siracusa, V., Finelli, L., Munari, A., Dalla Rosa, M. Fully aliphatic copolyesters based on poly(butylene 1,4- cyclohexanedicarboxylate) with promising mechanical and barrier properties for food packaging applications. *Ind. Eng. Chem. Res.* **52**, 12876–12886 (2013).

6.   Gigli, M., Lotti, N., Gazzano, M., Siracusa, V., Finelli, L., Munari, A., Dalla Rosa, M. Biodegradable aliphatic copolyesters containing PEG-like sequences for sustainable food packaging applications. *Polym. Degrad. Stab.* **105**, 96–106 (2014).

7.   Blaine, R. L.; Hahn, B. K. Obtaining Kinetic Parameters by Modulated Thermogravimetry. *J. Therm. Anal. Calorim.* 695–704 (1998). doi:https://doi.org/10.1023/A:1010171315715

8.   Flynn, J. H. Schwenker, R. F.; Garn, P. D. The Historical Development of Applied Non-Isothermal Kinetics. in *Thermal Analysis* (ed. Press, E. A.) 1111−1126 (1969). doi:10.1016/b978-0-12-395734-4.50035-7

9.   Blaine, R. A faster approach to obtaining kinetic parameters. *Am. Lab.* **30**, 21–23 (1998).

10.   Thiyagarajan, S., Meijlink, M. A., Bourdet, A., Vogelzang, W., Knoop, R. J., Esposito, A., Van Haveren, J. Synthesis and Thermal Properties of Bio-Based Copolyesters from the Mixtures of 2,5- A nd 2,4-Furandicarboxylic Acid with Different Diols. *ACS Sustain. Chem.*

Eng. (2019). doi:10.1021/acssuschemeng.9b04463

11. Terzopoulou, Z., Tsanaktsis, V., Nerantzaki, M., Papageorgiou, G. Z. & Bikiaris, D. N. Decomposition mechanism of polyesters based on 2,5-furandicarboxylic acid and aliphatic diols with medium and long chain methylene groups. *Polym. Degrad. Stab.* **132**, 127–136 (2016).

12. Schawe, J. E. K. Mobile amorphous, rigid amorphous and crystalline fractions in isotactic polypropylene during fast cooling. *J. Therm. Anal. Calorim.* **127**, 931–937 (2017).

13. Soccio, M., Lotti, N., Finelli, L., Gazzano, M. & Munari, A. Aliphatic poly(propylene dicarboxylate)s: Effect of chain length on thermal properties and crystallization kinetics. *Polymer (Guildf).* **48**, 3125–3136 (2007).

14. Fortunati, E., Gigli, M., Luzi, F., Lotti, N., Munari, A., Gazzano, M., Kenny, J. M. Poly (butylene cyclohexanedicarboxylate / diglycolate) random copolymers reinforced with SWCNTs for multifunctional conductive biopolymer composites. **10**, 111–124 (2016).

15. Guidotti, G., Soccio, M., Siracusa, V., Gazzano, M., Munari, A., Lotti, N. Novel random copolymers of poly(butylene 1,4-cyclohexane dicarboxylate) with outstanding barrier properties for green and sustainable packaging: Content and length of aliphatic side chains as efficient tools to tailor the material's final performance. *Polymers (Basel).* **10**, (2018).

16. Cavallo, D., Azzurri, F., Floris, R., Alfonso, G. C., Balzano, L., Peters, G. W Continuous cooling curves diagrams of propene/ethylene random copolymers. The role of ethylene co-units in mesophase development. *Macromolecules* **43**, 2890–2896 (2010).

17. Mensitieri, G., Di Maio, E., Buonocore, G. G., Nedi, I., Oliviero, M., Sansone, L., Iannace, S. Processing and shelf life issues of selected food packaging materials and structures from renewable resources. *Trends Food Sci. Technol.* **22**, 72–80 (2011).

18. Genovese, L., Soccio, M., Gigli, M., Lotti, N., Gazzano, M., Siracusa, V., Munari, A Gas permeability, mechanical behaviour and compostability of fully-aliphatic bio-based multiblock poly(ester urethane)s. *RSC Adv.* **6**, 55331–55342 (2016).

9 1,4-CYCLOHEXANEDICARBOXYLIC ACID AND ISOPHTHALIC ACID FOR DESIGNING AN INNOVATIVE SOLUTION FOR SUSTAINABLE PACKAGING

9.1 Introduction

One of the most actual themes of discussion, involving both public opinion and scientific community, regards the impact of humans in the environment. As concern plastics, the debate is still open: the main part of polymers available on Global Market have a short time of use and no end-life fate, since the wastes are accumulating in the environment because of their non-biodegradable nature and the absence of efficient process of recycling. Moreover, the monomers are meanly derived from fossil resources, no longer available in the planet. Despite that, polymers have unique properties (lightness, low cost, mechanical resistance, easy processability) resulting irreplaceable. For this reason, new class of plastics, biodegradable and biobased named biopolymers, have been studies as long-term solution. Promising results are obtained from aliphatic/aromatic copolyesters, tested from the researchers[1–7] and the industrial world[2,8–10], becoming a suitable solution in packaging field, the main environmental impact due to the high volume and low time of used, by which the envelopes are characterized.

In the present work, the aliphatic moiety selected was trans 1,4-cyclohexanedicarboxylic acid, a bio-based diacid characterized by 6 carbon ring that confers thermal stabily[11–13] and compostability[14] to its derivate. As concern the aromatic monomer, despite benzene moiety was the most common and widely used as aromatic element, the research was oriented to find alternatives. Good results were obtained employing its meta-isomer, isophthalic acid, easily synthetized from renewable sources[15–17]. The derived isophthalic polyesters were characterized by low rate of crystallization but still able to reorganize in ordered structure, forming an hard and opaque material[18]. Despite that, thermal stability was high[19] and the barrier properties[20,21] observed were very good.

Considering the good characteristics bared from the aliphatic acid, trans 1,4-cyclohexanedicarboxylic acid and the aromatic one, isophthalic acid, were chosen as fundamental moieties of the new bio-based aliphatic/aromatic system together with 1,4-butanediol, for its well-known sustainable nature and the good results obtained during homopolymerization in presence

of the two diacid selected. In the present work, a series of copolyesters were synthesized employing different amount of 1,4-cyclohexanedicarboxylic acid and isophthalic acid, with 1,4-butandiol. The so-obtained copolymers were deeply characterized from the chemical, thermal and mechanical point of view. On the basis a possible application for flexible packaging, the copolymers were filmed and barrier performances were evaluated.

9.2 Synthesis and molecular characterization

In order to establish clear structure-property relations, fundamental to design the most suitable material for the intended application, i.e. food packaging, the whole range of compositions was considered. The random copolymers $(P(BCE_mBI_n))$ as well as the two parent homopolymers poly(butylene 1,4-cyclohexanedicrboxylate) (PBCE) and poly(butylene isophthalate) (PBI) were synthesized according to the well-known two-step melt polycondensation. The polymerization conditions and the catalyst employed were carefully described in the "Methods and Materials" section. The polymers synthesized after purification appeared as white crystalline powders.
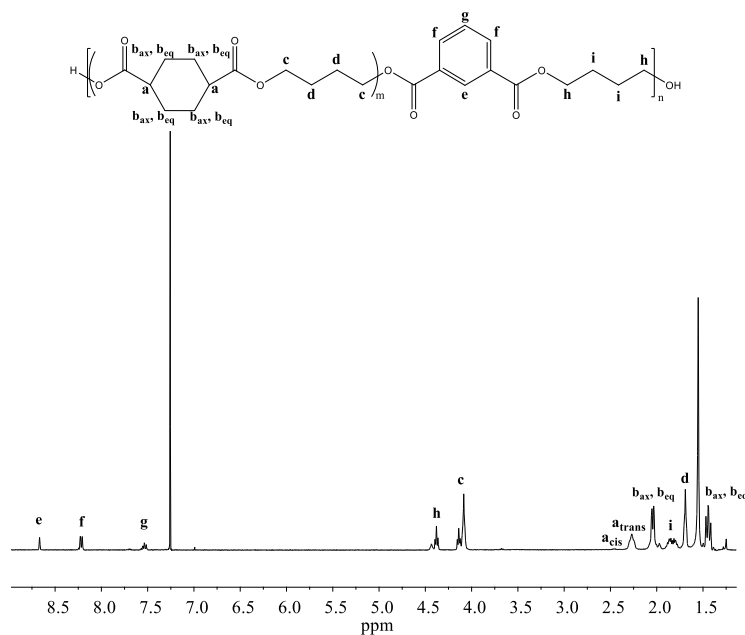
Figure 9.1: ^{1}H-NMR spectrum of $P(BCE_{80}BI_{20})$ with the relative peak assignments.

As usual, the samples were subjected to molecular characterization by ^{1}H-NMR in order to verify the chemical structure of the products of synthesis, and, in case of copolymers, to obtain info on real copolymer composition and on sequence distribution. As example, the spectrum obtained analyzing $P(BCE_{80}BI_{20})$ was reported in **Figure 9.1**.

As one can see, the signals agreed with the predicted chemical structure without unexpected peaks, proving the condition used for the synthesis were optimized. In details, in the range 7.75 - 8.70 ppm the aromatic protons, e, f and g, of the isophthalic moiety were resonating. The α protons (h) bond to the carboxylic groups of isophthalic were located at 4.40 ppm. More complex, the part of aliphatic counit. In this case, the α protons (c) bond to the carboxylic groups were found at 4.10 ppm. At 2.25 ppm the protons characteristic of *trans* isomer identified as a_{trans} were observed. Close to them, another peak was evident due to *cis* isomer (a_{cis})[11,22]. The exact amount of *cis* isomer, for each sample, was reported in **Table 9.1**.

Table 9.1: *Molecular characterization data of the two homopolymers, PBCE and PBI, and of P(BCE$_m$BI$_n$) random copolymers*

Sample	% BCE feed	% BCE from ^{1}H-NMR	M_n[a]	D[a]	b	L_{BCE}	L_{BI}	%cis
PBCE	1.00	1.00	57100	2.3	/	/	/	10.7
P(BCE$_{90}$BI$_{10}$)	0.90	0.88	43200	2.2	0.95	6.49	1.29	6.1
P(BCE$_{80}$BI$_{20}$)	0.80	0.81	43500	2.0	0.96	4.72	1.37	5.8
P(BCE$_{70}$BI$_{30}$)	0.70	0.74	42000	2.1	0.96	3.39	1.51	7.4
P(BCE$_{50}$BI$_{50}$)	0.50	0.52	52500	1.6	0.99	2.01	2.00	5.8
P(BCE$_{30}$BI$_{70}$)	0.30	0.33	39400	1.3	0.97	1.77	2.77	5.7
P(BCE$_{20}$BI$_{80}$)	0.20	0.25	33000	2.3	1.0	1.27	4.52	6.1
P(BCE$_{10}$BI$_{90}$)	0.10	0.12	31100	1.9	1.0	1.13	7.63	5.2
PBI	0	0	33150	2.0	/	/	/	/

a) Obtained from GPC analysis

As you can see, the homopolymer PBCE was the sample containing the highest amount of *cis* isomer (≈ 11%), among the samples under investigation. All the copolymers were characterized by similar *cis* isomer content. PBCE polyester previously synthesized by Prof. Lotti's research group contained a lower amount of *cis* isomer, ranging from 2 to 4%, although the adopted polymerization conditions were kept the same. The difference was due to the monomer utilized in this case, which initially contained higher amounts of *cis* isomer (4-5%). In the last part of the spectrum, -CH$_2$- proton signals, d and i, were observed and located respectively at 1.69 ppm and 1.82 ppm. The six-carbons ring had a complex system of signals at low chemical shift, 1.40 ppm, where the axial and equatorial protons, b_{ax} and b_{eq}, could be observed.

Two signals characteristic of the counits, butylene ciclohexane dicarboxylate, BCE, and butylene isophthalate, BI, were chosen to evaluate the real chemical composition. Two isolated signals were

found at 1.69 ppm (d) for BCE and at 8.75 ppm, e protons, for BI. The resulting actual copolymer compositions were listed in **Table 9.1**. As one can see, the real amount of the two comonomeric units was not far from feed ratio.

For copolymers, it was important to know the sequence distribution beside copolymer composition. In this view, ^{13}C-NMR measurements were carried out. As example, a spectrum with relative peak assignments was reported in **Figure 9.2** for P(BCE$_{80}$BI$_{20}$).
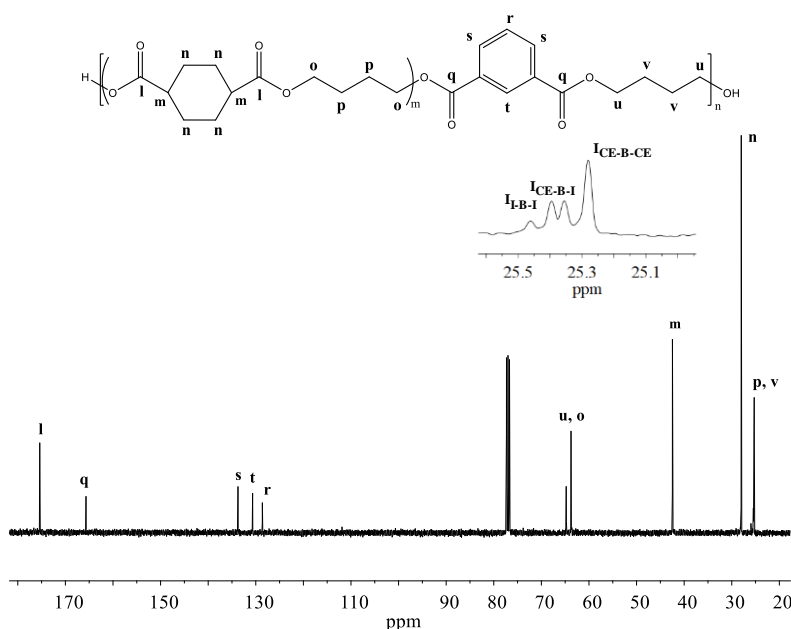
Figure 9.2: *^{13}C-NMR spectrum of P(BCE$_{80}$BI$_{20}$) with the relative peak assignment and magnification of the range 25.7-24.9 ppm.*

The sp^2 carbon of the COOR- groups bond to the cyclohexane ring, l, and to the isophthalate ring, q, were resonating respectively at 175 ppm and at 165 ppm. The aromatic carbon, r, s and t, could be recognized in the range 135 ppm and 125 ppm, while, the external methylene carbons, proper of the glycol subunit bonded to the isophthalic moieties, u, and to the cyclohexane ring, o, were resonating at 65 and 64 ppm, respectively. The carbon of the ring directly bonded to -COOR group, m, was located at 41 ppm, whereas the C atoms of the cyclohexene were observed at 28 ppm. At low chemical shift, 24 ppm, the inner carbon atoms of the glycol sub-unit were located. These latter signals were magnified and used to determine the length of the sequence of BCE and BI, and to calculate the degree of randomness, b. The set of signals observed in this zone was related to the possible triads, i.e. the glycol subunit (Butanediol: B) could be bonded to the same acid subunits (in case of cyclohexane dicarboxylate (CE), CE-B-CE, the signal was resonating at 25.35

ppm), while at 25.40 ppm the triads of butanediol bonded to isophthalic ring (I), I-B-I, could be observed. In between the two peaks, around 25.40 ppm, the mixed triads could be identified, I-B-CE and CE-B-I.

From the calculations of the integrals of the overmentioned signals, the degree of randomness, b, was estimated, as follow:

$$b = P_{CE-B-I} + P_{I-B-CE} \qquad\qquad Eqn.\ 1$$

$$P_{CE\_I} = \frac{(I_{CE-B-I} + I_{I-B-CE})/2}{(I_{CE-B-I} + I_{I-B-CE})/2 + I_{CE-B-CE}} \qquad\qquad Eqn.\ 2$$

$$P_{I\_CE} = \frac{(I_{CE-B-I} + I_{I-B-CE})/2}{(I_{CE-B-I} + I_{I-B-CE})/2 + I_{I-B-I}} \qquad\qquad Eqn.\ 3$$

where the probability to find a glycol subunit bond to the cyclohexane carboxylate ring and to the isophthalic moiety is expressed with P_{CE_I}, while the probability to find a glycol subunit bond to the isophthalic and cyclohexane carboxylate ring is defined P_{I_CE}. The just mentioned I_{CE_I}, I_{I_CE}, I_{CE_CE} and I_{I_I} are used to define the integrals of the peaks related to the triads previously described, CE-B-I, I-B-CE, CE-B-CE and I-B-I.

The results, listed in **Table 9.1**, were ranging between 1 and 0.95, indicating the random nature of the synthetized copolymers. The length of the two subunits BCE and BI, named L_{BCE} and L_{BI} could be evaluated as the inverse of the two calculated probability, P_{CE_I} and P_{I_CE}, respectively (these values were also collected in **Table 9.1**).

As expected, the sequence length of each comonomeric unit was strictly correlated to its amount: the high the counit content, the longer the sequence. Gel permeation chromatography was employed to evaluate the molecular weight and the polydispersity (see **Table 9.1**). All the synthetized samples were characterized by high molecular weight and by polydispersity about two, proving the polymerization process was optimized. As a matter of fact, free-standing films via compression molding were easily obtained.

9.3 Thermal characterization

The samples under study were then subjected to an accurate thermal characterization, by means of TGA and DSC techniques. Firstly, the thermal stability under nitrogen atmosphere was investigated. The experimental procedure was described in detail in the experimental part. The results obtained were collected in **Table 9.2**. As concerns the two homopolymers, PBCE and PBI, the thermal stability was found very good; noteworthy, PBCE resulted more thermally stable than PBI, despite the aromatic nature of this latter, due to the bulky and thermally stable cyclohexene ring[23]. PBCE resulted more thermally stable than PBI, despite less stable than PBCE with lower *cis* isomer content previously investigated[24]. The copolymer thermal stability was strictly related to the amount of BCE comonomeric unit, i.e. the higher the BCE unit content, the higher the sample thermal stability.

Table 9.2: TGA results for PBCE, PBI, and their random copolymers under nitrogen atmosphere.

Sample	T_{onset} °C	$T_{95\%}$ °C	T_{max} °C
PBCE	382	394	417
$P(BCE_{90}BI_{10})$	345	394	420
$P(BCE_{80}BI_{20})$	340	394	419
$P(BCE_{70}BI_{30})$	332	390	417
$P(BCE_{50}BI_{50})$	336	393	415
$P(BCE_{30}BI_{70})$	338	394	415
$P(BCE_{20}BI_{80})$	336	388	412
$P(BCE_{10}BI_{90})$	337	387	411
PBI	325	382	404

Afterwards, a deep calorimetric analysis was conducted. Firstly, the thermal behavior of the purified powders was investigated, in order to evaluate how the tendency to crystalize was affected by solvent evaporation. The results were listed in **Table 9.3**, while the calorimetric traces were collected in **Figure 9.3 A**. The curves were typical of semicrystalline samples, showing a little glass to rubber transition followed by a melting phenomenon at higher temperature.

PBCE under study had similar melting temperature respect to PBI, despite the lower symmetric architecture of this latter. It was worth noting melting temperature of PBCE previously investigated by Lotti's research group was ten degrees higher (T_m= 166°C). The discrepancy could again be explained as due to the quintupled amount of *cis* isomer (≈11%) present in the sample under study. The PBCE investigated in the present work had to be considered a random copolymer of *trans* and *cis* isomers, whereas the copolymer were exactly tercopolymers with three different comonomeric units.
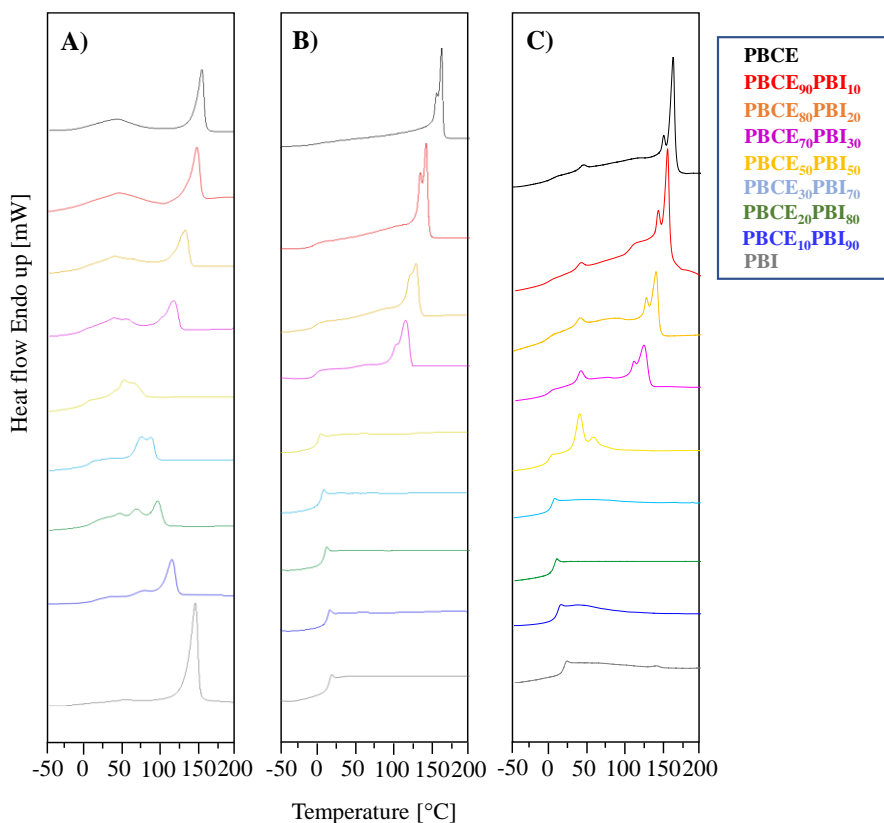
Figure 9.3*: (A) I^{st} scan calorimetric traces of PBCE, PBI and $P(BCE_mBI_n)$ purified powders; (**B**) IInd scan after melt quenching; (**C**) DSC I^{st} scan of PBCE, PBI and $P(BCE_mBI_n)$ compression molded films. Heating rate: 20 °C/min under nitrogen flow.*

As far as the fraction of crystalline phase developed during solvent evaporation was concerned, this was significantly higher for PBI (higher melting heat). It seems PBI tendency to develop the 3D-ordered phase during solvent evaporation was greater compared to PBCE. As regards the copolymers, melting temperature trend could be explained, dividing the copolymer series into two groups: the one composed of samples richer in BI co-unit content, the remaining samples being those containing higher amounts of BCE co-units. The copolymers containing 90 ≤ BCE mol %

≤ 70 were characterized by a melting phenomenon at high temperature, whose peak temperature and width decreased and increased, respectively, as the amount of BI unit content increased. This was typically observed in random copolymers with both comonomeric units able to crystallize, but only the one present in major amount taking part to crystallization process.

Table 9.3: Thermal characterization data of PBCE, PBI and P(BCE$_m$BI$_n$) powders.

Powder	Ist scan		IInd scan			
	T$_m$ °C	ΔH$_m$ J/g	T$_g$ °C	ΔCp J/g*°C	T$_m$ °C	ΔH$_m$ J/g
PBCE	156	13.0	17	0.209	156	36.3
P(BCE$_{90}$BI$_{10}$)	149	18.0	8	0.217	148	23.8
P(BCE$_{80}$BI$_{20}$)	135	26.8	9	0.164	135	18.4
P(BCE$_{70}$BI$_{30}$)	120	23.0	10	0.184	122	19.3
P(BCE$_{50}$BI$_{50}$)	70	21.0	11	0.294	/	/
P(BCE$_{30}$BI$_{70}$)	92	25.1	15	0.333	/	/
P(BCE$_{20}$BI$_{80}$)	100	26.7	19	0.353	/	/
P(BCE$_{10}$BI$_{90}$)	118	29.7	22.5	0.323	/	/
PBI	147	62.9	25	0.326	/	/

The no crystallizing counit could be rejected in the amorphous or could partially enclosed in crystal phase. The DSC trace of copolymer containing 30 mol % BI counits showed at lower temperature (around 50-70°C) a double melting phenomenon of small entity, which became more evident in the copolymer containing equimolar amounts of the two comonomeric units. In this latter sample, the peaks were also slightly shifted at higher temperature. As to the group of copolymers rich in BI unit content, a complex multiple endothermic phenomenon was observed, the most intense endothermic peak occurring at a temperature, which regularly decreased as the amount of BCE co-unit was increased. The intensity of the endothermic peak at lower temperature also increased with the amount of comonomeric units. Even for copolymers rich in BI co-units, the formation of the crystalline phase characteristic of parent homopolymer (PBI) seemed to occur, with BCE co-units excluded or partially included into the crystals. For the copolymers containing from 20 to 60 mol% of BCE co-units, just from the DSC curves, it was difficult to establish whether a single or two different crystalline phases coexisted. X-ray diffractometric analysis could help to shed light on this aspect (see in the following).

Figure 9.3 B reported the IInd scan after melt quenching, in order to better analyze the glass transition process; the derived thermal data were collected in **Table 9.3**. In case of PBCE, the fast cooling performed was not allowing the complete formation of an amorphous material. Differently, PBI revealed to be a slow-rate crystallizing polymer, the cooling rate applied being fast enough to block the crystallization. As regard the copolymers, those rich in BCE counits - P(BCE$_{90}$BI$_{10}$), P(BCE$_{80}$BI$_{20}$) and P(BCE$_{70}$BI$_{30}$)- crystallized during quenching, resembling the behavior of the parent homopolymer (PBCE). Of course, the crystalline phase formed during cooling step was characterized by lower T$_m$ and ΔH$_m$ values, which regularly decreased with the increment of BI unit content. Summarizing, the copolymer phase behavior depended on copolymer composition: the copolymer with high content of BCE counis were semicrystlline, whereas those containing BI unit content ranging from 90 to 50 mol% were completely amorphous. The DSC traces of these last samples showed indeed exclusively the endothermal baseline deviation associated to the glass to rubber transition. As far as the trend of T$_g$ values with copolymer composition was concerned, as one can see from **Table 9.3** and **Figure 9.3 B**, the measured values increased as the amount of BI unit content increased, as expected considering T$_{g,PBI}$ > T$_{g,PBCE}$, due to the presence in PBI of the more rigid aromatic isophthalic moiety.

In **Figure 9.3 C** the DSC traces of compression molded films were reported, the corresponding thermal data being collected in **Table 9.4**.

Table 9.4: Calorimetric data of PBCE, PBI and P(BCE$_m$BI$_n$) compression molded films.

Film	Ist scan			
	T$_g$ °C	ΔCp J/g·°C	T$_m$ °C	ΔH$_m$ J/g
PBCE	13	0.105	156	34
P(BCE$_{90}$BI$_{10}$)	5.5	0.173	149	30
P(BCE$_{80}$BI$_{20}$)	9	0.142	135	22
P(BCE$_{70}$BI$_{30}$)	5	0.165	120	20
P(BCE$_{50}$BI$_{50}$)	6.5	0.289	61	17
P(BCE$_{30}$BI$_{70}$)	9	0.432	/	/
P(BCE$_{20}$BI$_{80}$)	13	0.300	/	/
P(BCE$_{10}$BI$_{90}$)	17	0.406	/	/
PBI	25	0.346	/	/

From the analysis of the collected curves, it was clear PBCE was also able to crystallize during ballistic cooling occurring after compression molding. Such ability was characteristic of the copolymers containing high amounts of BCE co-units too (50≤ BCE mol% ≤90). However, the corresponding melting peaks became broader with increasing BI co-unit content, due to the disturbing effect exerted by isophthalic moieties on PBCE crystal packing. In all the copolymers, at the constant temperature of 45°C, an endothermic peak was observed, whose intensity increased with the amount of BI unit content. The endothermic process at high temperature manifested a double peak, whose origin could be ascribed to two possible reasons: *i)* melting-recrystallization-remelting processes typical of polyesters; *ii)* coexistence of two different crystal populations. Diffractometric analysis could help to clarify the nature of the complex endothermic phenomena observed by DSC.

9.4   Structural characterization

The purified powders and the filmed materials were submitted to wide angle X-ray scattering. The diffraction profiles of PBCE, P(BCE$_m$BI$_n$) and PBI samples were shown in **Figure 9.4**; the crystallinity degree values were reported in **Table 9.5**.

Table 9.5: Crystallinity degree by WAXS for PBCE, PBI and their random copolymers.

Sample	$\chi_{c,powder}$ %	$\chi_{c,film}$ %
PBCE	7.5	32
P(BCE$_{90}$BI$_{10}$)	9.4	30
P(BCE$_{80}$BI$_{20}$)	30	27
P(BCE$_{70}$BI$_{30}$)	26	25
P(BCE$_{50}$BI$_{50}$)	19	21
P(BCE$_{30}$BI$_{70}$)	24	/
P(BCE$_{20}$BI$_{80}$)	27	/
P(BCE$_{10}$BI$_{90}$)	34	/
PBI	46	/

On the basis of WAXS profile, powder samples (**Figure 9.2 A**) could be divided into three groups:

1) both PBCE and P(BCE$_{90}$BI$_{10}$) WAXS patterns displayed an intense band between 10° and 30° 2Θ with small shoulders, which could be the diffractometric reflections of samples with very low

246

crystallinity. Such band, even not structured, did not seem broad as the one usually observed in fully amorphous samples, suggesting the eventual presence of nanostructured or mesomorphic phase too;

2) the samples containing BI unit content ranging from 20 to 50 mol % showed the characteristic profile of PBCE crystalline phase as reported for other PBCE-based copolymers[14,25,26];

3) the samples with high BI unit content displayed the WAXS profile of PBI. All the samples showed an increase in the baseline in the 2Θ region around 20° that corroborated the presence of certain amount of amorphous and/or low ordered material; that was particular evident for the copolymer containing equimolar amount of the two comonomeric units.
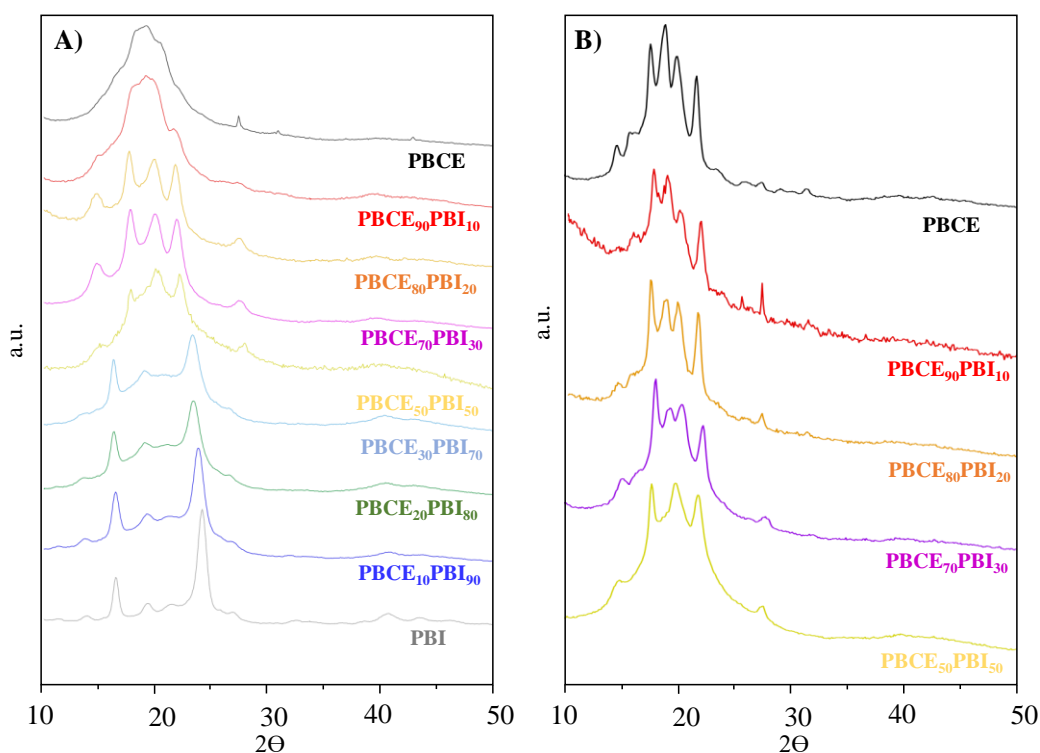
Figure 9.4*: XRD diffraction profiles of PBCE, P(BCExBIy) and PBI samples, **A)** in the form of powder and **B)** compression molded film.*

As far as the filmed polymers were concerned, the WAXS profiles showed diffraction peaks only for copolymers containing BI unit content comprised between 0 and 50 mol% (see **Figure 9.4 B**). The observed patterns were PBCE-like, even though two extra peaks at 16.3° and 19.7° 2Θ were present. These could be ascribed to the contemporary presence of a secondary crystal phase. It was worth noting such two further peaks were not evident in the sample P(BCE$_{50}$BI$_{50}$).

247

In the film samples, the crystallinity degree decreased as the BI unit content was increased, due to the disturbing effect of the foreign BI units.

Considering the results obtained by WAXS analysis, it was plausible that the double melting phenomenon observed at high temperature in the BCE-rich copolymers was due to the coexistence of two different crystal phases, whereas the endothermic peak well evidenced in equimolar copolymer at fix temperature (≈45°C) could be related to a mesophase, originating from stacking of cycloaliphatic rings.

9.5 Mechanical properties

The film obtained via compression moulding were subjected to stress-strain test, in order to collect information about their mechanical properties, which were fundamental for a future application. The obtained data were collected in **Table 9.6**, while some stress-strain curves were reported in **Figure 9.5**.
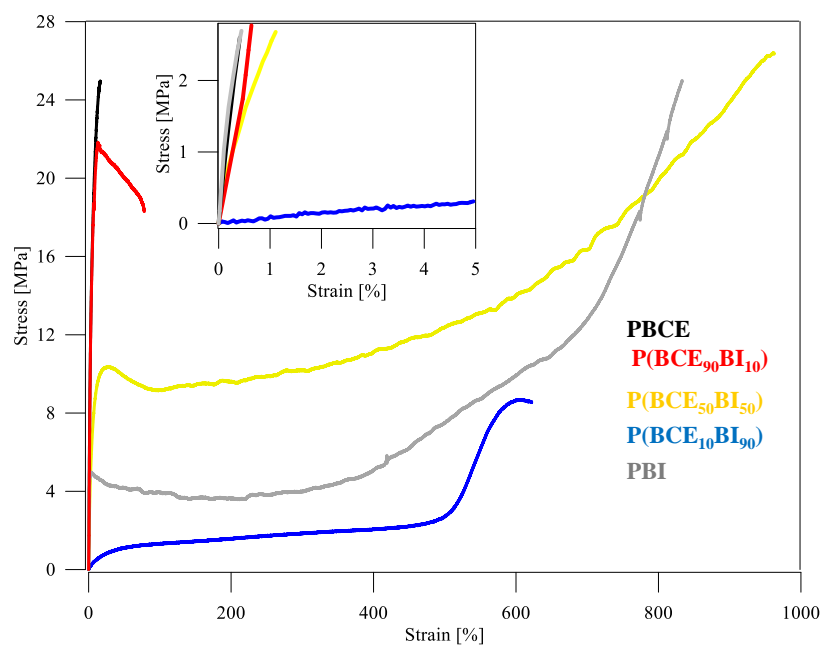
Figure 9.5*: Stress strain curves of PBCE, PBI and P(BCE$_{90}$BI$_{10}$), P(BCE$_{50}$BI$_{50}$), P(BCE$_{10}$BI$_{90}$) random copolymers.*

PBCE film was characterized by higher elastic modulus, lower stress at break and elongation at break compared to PBI film. The results could be explained taking into account that the former was semicrystalline (high E and σ_B) with a mobile amorphous phase (T_g below room temperature),

248

constrained by crystals (low ε_B). On the contrary, PBI was fully amorphous (lower E, higher ε_B), with however a particularly dense and not completely mobilized amorphous phase ($T_g \approx$ room temperature, high σ_B).

Table 9.6: *Mechanical characterization data of the analyzed films.*

Sample	σ_b MPa	ε_b %	E MPa
PBCE	23 ±3	15.0 ±4.5	558 ±45
P(BCE$_{90}$BI$_{10}$)	19 ±2	75 ±18	482 ±55
P(BCE$_{80}$BI$_{20}$)	9 ±1	36 ±23	383 ±37
P(BCE$_{70}$BI$_{30}$)	10 ±3	120 ±60	327 ±33
P(BCE$_{50}$BI$_{50}$)	10 ±1	914 ±52	229 ±3
P(BCE$_{30}$BI$_{70}$)	6 ±1	1623 ±194	4 ±1
P(BCE$_{20}$BI$_{80}$)	4 ±2	935 ±82	4 ±1
P(BCE$_{10}$BI$_{90}$)	6 ±3	573 ±60	5.5 ±0.3
PBI	39 ±10	795 ±39	426 ±39

As regards the copolymers P(BCE$_m$BI$_n$), one could see the elastic modulus E and strain at break ε_B decreased and increased, respectively, with the increasing of BI unit content. The copolymers containing from 90 to 50 mol% BCE co-units had a high elastic modulus value, due to their semicrystalline nature. On the contrary, copolymers rich in BI counits (P(BCE$_{10}$BI$_{90}$), P(BCE$_{20}$BI$_{80}$) and P(BCE$_{30}$BI$_{70}$)) were characterized by low E values. The mechanical response of these last could be explained considering firstly their amorphous nature, then their glass transition temperature below room temperature. In these samples, the amorphous phase was fully mobile with complete loosing of resistance to applied strain (indeed low values of E and stress at break were measured in these cases). Strain at break progressively increased with increasing BCE unit content, parallel to a decrease in the T_g value.

Comparing PBCE homopolymer under investigation with the one previously reported, one can see the former was characterized by lower E and higher ε_B, as expected if we considered it was less crystalline, due to higher cis isomer content.

9.6 Barrier properties

In order to evaluate the possible use of these new materials in food packaging, a study of the gas barrier properties was carried out. Specifically, the gas transmission rate (GTR) to dry oxygen and carbon dioxide was measured. The values obtained were collected in **Table 9.7**, and shown in **Figure 9.6**.

As indicated by the values reported in **Table 9.7** and clearly shown in **Figure 9.6**, gas barrier performances were correlated strictly to copolymer composition, the GTRs decreasing with the amount of BI counits present in the samples. A particularly consistent improvement (two order of magnitude) was observed for copolymers rich in BI counits (($P(BCE_{20}BI_{80})$) and ($P(BCE_{10}BI_{90})$)), which showed performances close to the outstanding ones of the homopolymer PBI, despite their amorphous nature.

Table 9.7: Gas barrier properties to oxygen and carbon dioxide of the analyzed films.

Sample	GTR-O_2 23 °C; 0%RH cm^3 cm/m^2 d atm	GTR-CO_2 23 °C; 0%RH cm^3 cm/m^2 d atm
PBCE	2.7	8
$P(BCE_{90}BI_{10})$	1.24	3.48
$P(BCE_{80}BI_{20})$	0.75	3.0
$P(BCE_{70}BI_{30})$	0.95	2.95
$P(BCE_{50}BI_{50})$	0.16	2.76
$P(BCE_{30}BI_{70})$	0.005	0.02
$P(BCE_{20}BI_{80})$	0.001	0.005
$P(BCE_{10}BI_{90})$	0.001	0.004
PBI	0.001	0.003

The less performant samples, even though slightly better than PBCE homopolymer, were semicrystalline with a mobile amorphous phase at the temperature of measurement (23°C). The copolymer rich in BI counits were on the contrary glassy amorphous.

From the trend observed, we can evict the gas barrier properties were mainly determined by the reasons which explained the outstanding performances of PBI (see Paragraph 7.5).
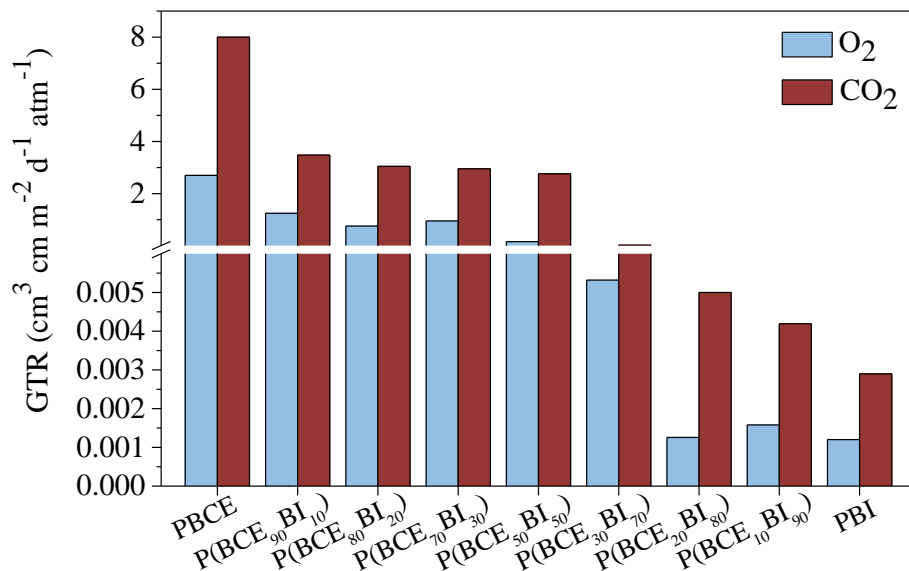
Figure 9.6*: GTR values to oxygen and carbon dioxide for PBCE, PBI and their random copolymers.*

9.7   Conclusions

The design of the new polymers revealed to be perfectly centered with respect to the intended application and copolymerization appeared to be a winning strategy to combine in the new polymer the optimal characteristics of each reference homopolymer.

The copolymers of PBI and PBCE showed indeed high thermal stability, very good mechanical performances and smart gas barrier properties. In particular, the functional properties (mechanical and gas barrier) could be nicely tuned changing copolymer composition, thus allowing the preparation of a wide *plethora* of new polymers, which range from rigid to flexible. The copolymers rich in BI counits were characterized by huge gas barrier properties, similar to those of EVOH, which currently was employed as high gas barrier layer in commercial multilayered films. Such films were moreover characterized by a mechanical response which render them suitable for high barrier flexible packaging films.

9.8   Bibliography

1.   Jin, H. J., Lee, B. Y., Kim, M. N., Yoon, J. S. Thermal and mechanical properties of mandelic acid-copolymerized poly(butylene succinate) and poly(ethylene adipate). *J. Polym. Sci. Part B Polym. Phys.* **38**, 1504–1511 (2000).

2.   Witt U, Muller R.J., D. W. *J Macromol Sci Pure Appl Chem* **A43**, 851 (1994).

3. Witt U., Muller R.J., Augusta J., Widdecke H, D. *Macromol Chem Phys* **195**, 793 (1994).

4. Nagata, M., Goto, H., Sakai, W., Tsutsumi, N. Synthesis and enzymatic degradation of poly(tetramethylene succinate) copolymers with terephthalic acid. *Polymer (Guildf)*. **41**, 4373–4376 (2000).

5. Ki, H. C., Ok Park, O. Synthesis, characterization and biodegradability of the biodegradable aliphatic-aromatic random copolyesters. *Polymer (Guildf)*. **42**, 1849–1861 (2001).

6. Kim, Y. J., Park, O. O. Miscibilities and rheological properties of poly(butylene succinate)-poly(butylene terephthalate) blends. *J. Appl. Polym. Sci.* **72**, 945–951 (1999).

7. Kint, D. P. R., Alla, A., Deloret, E., Campos, J. L., Muñoz-Guerra, S. Synthesis, characterization, and properties of poly(ethylene terephthalate)/poly(1,4-butylene succinate) block copolymers. *Polymer (Guildf)*. **44**, 1321–1330 (2003).

8. Shah, A. A., Kato, S., Shintani, N., Kamini, N. R., Nakajima-Kambe, T. Microbial degradation of aliphatic and aliphatic-aromatic co-polyesters. *Appl. Microbiol. Biotechnol.* **98**, 3437–3447 (2014).

9. Jacquel, N., Saint-Loup, R., Pascault, J. P., Rousseau, A., Fenouillot, F. Bio-based alternatives in the synthesis of aliphatic-aromatic polyesters dedicated to biodegradable film applications. *Polymer (Guildf)*. **59**, 234–242 (2015).

10. Witt, U., Müller, R. J., Deckwer, W. D. Studies on sequence distribution of aliphatic/aromatic copolyesters by high-resolution 13C nuclear magnetic resonance spectroscopy for evaluation of biodegradability. *Macromol. Chem. Phys.* **197**, 1525–1535 (1996).

11. Berti, C., Celli, A., Marchese, P., Marianucci, E., Barbiroli, G., & Di Credico, F. Influence of molecular structure and stereochemistry of the 1,4-cyclohexylene ring on thermal and mechanical behavior of poly(butylene 1,4-cyclohexanedicarboxylate). *Macromol. Chem. Phys.* **209**, 1333–1344 (2008).

12. Berti, C., Binassi, E., Celli, A., Colonna, M., Fiorini, M., Marchese, P., ... & Brunelle, D. J Poly(1,4-cyclohexylenedimethylene 1,4- cyclohexanedicarboxylate): Influence of Stereochemistry of 1,4-Cyclohexylene Units on the Thermal Properties. **46**, 619–630 (2008).

13. Genovese L., Lotti N., Gazzano M., Finelli L. New eco-friendly random copolyesters based on poly(propylene cyclohexanedicarboxylate): Structure-properties relationships. *Express Polym. Lett.* **9**, 972–983 (2015).

14. Gigli, M., Lotti, N., Vercellino, M., Visai, L., Munari, A. Novel ether-linkages containing aliphatic copolyesters of poly(butylene 1,4-cyclohexanedicarboxylate) as promising candidates for biomedical applications. *Mater. Sci. Eng. C* **34**, 86–97 (2014).

15. Frost, J. W. Synthesis of biobased and substituted terephthalic acids and isophthalic acids. 5–6 (2016).

16. He, Y. C., Wu, Y. D., Pan, X. H., Ma, C. L. Biosynthesis of terephthalic acid, isophthalic acid and their derivatives from the corresponding dinitriles by tetrachloroterephthalonitrile-induced Rhodococcus sp. *Biotechnol. Lett.* **36**, 341–347 (2014).

17. Bramucci, A. US 6,187,569 B1 (2001).

18. Conix, A., Van Kerpel, R. Crystallization behavior and melting properties of m-phenylene group containing polyesters. *J. Polym. Sci.* **40**, 521–532 (1959).

19. Roupakias, C. P., Bikiaris, D. N., Karayannidis, G. P. Synthesis, thermal characterization, and tensile properties of alipharomatic polyesters derived from 1,3-propanediol and terephthalic, isophthalic, and 2,6-naphthalenedicarboxylic acid. *J. Polym. Sci. Part A Polym. Chem.* **43**, 3998–4011 (2005).

20. Kotek, R., Pang, K., Schmidt, B., Tonelli, A. Synthesis and gas barrier characterization of poly(ethylene isophthalate). *J. Polym. Sci. Part B Polym. Phys.* **42**, 4247–4254 (2004).

21. Karayannidis, G. P., Sideridou, I. D., Zamboulis, D. N., Bikiaris, D. N., Sakalis, A. J. Thermal behavior and tensile properties of poly(ethylene terephthalate-co-ethylene isophthalate). *J. Appl. Polym. Sci.* **78**, 200–207 (2000).

22. Colonna, M., Berti, C., Binassi, E., Celli, A., Fiorini, M., Marchese, P., Brunelle, D. J. Poly(1,4-cyclohexylenedimethylene-1, 4-cyclohexanedicarboxylate): Analysis of parameters affecting polymerization and cis-trans isomerization. *Polym. Int.* **60**, 1607–1613 (2011).

23. Sun, Y. M., Wang, C. S. Preparation and characterization of poly(ethylene-1,4-cyclohexanedimethylene arylate). *Eur. Polym. J.* **35**, 1087–1096 (1999).

24. Guidotti, G., Soccio, M., Siracusa, V., Gazzano, M., Munari, A., Lotti, N. Novel random copolymers of poly(butylene 1,4-cyclohexane dicarboxylate) with outstanding barrier properties for green and sustainable packaging: Content and length of aliphatic side chains as efficient tools to tailor the material's final performance. *Polymers (Basel).* **10**, (2018).

25. Gigli, M., Lotti, N., Gazzano, M., Siracusa, V., Finelli, L., Munari, A., Dalla Rosa, M. Fully aliphatic copolyesters based on poly(butylene 1,4- cyclohexanedicarboxylate) with promising mechanical and barrier properties for food packaging applications. *Ind. Eng. Chem. Res.* **52**, 12876–12886 (2013).

26. Gigli, M., Lotti, N., Gazzano, M., Siracusa, V., Finelli, L., Munari, A., Dalla Rosa, M. Biodegradable aliphatic copolyesters containing PEG-like sequences for sustainable food packaging applications. *Polym. Degrad. Stab.* **105**, 96–106 (2014).

10 BLOCK COPOLYMERS OF POLY(3-HYDROXYBUTYRATE) (PHB) AND POLY(BUTYLENE/2-BUTYL-2-ETHYL-PROPYLENE 1,4-CYCLOHEXANE DICARBOXYLATE) (PBBEPCE): A BIOBASED PLASTIC SOLUTION FOR AN ENVIRONMENTALLY SUSTAINABLE SOCIETY

10.1 Introduction

A promising alternative to traditional and recalcitrant petroleum-based plastics are the polyhydroxyalkanoates (PHAs), bacterially synthesized polyesters[1]. PHAs attract the attention of both industries and researchers thanks to their versatility and green origin, making this class of materials a key player in the construction of an environmentally sustainable society. Nowadays, over 90 different types of PHAs, composed by various monomers, are reported and the number keeps growing. Some PHAs behave similarly to conventional plastics as polyethylene and polypropylene, while others present an elastomeric behavior[2]. One of the most representative – and investigated- member of this family is poly(3-hydroxybutyrate) (PHB). Despite its bio-based, biodegradable and biocompatible[2–5] nature, this polymer is characterized by high fragility, narrow processability window, high rate of crystallization and quite good barrier performance[6], that make its application in packaging field quite difficult. A possible approach to make PHB a real alternative to common polymers, improving in mechanical and barrier properties but maintaining its bio-based and biodegradable nature, could be copolymerization. In accordance with this idea, a random copolyester containing side aliphatic chains of different lengths was employed. In detail poly(butylene *trans*-1,4-cyclohexane dicarboxylate) was copolymerized in presence of 2-butyl-2-ethyl propanediol on the basis of our previous investigation, where the material demonstrated high flexibility and outstanding barrier properties. The two selected materials, PHB and poly(butylene cyclohexane dicarboxylate)-based copolyester, were combined by chain extension reaction, obtaining a new bio-based multiblock copolymer, for which the impact of different component ratio on the final properties was evaluated.

10.2 Synthesis and molecular characterization of prepolymers

PHB-block prepolymer, PHB-OH, was synthetized starting from commercial PHB (containing 7 mol% hydroxyvalerate) conducting the depolymerization procedure in presence of 1,4-butanediol described in "Methods and Materials" section.

The production of low molecular weight prepolymer was essential to produce block copolymeric system, being commercial PHB characterized by long chains where the reacting terminal groups were not easily available for the reaction. The so-obtained prepolymer PHB-OH was characterized from the molecular point of view by means of ^{1}H-NMR.
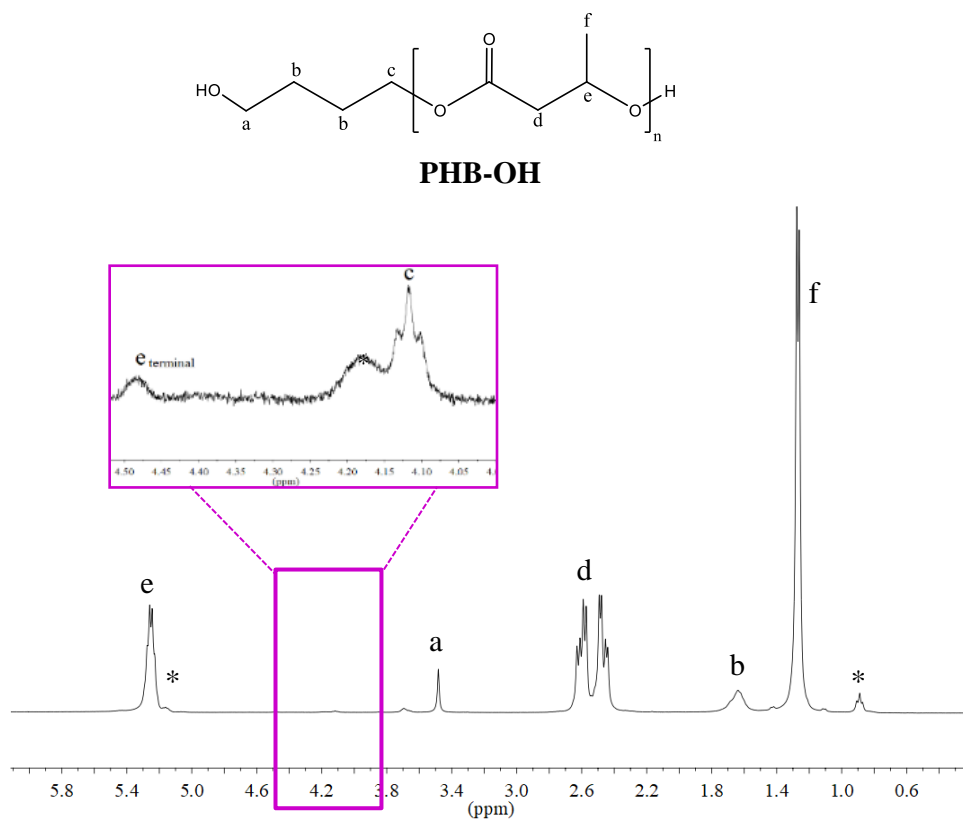
PHB-OH

Figure 10.1: *^{1}H-NMR spectrum of PHB-OH prepolymer with the relative peak assigned, identified as letters. Hydroxyvalerate signals are marked with *.*

The spectrum of PHB-OH was reported in **Figure 10.1**. In details, at 5.28 ppm the e proton, α located to the ester bond, resonated. As regards the remaining signals of the hydroxybutyrate repeating unit: at 2.52 ppm the signal of the d -CH$_2$- groups was located while at 1.22 ppm the peak of the f -CH$_3$ moiety was observed. In the inset, the signals proper of terminal moieties were showed: the e$_{terminal}$ and c protons of the terminal hydroxybutyrate and butanediol, at 4.48 and 4.12 ppm, respectively. The signals at 3.44 and 1.65 ppm were due to the 1,4-butandiol used in excess to promote depolymerization. The peaks identified as * were referred to the traces of hydroxyvalerate (**Figure 10.1**).

As one can see, no unexpected peaks were observed, therefore, the depolymerization process could

be considered adequately set.

The second prepolymer, poly(butylene/2-butyl-2-ethyl-propylene trans 1,4-cyclohexane dicarboxylate), P(BCE$_{70}$BEPCE$_{30}$), was constituted by a random distribution of butylene *trans* 1,4-cyclohexane dicarboxylate (70 mol%) and 2-butyl-2-ethyl propylene 2-butyl-2-ethyl-propylene trans 1,4-cyclohexane dicarboxylate (30 mol%). A standard two step polycondensation process was conducted with an excess of the two diols with respect to the acid, in order to obtain hydroxyl-ended chains; further details about the synthetic strategy were reported in "Methods and Materials" section. P(BCE$_{70}$BEPCE$_{30}$) was investigated via ^{1}H-NMR and ^{13}C-NMR (**Figure 10.2** and **Figure 10.3**) confirming the predicted structure and a random distribution of the sequences.
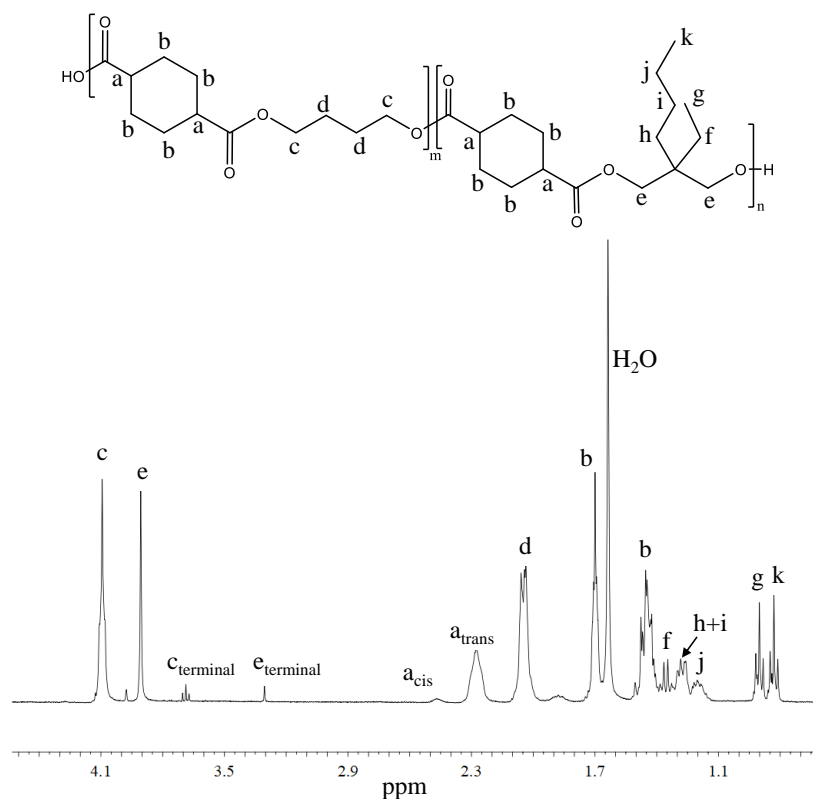
Figure 10.2*: ^{1}H-NMR spectrum of P(BCE$_{70}$BEPCE$_{30}$) with the relative peak assignment.*

In **Figure 10.2**, the spectrum of P(BCE$_{70}$BEPCE$_{30}$) was reported together with the peak assignment. The composition, reported in **Table 10.1**, was calculated from the area of the peaks of butylene sub-unit, the c signal at 4.11 ppm, and of the signal of butyl-ethyl propylene moiety, the e peak at 3.90 ppm.

The percentage of *cis* isomer present in the final product was calculated by the integral of a_{trans}, at 2.31 ppm and a_{cis}, at 2.43 ppm, and resulted close to 3%. Therefore, negligible isomerization processes took place during the polycondensation. The feed composition was closed to the obtained one, confirming a good control of the process.
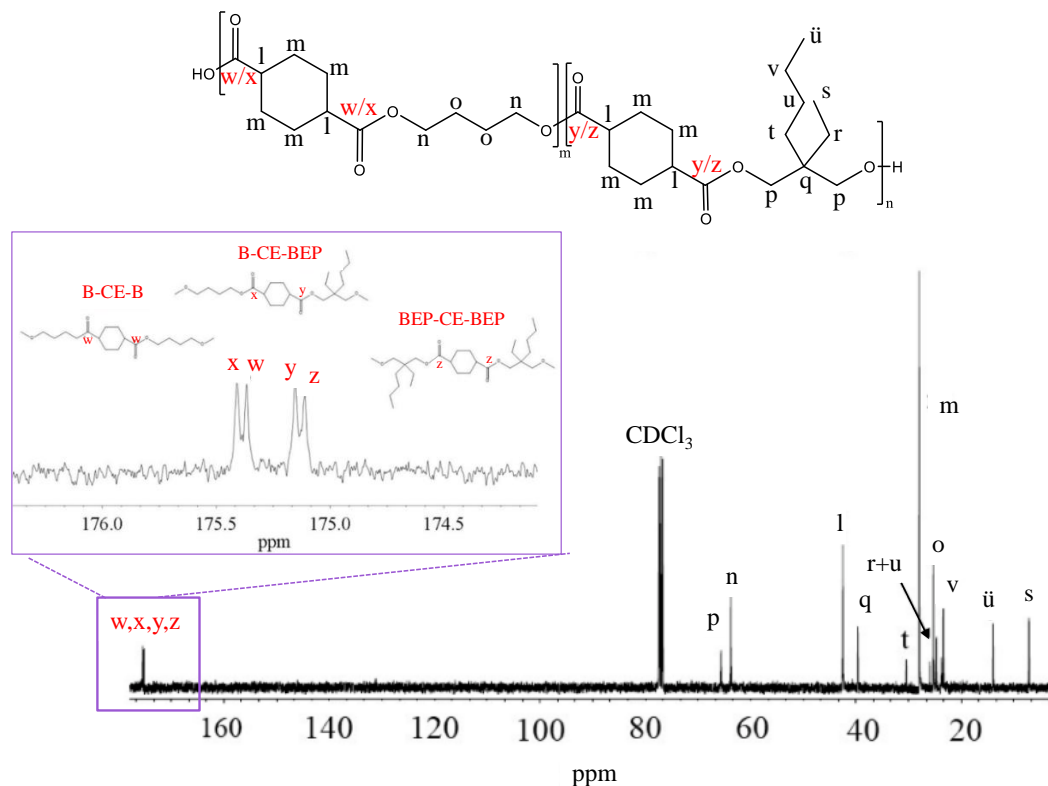
Figure 10.3: ^{13}*C-NMR spectrum recorded for P(BCE$_{70}$BEP$_{30}$) with the relative peak assignment. A magnification of the zone 179-174 ppm is inserted.*

^{13}C-NMR spectroscopy, besides confirming the chemical structure expected (see the ^{13}C-spectrum of P(BCE$_{70}$BEPCE$_{30}$) **Figure 10.3** with the relative peak assignment), was employed to calculate the degree of randomness (b). In particular, the carbon atoms of carboxylic groups located between 176.50 and 174 ppm, were used: the w signal due to the triad butanediol-cyclohexane-butanediol (B-CE-B) at 175.38, the z peak of the BEP-CE-BEP sequences at 175.13 ppm and the x and y peaks due to the B-CE-BEP and BEP-CE-B triads. The integrals of these peaks were employed in following equation.

$$b = P_{B-BEP} + P_{BEP-B} \qquad\qquad Eqn.\ 1$$

where $P_{B\text{-}BEP}$ and $P_{BEP\text{-}B}$ represent the probability of finding 1,4-butandiol, B, next to a 2-butyl-2-ethyl propanediol BEP, and the probability of finding a BEP moiety followed by a B one.

$P_{B\text{-}BEP}$ and $P_{BEP\text{-}B}$ could be defined by the following equations:

$$P_{B-BEP} = \frac{I_x}{I_x+I_w};$$ *Eqn. 2*

$$P_{BEP-B} = \frac{I_y}{I_y+I_z}$$ *Eqn. 3*

where I_x, I_w, I_y, I_z represent the integrated intensities of the peaks of the B-CE-BEP, B-CE-B, BEP-CE-B and BEP-CE-BEP.

The final value of b resulted 1.01, corresponding to random copolymers, confirming the good reaction control.

The molecular weight (M_n) reported for both the prepolymers, PHB-OH and P(BCE$_{70}$BEPCE$_{30}$), was evaluated via ^{1}H-NMR as follows:

$$DP = \left[\frac{I_{Int}/2}{I_{ext}} * 2 \right] + 1$$ *Eqn. 4*

$$Mn = DP * MW_{r.u.} + MW_t$$ *Eqn. 5*

Where, DP represents the degree of polymerization, I_{Int} is the area of a signal of the inner repeating unit and I_{ext} represents the area of the same proton in the terminal unit. $MW_{r.u.}$ is the molecular weight of the repeating unit while MW_t the molecular weight of the terminal unit.

In details, for PHB-OH, the calculation was made using the integrals of the e and e$_{terminal}$ protons (see **Figure 10.1**) as I_{Int} and I_{ext}, respectively; while in case of P(BCE$_{70}$BEPCE$_{30}$) (see **Figure 10.2**), the DP was obtained by considering the sum of c and e signals, as I_{Int}, and the sum of c$_{terminal}$ and e$_{terminal}$ peaks, as I_{ext}.

***Table 10.1**: Molecular characterization data of PHB-OH and P(BCE$_{70}$BEPCE$_{30}$) prepolymers.*

	M_n g/mol ^{1}H-NMR	DP	BCE mol% ^{1}H-NMR	BEPCE mol% ^{1}H-NMR
PHB-OH	12000	130	-	-
P(BCE$_{70}$BEPCE$_{30}$)	7300	29	70	30

10.3 Synthesis and characterization of block copolymers

PHB-OH and P(BCE$_{70}$BEPCE$_{30}$) were mixed in presence of a chain extender, hexamethylene diisocyanate (HDI), this latter reacting with the hydroxylic terminal groups of the two prepolymers formed the block copolymeric structure. Further details of the synthesis were reported in "Methods and Materials" section. Two multiblock copolymers with different weight composition were prepared (**Table 10.2**) and analysed.

Table 10.2: *Molecular characterization data P(HB$_x$-b-(BCE$_{70}$BEP$_{30}$)$_y$).*

Sample	PHB-OH wt% ^{1}H-NMR	M$_n$ g/mol	DP
P(HB$_{50}$-b-(BCE$_{70}$BEPCE$_{30}$)$_{50}$)	50	12300	21
P(HB$_{72}$-b-(BCE$_{70}$BEPCE$_{30}$)$_{28}$)	72	22000	39

The products were subjected to nuclear magnetic resonance spectroscopy in order to verify the structure. As an example, the spectrum recorded for P(HB$_{72}$-b-(BCE$_{70}$BEPCE$_{30}$)$_{28}$) was reported in **Figure 10.4**.
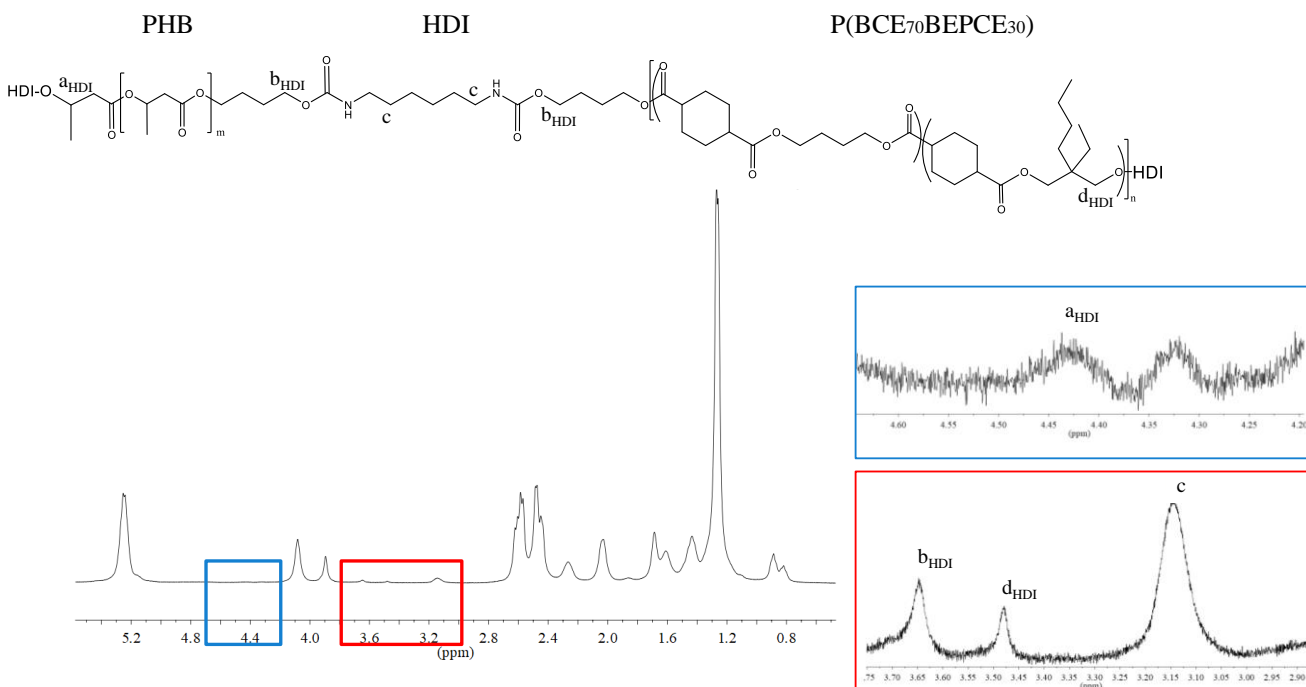
Figure 10.4: *^{1}H-NMR spectrum of P(HB$_{72}$-b-(BCE$_{70}$BEPCE$_{30}$)$_{28}$). For sake of clarity, just the new resonance peaks, i.e. the ones coming from the reaction with HID, are indicated in the inset (4.65-4.20 and 3.75-2.90 ppm).*

As one can see, the peaks agreed with the predicted structure; also, the presence of the signal at 3.15 ppm proper of the reacted HDI, confirmed the incorporation of the chain extender in the polymer chain.

10.4 Thermal and structural characterization

Thermogravimetric analysis was used to evaluate the thermal stability of the synthetized samples, evaluating the gravimetric weight loss by heating the sample from 40°C to 800°C at 10°C/min, under inert atmosphere.

The data collected were reported in **Table 10.3** while the curves were reported in **Figure 10.5.**

Table 10.3: *TGA data collected for the prepolymers, PHB-OH and P(BCE$_{70}$BEPCE$_{30}$), and for the block copolymers.*

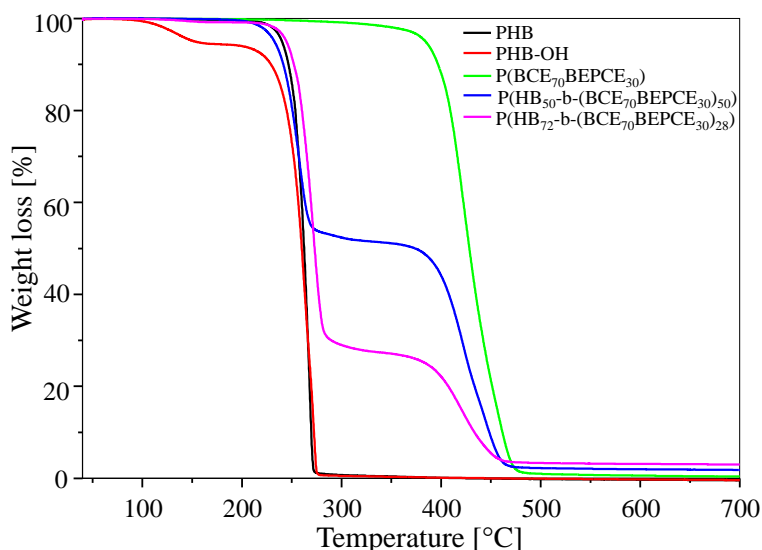|	$T_{5\%}$ °C	$T_{onset\ I}$ °C	$T_{onset\ II}$ °C	$T_{max\ I}$ °C	$T_{max\ II}$ °C
PHB	223	255	-	268	-
PHB-OH	154	251	-	273	-
P(BCE$_{70}$BEPCE$_{30}$)	384	-	421	-	399
P(HB$_{50}$-b-(BCE$_{70}$BEPCE$_{30}$)$_{50}$)	232	240	399	258	422
P(HB$_{72}$-b-(BCE$_{70}$BEPCE$_{30}$)$_{28}$)	244	256	394	272	421

Figure 10.5: *TGA traces of prepolymers and block copolymers, by heating at 10°C/min under inert atmosphere.*

The analysis confirmed the exceptional stability of P(BCE$_{70}$BEPCE$_{30}$), promoted by the cyclohexane ring, as previously reported[7]. In case of PHB the temperature of the maximum rate of degradation was much lower compared to P(BCE$_{70}$BEPCE$_{30}$), but in both cases the same one-step degradation mechanism occured. PHB thermal stability was not affected by depolymerization process, being the T$_{max}$ value practically the same for PHB and PHB-OH. The only difference regarded the weight loss around 100°C, for PHB-OH, probably due to the release of water previously adsorbed as a consequence of the high hidrophylicity character of the prepolymer.

As regards the block copolymers synthetized, the stability was comprised between the values of the two prepolymers, P(BCE$_{70}$BEPCE$_{30}$) and PHB-OH. In particular, the degradation occurred in a two-step mechanism. In case of P(HB$_{50}$-b-(BCE$_{70}$BEPCE$_{30}$)$_{50}$), in the first degradation step almost 50% of the initial weight was lost, corresponding to the percentage of PHB-OH prepolymer used; then, P(BCE$_{70}$BEPCE$_{30}$) component underwent degradation for the remaining 50%. In the same way, P(HB$_{72}$-b-(BCE$_{70}$BEPCE$_{30}$)$_{28}$) lost 70% of its weight corresponding to the percetage of PHB-OH, while the second step of degradation was corresponding to the final 30% of P(BCE$_{70}$BEPCE$_{30}$).
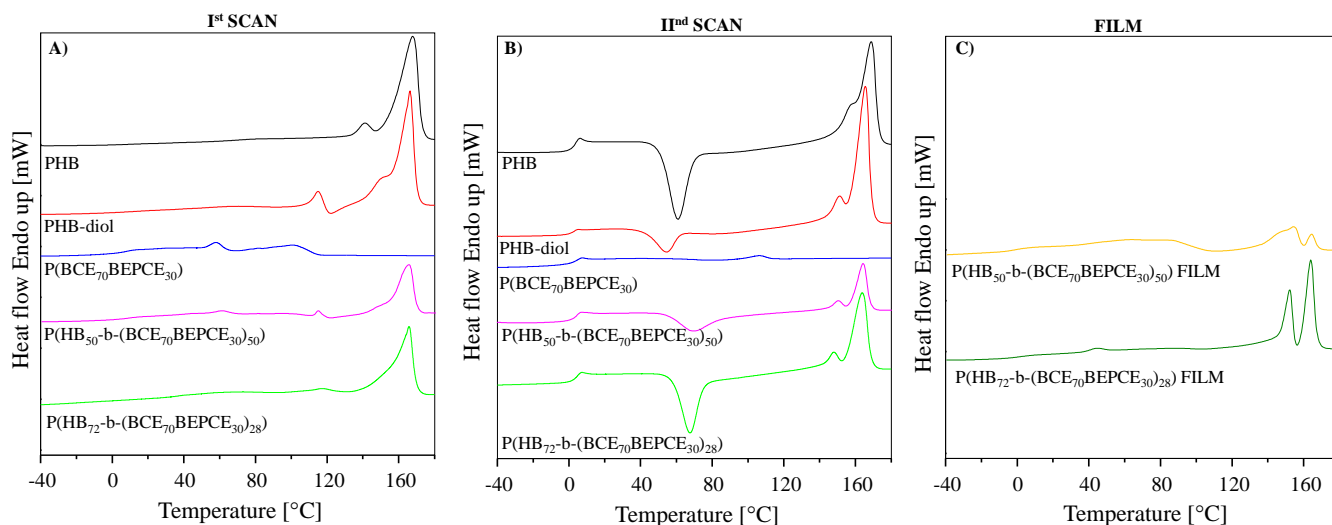

***Figure 10.6**: A) DSC curves recorded during Ist A) and IInd heating B) scans of the as-synthesized PHB homopolymer, prepolymers and block copolymers; C) DSC curves obtained from the compression moulded films of P(HB$_{50}$-b-(BCE$_{70}$BEPCE$_{30}$)$_{50}$) and of P(HB$_{72}$-b-(BCE$_{70}$BEPCE$_{30}$)$_{28}$).*
Heating rate: 20 °C/min under nitrogen flow.

The specific thermal transitions were evaluated by means of differential scanning calorimetry analysis. The details of the conducted measurements were reported in "Methods and Materials" section, while the so-obtained curves and results were respectively reported in **Figure 10.6** and **Table 10.4.**

As one can see, the Ist scan (**Figure 10.6 A**) showed a semicrystalline nature for all the reported samples, both prepolymers and block copolymers as well as the neat PHB homopolymer. PHB-OH presented the main melting peak close to the commercial PHB, around 168°C. Then, a second peak was observed at lower temperature for both the samples and attributed to two possible processes: melting of less perfect crystalline phase or a sequence of melting, recrystallization and melting of crystals. In case of PHB-OH, the low-melting peak was shifted to lower temperature followed by an exothermic process more marked compared to PHB. In this case, a sequence of melting-recrystallization-melting could be supposed, being the polymer chains present in PHB-OH shorter than the macromolecules of the high molecular weight PHB, and consequently more likely to rearrange and crystallize than longer polymer chains. As concerns P(BCE$_{70}$BEPCE$_{30}$) prepolymer, it was characterized by two melting peaks, one around 58°C and the second at 101°C. Both the phenomena were large and not very intense, since a defective and not abudant crystalline phase could be supposed. The absence of well-ordered lattice could be attributed to the intrinsic chemical structure of P(BCE$_{70}$BEPCE$_{30}$), where the long side branches of BEP moiety hampered the packing of the polymeric chains leading to low-crystalline sample.

As concern the two block copolymers synthetized, they presented a main melting peak around 164°C, corresponding to the melting of PHB-blocks. The enthalpy of melting (see ΔH_m values in **Table 10.4**) gave information about the crystals populating the samples, that resulted lower compared with pure PHB. In details, the higher the amount of the P(BCE$_{70}$BEPCE$_{30}$) block, the lower the crystalline phase developed. Indeed, P(HB$_{50}$-b-(BCE$_{70}$BEPCE$_{30}$)$_{50}$) had lower ΔH_m value compared to P(HB$_{72}$-b-(BCE$_{70}$BEPCE$_{30}$)$_{28}$) one. Despite that, in P(HB$_{50}$-b-(BCE$_{70}$BEPCE$_{30}$)$_{50}$), a small melting peak was observed around 60°C coinciding with the one observed for the pure block, P(BCE$_{70}$BEPCE$_{30}$).

In order to analyse the glass to rubber transition, more visible in fully amorphous materials, the samples were melted and fast cooled to hamper the crystallization process (see **Figure 10.6 B**). Except for PHB-OH, all the materials were quenched by applying the thermal treatment described.

During the subsequent heating (IInd scan) all the polymers were able to organize in ordered structures in correspondence of cold crystallization temperature, T_{cc}, and then melted at higher temperature (T_m). Nevertheless, the similar values of ΔH_{cc} and ΔH_m testify the effectiveness of quenching. Despite the fast cooling, PHB-OH molecules were still able to crystallize during cooling being $\Delta H_c < \Delta H_m$. This behaviour was in line with the results of the previous DSC scan that had highlighted how shorter polymer chains present higher crystallization rate. As concern the amorphous phase, glass transition resulted very similar for all the materials and below room temperature (see **Table 10.4**), thus, at room temperature the samples could be considered in rubbery state.

Table 10.4*: Thermal and structural characterization data of prepolymers and block copolymers.*

	I^{st} SCAN		IInd SCAN					
	T_m °C	ΔH_m J/g	T_g °C	ΔC_p J/g°C	T_{cc} °C	ΔH_{cc} J/g	T_m °C	ΔH_m J/g
Prepolymers								
PHB	168	89	2	0.479	61	60	169	63
PHB-OH	166	84	2	0.197	54	13	166	76
P(BCE$_{70}$BEPCE$_{30}$)	58 101	3 1	3	0.275	82	1	106	1
Block copolymers								
P(HB$_{50}$-b-(BCE$_{70}$BEPCE$_{30}$)$_{50}$)	60 165	2 29	3	0.351	69	21	164	22
P(HB$_{72}$-b-(BCE$_{70}$BEPCE$_{30}$)$_{28}$)	166	54	3	0.437	67	43	164	47

P(HB$_{50}$-b-(BCE$_{70}$BEPCE$_{30}$)$_{50}$) and P(HB$_{72}$-b-(BCE$_{70}$BEPCE$_{30}$)$_{28}$) were subjected to compression molding to obtain thin free-standing film. In order to investigate their thermal behaviour, the samples were characterized by DSC. The curves and the collected data were reported in **Figure 10.6 C** and **Table 10.5**.

Both the samples showed semicrystalline nature, since the ballistic cooling of the films allowed crystallization; the high temperature melting peak could be attributed to the melting of the ordered phase constituted by PHB blocks. Indeed, in case of P(HB$_{72}$-b-(BCE$_{70}$BEPCE$_{30}$)$_{28}$) where PHB portion was more abundant, the value of ΔH_m was higher compared to P(HB$_{50}$-b-

($BCE_{70}BEPCE_{30})_{50}$). Moreover, the melting phenomeon took place in a shorter range of temperature since the population of crystals was narrow, compared with $P(HB_{50}$-b-$(BCE_{70}BEPCE_{30})_{50})$ where the broad peak was due to the more impactant disturbing effect of $P(BCE_{70}BEPCE_{30})$ segments. As regards the shape of melting peaks, a double transition was recorded. Generally, this shape could be attributed to two different process, as explained before. Similar to the previous case, a melting-recrystallization- melting could be supposed.

Table 10.5: Thermal characterization of compression moulded films.

Block copolymers FILM	Ist SCAN					
	T_g °C	ΔC_p J/g°C	T_{cc} °C	ΔH_{cc} J/g	T_m °C	ΔH_m J/g
$P(HB_{50}$-b-$(BCE_{70}BEPCE_{30})_{50})$	2	0.220	109	9	62 164	13 21
$P(HB_{72}$-b-$(BCE_{70}BEPCE_{30})_{28})$	2	0.131	/	/	44 163	2 59

The second peak observed, around 62°C for $P(HB_{50}$-b-$(BCE_{70}BEPCE_{30})_{50})$ and 44 °C for $P(HB_{72}$-b-$(BCE_{70}BEPCE_{30})_{28})$, was related to the melting of $P(BCE_{70}BEPCE_{30})$ lattice. Indeed, the higher $P(BCE_{70}BEPCE_{30})$ containing copolymer, $P(HB_{50}$-b-$(BCE_{70}BEPCE_{30})_{50})$, presented higher ΔH_m as well.

It was worth noting the melting temperature of the PHB block was not affected by the presence of $P(BCE_{70}BEPCE_{30})$ block, thus evidencing no transesterification reactions had occurred during the chain extension synthesis.

Wide angle X-ray scattering was performed on the samples under study, in order to deeply investigate their crystalline phase. The obtained patterns for powders and for films were reported respectively in **Figure 10.7 A** and **Figure 10.7 B**.

As concern the materials in form of powders, PHB homopolymer presented an abundant crystalline phase, confirming the data collected during DSC measurements. Differently, $P(BCE_{70}BEPCE_{30})$ had a wide amorphous halo and just some undefined peak, due to the defective crystalline phase formed.

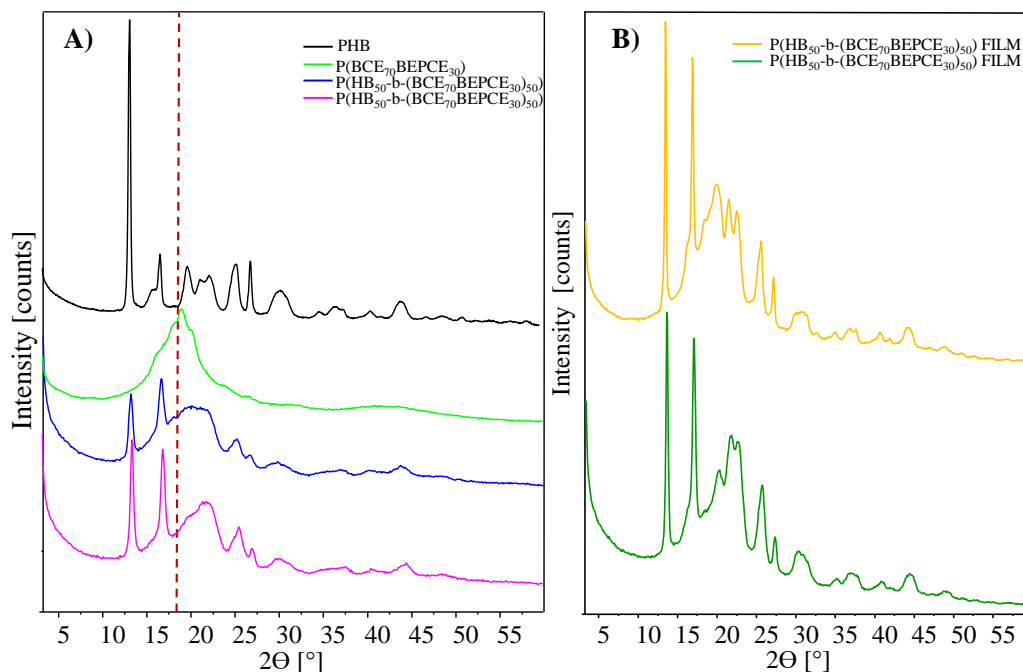***Figure 10.7***: ***A)*** *WAXS spectra of PHB homopolymer, P(BCE₇₀BEPCE₃₀) and the multiblock copolymers derived, in form of powders;* ***B)*** *WAXS spectra of P(HB₅₀-b-(BCE₇₀BEPCE₃₀)₅₀) and P(HB₇₂-b-(BCE₇₀BEPCE₃₀)₂₈) multiblock copolymers, in form of film.*

The two copolymers, P(HB$_{50}$-b-(BCE$_{70}$BEPCE$_{30}$)$_{50}$) and P(HB$_{72}$-b-(BCE$_{70}$BEPCE$_{30}$)$_{28}$), presented reflections typical of both blocks, since two different families of crystals were formed. In details, PHB-block crystallized easily as suggested by calorimetric traces, indeed the more defined peak observed were identified as due to PHB segments, while at around 20°, a wide peak proper of the lattice formed by P(BCE$_{70}$BEPCE$_{30}$) was reported, even if shifted respect to the prepolymer position. The comparison between the powders of P(HB$_{50}$-b-(BCE$_{70}$BEPCE$_{30}$)$_{50}$) and P(HB$_{72}$-b-(BCE$_{70}$BEPCE$_{30}$)$_{28}$) showed higher crystallinity degree and more intense peaks for the copolymer richer in PHB-block.

In **Figure 10.7 B**, the patterns collected for the moulded film were reported. Both the samples were able to develop a crystalline phase more efficiently packed compared with the powder one. Probably the ballistical cooling on one side, and the pressure on the other favoured the organization of the block segments. In particular, PHB-block still well organized as in the powders while P(BCE$_{70}$BEPCE$_{30}$) was presenting a more intense reflection, suggesting a better packed lattice, even if, as confirmed from DSC analysis, the final amount of crystals was not differing too much

265

from the ordered phase obtained during solvent evaporation. Comparing the two copolymers, a small shift of the signals with the composition was recorded.

10.5 Mechanical properties

The results of the mechanical analysis summarized in **Figure 10.8** and **Table 10.6**, showed the effect of the copolymerization strategy on the mechanical behaviour. In details, PHB resulted rigid, with an elastic modulus of 2185 MPa, with a breaking point at 3% of elongation, in good agreement with the high crystallinity degree recorded by DSC and WAXS analyses. The introduction of P(BCE$_{70}$BEPCE$_{30}$) prepolymer, thanks to its low elastic modulus and high elongation at break related to an abundant rubbery amorphous phase, mitigated the high rigidity of PHB. In both the copolymers the mechanical behaviour changed as a function of the amount of P(BCE$_{70}$BEPCE$_{30}$)-block. In details, the higher the amount of P(BCE$_{70}$BEPCE$_{30}$)-block the lower the elastic modulus and the stress at break (σ_b). In particular, E values was halved for P(HB$_{72}$-b-(BCE$_{70}$BEPCE$_{30}$)$_{28}$) and five times lower in case of P(HB$_{50}$-b-(BCE$_{70}$BEPCE$_{30}$)$_{50}$). The same trend was described by σ_b values. As concerns the elongation at break, ε_b, no significant effects were detected. This result could be explained considering the still high crystallinity degree of both the block-copolymers.
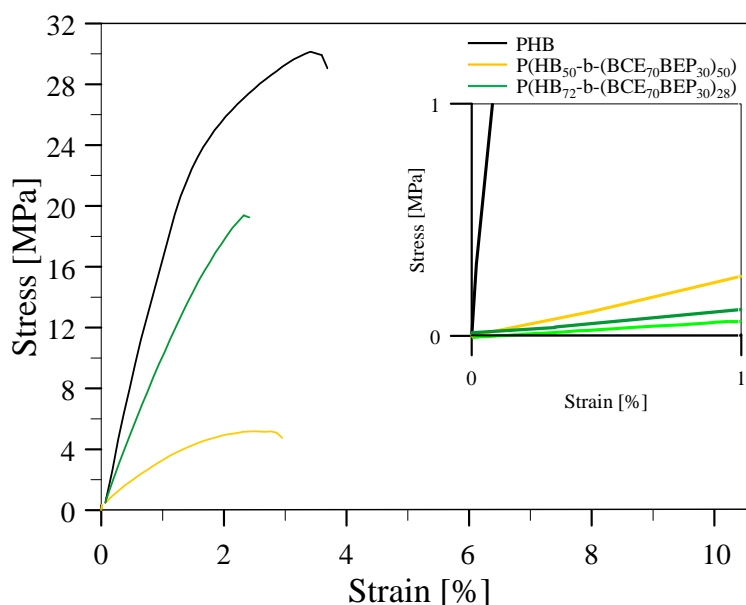

Figure 10.8*: Stress-strain curves of PHB homopolymer and P(HB$_{50}$-b-(BCE$_{70}$BEPCE$_{30}$)$_{50}$) and P(HB$_{72}$-b-(BCE$_{70}$BEPCE$_{30}$)$_{28}$) block-copolymers.*

Table 10.6: *Mechanical characterization data of PHB homopolymer and P(HB$_{50}$-b-(BCE$_{70}$BEPCE$_{30}$)$_{50}$) and P(HB$_{72}$-b-(BCE$_{70}$BEPCE$_{30}$)$_{28}$) block-copolymers.*

	E MPa	σ$_b$ MPa	ε$_b$ %
PHB	2185 ± 119	29 ± 3	3.1 ± 0.6
P(HB$_{50}$-b-(BCE$_{70}$BEPCE$_{30}$)$_{50}$)	386 ± 48	4.6 ± 0.3	3.3 ± 0.6
P(HB$_{72}$-b-(BCE$_{70}$BEPCE$_{30}$)$_{28}$)	1220 ± 37	15 ± 3	1.6 ± 0.5

10.6 Compostability

Biodegradability in compost of the multiblock copolymers was tested following the procedure presented in "Methods and Materials" section. The study was conducted considering the gravimetric weight loss (**Figure 10.9 A**), the changing in composition (**Figure 10.9 B**), the macroscopic evolution of film surface (**Figure 10.9 C**) and the thermal analysis (**Figure 10.9 C and D**).
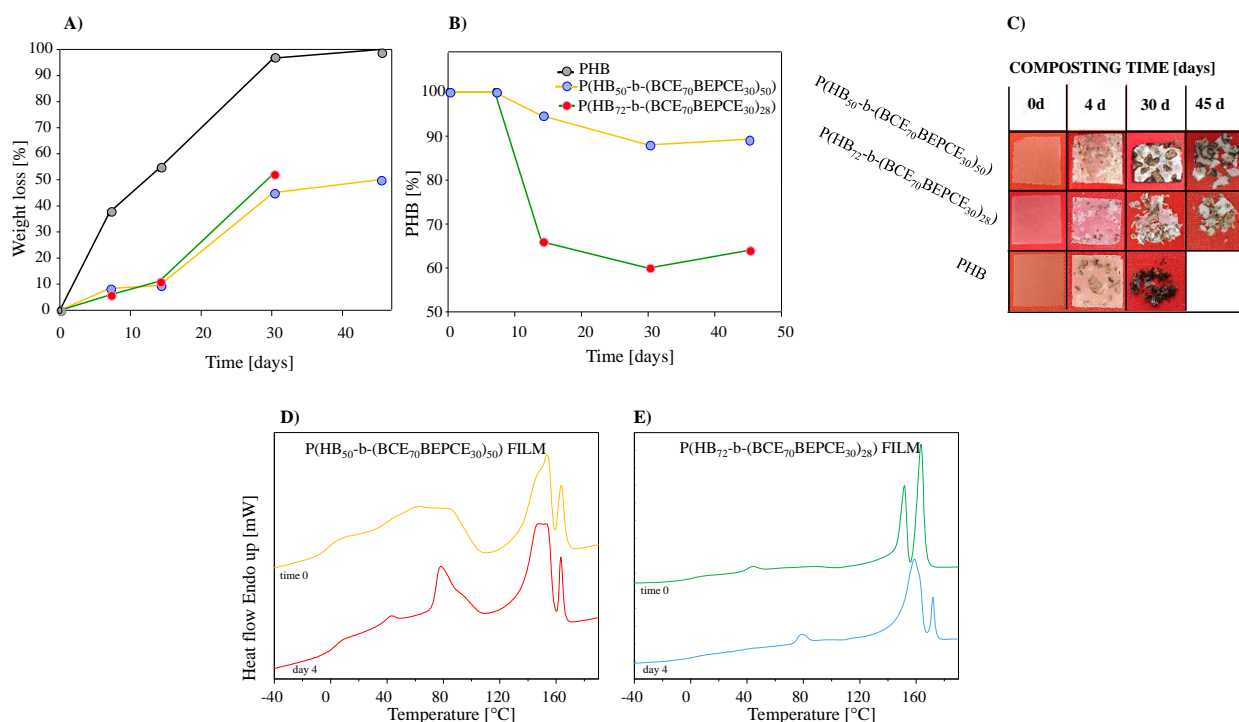

Figure 10.9: *A) Gravimetric weight loss as a function of incubation time; B) Composition (in terms PHB percent variance) as a function of incubation time; C) Macrographs of the samples incubated in compost for different time; D) and E) DSC traces of the two block-copolymers: neat film vs film incubated for 4 days.*

As one can see from **Figure 10.9 A**, after just 7 days the degradation process produced appreciable weight loss for all the materials. As concerns the neat PHB, surprisingly, it was the fastest degrading polymer regardless its high crystallinity degree, reaching the complete disintegration after just 30 days. As concern the copolymers, the disintegration rate was directly proportional to the PHB-block amount, due to the more degradable nature of PHB moiety, more easily consumed by the bacteria and fungi present in compost. Indeed, high weight loss was recorded together with a decreasing of PHB block amount as confirmed by ^{1}H-NMR analysis (**Figure 10.1 B**). The macroscopic appearance of the incubated films was in line with the weight loss and composition results, revealing firstly an increment of opacity and then of disintegration degree due to the increasing of crystalline phase, related both to annealing phenomena and to the tendency of microorganisms to degrade faster the amorphous zone of the sample. These two aspects were useful to understand the results of DSC analysis, conducted only on samples withdrawn after 4 days in compost, because at longer time of incubation the amount of compost sticked to the samples hampered the collection of meaningful data. As general consideration, an increasing of crystallinity degree, i.e. area under the endothermic curves, was observed due to the decreasing of the amorphous phase and the formation of new ordered phase by annealing. In details, as concerns $P(HB_{50}\text{-}b\text{-}(BCE_{70}BEPCE_{30})_{50})$, at the incubation temperature (56°C), the low melting block, $P(BCE_{70}BEPCE_{30})$, was able to reorganize. Indeed, a shift of its melting peak from around 60°C (time$_0$) to higher temperature, 80°C (after 4 days in compost) was observed. Together with this effect, the degradation activity of the bacteria played a role to explain the change of shapes of melting peaks. As well known, microorganisms firstly degraded the amorphous regions and then the more defective crystals; as a consequence the melting peak of $P(BCE_{70}BEPCE_{30})$-rich crystals was narrower and more defined. No appreciable effect was evidenced for the higher melting multiple peaks due to PHB-block sequences. As regards the $P(HB_{72}\text{-}b\text{-}(BCE_{70}BEPCE_{30})_{28})$ multiblock copolymer, again, an effect of composting time on the endotherms position/shape could be detected, in particular they moved to higher temperature. This result was related to the preferential degradation of the less perfect and lower melting crystal population.

10.7 Barrier properties

As previously stated, the main goal of the introduction of $P(BCE_{70}BEPCE_{30})$ sequences in the PHB backbone was the enhancement of flexibility without compromising its quite good barrier

properties. To check the barrier performance of the multiblock copolymers of PHB, the corresponding compression molded films were subjected to permeability test, according to the procedure reported in "Method and Materials". The results were shown as gas transmission rate (GTR) values to O_2 and CO_2 in **Figure 10.10**.
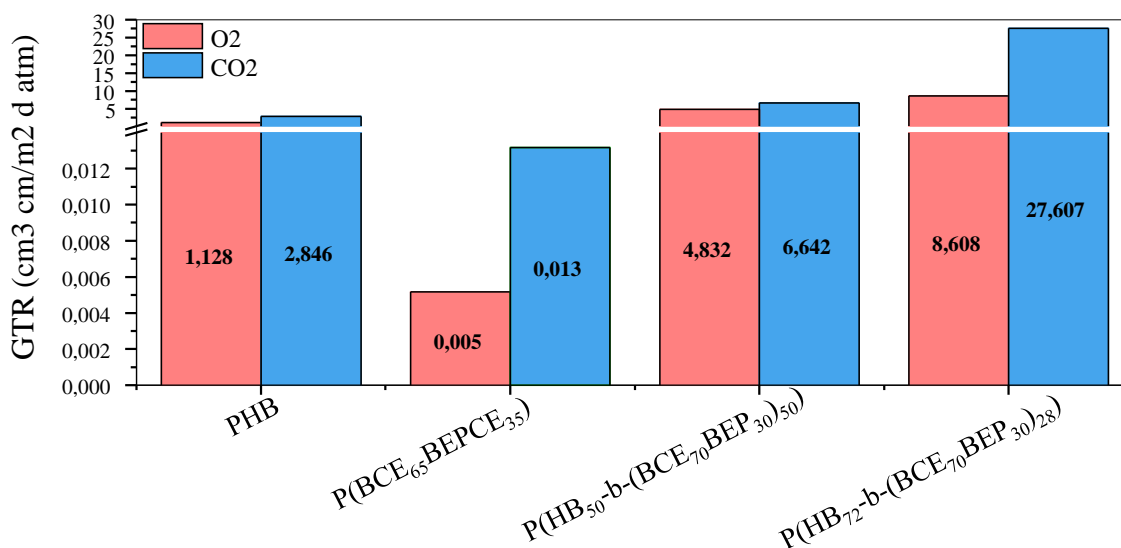

Figure 10.10. *GTR of O_2 and CO_2 through PHB, P(BCE$_{65}$BEPCE$_{35}$) and PHB$_n$P(BCE$_{70}$BEPCE$_{30}$)$_m$ copolymers films at 23°C and 0% RH.*

As reported in the literature[8], P(BCE$_{70}$BEPCE$_{30}$) polymer matrix was characterized by an outstanding ability of blocking the passage of both oxygen and carbon dioxide gases. This behavior was ascribed to the formation of a particular microstructure involving the cyclohexane ring moieties, particularly efficient in terms of gas barrier. The introduction of quite high amount of P(BCE$_{70}$BEPCE$_{30}$) block, 28 and 50 wt%, respectively, along polymer chains determined an increment of GTR values, both to O_2 and CO_2, with respect to neat PHB film. Quite surprisingly, the GTR increment was more pronounced for the less co-unit-containing copolymer, PHB$_{72}$P(BCE$_{70}$BEPCE$_{30}$)$_{28}$. This effect could be explained considering that, for lower co-unit content (28 wt%) the factor affecting mostly GTR value was the increment of interphase regions, due to the different crystalline phases related to the two different sequences. If the P(BCE$_{70}$BEPCE$_{30}$) block amount was further increased (up to 50 wt%), the factor due to inter-chain interactions among cyclohexane rings prevailed on the disclinations. In conclusion, the less rigid polymer material, PHB$_{50}$P(BCE$_{70}$BEPCE$_{30}$)$_{50}$ was also the more performant of the two. In

particular, this multiblock copolymer presented GTR values of the same order of magnitude as PHB homopolymer.

10.8 Conclusions

New fully-biobased multiblock copolymers of PHB were successfully synthesized. The introduction of P(BCE$_{70}$BEPCE$_{30}$) sequences in the PHB backbone conferred higher thermal stability to the copolymers compared to PHB homopolymer and reduced the polymer rigidity, as evidenced by significant reduction of Young´s Modulus and stress at break, strictly related to the amount of P(BCE$_{70}$BEPCE$_{30}$) used. Compostability tests were also conducted, proving the possibility to favourably increase the final material stability in compost, by introducing P(BCE$_{70}$BEPCE$_{30}$) moieties. As a matter of fact, PHB blocks were preferentially attacked even if more crystalline than the comonomeric segments. As concern the barrier ability of the multiblock copolymers, the results obtained evidenced how the quite good properties of PHB were not compromised by the P(BCE$_{70}$BEPCE$_{30}$) block presence. To conclude, chain extension strategy resulted an interesting approach to produce multiblock copolymers and a useful tool to tune the final properties of materials. In our specific case, P(BCE$_{70}$BEPCE$_{30}$) inserted in PHB polymer chain, acted on the main drawbacks of the homopolymer, as rigidity and high crystallinity, leading to two examples of suitable materials for flexible packaging application.

10.9 Bibliography

1.   Zhao K, Deng Y, Chen J. C, C. G. Polyhydroxyalkanoate (PHA) scaffolds with good mechanical properties and biodegradability. *Biomaterials* **24**, 1041–1045 (2003).

2.   Yang X, Zhao K, Chen G. Q. Effect of surface treatment on the biocompatibility of microbial polyhydroxyalkanoates. *Biomaterials* **23**, 1391–1397 (2002).

3.   Gan, Z., Abe, H., Doi, Y. Crystallization, melting, and enzymatic degradation of biodegradable poly(butylene succinate-co-14 mol % ethylene succinate) copolyester. *Biomacromolecules* **2**, 313–321 (2001).

4.   Deng Y, Zhao K, Zhang XF, Hu P, C. G. Study on the three-dimensional proliferation of rabbit articular cartilage-derived chondrocytes on polyhydroxyakanoate scaffolds. *Biomaterials* **23**, 4049–4056 (2002).

5.   Zhao K, Deng Y, C. G. Effect of surface morphology on the biocompatibility of polyhydroxyalkanoates. *Bio- chem Eng J* **15**, 115–123 (2003).

6.   Yu, L., Dean, K., Li, L. Polymer blends and composites from renewable resources. *Prog. Polym. Sci.* **31**, 576–602 (2006).

7. Sun, Y. M., Wang, C. S. Preparation and characterization of poly(ethylene-1,4-cyclohexanedimethylene arylate). *Eur. Polym. J.* **35**, 1087–1096 (1999).

8. Guidotti, G., Soccio, M., Siracusa, V., Gazzano, M., Munari, A., Lotti, N. Novel random copolymers of poly(butylene 1,4-cyclohexane dicarboxylate) with outstanding barrier properties for green and sustainable packaging: Content and length of aliphatic side chains as efficient tools to tailor the material's final performance. *Polymers (Basel).* **10**, (2018).

11 ECO-FRIENDLY APPROACH THROUGH CATECHOL CARBONATE FOR POLYUREAS PRODUCTION

11.1 Introduction

In the recent years great interest has been focused on organic carbonates (OCs), resulting an important class of molecules with a wide range of applications. OCs can be employed with success as chemical intermediates, thanks to their non-toxicity and biodegradability,[1,2] but also as green aprotic solvents, due to their high boiling point and high solvency[3]. Moreover, OCs in presence of ammine can react leading to ureas and polyureas (PU). These materials boast higher chemical, thermal and mechanical stabilities compared to polyurethane counterpart [4] and can be processed in form of fibers and film for suitable applications in medical filed and food preservation[5]. Despite PU have been known since years, recently, on the base of their high performance[6], new applications are under studies (special coatings[7], innovative elastomers[8], production of special composite materials with unique properties[9,10]). The main drawback of PU is related to their most common process of synthesis that employed the addition of pretty toxic compounds as polyisocyanates with polyamines even if the notorious toxicity of isocyanate[11–13]. For this reason, the possibility to use OCs for the production of PUs represents a hot topic. An added value is done also by recent development of different bio-based amines; butane diamine and pentane diamine has been obtained from lysine and ornithine, respectively, opening new perspectives for the synthesis of bio-PU[14,15]. Among the different routes proposed, the reaction of cyclic carbonates - as propylene carbonate or diphenyl carbonate, DPC- with diamines or polyamines[1617181920] is pretty promising. Nevertheless, these reactions need to be conducted at above 90°C and take hours to achieve high conversions; moreover, catalyst is required to increase the rate and the final yield and, in order to guarantee homogeneous solutions, solvents as tetramethylene sulfone or toluene are often used. With the aim of overcoming these drawbacks, a new synthesis performed in presence of catechol carbonate, a very promising OC molecule, was proposed. The few papers available reported its good reactivity in presence of aliphatic alcohols and polyols, as glycerol, to obtain the corresponding symmetric carbonates and glycerol carbonate[21–23]. For this reason, CC was employed in a new solvent/catalyst free polycondensation process in presence of different potentially biobased diamines, as 1,4-butanediamide, 1,5-pentandiamine and 1,6-hexandiamine, in order to obtain bio-PUs.

11.2 Molecular characterization

The synthesized polyureas, polyurea 4 polyurea 5 and polyurea 6, were obtained via two step polyondensation process, conducted in mass in absence of catalyst. Considering the bio-based nature of the diamine used, 1,4-butandiamine, 1,5-pentandiamine 1,6-hexametilendiammine, which could be derived from lysine and ornithine or via fermentation, the process resulted in line with the principles of the Green Chemistry.
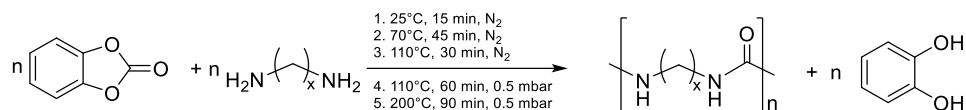

Figure 11.1: *Chemical pathway conducted to obtain polyurea 4 (x=4), polyurea 5 (x=5), polyurea (x=6).*

In a thermostated and mechanically stirred glass vial, equipped with an ice-cooled trap, catechol carbonate, CC, and an equimolar amount of diamine were added at 25°C. The temperature was raised and an increasing of the molecular weight was observed, indicated from the solidification of the reacting mass. Afterwards, the pressure was gradually decreased favoring the sublimation of catechol, accumulated in form of pure crystals and easily recycled. More details of the synthesis were reported in "Method and Materials" section. The so obtained products were fully characterized but firstly their chemical nature was verified via ^{1}H and ^{13}C NMR. The polyureas resulted not soluble in most common organic solvents, due to their high crystallinity degree, evidenced by calorimetric analysis described below, and for the inter-chain hydrogen bonds formed. As a matter of fact, NMR analysis was carried out in TFA-d solvent.

Table 11.1: *Molecular details of polyurea 4, polyurea 5 and polyurea 6.*

Sample	Yield NMR %	M_n NMR g/mol	PU isolated Yield %	Catechol isolated Yield %
Polyurea 4	>99	1370	82	85
Polyurea 5	>99	1030	83	85
Polyurea 6	>99	3200	90	90

The spectra collected revealed a good control of the process leading to clean product with high conversion and yield (**Table 11.1**). For all the materials prepared the sub-product of reaction, catechol, could be easily recovered in quantitative amount.
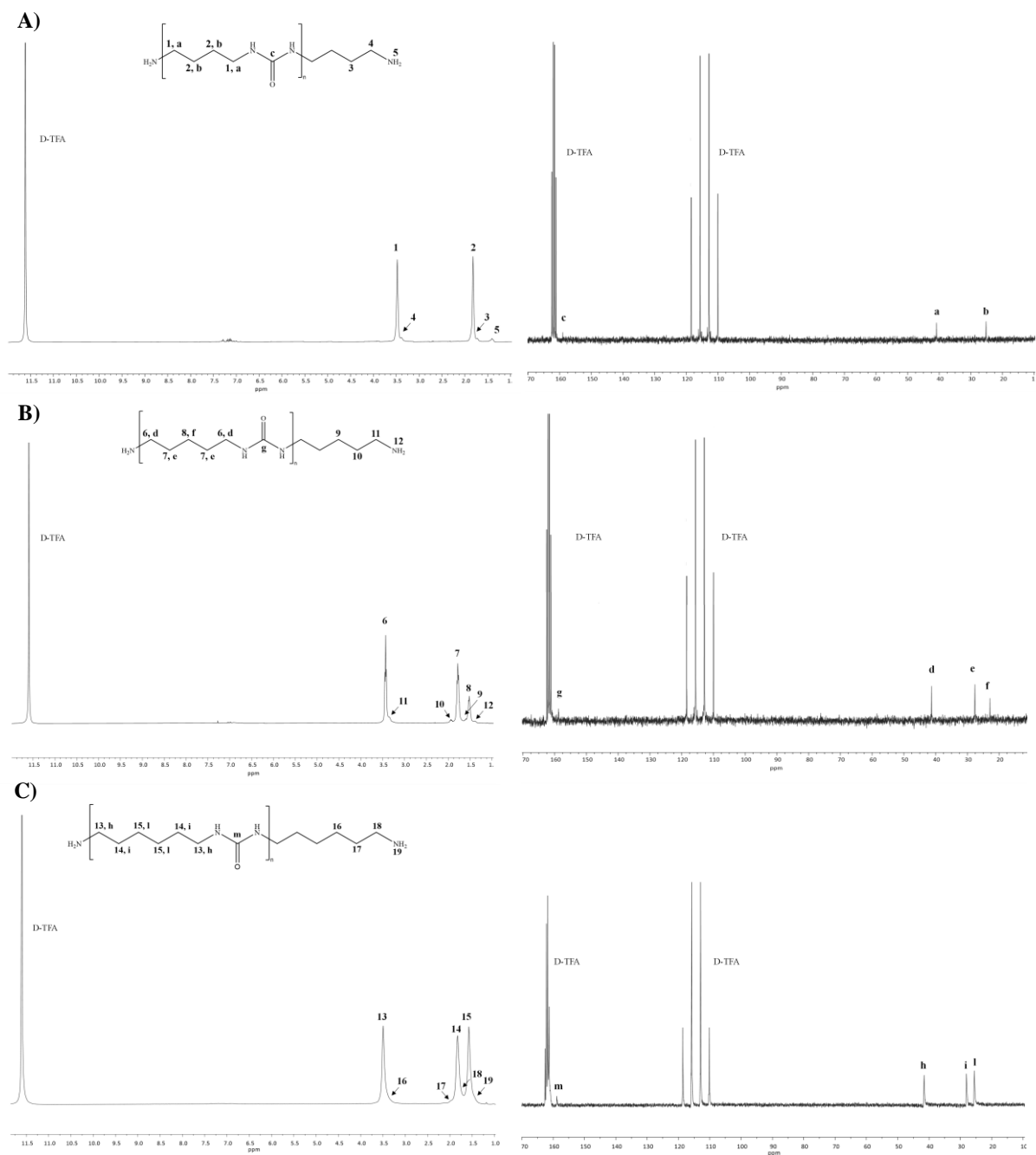
Figure 11.2: ^{1}*H-NMR and* ^{13}*C-NMR spectra recorded for A) polyurea 4, B) polyurea 5, C) polyurea 6.*

Figure 11.2 panel **A** showed the ^{1}H-NMR spectrum of polyurea 4 with the relative peak assignment. The chemical structure was confirmed: the hydrogen atoms in α position to the ureic group (1) resonated at 3.50 ppm, overlapped to the -CH$_2$- protons of the external repeating units (11) located at 3.40 ppm. At 1.75 ppm the signal assigned to protons 2 of the alkyl moiety could

be detected, again, an overlapping was observed with the signal of the same group numbered as 4, coming from the outer segments. The spectrum also reported the signal due to -NH$_2$ group at 1.25 ppm (5).

As well as ^{1}H-NMR just reported, ^{13}C-NMR spectrum, in **Figure 11.2** panel **A** right**,** confirmed the good control of the reaction. Indeed, no unexpected peaks were detected, other than those due to the a and b methylene groups of alkyl subunit at 41 ppm and 25 ppm, respectively, and the signal at 159 ppm ascribed to c ureic carbon whose presence was an evidence of the reaction occurrence.

Figure 11.2 B reported the ^{1}H-NMR (left) and ^{13}C-NMR (right) spectra of polyurea 5 with the relative peak assignments. As one can see from ^{1}H-NMR spectrum, 6, 7 and 8 protons of the alkyl subunit resonate at 3.50, 1.75 and 1.50 ppm, respectively. The other signals observed (9, 10, 11 and 12) were proper of the external subunits. Again, ^{13}C-NMR analysis allowed confirming the structure revealing the presence of the d, e and f secondary carbons at 41, 27, and 22 ppm, respectively, and the g quaternary carbon at 158 ppm.

Lastly, **Figure 11.2 C** reported the spectra recorded for polyurea 6. ^{1}H-NMR (left) confirmed the chemical structure with the signals of the alkyl subunit, 13, 14 and 15, clearly resonating at 3.50, 1.83 and 1.63 ppm. -NH$_2$ group was observed at 1.25 ppm (19), while the other peaks were attributed to the external part of the chain. At the right of **Figure 11.2 C**, ^{13}C-NMR reported the detection of carbons in line with the predicted chemical structure.

^{1}H-NMR analysis has also been used to calculate the molecular weight (see **Table 11.1**) from the normalized area of the signals relative to the external subunits (4 for polyurea 4; 11 for polyurea 5; 16 for polyurea 6) and of the peak ascribed to the inner moieties (1 for polyurea 4; 6 for polyurea 5; 13 for polyurea 6), according to the following equation:

$$DP = \frac{2*(Integral\ \textbf{\textit{ext}}+Integral\ \textbf{\textit{int}})}{Integral\ \textbf{\textit{ext}}} * Mn\ repeat\ unit \qquad\qquad Eqn.\ 1$$

Molecular characterization was completed by FTIR analysis (**Figure 11.3**). Besides the righthand region comprised between 1550 to 500 cm^{-1}, identified as fingerprint region and characteristic of each individual molecule, the spectra collected clearly showed for polyurea 4, polyurea 5 and polyurea 6 the typical stretching bands. Carbonyl of the urea functional group and the amide stretching of CO–NH were observed at 1625 and 1550 cm^{-1}, respectively, while at 3300 cm^{-1} was

located the secondary amine group, proper of all the prepared polyureas. The remaining peaks in between 3000 and 2800 cm^{-1} referred to the C-H bonds of the alkyl segments. In the series of polyurea 4, 5 and 6, the higher the length of the aliphatic segments of the repeating unit the more intense the C-H peak compared with the signal of the secondary amine group.
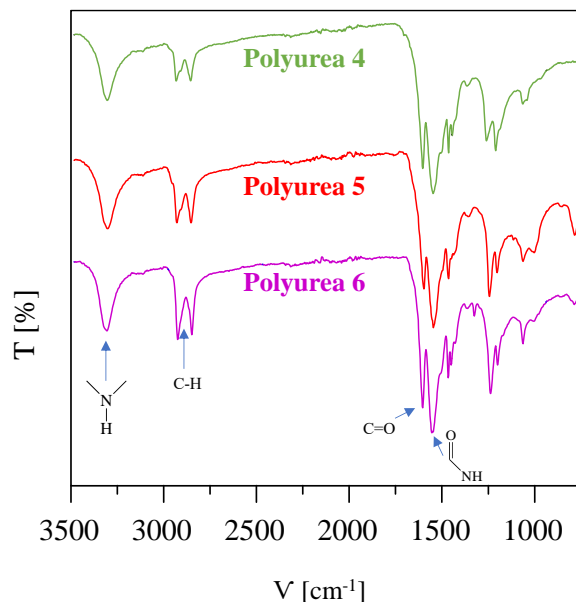

Figure 11.3: FTIR spectra of polyurea 4 (green line), polyurea 5 (red line) and polyurea 6 (purple line).

The polycondensation process adopted, despite overcoming environmental drawback typical for PUs synthesis, was leading to modest M_n as reported in **Table 11.1** due to the solid state reached during the reaction. In this regard, one interesting option could be the synthesis of lower melting polyureas, that keeping in the molten state under the used conditions, were able to further react reaching higher molecular weight. In case of polyurea 6 the higher M_n resulted, was related with the lower viscosity compared to the other melt systems, due to the higher aliphatic sequence reducing the hydrogen bond for repeating unit.

11.3 Thermal characterization

Polyurea 4, polyurea 5 and 6 have demonstrated high thermal stability, as shown by the TGA curves in **Figure 11.4**, making them suitable for high temperature applications. In detail, the first weight loss of about 5% was recorded around 300°C, associated to volatile cyclic derivatives forming during the backbiting reaction of the ammine end groups[24]. The maximum degradation rate took place at 355°C for polyurea 4, at 389°C for polyurea 5 while polyurea 6 had a T_{max} at

389°C. The intrinsic chemical structure of polyurea 4, characterized by higher density of ureic bonds along the macromolecular chain, being responsible of the main degradation process involving isocyanate group formation[18–20], decreased the thermal stability.
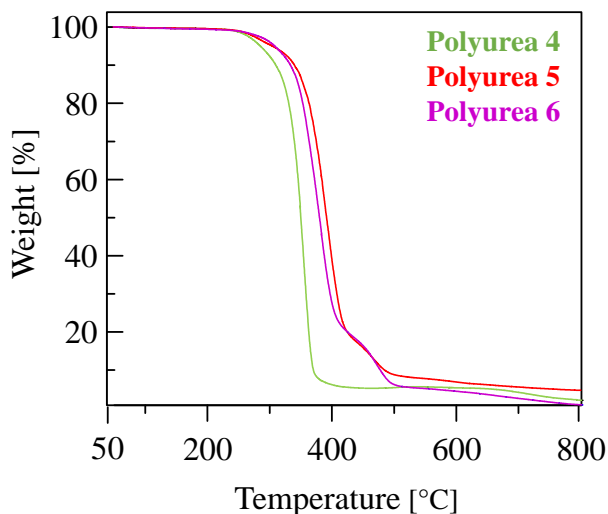

Figure 11.4: *TGA curves recorded for polyurea 4 (green line), polyurea 5 (red line) and polyurea 6 (purple line).*

The calorimetric traces and data reported respectively **Table 11.2** and **Figure 11.5**, for polyurea 4, polyurea 5 and polyurea 6 indicated their semicrystalline nature. The three samples presented very high melting temperatures (375°C for polyurea 4; 278°C for polyurea 5; 292°C for polyurea 6) accompanied with a huge melting enthalpies, ΔH_ms. These values were in line with previous results reported in literature[6].

Table 11.2: *Thermal characterization of polyueras synthetized.*

Sample	DSC				TGA	
	Ist scan		IInd scan			
	T_m °C	ΔH_m J/g	T_m °C	ΔH_m J/g	$T_{5\%}$ °C	T_{max} °C
Polyurea 4	375	730	-	-	283	355
Polyurea 5	278	130	277	120	300	389
Polyurea 6	292	118	278-276	90	305	375

The well packed structure of the crystalline phase was responsible for the elevated melting temperatures observed. The high grade of order reached was strictly related to the alkyl segment mobility and symmetry that favored the formation of inter-chain hydrogen bonds. The value of

ΔH_m, related to the amount of crystals developed, suggested a predominant development of crystal phase at the expense of the amorphous one, which was almost not visible. As regards polyurea 4, the endothermic peak had a relevant area that could not be explained only on the basis of melting phenomenon.
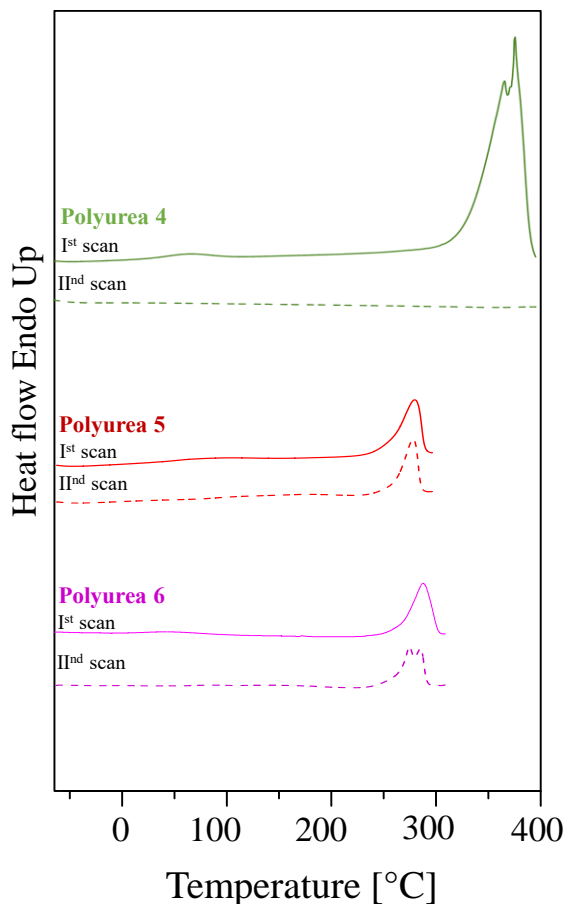

Figure 11.5: DSC curves for polyurea 4 (green line) polyurea 5 (red line) and polyurea 6 (purple).

Considering the data reported form thermogravimetric analysis, where the maximum degradation rate of polyurea 4 was observed around 355°C, it could be supposed that the melting process was presumably taking place in concomitance with the degradation. Indeed, during second scan no peaks were detected, meaning the complete degradation of polyurea 4 during the first heating step. Considering polyurea 5 and polyurea 6, they presented lower melting temperature respect to polyurea 4 but still presented pretty high ΔH_m value, indicating the predominant amount of crystalline material. Being T_m lower and their degradation temperature, polyurea 5 and 6 were melting without degrading, indeed the second heating scan reported thermal transitions retracking the first scan.

11.4 Conclusions

 "One-pot" process for the preparation of polyurea's was successfully applied, leading to highly crystalline PUs. This novel synthetic strategy opens new possibilities in the non-isocyanate route toward polyureas production. Moreover, the simple and quantitative recovery of cathecol, produced as product, could be isolated as pure crystals in amount between 85 to 100%, together with the use of bio-based diamine building blocks, as 1,4-butandiamine,1,5-pentandiamine and 1,6-hexametilendiammine, confers to this process a green basis. The products were completely characterized showing a really high thermal stability that make them suitable for high temperature applications.

11.5 Bibliography

1. Tundo, P., Selva, M. The chemistry of dimethyl carbonate. *Acc. Chem. Res.* **35**, 706–716 (2002).

2. Schäffner, B., Schäffner, F., Verevkin, S. P., Börner, A. Organic carbonates as solvents in synthesis and catalysis. *Chem. Rev.* **110**, 4554–4581 (2010).

3. Clements, J. H. Reactive applications of cyclic alkylene carbonates. *Ind. Eng. Chem. Res.* **42**, 663–674 (2003).

4. K.E. Fuger, J.J. McCoy, J. G. Z. US Patent 3,895,054 A,. (1975).

5. Jiang, S.; Cheng, H. Y.; Shi, R. H.; Wu, P. X.; Lin, W. W.; Zhang, C.; Arai, M.; Zhao, F. Y. Direct Synthesis of Polyurea Thermoplastics from CO2 and Diamines. *ACS Appl. Mater. Interfaces* **11**, 47413–47421 (2019).

6. Kébir, N., Benoit, M., Legrand, C., Burel, F. Non-isocyanate thermoplastic polyureas (NIPUreas) through a methyl carbamate metathesis polymerization. *Eur. Polym. J.* **96**, 87–96 (2017).

7. Tripathi, M., Parthasarathy, S., Roy, P. K. Spray processable polyurea formulations: Effect of chain extender length on material properties of polyurea coatings. *J. Appl. Polym. Sci.* **137**, 1–9 (2020).

8. Sánchez-Ferrer, A., Rogez, D., Martinoty, P. Synthesis and characterization of new polyurea elastomers by Sol/Gel chemistry. *Macromol. Chem. Phys.* **211**, 1712–1721 (2010).

9. Chin, D. C. H., Palaniandy, K., Hia, I. L., Pasbakhsh, P. High performance aliphatic polyurea films reinforced using nonfunctionalized multiwalled carbon nanotubes. *Polym. Compos.* **41**, 1036–1044 (2020).

10. Zhang, T.; Cai, W.; Chu, F.; Zhou, F.; Liang, S.; Ma, C.; Hu, Y. Hydroxyapatite/polyurea nanocomposite: Preparation and multiple performance enhancements. *Compos. Part A Appl. Sci. Manuf.* **128**, 105681 (2020).

11. Tang, S. L. Y., Smith, R. L., Poliakoff, M. Principles of green chemistry: Productively. *Green Chem.* **7**, 761–762 (2005).

12. H.G. Schmelzer, R.M. Mafoti, J. Sanders. The polyurea structure and the role of Amine-Terminated Polyethers and Polyesters in Polyurethanes. *J. Prakt. Chem.,* **336**, (1994).

13. Cornille, A., Auvergne, R., Figovsky, O., Boutevin, B. Caillol, S. A perspective approach to sustainable routes for non-isocyanate polyurethanes. *Eur. Polym. J.* **87**, 535–552 (2017).

14. Froidevaux, V., Negrell, C., Caillol, S., Pascault, J. P., Boutevin, B. Biobased Amines: From Synthesis to Polymers; Present and Future. *Chem. Rev.* **116**, 14181–14224 (2016).

15. Włoch, M., Datta, J., Błażek, K. The Effect of High Molecular Weight Bio-based Diamine Derivative of Dimerized Fatty Acids Obtained from Vegetable Oils on the Structure, Morphology and Selected Properties of Poly(ether-urethane-urea)s. *J. Polym. Environ.* **26**, 1592–1604 (2018).

16. Q. Liu. A simple conversion of amines into monosubstituted ureas in organic and aqueous solvents. *Tetrahedron Lett.* **42**, 1445–1447 (2001).

17. S. M. Hutchins, K. T., Chapman. A general method for the solid phase synthesis of ureas. *Tetrahedron Lett.* **35**, 4055–4058 (1994).

18. Pan, W. C., Lin, C. H., Dai, S. A. High-Performance Segmented Polyurea by Transesterification of Diphenyl Carbonates with Aliphatic Diamines. 2781–2790 (2014). doi:10.1002/pola.27302

19. A. K. Qaroush, A. S. Al-Hamayda, Y. K. Khashman, S. I. Vagin, C. T., B. R. Highly efficient isocyanate-free microwave-assisted synthesis of [6]-oligourea. *Catal. Sci. Technol.* **3**, 2221 (2013).

20. Pan, W. C., Liao, K., Lin, C. Dai, S. A. Solvent-free processes to polyurea elastomers from diamines and diphenyl carbonate. (2015). doi:10.1007/s10965-015-0747-x

21. T. Tabanelli, E. Monti, F. Cavani, M. Selva. The design of efficient carbonate interchange reactions with catechol carbonate. *Green Chem.* **19**, 1519–1528 (2017).

22. T. Tabanelli, C. Giliberti, R. Mazzoni, R. C. An innovative synthesis pathway to benzodioxanes: the peculiar reactivity of glycerol carbonate and catechol. *Green Chem.* **21**, 329–338 (2019).

23. Gjyli, S.; Korpa, A.; Tabanelli, T.; Trettin, R.; Cavani, F.; Belviso, C. Higher conversion rate of phenol alkylation with diethylcarbonate by using synthetic fly ash-based zeolites. *Microporous Mesoporous Mater.* **284**, 434–442 (2019).

24. Maisonneuve, L., Lamarzelle, O., Rix, E., Grau, E., Cramail, H. Isocyanate-Free Routes to Polyurethanes and Poly(hydroxy Urethane)s. *Chem. Rev.* **115**, 12407–12439 (2015).

Chapter V
CONCLUSIONS

The experimental activities conducted were focused on the development of new bio-based and/or biodegradable materials to replace the widely used oil-based polymers, especially in food packaging application. All the syntheses conducted were designed as eco-friendly and solvent free processes, with parameters easily to scale-up to the industrial level. In details, the research was developed in two main lines; the first one was centered on the modification of well-known bio-plastics via physical blending and mainly copolymerization process, this last resulting an effective tool to get *ad hoc* functional properties, improving the no optimal characteristics without compromising the satisfactory ones. A second line was focused on the development of new polymers with bio-based building blocks, derived from biomasses, adequately modified according to the principles of the "Green Chemistry".

The so-obtained materials were completely characterized from the chemical, structural and thermal point of view; then, different specific studies were conducted in order to evaluate the suitability in food packaging sector. For this reason, water contact angle and biodegradability were evaluated together with mechanical response and gas barrier properties. The results obtained were rationally explained with support of experimental data and structure-property correlations were defined.

The results obtained can be considered relevant for the academic as well as industrial world. In details, the well-known bioplastics, copolymerized with adequate co-units, improved the specific features that have been hampering the conquest of the market, maintaining the promising characteristics. Moreover, the high versatility of this class of material was tested, acting on both chemical structure and molecular architecture. The presence of short/long ramifications along the main chain and of heteroatoms and glycol sub-unit with different length resulted a very effective tool to control and properly tune the properties of the final material, such as flexibility, crystallization capability, hydrophilic/hydrophobic balance, mechanical response, biodegradation rate and barrier performances. Regards the molecular architecture, random or block distribution of co-units revealed to play a key role in determining the specific characteristics of the polymer. Several processing were performed, as compression moulding and extrusion, showing another

level of modification. Based on the promising barrier performances, obtained with adequate modification, together with the flexibility improvement, these materials become suitable candidates for monolayer packaging. In this way, recycling, currently recognized as the preferred option as post-used strategy, would be easier and cheaper, and mainly really possible, thanks to the lower complexity of the packages.

As regards polymers obtained employing bio-based building blocks, the synthesis of the final materials as well as the production of the monomers from biomasses followed the principles of the "Green Chemistry". The polymers obtained resulted high in molecular weight with adequate mechanical responses, becoming a good starting point for the development of a new class of oil-free materials.

In conclusion, the systems designed for food packaging applications during this PhD experimental activity resulted promising candidate to build a more sustainable industry and society. Despite that, upscaling needs to be tested and more detailed investigations, focused on the interaction materials-foods, need to be conducted before the entrance in the market.